NASA CR-114362

AVAILABLE TO THE PUBLIC

TRIM, CONTROL, AND STABILITY OF A GYRO-STABILIZED

HINGELESS ROTOR AT HIGH ADVANCE RATIO

AND LOW ROTOR SPEED

By G. A. Watts, R. J. London, and R. J. Snoddy

May 1971

TRIM, CONTROL, AND STABILITY OF A GYRO-STABILIZED

HINGELESS ROTOR AT HIGH ADVANCE RATIO

AND LOW ROTOR SPEED

By G. A. Watts, R. J. London, and R. J. Snoddy
May 1971

Distribution of this report is provided in the interest of information exchange. Responsibility for the contents resides in the author or organization that prepared it.

Prepared under Contract No. NAS 2-5168 by
LOCKHEED-CALIFORNIA COMPANY
ROTARY WING DIVISION
VAN NUYS, CALIFORNIA

for

U.S. ARMY AIR MOBILITY RESEARCH AND DEVELOPMENT LABORATORY
AMES DIRECTORATE
and
NATIONAL AERONAUTICS AND SPACE ADMINISTRATION
AMES RESEARCH CENTER

SUMMARY

Methods are developed for predicting the behavior of hingeless rotors
with stiff blades, at high advance ratios and low rotor speeds. The
methods are simple and expository in nature, and are developed for the
purposes of (1) providing insight into the influences of various rotor and
control parameters on rotor system behavior, (2) examining the suitability
of existing methods which contain more comprehensive analytic descriptions
for predicting behavior of hingeless rotors at high advance ratios at low
rotor speeds, and (3) to provide analysis techniques which are flexible
enough to be useful in preliminary design studies.

Cyclic angles required to trim rotor hub and swashplate moments are
calculated and compared with experimental data. Longitudinal cyclic angles
agree well over the advance ratio and rotor speed ranges studied. Lateral
cyclic angles do not agree well, but the discrepancy is systematic, sug-
gesting a lack in the theory.

The dependence of hub moment, thrust, and swashplate moment on cyclic
angles, collective angles, and rotor angle of attack was investigated both
analytically and experimentally at rotor speeds ranging from 8.5 to 90 per-
cent of nominal and at forward speeds ranging from 50 to 120 knots. Theoret-
ical predictions based on a simple analytical description of aerodynamics
agree well with experiment.

The control system used in the analyses and tests included a constant
speed gyroscope to stabilize the rotor. Rotor moments were controlled by
applying moments to the swashplate. The system was designed such that the
swashplate was not restrained by the control-force servos while in the
normal operating mode.

Theoretical estimates of hub moments produced by unit moments applied to
the swashplate show a trend toward very small changes in amplitude and phase
over large ranges of advance ratio and rotor speed. The trend toward

1

constancy in control effectiveness was verified by wind tunnel tests.

Stability of the gyro-stabilized cyclic feathering system was examined experimentally by applying "step" control moments at the swashplate and observing the decay of induced oscillations. Frequencies, damping, and precessive direction noted in the experiments compared well with values predicted by theory.

A description of the theoretical development, a summary of measured data, and some comparative evaluations are presented in this report.

CONTENTS

INTRODUCTION

In the search for higher cruising speeds and lower drag in helicopters, it became apparent that relieving the rotor of its propulsive task (employing auxiliary propeller or fanjet propulsion) would reduce retreating blade stall and permit a higher cruising speed. If, in addition, the rotor did not have to support the weight of the vehicle, that function being performed by wings, then the effects of retreating blade stall could be virtually eliminated (except in maneuvers) and a much greater speed attained. However, increasing flight speed, while maintaining a relatively constant rotor rotational speed brings on another limitation: the tips of the rotor blades on the advancing side encounter Mach number difficulties. It becomes desirable, therefore, to slow the rotor speed as forward flight speed is increased. Finally, if the rotor were completely eliminated, i.e., stowed away, the speed and cruise efficiency of conventional jet aircraft could be attained.

It becomes of interest to investigate slowing and stopping rotors in flight, and from a technological point of view, to develop knowledge and analytical tools that would be prerequisites to developing slowed-rotor or composite aircraft. Although industry has already developed analytic techniques for studying helicopters, many questions arise as to their suitability for predicting the behavior of rotors at high advance ratios and the high flight speeds expected to be encountered in the operation of slowed-rotor or stoppable-rotor aircraft. Therefore, the study reported here was undertaken to investigate the behavior of, and develop analytic design tools for, slowed/stopped rotors.

It was recognized that a rotor with very stiff blades would be required for in-flight stops, so a full-scale rotary-wing aircraft wind tunnel model, which had previously been used to demonstrate the feasibility of in-flight stops (in the NASA-Ames 40 x 80 ft wind tunnel), was selected as a baseline vehicle for this investigation.

The requirements for stiffness of rotor blades for slowed-rotor aircraft are not yet established. Since it is possible that blades may be stiffer than those used in conventional helicopters, and since wind tunnel tests of the stoppable rotor would span a complete range of advance ratios, from very low to infinity, it was decided that the same model would be used as a baseline vehicle for the slowed-rotor studies. Therefore, analytical methods are developed which describe the behavior of the rotor system over a complete range of rotor speeds, from nominal (for conventional helicopters) to zero; and data measured in wind tunnel tests of the baseline vehicle are used to corroborate the analyses.

Development of VTOL aircraft with hingeless rotors has progressed from a helicopter through jet-propelled and propeller-driven compound helicopters. Good handling qualities have been demonstrated in the helicopter, and greatly increased speed has been demonstrated in the compound helicopter. The next step in the direction of speed increase appears to be the development of the slowed-rotor compound helicopter. A 100-knot increase in flight speed appears to be realizable with a 50-percent reduction in rotor speed. This will extend the range of operating advance ratio to $\mu = 1.5$. Control system stability, damping of in-plane resonance, and blade stresses due to reduced centrifugal stiffness are areas that must be investigated.

A horizontally stoppable, retractable rotor aircraft could follow the development of the slowed-rotor compound. Its problems would be associated with extreme advance ratios, to infinity, and with alleviation of periodic forces at low rotor speeds due to gust response.

The research reported herein complements investigations made over the last ten years into the effects of: high advance ratio, blade dynamics, gyroscope stabilization, low rotor speed operation, and blade loads on a rotor stopped in flight. Some of these investigations employed the rotor used in this work.

A main purpose of the present investigation was the development of an understanding of the physics of low rotor speed, high advance ratio, gyro-

6

stabilized rotor operation, with an aim toward facilitating the rational design of high-speed, high-efficiency, VTOL aircraft.

Since the objective of this study was primarily an understanding of the behavior of a system, rather than precise numerical results, simplified "expository" methods based on key physical aspects were derived. The results of the approximate calculations are compared with experimental data. Expository methods were derived to determine the following:

- Stability of the fixed-shaft rotor-gyro system (representing the model in the wind tunnel)
- Stability of a free-flying vehicle with the same rotor-gyro system
- Aeroelastic derivatives of the fixed-shaft rotor
- Cyclic pitch angles required to trim the rotor
- Control effectiveness

All but the free-flight vehicle stability were checked experimentally by wind tunnel testing.

Although experimental data contained shaft vibration moments and blade harmonic loads, only the consequences of mean rotor coefficients were analyzed theoretically and are reported in this report. It is planned to reduce the vibration data and correlate it with theory at a later date.

$[A]$	Aerodynamic stiffness matrix (rotating axes)
$[A_r]$	Aerodynamic damping matrix (rotating axes)
AR	Aspect ratio of wing
b	Number of blades
b	Wing span, ft
bm	Blade root bending moment, ft lb
B	Tip loss factor
$[B]$	Aerodynamic stiffness matrix (stationary axes)
$[B_r]$	Aerodynamic damping matrix (stationary axes)
c	Blade chord, ft
C_R	Rotating damping (feathering friction), ft lb/rad/sec
C_S	Stationary damping (swashplate damping), ft lb/rad/sec
$\bar{c}$	Wing mean aerodynamic chord, ft
$c_{\ell \alpha_t}$	Tailplane lift curve slope
Cm	Hub pitching moment coefficient, $M/q \pi R^3$
C_ℓ	Hub rolling moment coefficient, $L/q \pi R^3$
Cm_{sp}	Swashplate pitching moment coefficient, $M_\theta/q \pi R^3$
$C_{\ell sp}$	Swashplate rolling moment coefficient, $M_\phi/q \pi R^3$
C_L	Lift coefficient, $L/q \pi R^2$
C_D	Drag coefficient, $D/q \pi R^2$
C/C_r	Fraction of critical damping
$[CF_b]$	Blade centrifugal force matrix
D	Drag, lb
[Damp]	Damping matrix

$[D]$	Transformation matrix – rotor to blade
e	Base of Naperian logarithms
fm	Blade feathering moment, ft lb
$\{GF\}$	Vector of rotor generalized forces
$\{GF_b\}$	Vector of blade generalized forces
H	Blade parabolic flapping generalized force, lb
H_{δ_0}	Collective flapping generalized force, lb
H_{δ_θ}	Pitch flapping generalized force, lb
H_{δ_ϕ}	Roll flapping generalized force, lb
I_b	Blade linear flapping moment of inertia, slugs ft^2
I_G	Gyroscope diametral moment of inertia, slugs ft^2
I_R	Feathering moment of inertia of rotor, slugs ft^2
I_o	Blade moment of inertia about $c/4$, slugs ft^2
Iyy	Body pitching moment of inertia, slugs ft^2
I_{xx}	Body rolling moment of inertia, slugs ft^2
$[I]$	Rotor inertia matrix
$[I_b]$	Blade inertia matrix
k	Mechanical advantage; gyro tilt: cyclic pitch ratio
K_R	Rotating spring constant, ft lb/rad
K_S	Stationary spring constant, ft lb/rad
ℓ_t	Tail length, ft
L	Hub rolling moment, ft lb
L_p	Body aerodynamic coefficient (damping in roll), $C_{\ell_p} \frac{b}{2V} q \, S t$
m	Mass, slugs
M	Hub pitching moment, ft lb

M Airframe mass, slugs

M_q Body aerodynamic coefficient (damping in pitch), $C_{m_q} \dfrac{\bar{c}}{2V} qS\bar{c}$

M_α Body aerodynamic coefficient (static stability), $C_{m\alpha} qS\bar{c}$

$M_{\dot\alpha}$ Body aerodynamic coefficient (plunge damping), $C_{m\dot\alpha} \dfrac{\bar{c}}{2V} qS\bar{c}$

M_θ Swashplate pitching moment, ft lb

M_ϕ Swashplate rolling moment, ft lb

M_{tip} Tip mass, slugs

M_δ Blade flapping generalized mass, slugs

$M_{()()}$ Generalized mass (subscripts denote coupling)

p The pth blade

P Per revolution

P Power, ft lb/sec

q Dynamic pressure, $\rho V^2/2$, lb/ft^2

r Distance from center of rotation, ft

R Rotor radius, ft

S_t Tail plane area, ft^2

S Wing area, ft^2

S_w πR^2 , ft^2

$[S]$ Structural matrix

T Thrust, lb

$T_{\frac{1}{2}}$ Time to half amplitude, sec

$[T]$ Transformation matrix, between sets of rotating axes

$[\ ]^T$ Matrix transpose operation

V Airspeed, ft/sec

V Blade root shear, lb

x	Roll axis (rotating)
X	Roll axis (stationary)
y	Pitch axis (rotating)
Y	Pitch axis (stationary)
z	Vertical displacement, ft
Z	Vertical axis
Z_α	Body aerodynamic derivative (lift curve slope), $C_{L_\alpha} qS$, lb/rad
α	Angle of attack, deg or rad
β	Blade linear flapping angle, deg or rad
β_o	Rotor precone angle, deg or rad
$\{\beta\}$	Vector of degree-of-freedom displacements
γ	Structural damping, fraction of critical
δ	Blade parabolic flapping displacement, ft
δ_o	Collective flapping displacement of the rotor, ft
δ_θ	Pitch flapping displacement of the rotor, ft
δ_ϕ	Roll flapping displacement of the rotor, ft
ϵ	Downwash angle of tail plane, rad
$\{\eta\}$	Vector of blade displacements
θ	Swashplate pitch angle, deg or rad
θ_f	Blade feathering angle, deg or rad
θ_t	Blade twist rate, deg/ft or rad/f
θ_o	Rotor collective angle (measured at root), deg or rad
$\theta_{.75R}$	Rotor collective angle (measured at 3/4 radius), deg or rad
θ_{1c}	Cyclic pitch, nose-up at $\psi = 0$, deg or rad
θ_{1s}	Cyclic pitch, nose up at $\psi = 90°$, deg or rad

11

Θ	Rotor pitch angle, rad
λ	Root of characteristic equation
Λ	Sweep angle between c/4 and feathering axis, rad
μ	Advance ratio $\dfrac{V}{\Omega R}$
ρ	Air density, slugs/ft^3
σ	Solidity
Σ	Summation sign
ϕ	Swashplate roll angle, rad
$\bar{\Phi}$	Rotor roll angle, rad
ψ	Azimuth angle measured counterclockwise from positive X axis (aft), rad
ψ_o	Cant angle, deg or rad
ω	Natural frequency 1/sec
Ω	Rotor rotation speed, rpm or rad/sec
Ω_G	Gyroscope rotation speed, rpm or rad/sec
$[\ ]^{-1}$	Reciprocal of matrix
.	First time derivative
..	Second time derivative

Subscripts

1, 2, 3	Blade numbers
n	The nth vibration mode
δ_o, δ_θ, δ_ϕ	Used to denote flapping degree-of-freedom

12

THEORETICAL DEVELOPMENT

The stability, fixed-shaft control effectiveness, and cyclic pitch required to trim a stiffened rotor, stabilized by a high-speed gyroscope system, while operating at high advance ratios were studied. The effects of operating at low rotor speeds were also studied.

An important aspect of the theoretical investigation was a determination to keep the analysis as elementary as possible consistent with explaining the behavior observed in experiments. Although elegant methods employing comprehensive mechanical descriptions for precise analysis were available, and were used for checking purposes, these methods were not expected to shed adequate light on the fundamental physical processes at work in the system. These more elaborate methods solve comprehensive differential equations in step-by-step procedures, either around the azimuth or vs time, and often require checking against desired conditions and iterating to a solution.

Elementary or "Expository" methods, in closed form where possible, are adopted for the purpose of gaining insight to the causes and effects of design variables, to the interrelated behavior of the rotor, control system, and the airframe. Expository methods also offer the possibility of becoming preliminary design tools for the design of new vehicles. Rapid solution to design parameter variations is a goal of the expository methods. Also, the character of the expository method makes it a good communication medium for use among technical people.

The expository methods are designed to open physical situations for viewing. An example is the capability to calculate the dynamic modes of an aeromechanical system. Any linear system without periodically varying coefficients is simply analyzed for its dynamic properties, the time constant or the period and damping of its transient modes. They may be divergent or damped, and the vector of degrees of freedom which describes the mode generally shows clearly the important elements of that mode of motion.

Equations of Motion

During its development, the expository method was assembled in three stages, enlarging the magnitude of description in each successive stage. At each stage, an understanding of the system behavior based on fundamentals was obtained before the next stage was attempted. In this way the effects of increasing the size of description of the system could be seen. Rationale for development of the method is discussed here. Details of the mathematical derivation are given in Appendices A and B.

The first stage of the expository method contained only two degrees of freedom: gyro pitch and gyro roll. Even with this extreme simplicity the fixed-shaft stability boundary was predictable, and the experimentally observed effects of feathering damping and swashplate damping on control mode stability were indicated up to rotor speeds of approximately 30-percent rpm (where nominal operating speed of the rotor, in a helicopter mode, is considered to be 100-percent rpm). Above 30-percent rpm, the fact that the blade flapping mode was not included in the analysis made the control mode appear to be unrealistically unstable. The calculated rotor hub moment response to cyclic pitch was largely in error at rotor speeds above 10-percent rpm. It is important, however, that the simple version showed the limiting physical case for extremely stiff cantilever blades, and so became a foundation for development of the second stage.

The second stage in the development of the expository method consisted of adding three rotor first flapping modes: pitch, roll and collective flapping of the tip path plane; thus increasing the degrees of freedom in the program from two to five. Again the rotor shaft was fixed. The five degree of freedom model calculated control mode stability well over the complete range of rotor speeds, except for an unexplained excessive damping which occurred at an intermediate rotor speed. The hub moment aeroelastic response to cyclic angles was predicted well at all rotor speeds. Trends of cyclic angles required to trim rotor hub moments were correctly calculated. The cyclic angle θ_{1s} (called longitudinal cyclic for its effect on articulated rotors, but with very stiff blades such as used in this study, this angle

produces more rolling than pitching moment) was very closely predicted. The measured values of lateral cyclic trim angle θ_{1_c} deviated considerably from those predicted, and in a sense suggested that some important contribution to nose up pitching moment had been omitted in the analysis; reasons for this are suspected but have not yet been checked. The method also predicted control effectiveness trends well. The effects of flapping on stability and on aeroelastic derivatives agreed well with the test measurements.

The third stage in the development of the method involved the addition of hub (and body) pitch, roll and plunge degrees of freedom. The resulting eight degree-of-freedom model was used to evaluate the feasibility and usefulness of testing the model mounted on gimbals in the wind tunnel (this evaluation was requested as part of an investigation into the possibility of performing tests with the model free to pitch and roll in the wind tunnel). The stability modes, frequenices, and dampings of the gimballed model were compared with those of a hypothetical free-flight version of the model. Results of this comparison are given later in this report.

The fundamental concepts involved in the derivation of the equations are few and are easily grasped. There are three rotational states in the total system: Those associated with the gyroscope, the rotor, and the airframe. Only small motions of mass elements in each rotating state, relative to the appropriate set of axes which rotates with each of the rotational states, need be considered in developing the equations of motion. This feature is the key to the simplifications included in the expository method. (The most complex parts of the method have to do with transferring equations among various sets of axes, and they are not difficult.) The fundamental concepts used are discussed in the following paragraphs.

Fundamental concept number 1. - Because motions of elements in a given state are small (in fact perturbational) the calculation of forces due to the motions is very simple. The forces may be inertial, centrifigual, aerodynamic, structural, or due to springs and dashpots. The force due to unit displacement or velocity may be independent of azimuth, or may vary periodically with azimuth (the fact that they're viewed in rotating axes permits

the simplification). Appendix A discusses calculation of all but the aero-dynamic forces. Reference (1) discusses calculation of aerodynamic forces.

Fundamental concept number 2. - Small displacements relative to a set of axes can be expressed relative to another set of axes by a simple time dependent transformation which relates the positions of the two sets of axes. In the present work it was necessary only to consider displacements normal to the (X, Y) plane (Z direction). These displacements are organized into pitch, roll, and plunge motions. They may be transformed from one axis system to another (from set ① to set ②) by the transformation

$$
\left\{ \begin{array}{c} \Theta \\ \Phi \\ z \end{array} \right\}_{②} = \left[\begin{array}{ccc} \cos\left(\Omega_{②} - \Omega_{①}\right)t & -\sin\left(\Omega_{②} - \Omega_{①}\right)t & 0 \\ \sin\left(\Omega_{②} - \Omega_{①}\right)t & \cos\left(\Omega_{②} - \Omega_{①}\right)t & 0 \\ 0 & 0 & 1 \end{array} \right] \left\{ \begin{array}{c} \Theta \\ \Phi \\ z \end{array} \right\}_{①}
$$

or in more compact form,

$$
\beta_2 = \left[T \right] \beta_1
$$

Fundamental concept number 3. - This concept is a corollary to number two in that the generalized forces relative to one axis system may be transformed relative to another by the transpose of the above transform,

$$
\left\{ \begin{array}{c} M \\ L \\ T \end{array} \right\}_{①} = \left[T \right]^{T} \left\{ \begin{array}{c} M \\ L \\ T \end{array} \right\}_{②}
$$

The two concepts enable the complete transformation of coefficients in the differential equations from one rotating state to another. To transform

16

time derivatives of displacements it is important to note that ;he time derivatives of the transform are as follows:

$$\dot{\beta}_2 = [T] \dot{\beta}_1 + [\dot{T}] \beta_1$$

$$\ddot{\beta}_2 = [T] \ddot{\beta}_1 + 2 [\dot{T}] \beta_1 + [\ddot{T}] \beta_1$$

For example, terms in one axis system:

$$[I] \ddot{\beta}_2 + [Damp] \dot{\beta}_2 + [S] \beta_2$$

may be transformed to another rotating system by:

$$[T]^T [I] \left\{ [T] \ddot{\beta}_1 + 2 [\dot{T}] \dot{\beta}_1 + [\ddot{T}] \beta_1 \right\}$$

$$+ [T]^T [Damp] \left\{ [T] \dot{\beta}_1 + [T] \beta_1 \right\} + [T]^T [S] [T] \beta_1$$

Fundamental concept number 4. - The centrifugal forces in a rotating state may be thought of as radial forces externally applied to each mass element and resisted by tension in the structure. The normal components of the resisting tensile forces may then be used to calculate moments and generalized forces on the various degrees of freedom. The transformation of centrifugally induced forces to stationary axes produces gyroscopic terms.

Fundamental concept number 5. - The kinematic and dynamic relationships between degrees of freedom of the entire rotor in rotating coordinates and of individual blade motions are easily expressed. In the rotor rotating state, correspondence can be deduced by inspection; this is shown in Appendix A. Couched in matrix form it is stated

$$\{\eta\}_{\text{blade motions}} = [D] \{\beta\} \quad \substack{\text{Rotor degrees of freedom} \\ \text{in rotating coordinates}}$$

17

The velocity and accelerations are related thus

$$\{\dot{\eta}\} \ = \ [D] \ \{\dot{\beta}\}$$

$$\{\ddot{\eta}\} \ = \ [D] \ \{\ddot{\beta}\}$$

With generalized forces on the blades easily calculable, be they inertial, centrifugal, or aerodynamic, the generalized forces on the degrees of freedom due to motions of the degrees of freedom can be obtained by noting that they are related to the blade generalized forces by

$$\left\{GF\right\}_\beta \ = \ [D]^{\ T} \ \left\{GF\right\}_{blades}$$

The rotor generalized forces $\left\{GF\right\}_\beta$ in terms of rotor motions is

$$\left\{GF\right\}_\beta \ = \ [D]^{\ T} \begin{bmatrix} \text{blade force due to} \\ \text{blade motions} \end{bmatrix} [D] \ \{\beta\}$$

and the rotor derivations are obtained in terms of blade forces

$$[D]^{\ T} \begin{bmatrix} \text{blade forces due to} \\ \text{blade motions} \end{bmatrix} [D]$$

Summary of the procedure. - Based on the preceding concepts, the equations of motion are derived in Appendix A as follows:

(1) Motions of the isolated gyroscope, in pitch and roll, are considered relative to axes which rotate with the gyroscope. The pitch and roll equations are not coupled.

(2) Equations for the isolated gyroscope are transformed to axes which rotate at rotor speed.

(3) Equations of motion of the rotor, in terms of motions of individual blades, are derived relative to axes which rotate with the rotor, and are added to the transformed gyroscope terms. Blade forces are inertial, centrifugal, structural damping, and aerodynamic.

(4) Rotating spring and rotating damping terms (terms involving rotating friction about the blade feathering axis) are added.

(5) All terms are transformed to stationary or earth-fixed axes.

(6) Terms representing swashplate damping and springs are added.

(7) Body inertia and aerodynamic derivative terms are added to the pitch, roll and plunge equations.

(8) The following forcing terms are added to the right hand side (RHS) of the equations:

- aerodynamic terms due to precone, twist, and collective angles
- aerodynamic terms due to gust angle of attack
- terms representing control moments which are applied to the swashplate
- a term representing the centrifugal flattening of the precone

Aerodynamics

Aerodynamics used in these investigations is organized into derivative form, or coefficients in the differential equations. Simple aerodynamic premises which are shown to be valid for high advance ratio and low rotor thrust are used. The derivatives, analogous to rigid-body derivatives for fixed wing aircraft, relate rotor forces, moments, and generalized forces to displacements and velocities in various degrees of freedom of the rotor. The derivatives are used relative to an earth-fixed axis system, but are derived from blade forces due to blade motions in rotating axes.

Aerodynamic derivatives as used in this study are of two types:

(1) response derivatives

(2) forcing derivatives

19

Response derivatives represent aerodynamic forces produced by motions of the degrees of freedom. The response derivatives are comprised of changes in

- thrust
- hub and swashplate moments
- rotor-flapping generalized forces

due to unit changes in the displacements and velocities of

- rotor pitch, roll, and plunge rigid body motion
- swashplate pitch and roll
- rotor (flapping) degrees of freedom.

Forcing derivatives represent those aerodynamic forces produced external to the dynamic system by

- gust angle of attack
- rotor precone
- blade twist
- swashplate collective (not considered a degree of freedom in this analysis)

The main difference between aerodynamic derivatives of fixed-wing and rotary-wing aircraft is that the rotary wing derivatives possess parts which vary periodically with time (azimuth) as well as mean parts. The forcing derivatives merely add steady oscillating forces to steady-state conditions. The periodic parts of the response derivatives, however, alter the basic mathematics of the differential equations.

The stationary axis derivatives consist of a mean value, independent of azimuth, and harmonic components at frequencies of 3, 6, 9..... times the rotor rotation rate. The 3P component is enough larger than the others to make it the only one of significance. The phase or relative magnitude of its sine and cosine components, is seen to remain unchanged over a large range of advance ratios.

Since the application considered in the analytical portion of this study involves winged aircraft, where the wing is expected to unload the rotor at appropriately high flight speeds, the rotor is considered to pro-

20

vide little lifting force. The lightly loaded rotor must traverse the
advance ratio spectrum from $\mu = 0.3$ to infinity during an in-flight start/
stop operation. In the case of a slowed-rotor compound helicopter, the rotor
is also lightly loaded, but its advance ratio is not expected to exceed
$\mu = 1.5$. Since the aerodynamic and vehicle behavior studies reported herein
are exploratory in nature (high advance ratios and very stiff blades are in-
volved), the simplest concepts which yield approximately correct answers are
used. It is therefore of interest to discuss some ramifications of advance
ratio μ.

The parameter is fundamental to rotary wing aerodynamics. It is the
ratio of forward speed to rotor tip speed, and it in effect controls the
geometry of air flow relative to the rotor blades. A combination of forward
(flight) speed and rotor local velocity (rotational speed) gives the velocity
and direction of flow relative to the blades. The flow pattern varies over
the disk from the purely rotational flow at $\mu = 0$ to the purely rectilinear
at $\mu = \infty$.

$$\mu = \frac{V}{\Omega R} = 0.5$$

Rectilinear Flow   +   Rotational Flow   =   Flow relative to blades
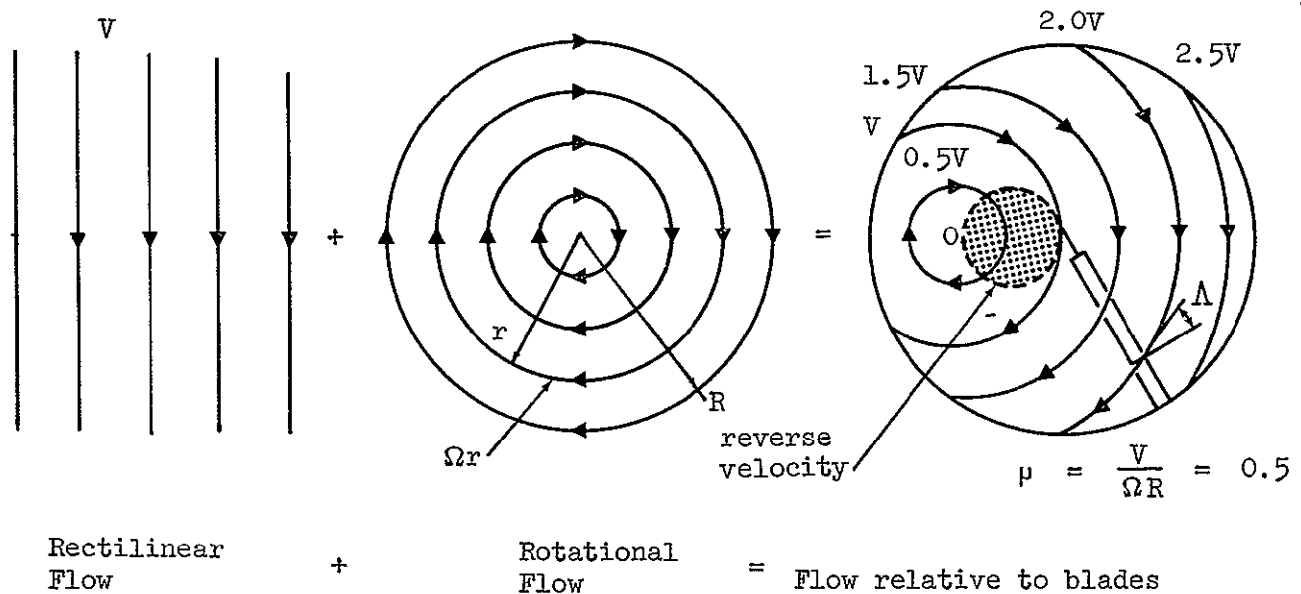
For rotors with infinitely stiff blades, similar geometries and common angles of attack, collective pitch and cyclic pitch; the aerodynamic forces are functions only of advance ratio, free stream dynamic pressure and size.

In a fundamental sense, advance ratio can also be considered to control the geometry of vortices shed by the blades; see Figure 1. At low advance ratio, the vortex structure and attendant downwash from many blade passages accumulate over the rotor disk and drift downstream causing large induced downwash over the disk especially toward its aft edge. At high advance ratio, on the other hand the tip vortices move straight downstream from the blade tips so that downwash cannot accumulate. Induced downwash at high advance ratios can therefore be considered negligible.

At any forward speed a reverse flow region exists just to the left of the rotor mast, where the net air flow moves over the blades from the trailing to the leading edge. This reverse velocity region can also be represented as a function of advance ratio: The region is very small at low advance ratios and approaches 50 percent of the disk area as the advance ratio approaches infinity; see Figure 1.

Assumptions used in formulating aerodynamics representation. - Since the nominal rotor lift of interest in this study is small, blade angles of attack are well below stall limits, even in the reverse flow region. Also, over most of the flight speed region of interest, tip speeds are well below the speed of sound. These two factors permit the use of linearized aerodynamics. Analyses and tests were limited to conditions which do not violate aerodynamic linearity. Fundamentally, linearity allows the use of procedures in which the effects of changing one angle at a time are determined; therefore, coefficients analogous to fixed wing aircraft derivatives can be used, and the superposition of these effects results in a good approximation.

In the calculation of a derivative, the effects of varying one degree of freedom at a time are considered. In the wind tunnel, however, flapping motions are not suppressed, so the measured derivatives are aeroelastic derivatives.

ROTOR DISK

WIND DIRECTION

REVERSE
VELOCITY
OVER BLADE
SECTIONS

PATH OF ONE
BLADE TIP

$\mu = 0.1$
LOW ADVANCE RATIO
- LARGE INDUCED DOWNWASH
- SMALL SWEEP
- SMALL REVERSE VELOCITY REGION

$\mu = 2.0$
HIGH ADVANCE RATIO
- SMALL INDUCED DOWNWASH
- LARGE SWEEP
- LARGE REVERSE VELOCITY REGION
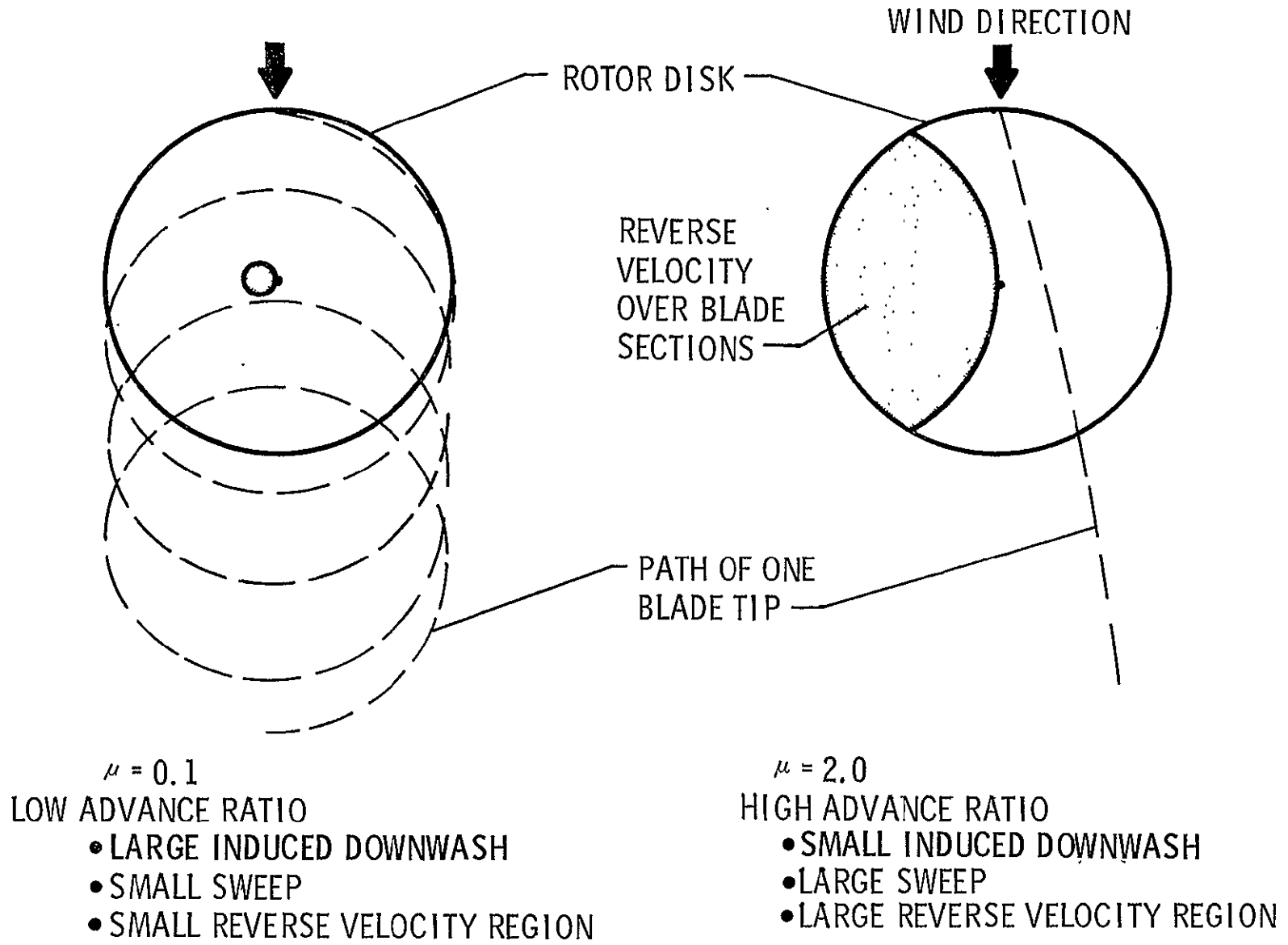
Figure 1.   Advance Ratio Effect on Flow Geometry

The differential equation coefficients vary with the azimuthal position of the rotor.

Consistent with the expository approach, the most simple formulation of aerodynamics which will yield results approximating reality are used. The following are the simplifications used, and their justifications:

(1) Induced downwash is ignored. At high advance ratios, if induced downwash is assumed uniform, it is small enough to be neglected.

(2) Spanwise induction effects are approximated. The most significant effect of spanwise induction is loss of lift near the blade tip. This effect depends on the aspect ratio of the lifting surface. For the blades of the wind tunnel model (AR=12) in uniform flow, the tip effect is hardly noticeable inboard of 80 percent of the blade radius. This effect is approximately accounted for by assuming the blade radius to be slightly smaller than it actually is, by a factor $B \approx 0.97$. The lift at any section can therefore be assumed to depend only on local dynamic pressure normal to the leading edge and on the normal angle of attack at the section.

(3) Blade sweep effects are ignored. At azimuth locations remote from 90 and 270 degrees, at high advance ratios, the flow approaches the blade obliquely. In the aft semicircle of the disk, the flow meets the blade flowing obliquely outboard, whereas in the forward semicircle it meets the blade flowing obliquely inboard. Wind tunnel tests have shown that resolving the flow into components parallel and normal to the blade and ignoring spanwise components yields a good approximation of the pressure distribution and lift, Reference 1. Recent tests have shown that the primary effect of sweep is to increase the maximum lift before stall, but not to change the lift-curve slope or the linearity, Reference 2.

(4) Unsteady aerodynamics are ignored. The primary effect of unsteady aerodynamics can be seen by examining the growth of lift after a sudden change in angle of attack. Lift growth is given by Wagner in terms of numbers of chords travelled, Reference 3. Lift starts almost immediately at 50 percent of maximum and grows to 90 percent within 6 chords of travel. In the tested rotor, where the blade chord is small (the chord of the blade of the wind tunnel model is 1.17 ft) the lift becomes 90 percent of steady-state in 7 ft of travel. At the rotor tip the perimeter is 104 ft. Therefore, in effect steady-state conditions are reached within 7 percent of total azimuth travel when the forward speed is zero. At high advance ratio, the tip velocity on the advancing side is greater than ΩR, so the lift would grow to steady state within a smaller azimuth displacement. On the retreating side, however, the opposite is true and longer azimuthal travel would be required to attain a near steady-state condition. Therefore, unsteady effects would cause some deviation from results based on steady aerodynamics. However, since the deviation is most significant in the reverse flow region where the low dynamic pressure makes lift sensitivity small, the effect is assumed to be lost in the total aerodynamic derivative. The net effect of unsteady aerodynamics is not expected to reduce the effective blade section lift-curve slope by more than a few percent; therefore, the assumption to neglect unsteady aerodynamics is not expected to change the basic characteristics of solutions in this study.

It is not the point of the foregoing discussion to suggest that crude assumptions are adequate for all rotor analyses. For example, helicopters to be efficient, must operate at high enough blade loading so that the blades on the retreating side are well into the stall region. Downwash can affect both loads and stability, and unsteady aerodynamics can damp or aggravate flutter.

Aerodynamic calculations are made to provide response and forcing aerodynamic coefficients (derivatives) for the differential equations of motion of a free-flying (slowed or stoppable rotor) aircraft. The differential equations contain two types of response derivatives: those due to displacements of the degrees of freedom, and those due to time rates of change of displacement (i.e., displacement and velocity derivatives).

Motions of the system considered in the analyses are those which produce vertical displacements of elements of mass of the rotor, gyroscope, and body. They are all either tilt or plunge motions. Fore and aft, lateral, and yawing degrees of freedom, and in-plane motions of the rotor blades are not considered. Each motion of the blades produces a unique spanwise and chordwise distribution of aerodynamic lift. The distribution depends only on advance ratio and azimuth position. The magnitude depends on dynamic pressure due to forward flight. In these analyses the effects of Mach number and Reynolds number are considered to be negligible.

Lift distributions are integrated to produce blade forces. The blade forces used in these analyses are:

- blade root bending moment, bm
- blade root shear, V
- feathering moment, fm
- generalized force in the first blade flap mode, H

Forces due to blade motions corresponding to the motion of any one degree of freedom of the rotor, existing at any rotor azimuth position, are combined to give overall or generalized forces to all the degrees of freedom of the rotor. That is, any motion, displacement or velocity, or any fixed geometry setting produces a distribution of aerodynamic lift over the blades which are integrated to form generalized forces in all modes of vehicle motion.

Aeroelastic Derivatives of the Rotor

The concept of aeroelastic derivatives is borrowed from fixed wing aircraft technology. Aeroelastic derivatives include the influences of structural deflections which occur as a result of equilibria of aerodynamic and shaft forces. Therefore, calculated derivatives which include aeroelastic effects are more appropriately compared with data derived from wind tunnel measurements.

Caution must be exercised in applying aeroelastic derivatives to helicopter analyses. Uses parallel to those of airplanes are not always valid due to lower rotor "structural" frequencies. For example, in computing flight motions of a fixed-wing aircraft, often only rigid-body motions are admitted as specific degrees of freedom. As long as the periods of the structural vibrations are short compared with those of the vehicle flight modes and rates of applying controls are slow, the air forces produced by the elastic deflections may be put into equilibrium with rigid body inertia forces. The effects of elastic distortion of the airframe are not, therefore, ignored. The static distortion of the body is calculated and the aerodynamic forces so produced are included with those due to an angle displacement to give a static aeroelastic derivative, which may be used in studying the aircraft dynamics and in calculating trimmed flight conditions. In the motions of a rotary-wing aircraft, however, the natural flapping frequencies of the rotor can be of the same order as the vehicle modes. It, therefore, seems inapplicable to compute helicopter stability by the use of aeroelastic derivatives as done with fixed wing aircraft. It is, however, valid to compute trimmed conditions for helicopters using aeroelastic derivatives, since they are a consequence of a steady state.

As well as being useful for calculating rotor steady state conditions, such as trim, calculated rotor aeroelastic derivatives may be compared directly with derivatives measured in the wind tunnel. In wind tunnel testing elastic degrees of freedom are not under the direct control of the experimenter but take up deflections in response to an equilibrium of aerodynamic forces and structural forces due to the displacement of one of the parameters (or

27

degrees of freedom) under direct control. The rotor aeroelastic derivatives therefore parallel the aeroelastic derivatives calculated for airplanes.

In making a unit change in one of the directly controlled parameters, airloads are created due to both the rigid geometry change and the resulting deflection shape change of the blades. The sum of all airloads due to the change yields the aeroelastic derivatives.

The parameters (or degrees of freedom) under the direct control of the experimenter were cyclic and collective pitch and angle of attack. The changes in lift, hub moment, and swashplate moment due to unit changes in these parameters were found experimentally and compared with theoretically calculated values.

In order to calculate the cyclic angles required to trim hub moments or swashplate moments to zero, it was convenient to calculate the aeroelastic derivatives due to twist and precone.

In summary the aeroelastic derivatives calculated were:

$$\frac{\partial \left(M, \ L, \ T, \ M_\theta, \ M_\phi \right)}{\partial \left(\theta, \ \phi, \ \beta_o, \ \ddot{z}, \ \theta_o, \ \theta_t \right)}$$

The aeroelastic derivatives were calculated using the eight degree-of-freedom equations shown in Appendix A. The forcing derivatives are not set to zero, as in computing the system stability, but are retained for the computation of aeroelastic derivatives.

The rigid aerodynamic derivatives calculated in Reference 1 contain a mean part and harmonic components, the most significant of which are the 3P components. Only the mean aeroelastic derivatives are calculated in this investigation and they are compared to the mean experimental derivatives. The harmonic components are important from a blade loads and shaft vibration point of view and could form the subject of a separate study.

In calculating the aeroelastic derivatives for the fixed-shaft case it may be noted that in stationary axes and steady operation the accelerations

28

and velocities of all degrees of freedom are zero. Therefore, the inertia $[I]$ and velocity matrices $\left[2\,[I]\,[\dot{T}] + [\text{Damp}]\right]$ and $\left[B_r\right]$ need no longer be considered and the system in steady state equilibrium is represented as follows:

$$\begin{Bmatrix} \text{Balancing} \\ \text{Forces} \end{Bmatrix} + \overbrace{\Big[[I][\ddot{T}] + [D][\dot{T}] + [S]\Big]}^{[\text{Mech Stiffness}]} \beta - \overset{\left[\begin{smallmatrix}\text{Aero}\\\text{Stiffness}\end{smallmatrix}\right]}{[B]} \beta = \left[\begin{bmatrix}\text{Forcing}\\\text{Deriv.}\end{bmatrix} + \begin{bmatrix}\text{CF}_{6,1}\end{bmatrix}\right] \begin{Bmatrix} \beta_o \\ \theta_o \\ \theta_t \\ \dot{z} \end{Bmatrix}$$

In the fixed-shaft case the shaft deflections Θ, Φ, and z are zero and the swashplate tilt angles θ and ϕ are specified (i.e., they are no longer free). The only free motions are the three flapping deflections δ_o, δ_θ, δ_ϕ.

In calculating the aeroelastic derivatives one of the angles – swashplate cyclic or collective, angle of attack, precone or twist – is made equal to unity and the rest are made zero. Under the influence of this specified unit angle the rotor flapping deflections are found. A second step then allows hub moments, lift, and swashplate moments to be found due to all airloads. These form the aeroelastic derivatives.

Blade structural damping and swashplate stationary damping are assumed to be zero. Rotating (feathering) damping is retained. The basic equation may then be written:

$$\begin{Bmatrix} M \\ L \\ T \\ M_\theta \\ M_\phi \\ H_{\delta_o} \\ H_{\delta_\theta} \\ H_{\delta_\phi} \end{Bmatrix} + \left[\begin{array}{c}\text{MECH}\\\text{STIFFNESS}\end{array}\right] - \left[\begin{array}{c}\text{AERO}\\\text{STIFFNESS}\end{array}\right] \begin{Bmatrix} 0 \\ 0 \\ 0 \\ \theta \\ \phi \\ \delta_o \\ \delta_\theta \\ \delta_\phi \end{Bmatrix} = \left[\begin{array}{c}\text{FORCING}\\\text{AERO}\\ +\\ \text{CF}\end{array}\right] \begin{Bmatrix} \beta_o \\ \theta_o \\ \theta_t \\ \dot{z} \end{Bmatrix} \quad\text{------(1)}$$

In the balancing forces matrix, the left hand column matrix, the rotor generalized flapping terms are set equal to zero. In turn, one of the values of θ, ϕ, β_o, θ_o, θ_t and $\dot{z}$ ($\dot{z}/V$ is rotor angle of attack) is set equal to unity and the rest set to zero. The unknowns in the matrix equation then become the hub and swashplate aeroelastic derivatives M, L, T, M_θ and M_ϕ and the rotor generalized flapping displacements δ_o, δ_θ and δ_ϕ. Equation (1) may then be rewritten (and partitioned):

$$
\begin{Bmatrix} M \\ L \\ T \\ M_\theta \\ M_\phi \\ \hline 0 \\ 0 \\ 0 \end{Bmatrix}
+
\left[\begin{array}{c|c} \text{(MECH STIFFNESS)} \\ \text{MS1} \\ \hline \text{MS2} & \text{MS3} \end{array} \right]
-
\left[\begin{array}{c|c} \text{(AERO STIFFNESS)} \\ \text{AS1} \\ \hline \text{AS2} & \text{AS3} \end{array} \right]
\begin{Bmatrix} \theta \\ \phi \\ \delta_o \\ \delta_\theta \\ \delta_\phi \end{Bmatrix}
=
\left[\begin{array}{c} \text{(FORCING AERO)} \\ \text{AF1} \\ \hline \begin{array}{c} + \\ \text{CF} \end{array} \text{AF2} \end{array} \right]
\begin{Bmatrix} \beta_o \\ \theta_o \\ \theta_t \\ \dot{z} \end{Bmatrix} \; ---\; (2)
$$

Note that the (6,1) element of the forcing aero matrix contains the non-aerodynamic part of the centrifugal force collective flapping term.

At this point it may be noted that the hub and swashplate unknown forces are not found in the last three algebraic equations. This allows the rotor flapping deflections to be solved for independently.

In the calculation procedure, the values for δ_o, δ_θ and δ_ϕ must first be found. This is carried out as follows:

$$
\left[[\text{MS2}] - [\text{AS2}] \right] \begin{Bmatrix} \theta \\ \phi \end{Bmatrix} + \left[[\text{MS3}] - [\text{AS3}] \right] \begin{Bmatrix} \delta_o \\ \delta_\theta \\ \delta_\phi \end{Bmatrix} = \left[\begin{array}{c} +\text{CF}_{1,1} \\ \\ \text{AF2} \end{array} \right] \begin{Bmatrix} \beta_o \\ \theta_o \\ \theta_t \\ \dot{z} \end{Bmatrix}
$$

Therefore:

$$\begin{Bmatrix} \delta_o \\ \delta_\theta \\ \delta_\phi \end{Bmatrix} = \left[\begin{bmatrix} MS3 \end{bmatrix} - \begin{bmatrix} AS3 \end{bmatrix}\right]^{-1} \left[\begin{bmatrix} +CF_{11} \\ \quad AF2 \end{bmatrix} \begin{Bmatrix} \beta_o \\ \theta_o \\ \theta_t \\ \dot{z} \end{Bmatrix} - \left[\begin{bmatrix} MS2 \end{bmatrix} - \begin{bmatrix} AS2 \end{bmatrix}\right] \begin{Bmatrix} \theta \\ \phi \end{Bmatrix}\right] \text{---}(3)$$

Then the body and swashplate aeroelastic derivatives may be determined:

$$\begin{Bmatrix} M \\ L \\ T \\ M_\theta \\ M_\phi \end{Bmatrix} = \left[\begin{bmatrix} MS1 \end{bmatrix} - \begin{bmatrix} AS1 \end{bmatrix}\right] \begin{Bmatrix} \theta \\ \phi \\ \delta_o \\ \delta_\theta \\ \delta_\phi \end{Bmatrix} + \begin{bmatrix} AF1 \end{bmatrix} \begin{Bmatrix} \beta_o \\ \theta_o \\ \theta_t \\ \dot{z} \end{Bmatrix} \text{-----------}(4)$$

A unit value of one of β_o, θ_o, θ_t, $\dot{z}$, θ or ϕ is substituted in equations (3) with zero for the others. The set of rotor flapping deflections obtained is then substituted in equations (4) along with the unit value of the chosen angle. The column matrix of hub and swashplate forces becomes the aeroelastic derivatives for the angle.

The above derivatives are dimensional, i.e., hub and swashplate moments in ft lb and thrust (the same as lift for small angles) in lb.

It is convenient to display the moment and force derivatives in a non-dimensional form. The moments are divided by dynamic pressure due to forward speed, disk area and radius $q \pi R^3$ and the forces by dynamic pressure and disk area $q \pi R^2$. The convenience is due to the fact that the basic aerodynamic derivatives upon which the calculation of the aeroelastic derivatives are based are functions only of advance ratio when so non-dimensionalized (for a given rotor geometry).

31

When the effects of blade flapping are included, for a given mass and stiffness distribution in the blades, the aeroelastic derivatives become a function of flapping frequency (P) and air density (Lock No.) and advance ratio. The aeroelastic derivatives are displayed in nondimensional form versus advance ratio μ and flapping frequency (P) for the Lock No. corresponding to nominal sea level air density. The variation with Lock No. is not shown, since tests were performed only at the one air density.

Lock No. is an index as to the ratio of air forces to mass forces on a root-hinged, articulated rotor blade. It serves approximately the same function for hingeless rotors. It is, perhaps, more properly thought of as a density relationship; the ratio of air density to blade density (for a given lift curve slope). It is defined as follows (Reference 4):

$$\text{Lock No.} = \frac{c \; \rho \; a \; R^4}{I_1}$$

$$= \frac{1.17(.002378) \; .95(2\pi)(16.5)^4}{268}$$

$$= 4.57$$

where:

c = blade chord

ρ = air density

a = lift curve slope

R = rotor radius

I_1 = blade moment of inertia in linear flapping

Lock No. = 4.57 in all tests.

Figure 2 shows an example of the theoretical variation of nondimensional derivatives with advance ratio and flap frequency ratio at sea level air density. Lines of constant forward speed are also shown to facilitate the comparison of the experimental data gathered along lines of constant speed with theoretical. The figures show the variation of hub moment coefficients
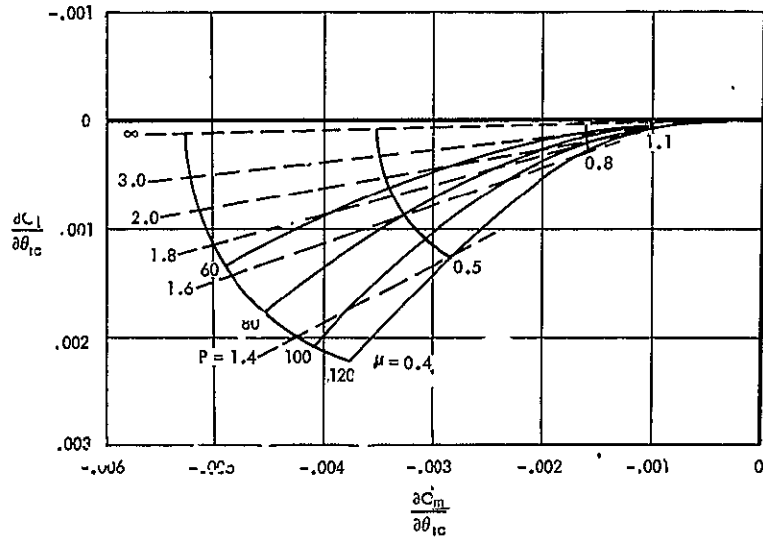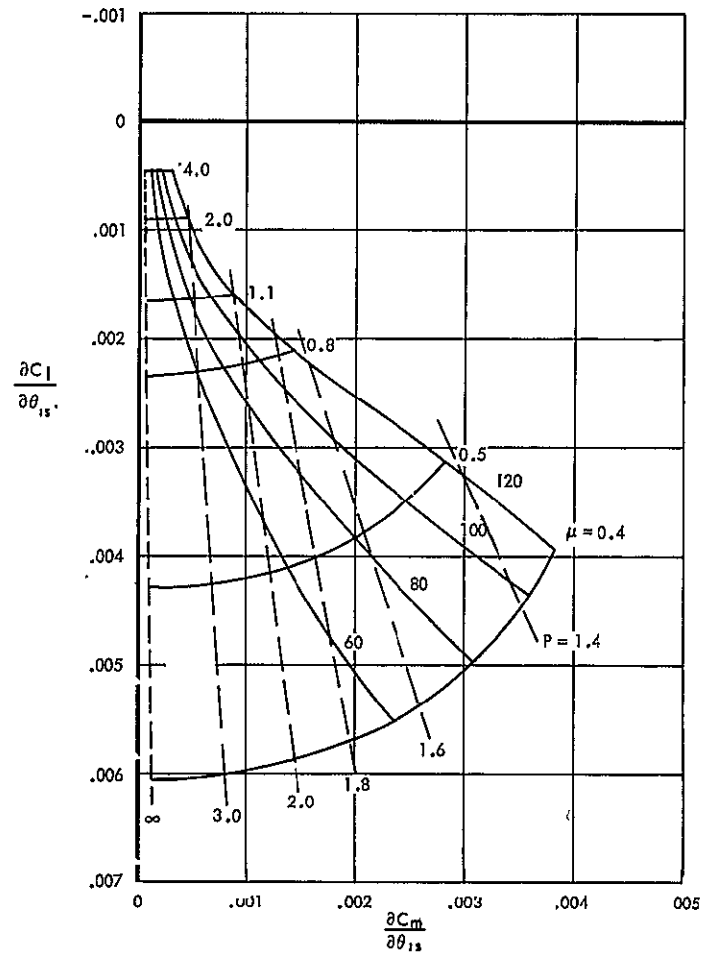
Figure 2. Analytically Derived Hub Moments Due to Cyclic Pitch Angles-Effect of Velocity

33

with the cyclic pitch components θ_{1_c} and θ_{1_s}. Hub moment is shown as a vector with its tail at the origin and head in the pitch-roll moment field. The right hand rule indicates its azimuth, viewed from above. The great reduction in the coefficients with increasing advance ratio is apparent and the change in azimuth due to increased flapping due to the rpm increase associated with increased forward speed is also apparent.

Moment Trim Using Cyclic Pitch

Two basic trim conditions are considered: hub mean moments trimmed to zero and swashplate (or gyro) mean moments trimmed to zero. These are referred to in this report as the hub trimmed or swashplate trimmed conditions.

Control of helicopters is accomplished through pitch and roll moments applied to the airframe by the rotor. These moments are produced primarily through blade cyclic pitch angles which have limited maximum amplitudes. The fraction of the available cyclic angles used in trimming rotor hub moments to zero is therefore very important since the angles remaining may seriously limit the moments which may be applied in some azimuth.

Cyclic angles can be applied to nullify the moments produced by blade geometry and flight operating condition. Rotor precone tends to apply a nose-up pitching moment to stiff bladed cantilever rotors and negative lateral cyclic pitch θ_{1_c} (so called for its effect on articulated rotors) is required to compensate it. Angle of attack, collective pitch and blade twist tend to apply rolling moments which can be cancelled by longitudinal cyclic pitch θ_{1_s}.

It is important to note that this study considers only the mean moments applied to the shaft and not the moments that occur periodically relative to rotor azimuth position. At low rpm these moments may be cancelled by judicious use of cyclic and collective pitch varying with azimuth. Trimmed conditions, being steady state, are well suited for computation by the use of aeroelastic derivatives. Hub moment trim is easily calculated using hub moment aero-

elastic derivatives. The cyclic angles required to trim hub moments to zero may be found by considering only the aeroelastic balance of hub moments.

$$
\begin{bmatrix} \dfrac{\partial M}{\partial \theta_{1_c}} & \dfrac{\partial M}{\partial \theta_{1_s}} \\[2ex] \dfrac{\partial L}{\partial \theta_{1_c}} & \dfrac{L}{\partial \theta_{1_s}} \end{bmatrix} \begin{Bmatrix} \theta_{1_c} \\[2ex] \theta_{1_s} \end{Bmatrix} + \begin{bmatrix} \dfrac{\partial M}{\partial \theta_{.75R}} & \dfrac{\partial M}{\partial \beta_0} & \dfrac{\partial M}{\partial \theta_t} & \dfrac{\partial M}{\partial \alpha} \\[2ex] \dfrac{\partial L}{\partial \theta_{.75R}} & \dfrac{\partial L}{\partial \beta_0} & \dfrac{\partial L}{\partial \theta_t} & \dfrac{\partial L}{\partial \alpha} \end{bmatrix} \begin{Bmatrix} \theta_{.75R} \\[1ex] \beta_0 \\[1ex] \theta_t \\[1ex] \alpha \end{Bmatrix} = \begin{Bmatrix} M \\[2ex] L \end{Bmatrix} = 0
$$

and the cyclic angles may be found directly:

$$
\begin{Bmatrix} \theta_{1_c} \\[2ex] \theta_{1_s} \end{Bmatrix} = - \begin{bmatrix} \dfrac{\partial M}{\partial \theta_{1_c}} & \dfrac{\partial M}{\partial \theta_{1_s}} \\[2ex] \dfrac{L}{\partial \theta_{1_c}} & \dfrac{L}{\partial \theta_{1_s}} \end{bmatrix}^{-1} \begin{bmatrix} \dfrac{\partial M}{\partial \theta_{.75R}} & \dfrac{\partial M}{\partial \beta_0} & \dfrac{\partial M}{\partial \theta_t} & \dfrac{\partial M}{\partial \alpha} \\[2ex] \dfrac{\partial L}{\partial \theta_{.75R}} & \dfrac{\partial L}{\partial \beta_0} & \dfrac{\partial L}{\partial \theta_t} & \dfrac{\partial L}{\partial \alpha} \end{bmatrix} \begin{Bmatrix} \theta_{.75R} \\[1ex] \beta_0 \\[1ex] \theta_t \\[1ex] \alpha \end{Bmatrix}
$$

The cyclic angles required to trim the swashplate moments to zero are found in identically the same way. The effects of rotating damping (feathering friction) C_R must be included in the calculation of the aeroelastic derivatives.

Swashplate moment trim is important for gyro controlled.feathering moment feedback rotors because the gyroscope responds to moments applied to the swashplate and trims them automatically to zero in the absence of pilot applied control moments. This also trims hub moments to zero up to an advance ratio of approximately $\mu = 0.8$, where the swashplate moments are more or less proportional to hub moments; but above this ($\mu > 0.8$), increasingly larger hub moments occur with zero swashplate moments due to the reverse velocity over the retreating blades and to feathering friction effects on the large cyclic angles. The cyclic angles to trim the swashplate, therefore, tend to increasingly disagree with those required to trim the rotor as the advance ratio increases. The hub moments due to swashplate trim, as calculated from equations (5) and (2) below, therefore, represent the free-gyro condition.

$$\begin{Bmatrix} \text{Rotor and} \\ \text{Swashplate} \\ \text{Moments} \end{Bmatrix} = \begin{bmatrix} \text{Aeroelastic} \\ \text{Derivatives} \end{bmatrix} \begin{Bmatrix} \text{Rotor} \\ \text{Parameters} \end{Bmatrix}$$

or:

$$\begin{Bmatrix} M \\ L \\ \hline M_\theta \\ M_\phi \end{Bmatrix} = \begin{bmatrix} \text{AMH1} & \vdots & \text{AMH2} \\ \hline \text{AMS1} & \vdots & \text{AMS2} \end{bmatrix} \begin{Bmatrix} \theta \\ \phi \\ \beta_o \\ \theta_o \\ \theta_t \\ \dot{z} \end{Bmatrix} \qquad \text{---------------(1)}$$

Partitioning:

$$\begin{Bmatrix} M \\ L \end{Bmatrix} = \begin{bmatrix} \text{AMH1} \end{bmatrix} \begin{Bmatrix} \theta \\ \phi \end{Bmatrix} + \begin{bmatrix} \text{AMH2} \end{bmatrix} \begin{Bmatrix} \beta_o \\ \theta_o \\ \theta_t \\ \dot{z} \end{Bmatrix} \qquad \text{-----------(2)}$$

$$\begin{Bmatrix} M_\theta \\ M_\phi \end{Bmatrix} = \begin{bmatrix} \text{AMS1} \end{bmatrix} \begin{Bmatrix} \theta \\ \phi \end{Bmatrix} + \begin{bmatrix} \text{AMS2} \end{bmatrix} \begin{Bmatrix} \beta_o \\ \theta_o \\ \theta_t \\ \dot{z} \end{Bmatrix} \qquad \text{----------- (3)}$$

Rearranging equations (2) and (3) after setting the left hand sides equal to zero:

$$
\begin{Bmatrix} \theta \\ \phi \end{Bmatrix}_{\text{Hub Trim}} = - \begin{bmatrix} \text{AMH1} \end{bmatrix}^{-1} \begin{bmatrix} \text{AMH2} \end{bmatrix} \begin{Bmatrix} \beta_0 \\ \theta_0 \\ \theta_t \\ \dot{z} \end{Bmatrix} \text{\textemdash\textemdash\textemdash\textemdash\textemdash\textemdash} (4)
$$

$$
\begin{Bmatrix} \theta \\ \phi \end{Bmatrix}_{\text{Swashplate Trim}} = - \begin{bmatrix} \text{AMS1} \end{bmatrix}^{-1} \begin{bmatrix} \text{AMS2} \end{bmatrix} \begin{Bmatrix} \beta_0 \\ \theta_0 \\ \theta_t \\ \dot{z} \end{Bmatrix} \text{\textemdash\textemdash\textemdash\textemdash\textemdash\textemdash} (5)
$$

The hub moment trimmed swashplate angles and corresponding swashplate moments are obtained by using equations (4) and (3) respectively. Similarly, the swashplate trimmed angles and hub moments are determined by employing equations (5) and (2). The swashplate angles may be transformed to blade cyclic angles by the sine cosine transformation:

$$
\begin{Bmatrix} \theta_{1_c} \\ \theta_{1_s} \end{Bmatrix} = \begin{bmatrix} -.4347 & .7530 \\ +.7530 & .4347 \end{bmatrix} \begin{Bmatrix} \theta \\ \phi \end{Bmatrix}
$$

(The effect of mechanical advantage k is also included. It gives the gyro an increased tilt per unit cyclic angle applied.)

Theoretical cyclic pitch angles required to trim hub moments to zero are shown in Figure 3 and to trim swashplate moments to zero in Figure 4. The conditions were as follows:

37
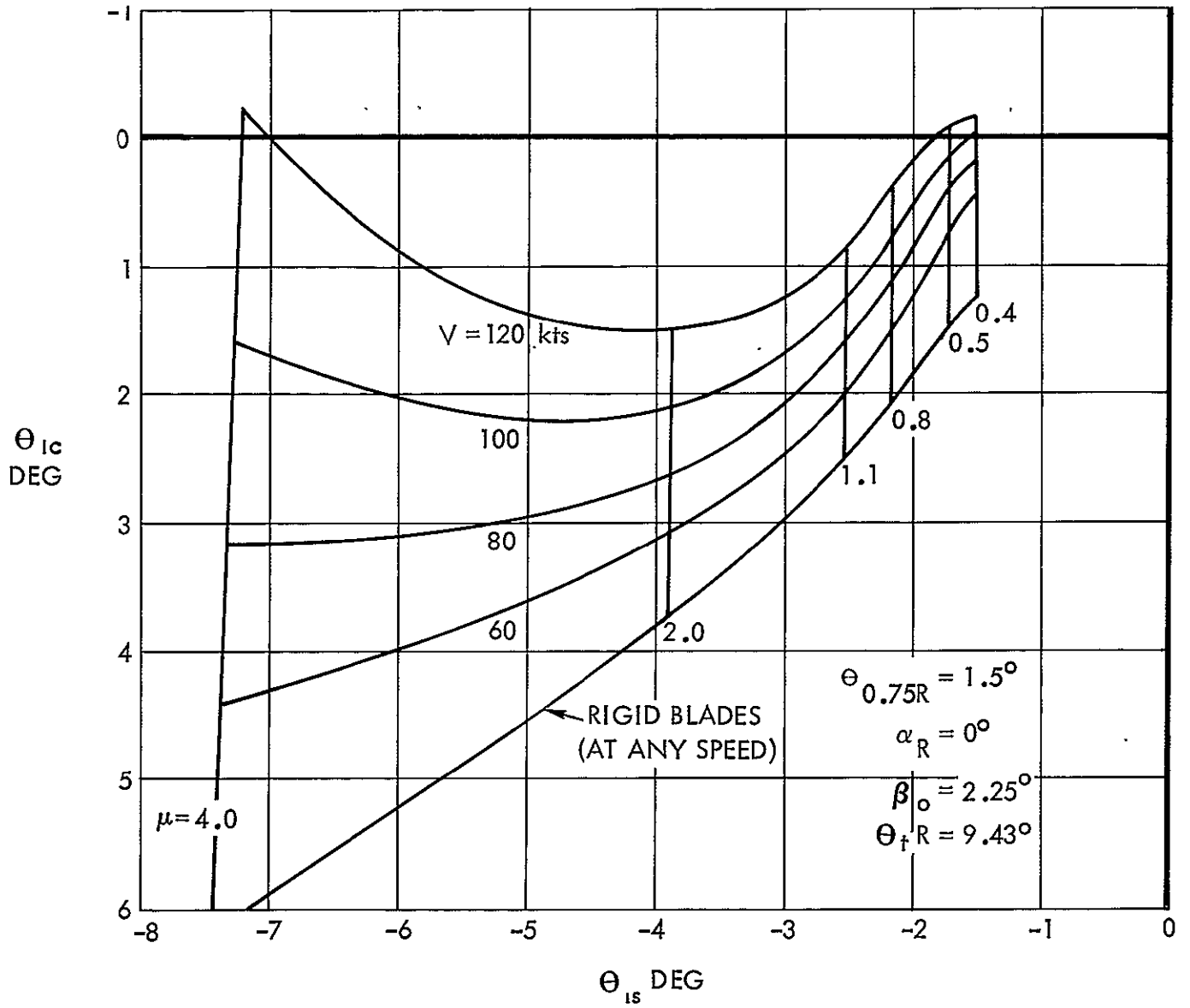
Figure 3. Analytically Derived Cyclic Pitch Angles For Hub Moment
Trim - Effect of Velocity
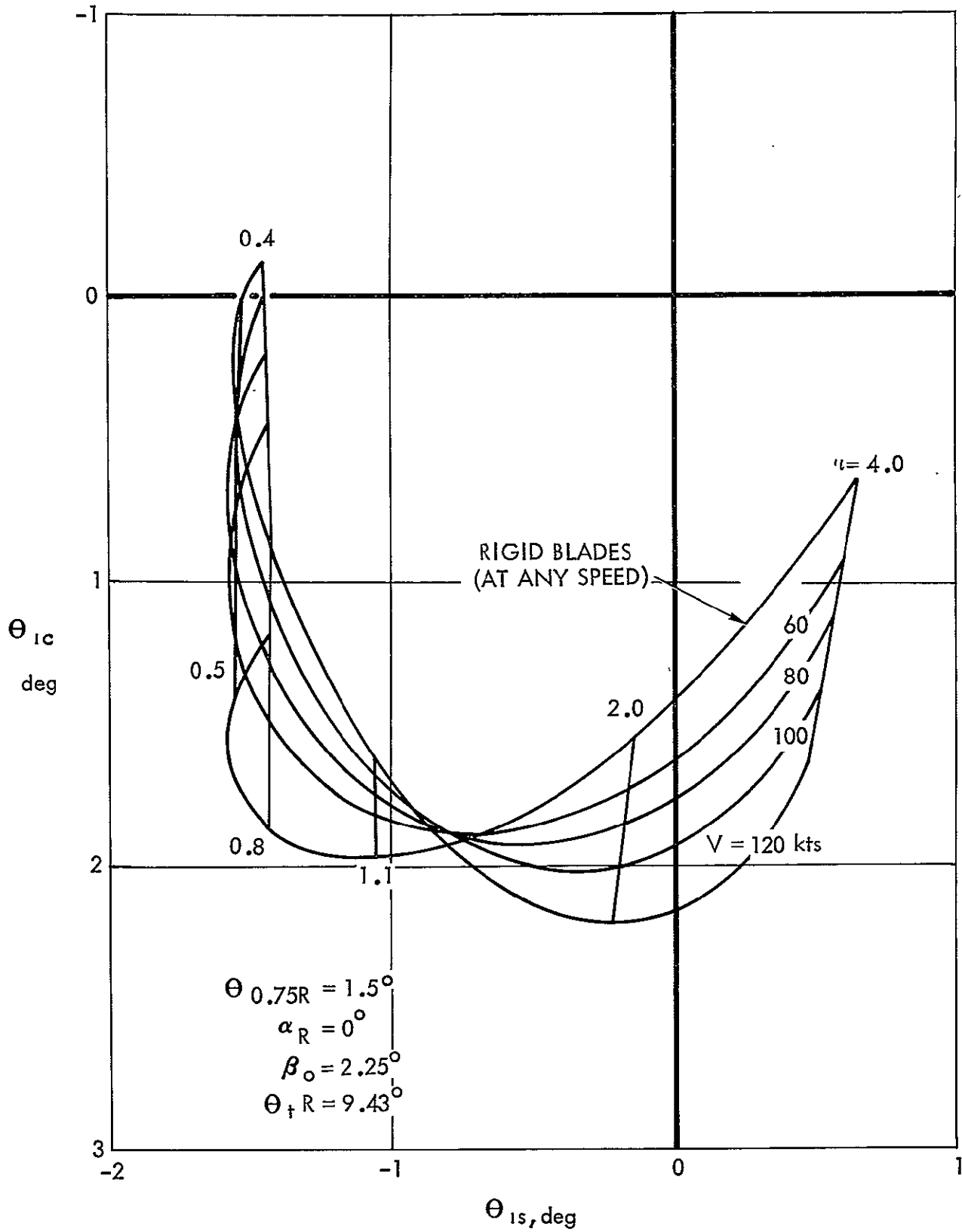
Figure 4. Analytically Derived Cyclic Pitch Angles for Swashplate Moment Trim - Effect of Velocity

$$\alpha \ = \ 0$$

$$\theta_{.75R} \ = \ 1.5°$$

$$\theta_t R \ = \ -9.43°$$

$$\beta_0 \ = \ 2.25°$$

The variation of the cyclic pitch vector is shown with respect to advance ratio and forward speed. The ranges of each were:

$$0.4 < \mu < 4.0$$

$$0 < V < 120 \text{ Kts.}$$

From the curves it may be seen that θ_{1_s} is a function only of advance ratio, but θ_{1_c} varies according to both advance ratio and forward speed, or more precisely, according to advance ratio and flap frequency ratio.

It is interesting to note that over the advance ratio range from $\mu = 0.4$ almost to $\mu = 0.8$ the cyclic pitch angles to trim both hub and swashplate moments to zero are almost the same. Rotating damping (feathering friction) was assumed to be zero.

Control Effectiveness

As used in this report, the term "control effectiveness" refers to the moments produced at the rotor hub by the application of unit control moments to the swashplate. The shaft is prevented from pitching or rolling both in the tests and in the analyses. In a free flying aircraft, control moments result in steady rates of roll and normal accelerations with somewhat different aerodynamic forces on the rotor, so the definition of "control effectiveness" is different in that case.

In the fixed-shaft case the free-gyroscope control system affords a simple method of applying hub moments to the rotor. The control system, in the absence of operator applied swashplate control moments, automatically trims hub moments to near zero. Then, as the operator applies control

40

moments through the free-floating swashplate, hub moments are produced as balancing feathering moments build up.

Feathering moments are proportional to root bending moments, and in the advancing flow region, the factor of proportionality is the blade sweep angle Λ. In the reverse flow region, the factor reverses sign and becomes variable with azimuth and advance ratio. Therefore, as long as effects of the reverse velocity region remain small relative to the effects of the advancing flow (at advance ratios less than, say, $\mu = 0.8$), the swashplate moments are approximately equal to hub moments factored by Λ (with unit mechanical advantage).

The mechanical advantage is the ratio of swashplate tilt to cyclic pitch and is denoted by "k". The ratio of swashplate moment to hub moment with zero cant angle therefore, becomes $\frac{\Lambda}{k}$ at modest advance ratio.

For purposes of flight stability, the feathering linkage is designed to rotate the swashplate moments in azimuth through the cant angle Ψ_0. This effect may be seen in the control effectiveness results.

Because the azimuth and amplitude of the reacting hub moment remain fairly constant the cyclic angles are forced to take on large azimuth and amplitude changes as the rpm and advance ratio change.

If a servo control moment is applied rapidly, the control mode (indicated by an advancing precessive motion of the gyroscope) will be excited. It is well damped down to a low rpm and then becomes unstable with further rpm reduction. The control effectiveness discussed here is a measure of the incremental hub moments remaining after the transient motions and forces have damped out for the stable system.

The control effectiveness ratios are easily evaluated using the aeroelastic derivatives. The steady-state moment equilibrium equation may be written as follows where the partitioned 4x6 matrix consists of aeroelastic derivatives:

$$\begin{Bmatrix} L \\ M \\ M_\theta \\ M_\phi \end{Bmatrix} = \left[\begin{array}{c:c} AMH1 & AMH2 \\ \hdashline AMS1 & AMS2 \end{array}\right] \begin{Bmatrix} \theta \\ \phi \\ \beta_o \\ \theta_o \\ \theta_t \\ \dot{z} \end{Bmatrix} \relbar\relbar\relbar\relbar\relbar\relbar\relbar\relbar \quad (1)$$

Rewriting:

$$\begin{Bmatrix} L \\ M \\ M_\theta \\ M_\phi \end{Bmatrix} = \left[\begin{array}{c} AMH1 \\ \hdashline AMS1 \end{array}\right] \begin{Bmatrix} \theta \\ \phi \end{Bmatrix} + \left[\begin{array}{c} AMH2 \\ \hdashline AMS2 \end{array}\right] \begin{Bmatrix} \beta_o \\ \theta_o \\ \theta_t \\ \dot{z} \end{Bmatrix} \relbar\relbar\relbar\relbar\relbar\relbar \quad (2)$$

If the rotor parameters in the right hand 4x4 matrix are held constant, then equation (2) may be rewritten:

$$\begin{Bmatrix} L \\ M \\ M_\theta \\ M_\phi \end{Bmatrix} = \left[\begin{array}{c} AMH1 \\ \hdashline AMS1 \end{array}\right] \begin{Bmatrix} \theta \\ \phi \end{Bmatrix} + \begin{Bmatrix} L_o \\ M_o \\ M_{\theta_o} \\ M_{\phi_o} \end{Bmatrix}$$

or:

$$\begin{Bmatrix} L - L_o \\ M - M_o \\ M_\theta - M_{\theta_o} \\ M_\phi - M_{\phi_o} \end{Bmatrix} = \begin{Bmatrix} \Delta L \\ \Delta M \\ \Delta M_\theta \\ \Delta M_\phi \end{Bmatrix} = \left[\begin{array}{c} AMH1 \\ \hdashline AMS1 \end{array}\right] \begin{Bmatrix} \theta \\ \phi \end{Bmatrix} \relbar\relbar\relbar\relbar\relbar\relbar\relbar \quad (3)$$

or:

$$\begin{Bmatrix} \Delta L \\ \Delta M \end{Bmatrix} = \begin{bmatrix} AMH1 \end{bmatrix} \begin{Bmatrix} \theta \\ \phi \end{Bmatrix} \text{------------------- (4)}$$

$$\begin{Bmatrix} \Delta M_\theta \\ \Delta M_\phi \end{Bmatrix} = \begin{bmatrix} AMS1 \end{bmatrix} \begin{Bmatrix} \theta \\ \phi \end{Bmatrix} \text{------------------- (5)}$$

Inverting $\begin{bmatrix} AMS1 \end{bmatrix}$

$$\begin{Bmatrix} \theta \\ \phi \end{Bmatrix} = \begin{bmatrix} AMS1 \end{bmatrix}^{-1} \begin{Bmatrix} \Delta M_\theta \\ \Delta M_\phi \end{Bmatrix} \text{------------(6)}$$

Combining (4) with (6) to eliminate the swashplate angles:

$$\begin{Bmatrix} \Delta L \\ \Delta M \end{Bmatrix} = \begin{bmatrix} AMH1 \end{bmatrix} \begin{bmatrix} AMS1 \end{bmatrix}^{-1} \begin{Bmatrix} \Delta M_\theta \\ \Delta M_\phi \end{Bmatrix} \text{-------- (7)}$$

And the control effectiveness ratios can be defined as:

$$\begin{Bmatrix} \Delta L \\ \Delta M \end{Bmatrix} = \begin{bmatrix} \text{CONTROL} \\ \text{EFF.} \\ \text{RATIOS} \end{bmatrix} \begin{Bmatrix} \Delta M_\theta \\ \Delta M_\phi \end{Bmatrix}$$

Therefore, the control effectiveness ratios are:

$$\begin{bmatrix} \text{CONTROL} \\ \text{EFF.} \\ \text{RATIOS} \end{bmatrix} = \begin{bmatrix} AMH1 \end{bmatrix} \begin{bmatrix} AMS1 \end{bmatrix}^{-1}$$

43

Fixed-Shaft, Rotor-Gyroscope Stability

The stability of a rotor-gyroscope system with the rotor shaft mounted
so that it could not pitch, roll, or plunge (as was tested in the wind tunnel),
is more simply predictable than a system mounted in a free-flying aircraft.
The differences are discussed in detail in a later section.

The equations of motion of the rotor-gyroscope-body, which are derived
in Appendix A for a free-flying aircraft, are easily reduced to the fixed-
shaft case since pitch, roll, and plunge displacements and velocities in the
fixed-shaft case are zero. All forces due to these motions are zero, which
permits the first three columns and the first three rows of all matrices to
be deleted. Therefore, the fixed-shaft equations of motion are obtained from
the free-flying equations of motion by extracting the lower right 5x5 terms
from the 8x8 matrices, thereby reducing the size of the mathematical repre-
sentation from eight degrees-of-freedom to five degrees-of-freedom.

The stability of the five degree-of-freedom linear system can be assessed
from the roots of the characteristic equation of the system (as long as the
periodic components of the differential equation coefficients are ignored).
The roots occur in pairs that indicate either damped or unstable oscillation,
or they occur singly indicating subsidence or divergence. Since the equations
are second order and five in number, the total number of roots is 10 (the
product of the order and the number of equations).

For the free gyro case, the roots generally consist of five oscillating
roots over a large range of rotor speeds. At some low value of rpm, as rotor
speed is reduced, one mode will split into two real roots, one subsident and
the other divergent or unstable.

Each of the modes of motion corresponding to the roots consists of comb-
inations of degrees of freedom in ratio to the one of maximum value. The
ratios of displacements are complex for oscillatory modes and real for
aperiodic modes. The modes are named so as to describe their most prominent
features. A typical example is shown (Figure 5, 6 and 7) in which the rpm is
reduced from 100 percent to zero at 100 knots. The swashplate is free of spring
restraint and the rotating (feathering) damping C_R = 7 ft lb/rad/sec and the
swashplate damping C_S = 80 ft lb/rad/sec.

44

Theory. - The five degree-of-freedom equations shown in Appendix C may be written in abbreviated form as follows:

$$[I]\, \ddot{\beta} + \left[[D] + \left[B_r\right]\right]\dot{\beta} + \left[[S] + [B]\right]\beta = 0$$

Where β is the vector of displacements of the degrees-of-freedom

$$\beta = \begin{Bmatrix} \theta \\ \phi \\ \delta_o \\ \delta_\theta \\ \delta_\phi \end{Bmatrix}$$

Assuming that the motions of the system are expressible in exponential form, their time derivatives become:

$$\beta = \beta_o\, e^{\lambda t}$$

$$\dot{\beta} = \lambda \beta_o\, e^{\lambda t}$$

$$\ddot{\beta} = \lambda^2 \beta_o\, e^{\lambda t}$$

and the differential equations become:

$$\left[\lambda^2 [I] + \lambda\left[[D] + \left[B_r\right]\right] + [S] + [B]\right]\beta_o = 0$$

For non-trivial solutions the determinant of the equations must equal zero:

$$\Delta \equiv \left| \lambda^2 [I] + \lambda\left[[D] + \left[B_r\right]\right] + [S] + [B] \right| = 0$$

45

The values of λ which cause this to occur are called the roots (sometimes eigenvalues) and indicate the frequency and damping in each of the modes of transient oscillation. The roots are complex in general:

$$\lambda = \lambda_r \pm i\lambda_i$$

The exponential decay or amplification and the frequency are determined as follows. First note that

$$\beta = \beta_o e^{(\lambda_r \pm i\lambda_i)t} = \beta_o e^{\lambda_r t} e^{\pm i\lambda_i t}$$

and

if λ_r is negative, the oscillations subside;

if λ_r is positive, the oscillations diverge and are unstable.

The frequency in radians/sec is given by $\lambda_i = \omega_{damped}$ and this is the damped natural frequency. The undamped natural frequency is given by:

$$\omega_{n_{undamped}} = \sqrt{\lambda_i^2 + \lambda_r^2}$$

The time required for the oscillation or subsidence to reduce to half the original amplitude may be found as follows:

the time to subside to $\frac{1}{e}$ amplitude $T_{1/e} = \dfrac{-1}{\lambda_r}$

and from this the time to subside to half the original amplitude

$$T_{1/2} = \log 2 \; T_{1/e}$$

$$= .693 \; T_{1/e}$$

$$T_{1/2} = - \frac{.693}{\lambda_r}$$

46

and the reciprocal of time to half amplitude is used as an index to stability in these analyses.

$$\frac{1}{T_{1/2}} = -1.442 \, \lambda_r$$

The critical damping ratio of a mode is given by:

$$\frac{c}{c_r} = \frac{-\lambda_r}{\sqrt{\lambda_i^2 + \lambda_r^2}}$$

The modes of motion corresponding to the roots of the equations (sometimes called eigenvectors) are determined by substituting the value of the nth root λ_n for λ and then evaluating the nondimensionalized vector of displacements for the nth root. The modal vector divided by one of its displacements could be as follows:

$$\text{Let} \quad \left\{ \beta_n \right\} = \left\{ \begin{array}{c} \theta/\theta \\ \phi/\theta \\ \delta_o/\theta \\ \delta_\theta/\theta \\ \delta_\phi/\theta \end{array} \right\} = \left\{ \begin{array}{c} 1 \\ \phi/\theta \\ \delta_o/\theta \\ \delta_\theta/\theta \\ \delta_\phi/\theta \end{array} \right\}$$

and the equation becomes

$$\left[\lambda_n^2 \, [I] + \lambda_n \left[[D] + \left[B_r \right] \right] + [S] + [B] \right] \left\{ \beta_n \right\} = 0$$

In the product of the square matrix and the mode vector, the first column will have no unknown quantities, in this example, as follows:

$$a_{11}\ 1\ +\ a_{12}\ \phi/\theta\ +\ a_{13}\ \delta_o/\theta\ +\ .\ .\ =\ 0$$

$$a_{21}\ 1\ +\ a_{22}\ \phi/\theta\ +\ a_{23}\ \delta_o/\theta\ +\ .\ .\ =\ 0$$

$$a_{31}\ 1\ +\ a_{32}\ \phi/\theta\ +\ a_{33}\ \delta_o/\theta\ +\ .\ .\ =\ 0$$

$$.\qquad\qquad.\qquad\qquad.\qquad\qquad.\ .\ .$$

$$.\qquad\qquad.\qquad\qquad.\qquad\qquad.\ .\ .$$

The equations may then be solved for the four unknown ratios by discarding any one of the five equations and the transferring the constant column to the right hand side

$$\begin{bmatrix} a_{12} & a_{13} & \cdot & \cdot \\ a_{22} & a_{23} & \cdot & \cdot \\ a_{32} & a_{33} & \cdot & \cdot \\ \cdot & \cdot & \cdot & \cdot \end{bmatrix} \begin{Bmatrix} \phi/\theta \\ \delta_o/\theta \\ \delta_\phi/\theta \\ \delta_\theta/\theta \end{Bmatrix} = \begin{Bmatrix} a_{11} \\ a_{21} \\ a_{31} \\ \cdot \end{Bmatrix}$$

Then

$$\begin{Bmatrix} \phi/\theta \\ \delta_o/\theta \\ \delta_\theta/\theta \\ \delta_\phi/\theta \end{Bmatrix} = \begin{bmatrix} a_{12} & a_{13} & \cdot & \cdot \\ a_{22} & a_{23} & \cdot & \cdot \\ a_{32} & a_{33} & \cdot & \cdot \\ \cdot & \cdot & \cdot & \cdot \end{bmatrix}^{-1} \begin{Bmatrix} a_{11} \\ a_{21} \\ a_{31} \\ \cdot \end{Bmatrix}$$

The modal vector then would consist of unit real gyro pitch angle and complex ratios of the other displacements to the unit pitch displacement, in the case of an oscillatory root. Modes with real roots have real modal vectors.

48

In the case of an oscillatory mode the projections in the real axis of the components of the vector represent the actual motion. All components maintain the same amplitude and phase, in the imaginary plane, relative to each other but rotate as time passes making one complete resolution in each period of oscillation, counterclockwise.

It should also be noted that the modes are orthogonal to each other; i.e., motions entirely in one mode do not create forces that disturb other modes.

Modal vectors may be nondimensionalized relative to any element of displacement. In this example, they have been arbitrarily scaled relative to the largest element.

Example: The variation of the roots and vectors of the characteristic equation over the rpm-range is shown in Figures 5, 6, and 7. The case chosen for examination was fixed-shaft at an airspeed of 100 knots EAS with a free (or unsprung) swashplate. The swashplate damping C_S was 80 ft lb/rad/sec and the rotating damping (or feathering friction) C_R was 7 ft lb/rad/sec.

Figure 5 shows four of the five oscillating roots of the system displayed relative to real-imaginary axes. The real part of the root is displayed along the abscissa (it is also the reciprocal of the time to 1/e amplitude). The imaginary part of the root is displayed along the ordinate and is the damped natural frequency in radians/sec.

This way of displaying the variations of roots with rpm is particularly useful since radial lines from the origin mark contours of constant critical damping ratio C/C_r and the stability of each root becomes immediately apparent.

The four roots displayed are the rotor nutating, rotor collective, rotor precessive and the gyro precessive. The gyro nutating mode is not shown because it is very high frequency and lightly damped and doesn't change with rotor rpm.
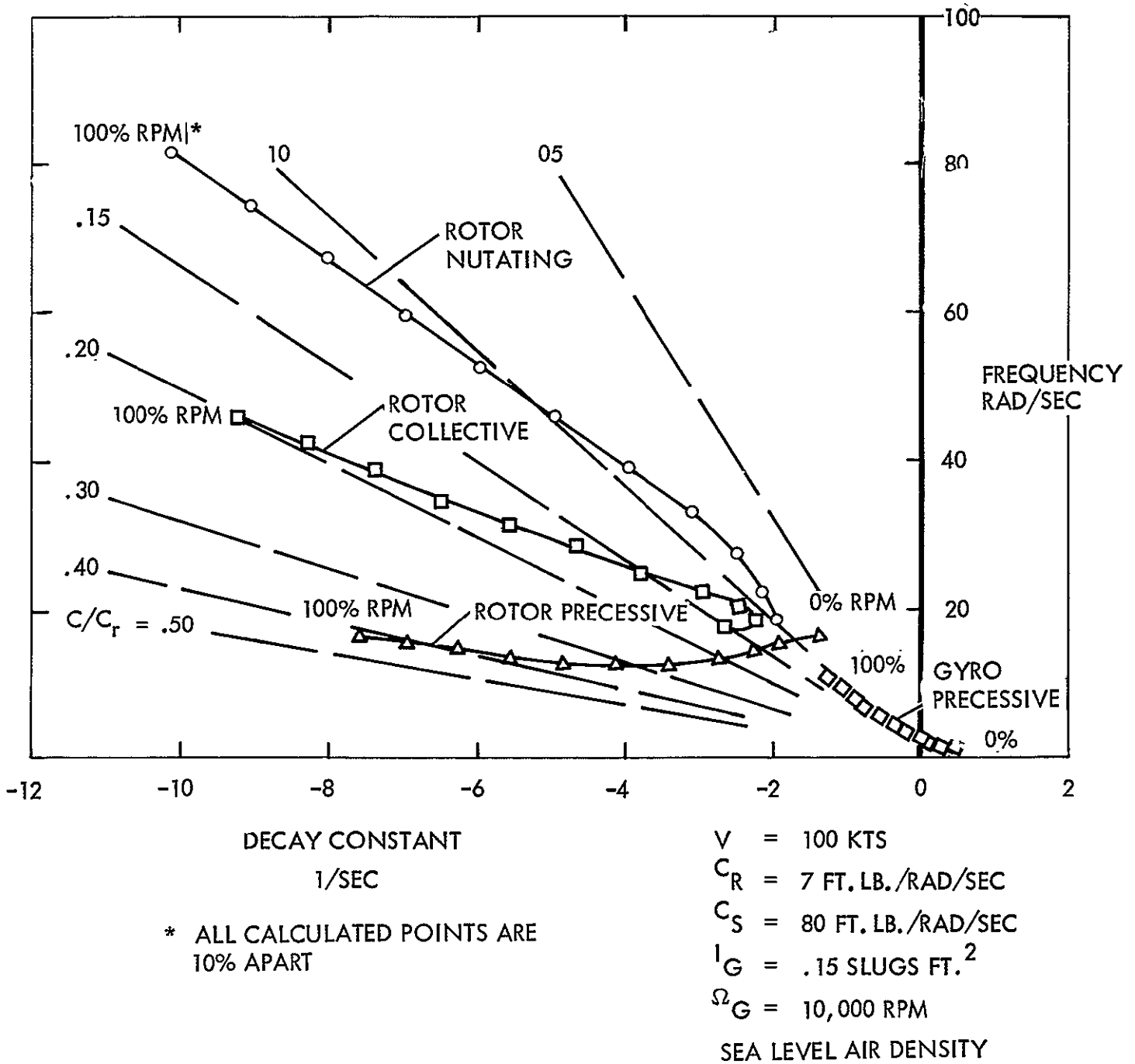
Figure 5. Typical Variation Of Roots With Rotor Speed For Fixed-Shaft, Free Swashplate Conditions
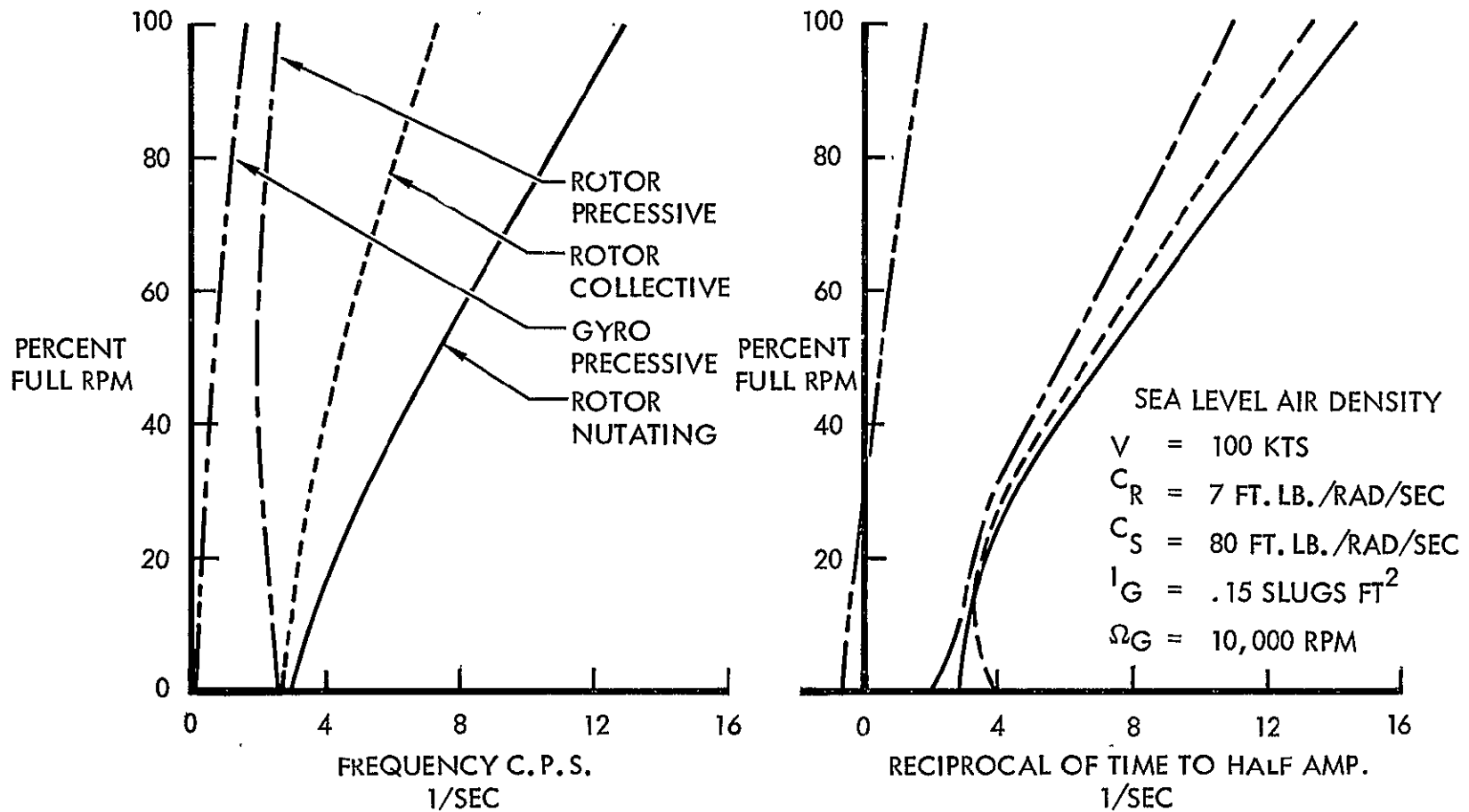
Figure 6.   Variation Of Mode Frequency And Damping With Rotor Speed For
The Fixed-Shaft, Free-Swashplate Case

51
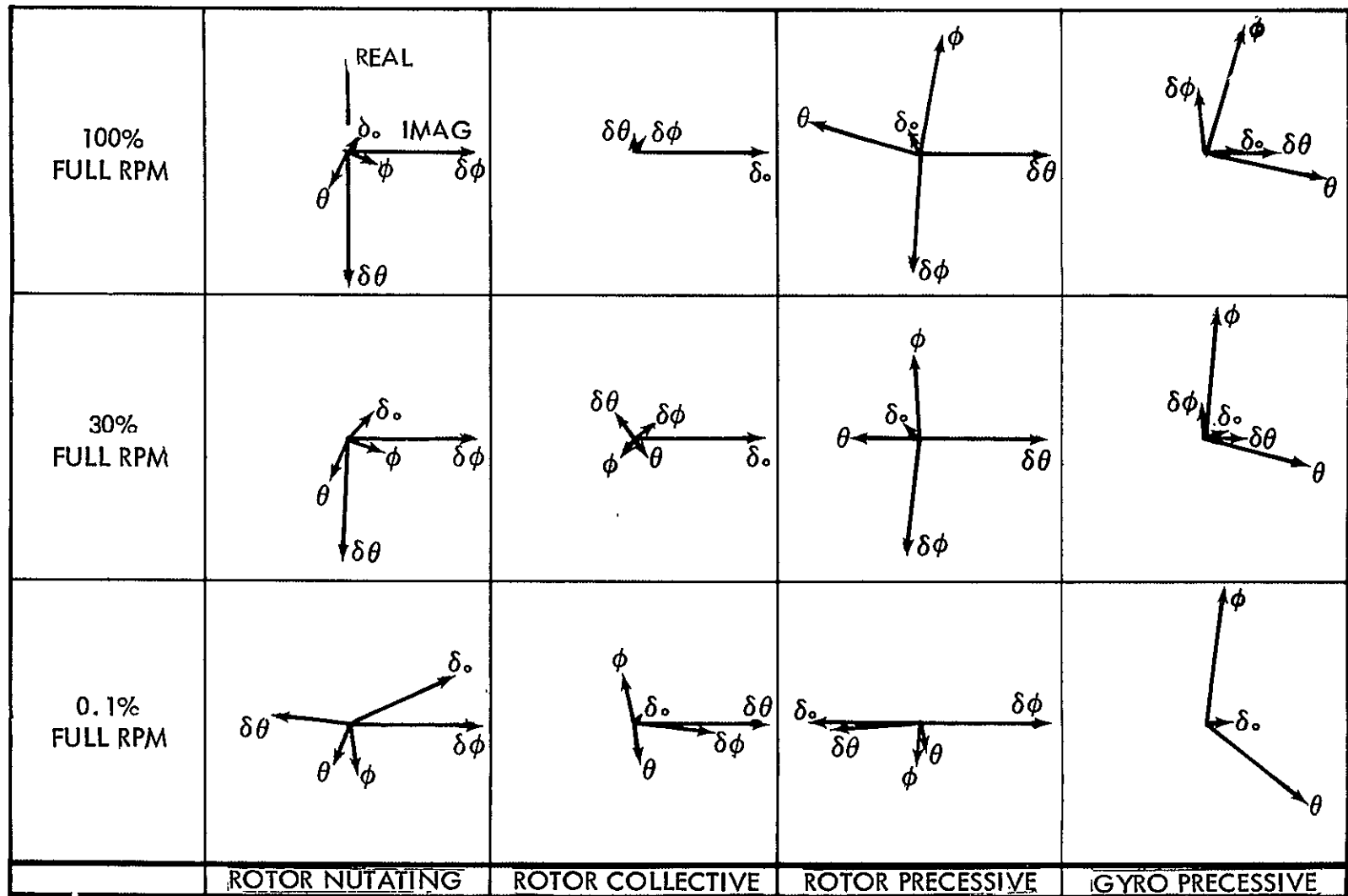
Figure 7. Mode Shape Vectors For The Fixed-Shaft Free Gyroscope Case

Another way of displaying the roots is shown in Figure 6. The damped natural frequency in cycles per second and the reciprocal of the time to half amplitude $1/T_{\frac{1}{2}}$ are displayed versus rotor rpm. This method allows the stability at any given rpm to be assessed at a glance.

Figure 7 shows the modes of oscillation. The vectors of degrees of freedom (mode shapes) are shown at full rpm, 30 percent, and 0.1 percent rpm (or essentially the stopped condition).

Analysis of transient motions of the rotor gyro mechanical system in terms of mode shapes, frequencies, and decay times, required that the equations be linear and without periodic coefficients. The linear mathematical model discussed here was abstracted from the more complex mechanical system, which contained nonlinearly coupled flap and in-plane modes, a spring-restrained gyro, plunge degree of freedom, lack of precise inertial and geometric symmetry, and a shaft that was mounted on a spring-supported mass.

Had the nonlinear complications been considered, then modes, frequencies, and damping could not have been found in closed form. The variations of the degrees of freedom with time could only have been found through step-by-step integration or electronic analog, and the stability inferred from this response.

Modelling only the principal aspects of the system allowed the basic motions, as discussed below, to be clearly seen.

The gyro precessive mode is characterized by a frequency lower than those of the rotor modes. Examination of Figure 7 shows that motion in the mode consists primarily of gyroscope, or swashplate precessive tilting. Since the physical motion of a mode is given by the projection of its modal vector components in the real, or horizontal, axis as it rotates counterclockwise at the mode frequency, it may be seen that the modal precession is advancing (or wobbling in the direction of rotation). Accompanying the gyro precessive wobble is a much smaller precessive wobble of the disk plane, which diminishes as the rpm reduces.

The rotor precessive mode frequency is somewhat higher than the gyro precessive frequency. but still much lower than the rotor rotation rate. From full rpm down to less than 30-percent rpm, the mode is a regressive precession (wobbling in the opposite direction to the rotor rotation), and the blade cyclic pitch is approximately the same magnitude as blade flapping but opposite in sign (but still regressive). At zero rpm, the mode degenerates to a negative pitch flapping relative to the airstream combined with a negative collective flapping.

Had the rotor blades been articulated and the aerodynamic forces been zero, the rotor precessive mode frequency would have been zero. Relative to rotating coordinates, the blades would have oscillated in flap at 1P. Any blade root spring effect added to the articulated blades would cause them to simulate hingeless rotor blades and would increase the flap frequency above 1P in rotating coordinates. This would result in a small frequency in stationary coordinates, and the cyclic flapping would have a regressive wobble.

At full rpm, the cyclic pitch angle participation in the mode is equal and opposite the flapping motion. When the rotor flaps down, the blades feather nose-up in that region of the disk so that the aerodynamics tend to reinforce the structural and centrifugal stiffness again increasing the frequency of the regressive flapping motion. At zero rpm the mode degenerates to a negative pitch flapping relative to the airstream combined with a negative collective flapping.

The rotor collective flapping mode is almost pure at full rpm. At zero rpm, it degenerates to almost pure roll flapping mode relative to the airstream. Its frequency is slightly higher than the rotor rotation rate due to the root spring effect.

The rotor nutating mode is characterized by a frequency slightly larger than twice the rotor rotating rate and an advancing precessive motion of the pitch and roll flapping degrees of freedom. The mode is similar to the nutating mode of a gyroscope, and derives its name from that fact.

As the rotor is stopped, the mode changes to a combined pitch flapping and coning (collective flapping) motion.

54

Wind Tunnel Simulation of Free-Flight

The most convenient way to test a rotor in the wind tunnel is with its shaft fixed against pitching, rolling and plunging. The results of such tests validly represent flight cases in which the shaft low frequency motions are insignificantly small. These cases include level flight of stable systems and should be valid for rotor performance, trimmed flight swashplate angles, and fluctuating loads provided that the vibrating shaft deflections are small.

On the other hand, the transient response of the system to sudden force applications would not possess representative frequencies, dampings, and influences of the degrees of freedom if the body in free flight would take on large motions following the force application. In fact it is conceivable that a control system that behaves well in the fixed-shaft condition could be unstable in free flight. One parameter must be carefully optimized for free flight stability but has absolutely no effect on fixed-shaft rotor gyroscope stability. It is the cant angle (ψ_o) between the gyro tilt axes and the feathering displacement axes.

The difficulty and expense involved in mounting a model in the tunnel sc as to be essentially free requires that a careful assessment be made of gains obtainable by freeing the various rigid-body degrees of freedom:
- pitch and roll
- plunge
- yaw and sideslip
- surge

The logic which led to the decision to test the fixed-shaft configuration was as follows. The significant aspects of slowing and stopping a rotor were assumed to be high advance ratio aerodynamics, effects of stiffened cantilever blades, and high-speed gyro control. These aspects played important parts in the:
- automatic trimming of hub moments
- effectiveness of the control system
- stability of the rotor-gyro system
- dynamic rotor loads and vibrations.

The procedure adopted was to develop methods of predicting the behavior of the fixed-shaft system - methods that adequately treated high advance ratio aerodynamics, very stiff blades, and a gyro-controlled feathering system. It was presumed that to extend the methods to include the effect of the rigid-body degrees of freedom would be straightforward. This logic does depend on how large an extrapolation is necessary to include the body degrees of freedom. There is some risk that basic rules learned on one system might not apply well, in extenso, to more complex situations. It is expected, however, that verification of the fixed-shaft tests greatly increases the likelihood that the free-flight analyses would be valid.

There is always the element of doubt which quasi-free-flight tunnel tests would clear up. The question to be assessed at this time is "Are gimballed-model wind tunnel tests worth the additional difficulty and expense?".

If gimballing a model in the tunnel is to represent an inflight stoppable rotor aircraft, the tests would be very difficult, because a full set of conventional airplane controls, elevators and ailerons (perhaps flaps) would have to be installed on the model and a full rotor harmonic cyclic-collective active swashplate control system would have to be developed. A pilot would have to remotely "fly" the vehicle in the wind tunnel.

In the case of the slowed rotor compound helicopter, with a rotor slowed to approximately 50 percent rpm, many of the expensive requirements vanish. The rotor controls can be used to control the aircraft. The existing passive high-speed gyro system might be adequate, at least for test purposes. In addition, the possibility that limited free-flight freedoms (pitch and roll) could yield a majority of the desired information leads to relatively simple mechanization of the freedoms.

The differences between fixed-shaft and free flight can be resolved by logic and the analyses discussed herein. Free flight involves:

- pitch and roll
- plunge
- yaw and sideslip
- surge.

The surging or axial degree of freedom involves the speeding up and slowing down of the aircraft. Leaving it out of analyses prevents the calculation of phugoid motion (of very long period) which involves the interchange of potential and kinetic energies of the airframe as a whole. The test section size of a wind tunnel is too small to permit the perturbation in position (from a mean) that would be necessary to include these motions. There is some logic to the point that the motions do not really reflect highly coupled rotor/airframe motions, because of the very long period, of the order of 10 seconds, of the motion compared to the periods of other rotor/airframe modes. Restraining the aircraft fore and aft motions is necessary for tunnel operations and is not expected to materially affect rotor/airframe interactions.

Yaw and sideslip are important to yaw control and stability and the effectiveness of the tail rotor. These modes are also of relatively long period, or are aperiodic. The dutch roll-like modes could be expected to be of the order of half the period of the phugoid-like modes, perhaps three to four seconds, and also reflect the effects of gravitational attraction. The motions are a bit too large to stay within the confines of the wind tunnel test section, but rotor sideslip derivatives are not fundamentally different from rotor symmetric derivatives; the azimuth change of air approach to the rotor in effect merely shifts the rotor reference axis. The motions are of long enough periods so as to not intimately react with the rotor-gyroscope-body motions.

Plunge is fundamental to the correct calculation of the short period pitch mode. Pitch-plunge coupling is the essence of this mode and is expected to couple with roll (due to the rotor in the system). So the pitch-roll-plunge motions should be important to the fundamental rotor-gyro-body modes. If the plunge mode is to be suppressed in the wind tunnel, knowledge of gimballed model representative rotor-gyro-body motions must first be obtained by analysis. Eliminating the plunge degree of freedom by supporting the model would simplify the suspension, and because the model is about twice as heavy as a free-flight vehicle (for the size of the rotor), would allow the wing to be properly loaded.

57

The study reported herein, therefore, is devoted to answering the two questions:

1. What are the differences between free-flight and fixed-shaft stability, and are the differences worth the expense of testing by gimballing the model?

2. Does suppressing the plunge degree of freedom (and effectively eliminating the overweight condition) and suffering the oversize pitch and roll inertias fundamentally change the behavior of the gimballed model from free-flight behavior?

These questions are answered under "Topics Related to Wind Tunnel Tests" by finding the roots and stability mode vectors of the characteristics equations of the rotor-gyroscope-body equations of Appendix A for both the free-flight aircraft and the gimballed model and comparing them with those of the fixed-shaft case.

WIND TUNNEL MODEL

Description

The wind tunnel test model, shown in Figure 8, has a 3-bladed
33-foot diameter hingeless rotor, and a mechanical-hydraulic control system
incorporating a high-speed gyro. The pertinent vehicle geometry is presented
in Table I. Power is provided by a Pontiac engine, driving through a
torque converter, transmission, slip differential and sprocket and chain to
the rotor shaft. Slowing and stopping the rotor are accomplished by a hy-
draulically actuated brake. The support structure, engine and drive train are
enclosed in an aerodynamic fairing simulating a compound helicopter fuselage.
Wings are also available for the model, but both analysis and tests were per-
formed in the wing-off configuration, to more correctly approximate the con-
ditions of the aerodynamic analyses.

The complete model was rigidly mounted in the wind tunnel on two forward
struts at the sponsons, and one telescoping tail strut. Ball and socket
joints at the attachment points permitted swivel freedom for angle of attack
changes, which were accomplished by remotely varying the tail strut length.
The three support struts reacted through the wind-tunnel model balance system
to provide basic aerodynamic force and moment data.

Although the model has been designed specifically for the investigation
of slowed/stopped rotor behavior, the rotor should be considered as repre-
sentative rather than optimum. The rotor is specially stiffened to resist
blade bending divergence when stopped. Figures 9 through 13 show the
blade mass and stiffness radial distribution. A previous tunnel entry with
the model demonstrated the structural integrity of the blades in the stopping,
starting, folding and unfolding operations and is discussed in Reference 5.

Control System

A feature of the vehicle is the provision of two essentially different
control system modes, the primary or free swashplate mode, and the locked
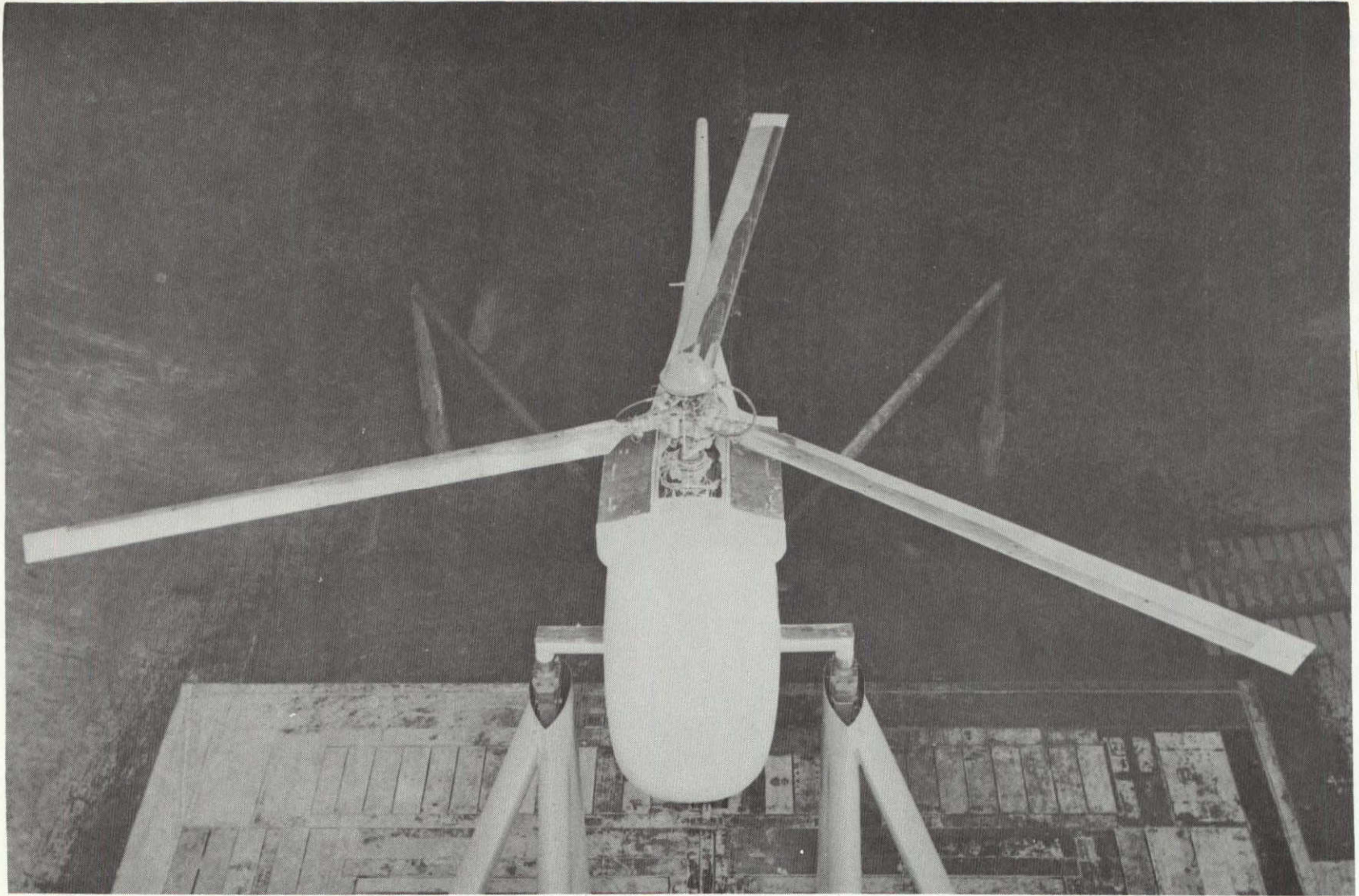
Figure 8. Specially Stiffened 33 Ft. Rotor With High Speed
Gyro In The Ames 40 x 80 Ft. Wind Tunnel

TABLE I

MODEL PHYSICAL PARAMETERS

Main Rotor

Number of blades	3
Radius	16.5 feet
Chord	1.17 feet (14 inches)
Airfoil	NASA 63_2015
Solidity	0.0675
Blade Area	57.7 ft^2
Disc Area	855.3 ft^2
Blade pre-cone angle	2.25°
Blade forward sweep	1.50°
Blade twist (down at tip)	9.43° (0.572°/ft)
Blade twist axis (passes through shaft C_L)	27% chord
Blade Feathering axis	32.5% chord at R.S. 30.85 inches
Rotor 100% rpm	355
Tip speed	613.4 ft/sec at 100% rpm
Mast angle (forward tilt)	0°
Rotor polar inertia	849 slug ft^2

Gyro

100% rpm	10,000
Gyro cant angle	60°
Gyro polar inertia (ring off)	0.30 slug ft^2
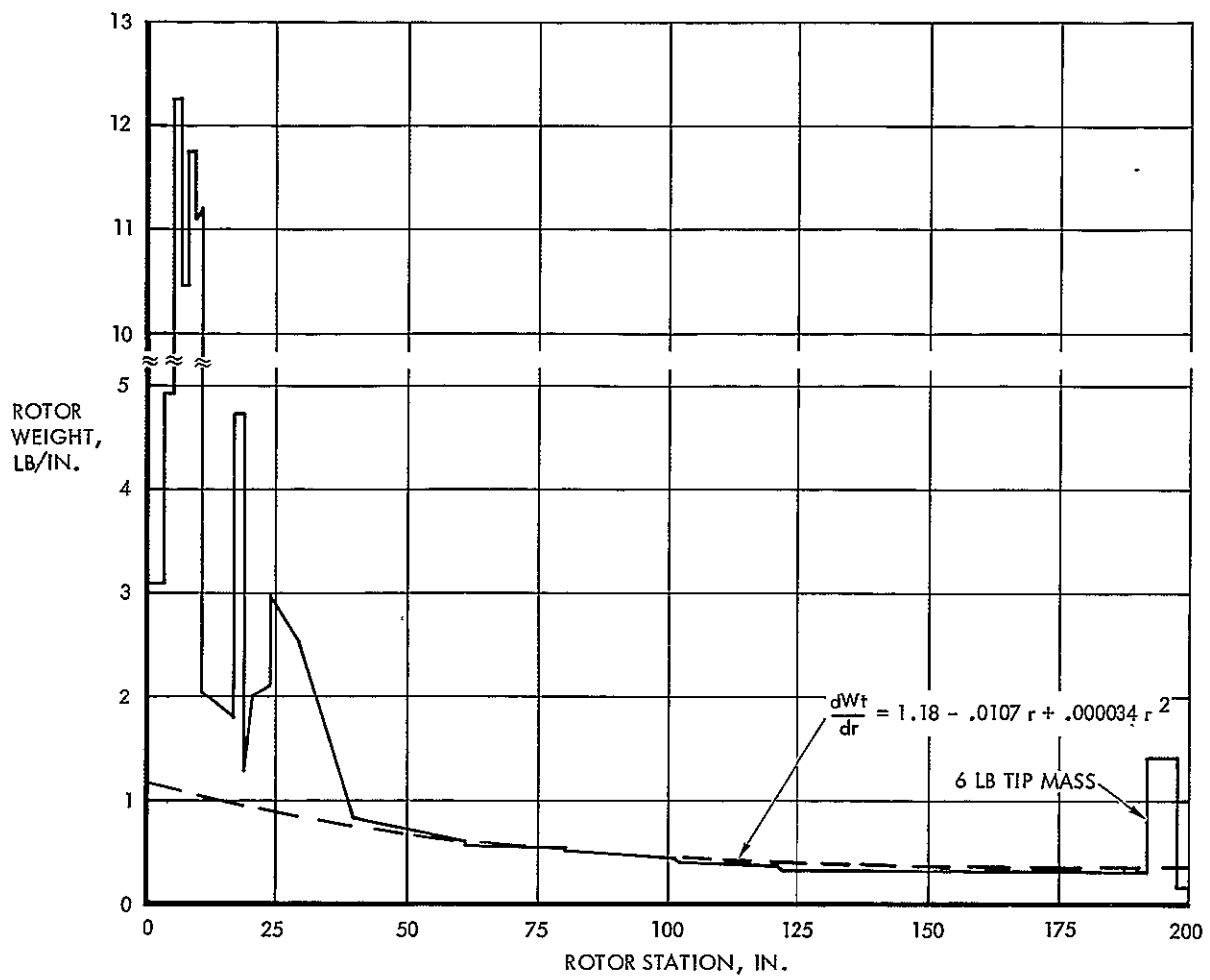
Figure 9. Rotor Blade Distributed Weight

$$\frac{dWt}{dr} = 1.18 - .0107\,r + .000034\,r^2$$

6 LB TIP MASS
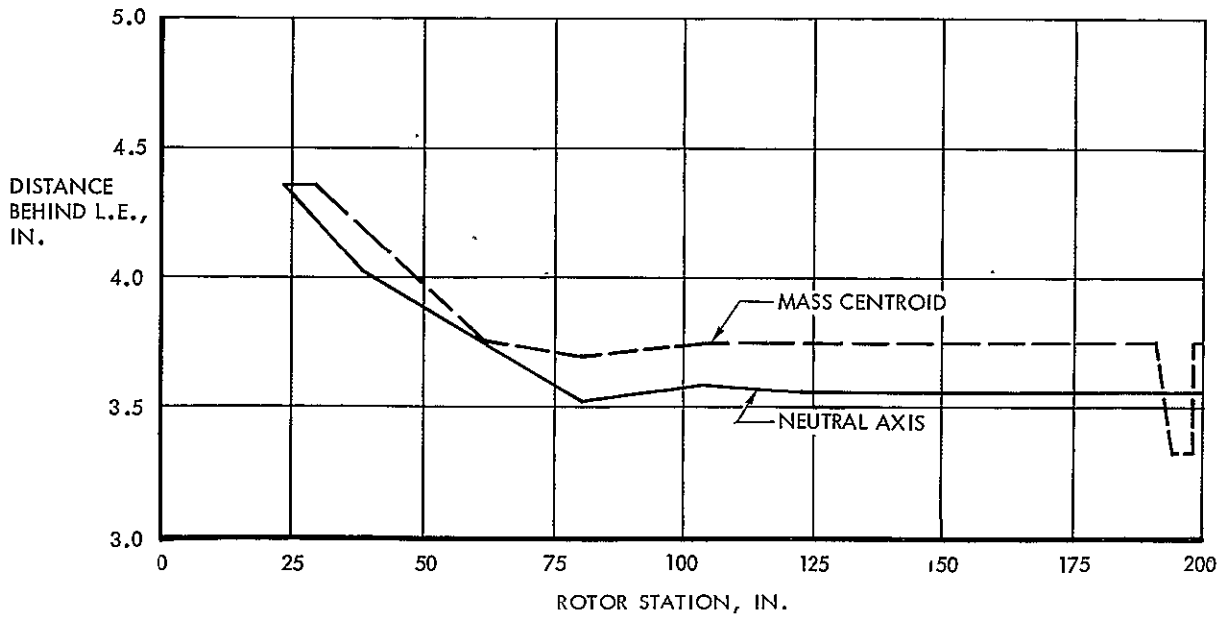
Figure 10. Rotor Blade Mass Centroid And Neutral Axis
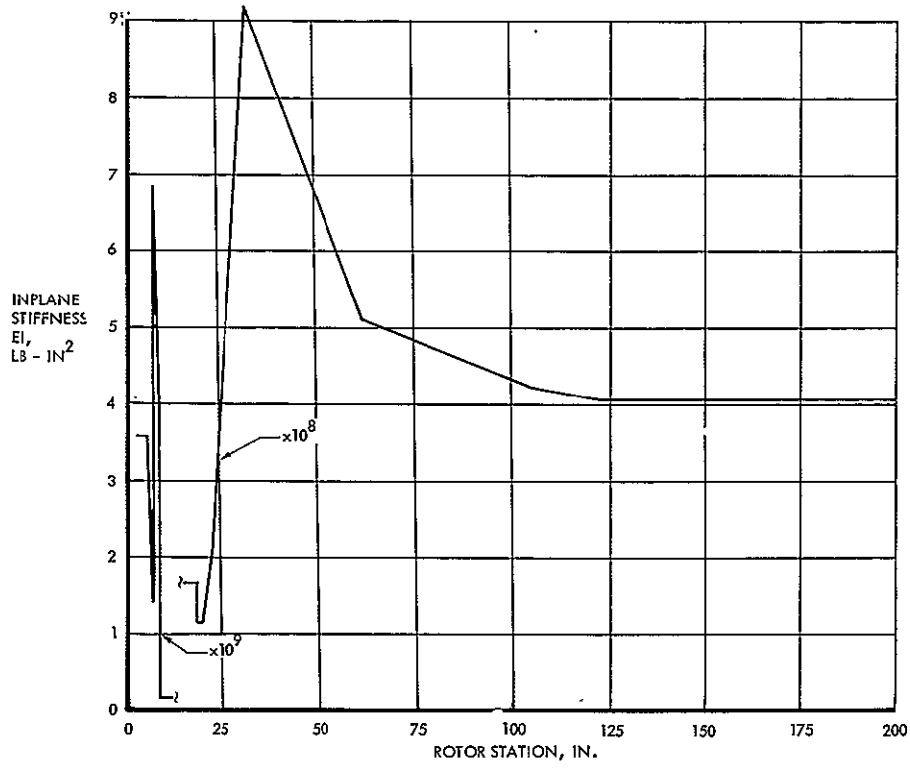
Figure 11. Rotor Blade Inplane Stiffness
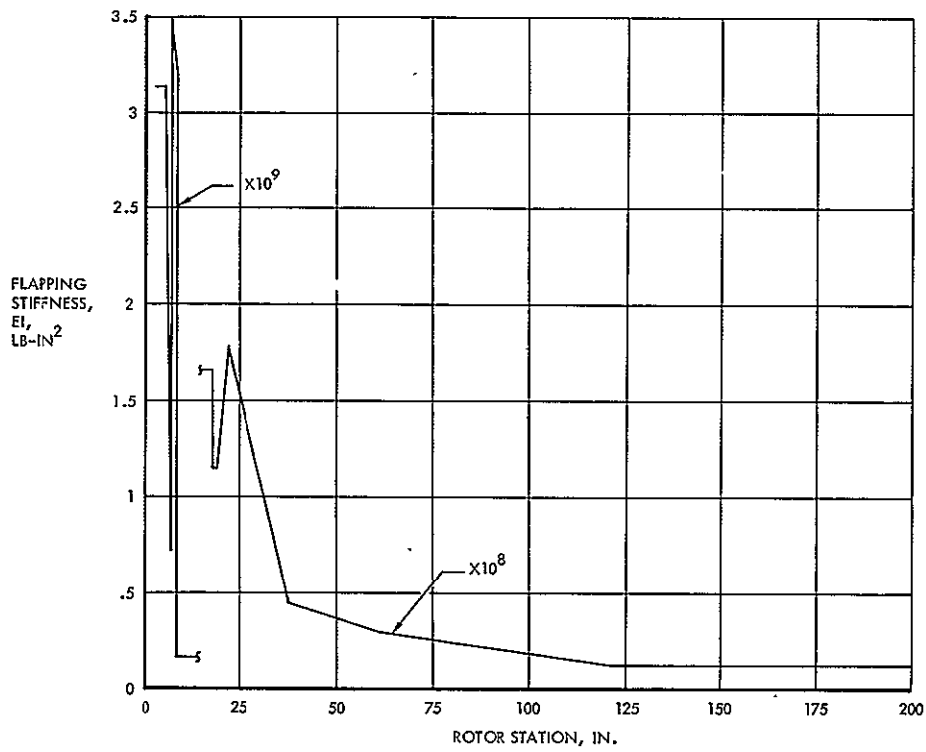
Figure 12. Rotor Blade Flapping Stiffness

63
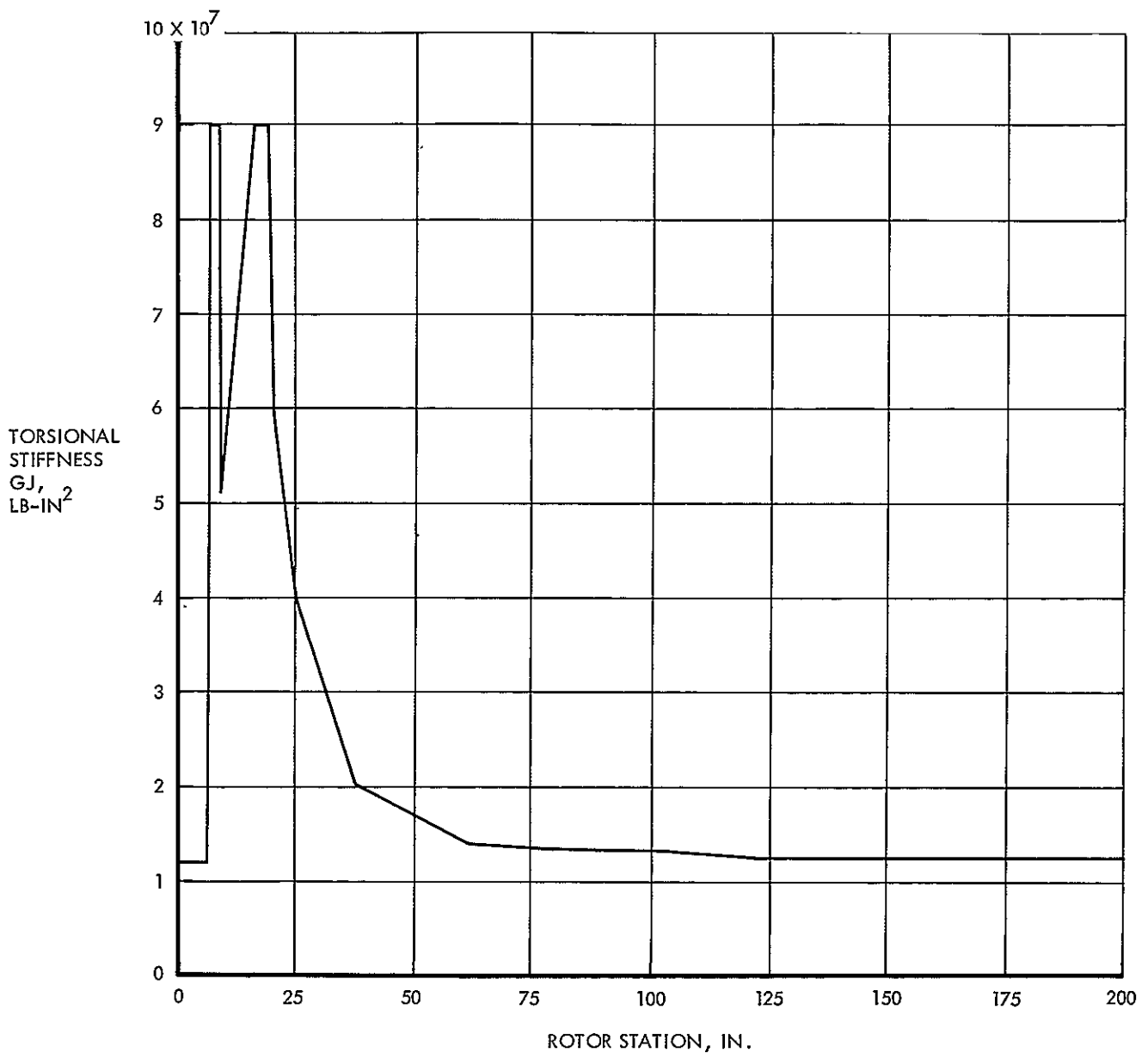
Figure 13. Rotor Blade Torsional Stiffness

swashplate mode, each having its own pair of cyclic control sticks. A schematic of the system is shown in Figure 14.

In the primary mode the characteristics of the high-speed gyro are utilized. Rotor control is achieved by use of pitch and roll servo-damper actuators, each of which applies a force to the swashplate independent of the position of the actuator piston in the cylinder. Motion of the control stick directs the net force upon it. The force is then transmitted to the gyro via the bellcrank, swashplate and control rods. For a stable system the gyro, in response to this input, will rapidly take up a position dictated by equilibrium of the moments applied to it by the controller and those fed back to it from the rotor.

At conversion speed, the rotor/gyro system is inherently stable at normal operating rpm, but stability deteriorates with decreasing rpm. At some low rpm the system becomes unstable. Since operation in this condition is unacceptable the primary control mode is supplemented by an augmentation spring at rpm less than 110, as indicated by an rpm sensing valve. The spring force provided by this unit acts to assist the gyro in preventing blade feathering divergence. Motion of the primary control stick will still result in a force output from the servo-damper actuator, but with the spring unit engaged the net output from the bell-crank will be significantly reduced, and the primary control will be relatively ineffective. The augmentation spring was not employed during these tests.

In the locked swashplate control mode, the locking function is performed by the spring augmentation unit. The gyro tilt angle is commanded by the position of the control stick, via the position servo-actuator within the unit, the gyro is thus constrained from precessing and is isolated from the control loop.

The spring augmentation unit serves an additional function in the Failure Prevention System. When flapwise blade loads reach a pre-set value (approximately 50% of failure load), the unit is automatically locked, preventing further control application in either mode until the system is disarmed.
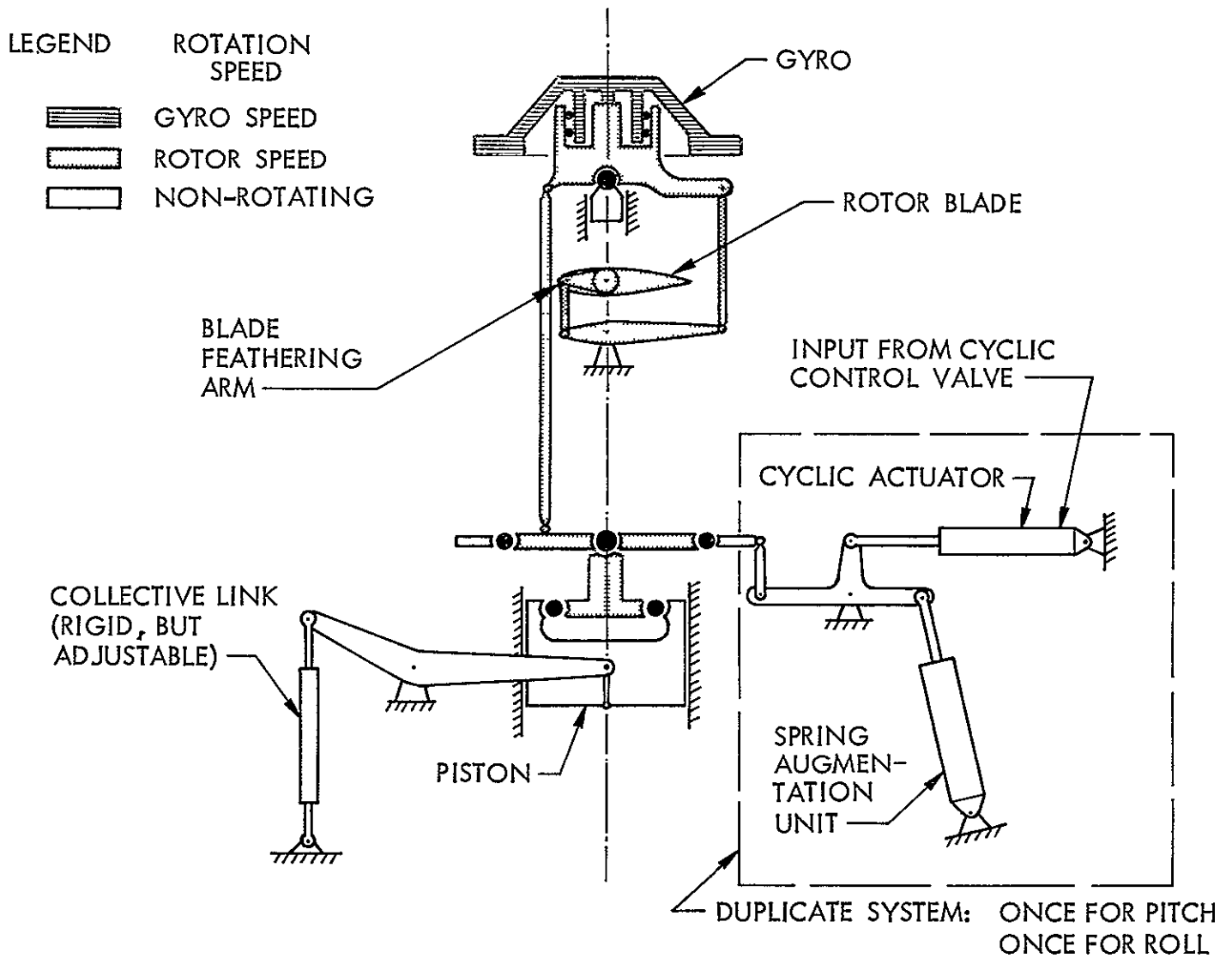
Figure 14. Control System Schematic

66

Because of the nature of the test program, remote control of collective pitch was not considered essential. To preclude an incident due to leakage in the collective servo-actuator, it was replaced by a solid, adjustable link.

Ground Tests

In preparation for tunnel entry, an extensive ground test program was conducted to functionally check out the vehicle operation and determine its strength and vibration characteristics. The fuselage shell was proof tested to a load distribution representative of the limit wind tunnel test condition for forebody loads, i.e., 180 KTS forward speed, and 4° shaft angle of attack. The limit aft body load was considered to occur at a 5° yaw angle, at 180 KTS and this condition was simulated by loading the vertical fin. The control system strength capability and stiffness characteristics were examined by replacing the actuators by solid links, then proof testing to represent both collective and cyclic loads. No evidence of structural failure or permanent deformation was present. The effect of measured cyclic and collective stiffness on the system aeroelastic stability was assessed analytically and found to be small.

Shake tests on the rotor were performed to identify the important blade flapwise and in-plane non-rotating natural frequencies and mode shapes. The model structural framework was anchored to the ground, and the control actuators were replaced by solid links. Figure 15 shows the test results, and the calculated effect of rpm on the mode frequencies.

The rotor whirl test program served as a checkout of vehicle systems operation, rotor stability and loads over a range of rpm, lift and body moments that encompassed the planned wind-tunnel test envelope. Based on this program, improvements were made to control system hardware, and the procedures for real-time monitoring of rotor and control system loads and stability were evolved.
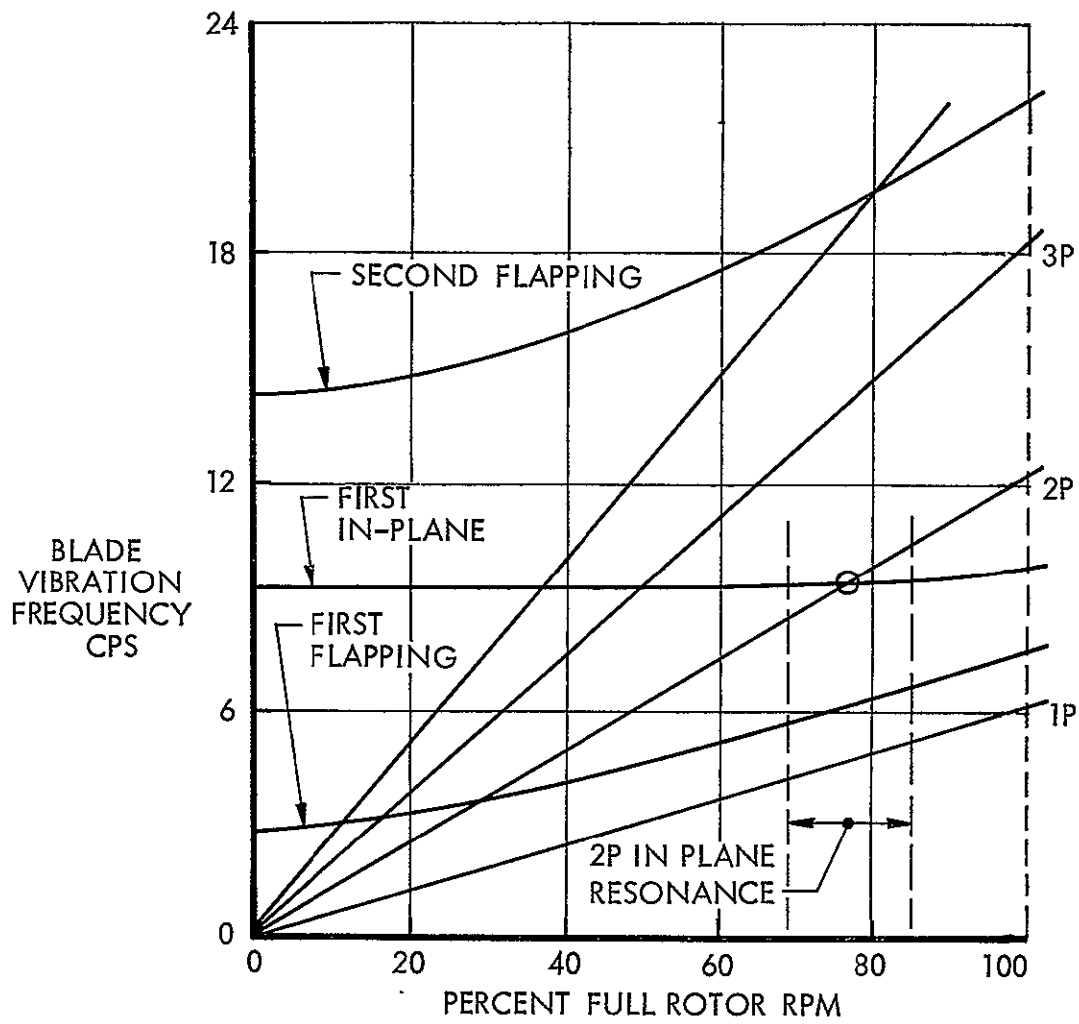
Figure 15. Blade Natural Frequencies

68

A safety engineering analysis of the system, operating within the prescribed test envelope, was made in sufficient depth to assure maximum safety consistent with operational requirements. The study encompassed the model and its components, interfacing subsystems, equipment, instrumentation and test crews. A Gross Hazard Analysis considered the probable nature and impact of failures within the model's power and drive system, rotor control system, hydraulic distribution system, electrical distribution system, control instruments and tunnel drive system. A Failure Mode and Effects Analysis examined in greater detail the hydraulic and electrical components of the rotor control system.

Instrumentation

Instrumentation was installed to provide a record of the rotor and control system behavior during the test program, to facilitate control of the vehicle and to permit real-time monitoring of critical system loads.

A summary of the parameters measured is given in Table II.

Loads data were obtained from foil type strain gages wired into bridge circuits, and position data from angular or linear potentiometers. Blade loads and rotating control system measurements were transmitted through shaft mounted slip rings. Lift, pitch moment and roll moment were measured by load cells mounted on longitudinal and lateral axes through the rotor center-line, 36 inches below the hub. As a consequence of this vertical location, the pitch and roll moment outputs reflected the presence of in-plane forces at the hub in addition to hub moments. The shaft bending bridges were located close to the hub (11 inches) and this data, when transformed to stationary axes, was preferred to the load cell output as an indication of hub moment.

Transducer sensitivities were measured by direct calibration over the expected operating range, and the electrical equivalent load obtained by inserting a shunt resistance on one leg of each bridge.

The parameters measured during the test program were recorded on three data acquisition systems, each tailored to a particular task. The basic recording instrument, a CEC oscillograph with 28 active channels was in

TABLE II

INSTRUMENTATION MEASUREMENTS

Item	Measurement	No. 1 Osc.	No. 2 Osc.	Tape Recorder
1	Lift	X		*
2	Pitch Moment	X	X	X
3	Roll Moment	X	X	X
4	Shaft Bending at $0°$	X		X
5	Shaft Bending at $90°$	X		X
6	Collective Position	X		
7	Swashplate Pitch Angle	X	X	X
8	Swashplate Roll Angle	X	X	X
9	Swashplate Pitch Moment	X	X	X
10	Swashplate Roll Moment	X	X	X
11	No. 1 Blade Angle	X		X
12	No. 2 Blade Angle	X		
13	No. 3 Blade Angle	X		
14	No. 2 Pitch Link Load	X		*
15	Swashplate to Gyro Rod Load	X		
16	Shaft Torque	X		
17	Shaft Lateral Vibration	X		
18	No. 2 Flap Bending at Station 10.7	X		
19	No. 2 Flap Bending at Station 21.3			*
20	No. 2 Flap Bending at Station 43.0	X		
21	No. 2 Flap Bending at Station 69.0	X		
22	No. 2 Flap Bending at Station 118.0	X		
23	No. 1 Flap Bending at Station 43.0	X		
24	No. 3 Flap Bending at Station 43.0	X		
25	No. 2 Chord Bending at Station 10.7	X		
26	No. 2 Chord Bending at Station 69.0	X		
27	Index Pip	X	X	X
28	Strain Gage Voltage	X		
29	Time Code	X	X	X

* No data due to faulty amplifiers

continuous operation throughout the tests, at high speed for data points and envelope expansion, and at low speed elsewhere. Supplementing this for the derivative and control effectiveness tests was a 14 channel FM tape recorder, the first item in an automated data analysis system. Rotor/gyro response to step control inputs was recorded on an additional oscillograph, with fewer channels for easier reading, and greater sensitivity for more accurate data. Time correlation of the three sets of data was achieved by recording time code on each.

WIND TUNNEL TESTS

PROCEDURES

When the detailed test plans were written, it was anticipated that rotor instability or high structural loads might make operation in some areas unsafe, and that severe rotor resonance at a planned test point might introduce a factor into the test data which had not been considered in the analysis, making a direct comparison invalid. In recognition of these factors, the criteria used in planning the test procedures were, first, assure the safety of the vehicle, then sequence the tests such that maximum useful data is obtained.

To obtain maximum useful data, the tests and theoretical work were conducted so as to isolate error. The experimental aeroelastic derivatives depended only on the slopes of the instrumentation calibration and were not subject to calibration zero error. Each of the derivatives depended on the variations of a restricted set of parameters, thus allowing errors to be isolated. Verification of rotor derivatives by test eliminated them as a source of error in the stability analyses.

In order to establish a safe operating envelope, a series of Safety Tests were performed at each forward speed prior to gathering technical data. In the fixed swashplate control mode the rotor was demonstrated to be free from low frequency instabilities by pulsing the cyclic control and observing the response, over the test rpm range. Resonant modes in the rotor-body-support strut system were located by making slow rpm sweeps, first at zero tunnel speed then with increasing forward speed.

Having established the "avoid" regions at each tunnel speed by the Safety Tests, the Technical Tests were performed in the following order:

(1) Fixed swashplate derivative tests
(2) Free swashplate stability tests
(3) Free swashplate controls effectiveness tests

Transition from fixed to free swashplate control mode was always accomplished at 40 knots in these tests to minimize possible transient loads. When changing, tunnel speed the rotor speed was set to 200 rpm where loads were generally small.

Fixed swashplate derivative tests. - The planned procedure called for the operator to trim out hub moments, then apply an increment in swashplate pitch angle holding roll angle constant, and vice versa, to give the variation of hub moment and lift due to each cyclic angle. However due to leakage in the servo-actuators, and air in the hydraulic lines, the actuators were not completely effective in locking the swashplate. When applying an incremental swashplate pitch angle from trim, for example, corrective action was necessary to maintain the roll angle at its trim value. Thus the elimination of cross-coupling in control application was dependent on the accuracy and resolution of the swashplate angle panel instruments.

Because of the vertical offset of the moment load cells from the hub, the panel moment indicators were not used to trim the rotor. An oscilloscope display of shaft bending moment was provided, so that the operator, by zeroing the 1P component, could achieve a satisfactory trim, except where harmonics higher than 1P obscured the trace.

In order to obtain accurate derivatives, a minimum of four swashplate angle increments from trim (two positive, two negative) were applied in each of pitch and roll, the maximum input being dictated in most cases by the blade flap-wise or chordwise strength relative to allowable endurance stresses. An X-Y oscilloscope presenting blade chord and flap bending moments, was used to monitor both blade loads and blade dynamic behavior. Rotor strength limits were rarely approached, and when high loads were experienced Failsafe System actuation prevented further control application. In such cases, the cause of the high loads was determined, the system was then disarmed, and corrective action taken.

To obtain the lift and moment derivatives with respect to angle of attack, the test procedure followed was to trim the rotor at $\alpha_R = 0°$, then increase α_R in 0.5 degree or 1.0 degree increments. As with the cyclic derivative tests, it was not possible to maintain the cyclic angles at the values for trim at $\alpha_R = 0°$, so the data reflected the changes in these parameters in addition to

the variation in angle of attack. Blade endurance loads dictated the maximum angle of attack achieved in the tests.

The majority of the test points in the program were performed at a collective angle setting of $\theta_{0.75R} = 1.5^\circ$. Time limitations prevented a thorough investigation of the effects of collective angle changes. The adjustable link in the collective control system was set to give a collective angle of $\theta_{0.75R} = 3$ degrees, and data was recorded at nominal trim for a number of test conditions.

Free swashplate stability tests. - With the gyro operating at its design speed of 10,000 rpm, the rotor/gyro stability in the primary control mode was obtained by applying step moment inputs about the swashplate roll axis, starting at 320 rpm and at gradually reduced rotor speeds. The stability and frequency of the swashplate angular response were determined from the oscillograph records after each test. The decay rate was plotted versus rotor rpm, and the trend examined before testing at a lower rpm. In this manner the rpm at which the system became neutrally stable was determined graphically. The unstable region was never penetrated during testing.

Free swashplate control effectiveness tests. - The test method here was similar to that employed in the fixed swashplate cyclic derivative tests, except that incremental swashplate moment, rather than angle, inputs were made, by means of the primary control system. Once again a minimum of four control increments from trim were applied in each axis, the other control being left untouched.

The free swashplate test envelope was severely restricted, because of the poor stability of the rotor/gyro system at low rpm and high advance ratio. No control effectiveness tests were conducted near the stability boundary.

Airspeed-RPM Envelope

The Wind Tunnel Test Plans called for testing at advance ratios between 0.4 and 4.0 at tunnel airspeeds in the range 60 to 120 knots. However, the preliminary safety tests exposed areas where model operation was hazardous, or where the model behavior was such as to preclude the gathering of useful data. Figure 16 presents the overall test envelopes in the fixed and free swashplate modes, and Figure 17 shows the regions within these envelopes which were avoided for continuous operation.

Continuous operation of the rotor was limited to a maximum of 320 rpm due to an anticipated engine drive train heating problem. The rotor was demonstrated to be free of flutter and pitch instabilities within the test rpm range. It should be noted that flutter checks made during the whirl tests indicated a flutter-free rotor to at least 390 rpm.
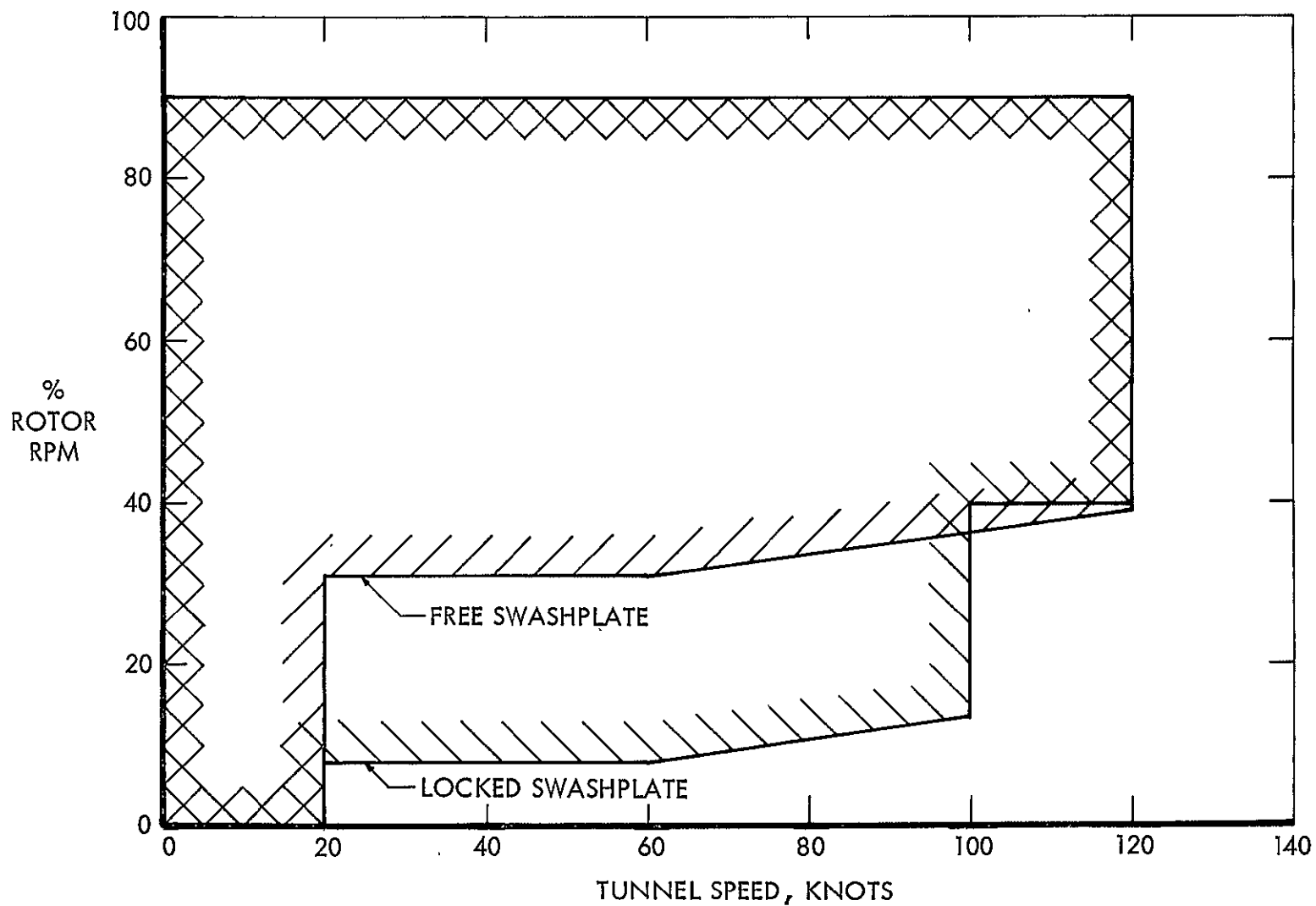
Figure 16. Test Envelope

76
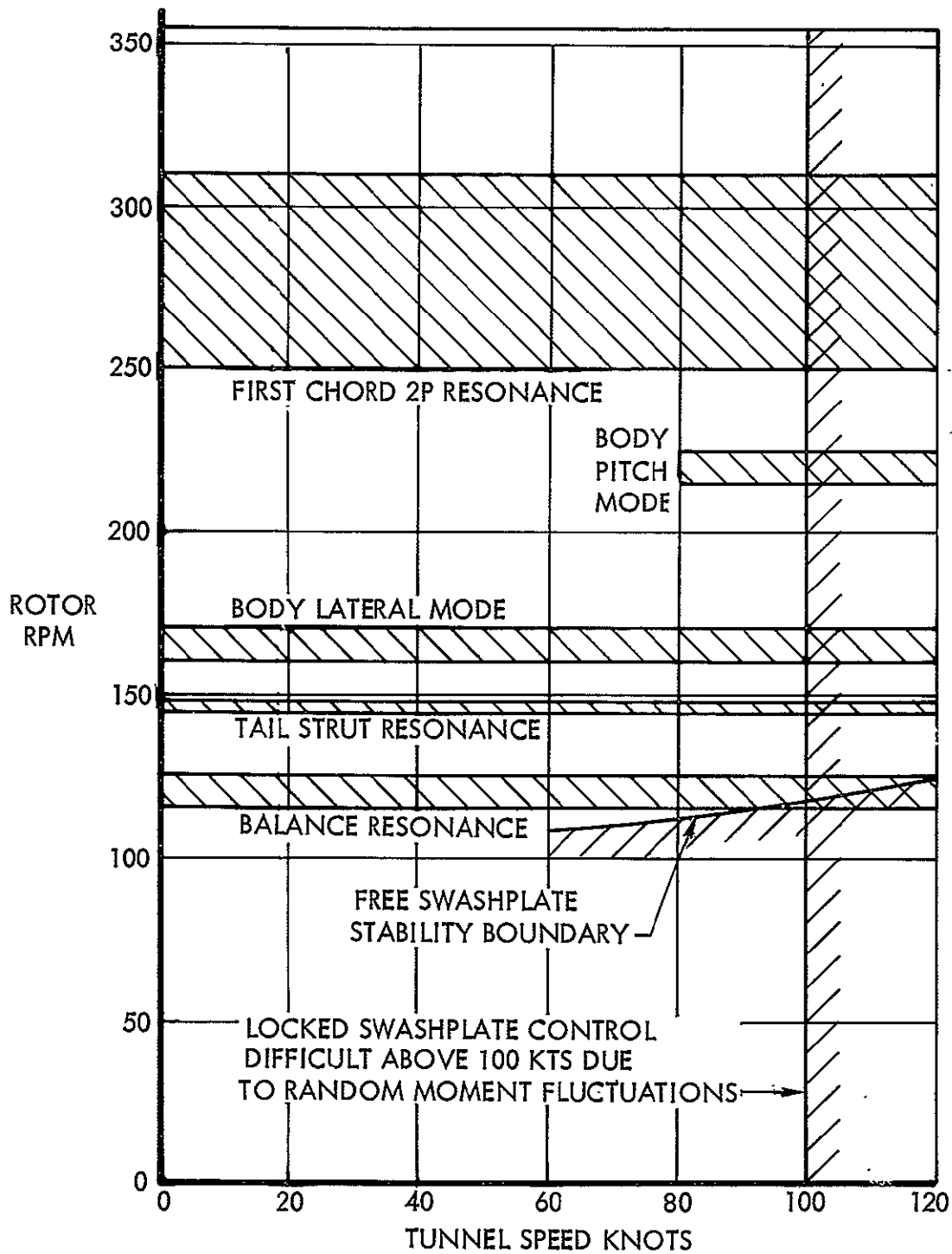
Figure 17. Test 'Avoid' Regions

<u>Model resonance</u>. — The model resonant modes that were potentially
bothersome and hence restricted the test envelope (Figure 17 were:

(1) Model lateral mode at 160 rpm which was characterized by strong
    lateral response at 3P in the stationary system and chordwise 2P
    response.

(2) Model pitch mode at 220 rpm which was characterized by pitch load
    cell 3P in the stationary system and strong chordwise response at
    2P. This mode was not detected at tunnel speeds less than 90 KTS.

(3) Rotor blade first inplane 2P crossing at 280 rpm (at 1.5° collective
    blade angle). Continuous testing was restricted between 250 and
    310 rpm to preclude a 1P x 2P instability.

(4) A tunnel balance system resonance was observed at 1.8 CPS (108 rpm).

<u>Control difficulties</u>. - In the fixed swashplate control mode, the opera-
tors had difficulty holding steady conditions at the higher tunnel airspeeds.
The model behavior was characterized by a random load cell moment fluctuation
which increased in amplitude with increasing airspeed and rotor rpm to
±12,000 in lb at 120 KTS, 320 rpm. As a consequence no fixed swashplate tech-
nical tests were performed above 100 KTS. It was thought that the problem
might be due to random blade feathering motion within the slop band of the
control system. However, examination of the oscillograph records of blade
angle did not substantiate this. It is postulated that the tunnel flow
straighteners in the return circuit were unable to remove all the swirl in the
airflow induced by the rotor. Since rotor control in the primary mode was
much steadier and the gyro took up random oscillations it is felt that the
gyro was effective in overcoming the effects of these external aerodynamic
"gusts."

Test Conditions

The fixed swashplate test conditions which were investigated in the
determination of derivatives with respect to cyclic pitch, collective pitch,
and angle of attack are summarized in Figures 18 and 19. The free swash-
plate control effectiveness test conditions are also shown.
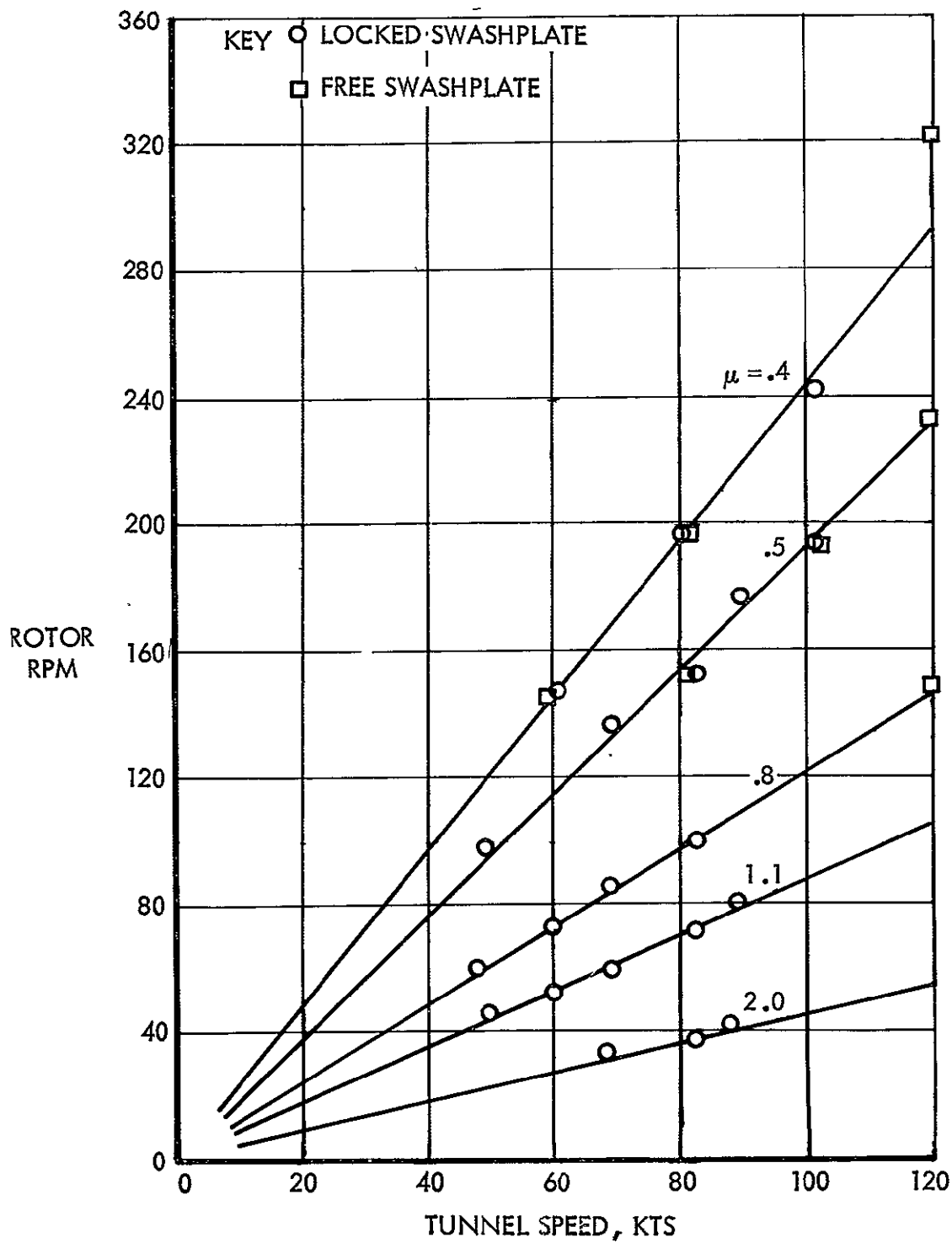
Figure 18. Rotor Velocity Diagram - Test Conditions
$\alpha_R = 0$ Deg, $\theta_{0.75R} = 1.5$ Deg
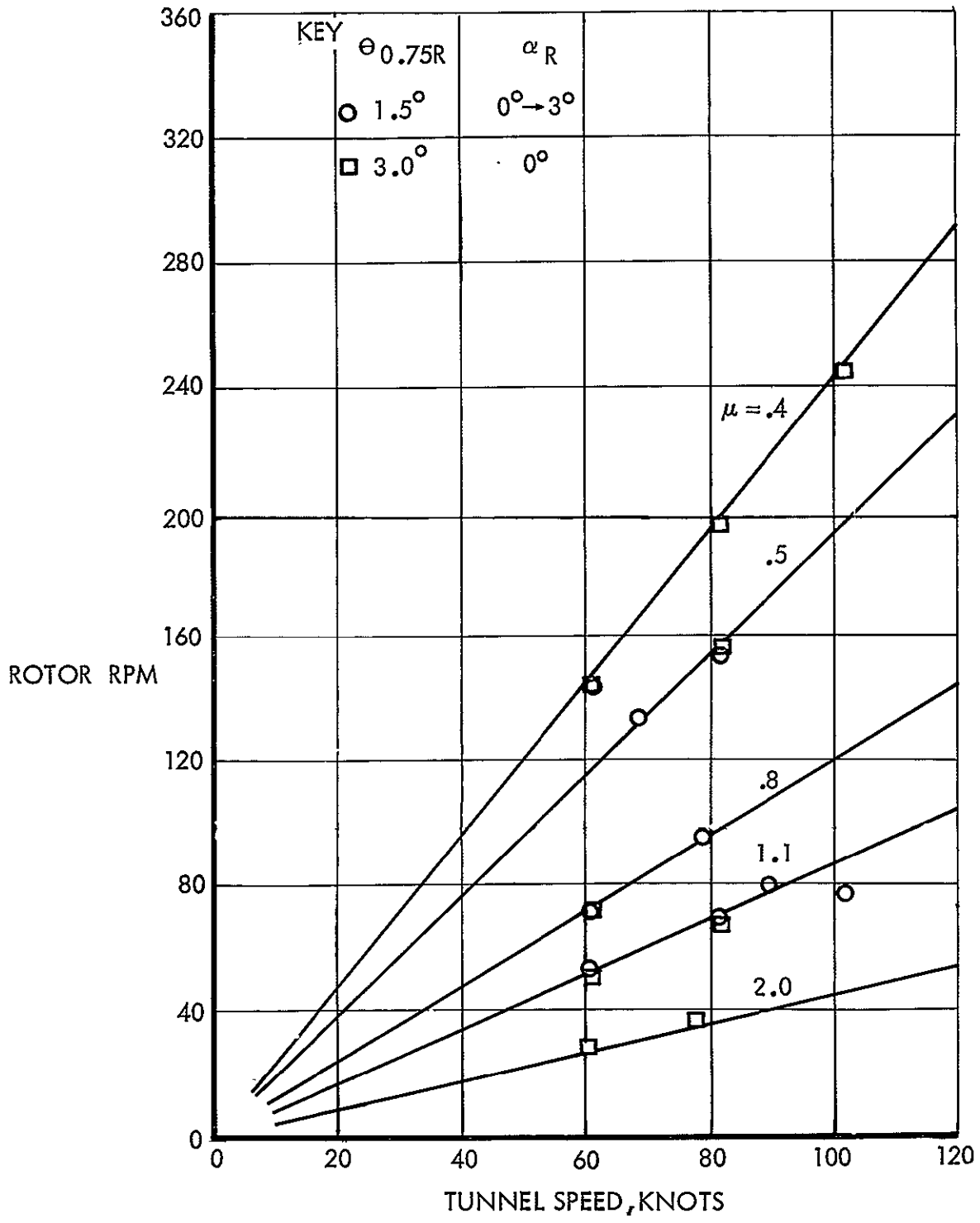
Figure 19. Rotor Velocity Diagram - Test Conditions. Angle
of Attack and Collective Angle Tests

Rotor and swashplate derivatives, and control effectiveness data were measured along lines of nominally constant advance ratio in order to simplify the isolation of the aerodynamic and aeroelastic effects.

Data Reduction and Analysis

The data of primary interest to the modification of theoretical methods was recorded on tape as well as oscillograph. It consisted of instrument output which yielded cyclic pitch angles and hub and swashplate moments. The analog data recorded in FM form on magnetic tape was chosen as the main source of information primarily because it lent itself to automatic data reduction with a minimum of manual operations. The test records were passed through an analog-to-digital conversion process, which picked off data every 0.004 seconds, to make them acceptable to computer equipment, then stored in digital form on magnetic tape.

The preliminary computer operations involved calibrating and smoothing the data. Calibration was performed by recording pre-run resistance shunts having known equivalent loads. This gave the parameter sensitivities, from which the conversion from data counts to engineering units were made. Electrical noise and wild points in the data were eliminated by a three point parabolic smoothing routine. The computer next recognized the rpm signal, which was triggered whenever the No. 1 blade was aft (at $\psi = 0^\circ$). The data within the cycles of interest were interpolated to give 72 data points per cycle.

In this form the data was suitable for the subsequent analysis procedures discussed below:

<u>Shaft bending moment transformation</u>. - As discussed in the Instrumentation section, the output of the 0 degree and 90 degrees shaft bending moment gages was preferred to the load cell moment measurements, because of their proximity to the rotor hub. In order to indicate pitch and roll moment, a transformation from rotating to non-rotating coordinates was required. The relationship at a particular instant, where the No. 1 blade is at an azimuth of ψ degrees, is given by

$$M = S.B._0 \cos \psi - S.B._{90} \sin \psi$$

$$L = S.B._0 \sin \psi + S.B._{90} \cos \psi$$

By this conversion process, derived time histories of shaft pitch and roll moment were available.

Harmonic Analysis of Data. - If $y = f(x)$ is periodic, so that the value of the function y is unaltered if the variable x is increased by any multiple of the period, then the function can be expressed in the form of a Fourier Series

$$y = A_0 + \sum_{j=1}^{\infty} A_j \cos jx + \sum_{j=1}^{\infty} B_j \sin jx$$

Given a set of observed values (x_i, y_i), $i = 1, 2, 3, \ldots N$, where N is the number of equally spaced input points in one cycle, it is desired to approximate $y(x)$ by a trigonometric polynominal

$$y(x) = A_0 + \sum_{j=1}^{n} A_j \cos jx + \sum_{j=1}^{n} B_j \sin jx$$

or, in the polar (amplitude - phase) form,

$$y(x) = A_0 + \sum_{n=1}^{n} C_j \cos (jx - \phi_j)$$

The required coefficients are:

$$A_0 = \frac{2}{N} \sum_{i=1}^{N} y_i$$

$$A_j = \frac{2}{N} \sum_{i=1}^{N} y_i \cos \left[\frac{2(i-1)\, j\pi}{N} \right]$$

82

$$B_j = \frac{2}{N} \sum_{i=1}^{N} y_i \sin\left[\frac{2(i-1)\,j\pi}{N}\right]$$

$$C_j = (A_j^2 + B_j^2)^{\frac{1}{2}}$$

and

$$\phi_j = \tan^{-1}\left(\frac{B_j}{A_j}\right)$$

for

$$j < \frac{N}{2}$$

Since $N = 72$ for the test data, the harmonic analysis is theoretically good for harmonics from 1 to 35. However, only the first ten harmonics, plus the mean, were calculated.

In the data analysis which follows, only the mean of rotor and swashplate forces and moments, and the first harmonic of blade angle (giving the cyclic control angles) were required. However, the digital format of the data made the results amenable to harmonic analysis, and the dynamic behavior of the rotor/gyro system within the aerodynamic environment was of interest for future studies.

Method of least squares. - To obtain the cyclic aeroelastic derivatives and the control angles for trim, hub and swashplate force and moment data were recorded for various combinations of pitch and roll control angles. In order to separate the effects of the combined input, a least squares solution of the equations for the rotor and swashplate moments was employed.

It has been hypothesized that changes in rotor and swashplate forces and moments are linearly related to changes in swashplate angles, e.g.,

$$M = M_{\theta=\phi=0} + \frac{\partial M}{\partial \theta} \cdot \theta + \frac{\partial M}{\partial \phi} \cdot \phi$$

83

and similarly for

$$L, \quad M_\theta, \quad M_\phi, \quad T$$

Alternatively, if the control positions are described by cyclic blade pitch, then

$$M = M_{\theta_{1_s} = \theta_{1_c} = 0} + \frac{\partial M}{\partial \theta_{1_c}} \cdot \theta_{1_c} + \frac{\partial M}{\partial \theta_{1_s}} \cdot \theta_{1_s}$$

For convenience, the method will be discussed in terms of swashplate angles only.

The problem is to determine the values of $M_{\theta=\phi=0}$, $\partial M/\partial\theta$, $\partial M/\partial\phi$ (denoted M_o, M_θ, M_ϕ hereafter) which will describe the best fit plane of M through θ and ϕ. If M_i, θ_i, and ϕ_i are particular measured values, then the deviation of this data from the best fit plane is given by the residual

$$v_i = M_i - M$$

If

$$S' = \sum_{i=1}^{n} v_i^2 = \sum_{i=1}^{n} (M_i - M)^2$$

then the best fit plane is defined by the requirement that S be minimum, i.e.,

$$\frac{\partial S}{\partial M_o} = \frac{\partial S}{\partial M_\theta} = \frac{\partial S}{\partial M_\phi} = 0$$

or

$$(n)\, M_o + \left(\sum_{i=1}^{n} \theta_i \right) M_\theta + \left(\sum_{i=1}^{n} \phi_i \right) M_\phi = \sum_{i=1}^{n} M_i$$

$$\left(\sum_{i=1}^{n} \theta_i \right) M_o + \left(\sum_{i=1}^{n} \theta_i^2 \right) M_\theta + \left(\sum_{i=1}^{n} \theta_i \phi_i \right) M_\phi = \sum_{i=1}^{n} M_i\, \theta_i$$

$$\left(\sum_{i=1}^{n} \phi_i \right) M_o + \left(\sum_{i=1}^{n} \theta_i \phi_i \right) M_\theta + \left(\sum_{i=1}^{n} \phi_i^2 \right) M_\phi = \sum_{i=1}^{n} M_i\, \phi_i$$

In matrix form this becomes

$$
\begin{bmatrix}
(1 + 1 + ..) & (\theta_1 + \theta_2 + ..) & (\phi_1 + \phi_2 + ..) \\
(\theta_1 + \theta_2 + ..) & (\theta_1^2 + \theta_2^2 + ..) & (\theta_1\phi_1 + \theta_2\phi_2 + ..) \\
(\phi_1 + \phi_2 + ..) & (\theta_1\phi_1 + \theta_2\phi_2 + ..) & (\phi_1^2 + \phi_2^2 + ..)
\end{bmatrix}
\begin{bmatrix} M_o \\ M_\theta \\ M_\phi \end{bmatrix}
=
\begin{bmatrix}
M_1 + M_2 + .. \\
M_1\theta_1 + M_2\theta_2 + .. \\
M_1\phi_1 + M_2\phi_2 + ..
\end{bmatrix}
$$

from which

$$
\begin{bmatrix} M_o \\ M_\theta \\ M_\phi \end{bmatrix}
=
\begin{bmatrix}
(1 + 1 + ..) & (\theta_1 + \theta_2 + ..) & (\phi_1 + \phi_2 + ..) \\
(\theta_1 + \theta_2 + ..) & (\theta_1^2 + \theta_2^2 + ..) & (\theta_1\phi_1 + \theta_2\phi_2 + ..) \\
(\phi_1 + \phi_2 + ..) & (\theta_1\phi_1 + \theta_2\phi_2 + ..) & (\phi_1^2 + \phi_2^2 + ..)
\end{bmatrix}^{-1}
\begin{bmatrix}
M_1 + M_2 + .. \\
M_1\theta_1 + M_2\theta_2 + .. \\
M_1\phi_1 + M_2\phi_2 + ..
\end{bmatrix}
$$

In the same manner we can solve the remaining hub and swashplate equations

$$
L = L_{\theta=\phi=o} + \frac{\partial L}{\partial \theta} \cdot \theta + \frac{\partial L}{\partial \phi} \cdot \phi
$$

$$
T = T_{\theta=\phi=o} + \frac{\partial T}{\partial \theta} \cdot \theta + \frac{\partial L}{\partial \phi} \cdot \phi
$$

$$
M_{SP} = M_{SP_{\theta=\phi=o}} + \frac{\partial M_{SP}}{\partial \theta} \cdot \theta + \frac{\partial M_{SP}}{\partial \phi} \cdot \phi
$$

$$
L_{SP} = L_{SP_{\theta=\phi=o}} + \frac{\partial L_{SP}}{\partial \theta} \cdot \theta + \frac{\partial L_{SP}}{\partial \phi} \cdot \phi
$$

Since the control inputs θ, ϕ are the same in each case, it is convenient to combine the analysis into one matrix equation,

$$
\begin{bmatrix}
M_o & L_o & T_o & M_{SP_o} & L_{SP_o} \\
M_\theta & L_\theta & T_\theta & M_{SP_\theta} & L_{SP_\theta} \\
M_\phi & L_\phi & T_\phi & M_{SP_\phi} & L_{SP_\phi}
\end{bmatrix}
=
\begin{bmatrix}
(n) & \left(\sum\limits_{i=1}^{n} \theta_i\right) & \left(\sum\limits_{i=1}^{n} \phi_i\right) \\
\left(\sum\limits_{i=1}^{n} \theta_i\right) & \left(\sum\limits_{i=1}^{n} \theta_i^2\right) & \left(\sum\limits_{i=1}^{n} \theta_i \phi_i\right) \\
\left(\sum\limits_{i=1}^{n} \phi_i\right) & \left(\sum\limits_{i=1}^{n} \phi_i \theta_i\right) & \left(\sum\limits_{i=1}^{n} \phi_i^2\right)
\end{bmatrix}^{-1}
$$

$$
\begin{bmatrix}
\left(\sum\limits_{i=1}^{n} M_i\right) & \left(\sum\limits_{i=1}^{n} L_i\right) & \left(\sum\limits_{i=1}^{n} T_i\right) & \left(\sum\limits_{i=1}^{n} M_{SP_i}\right) & \left(\sum\limits_{i=1}^{n} L_{SP_i}\right) \\
\left(\sum\limits_{i=1}^{n} M_i \theta_i\right) & \left(\sum\limits_{i=1}^{n} L_i \theta_i\right) & \left(\sum\limits_{i=1}^{n} T_i \theta_i\right) & \left(\sum\limits_{i=1}^{n} M_{SP_i} \theta_i\right) & \left(\sum\limits_{i=1}^{n} L_{SP_i} \theta_i\right) \\
\left(\sum\limits_{i=1}^{n} M_i \phi_i\right) & \left(\sum\limits_{i=1}^{n} L_i \phi_i\right) & \left(\sum\limits_{i=1}^{n} T_i \phi_i\right) & \left(\sum\limits_{i=1}^{n} M_{SP_i} \phi_i\right) & \left(\sum\limits_{i=1}^{n} L_{SP_i} \phi_i\right)
\end{bmatrix}
$$

which may be formed as follows

$$
\begin{bmatrix}
M_o & L_o & T_o & M_{SP_o} & L_{SP_o} \\
M_\theta & L_\theta & T_\theta & M_{SP_\theta} & L_{SP_\theta} \\
M_\phi & L_\phi & T_\phi & M_{SP_\phi} & L_{SP_\phi}
\end{bmatrix}
=
\begin{bmatrix}
1 & 1 & . & 1 \\
\theta_1 & \theta_2 & . & \theta_n \\
\phi_1 & \phi_2 & . & \phi_n
\end{bmatrix}
\begin{bmatrix}
1 & \theta_1 & \phi_1 \\
1 & \theta_2 & \phi_2 \\
. & . & . \\
1 & \theta_n & \phi_n
\end{bmatrix}^{-1}
$$

$$
\begin{bmatrix}
1 & 1 & . & 1 \\
\theta_1 & \theta_2 & . & \theta_n \\
\phi_1 & \phi_2 & . & \phi_n
\end{bmatrix}
\begin{bmatrix}
M_1 & L_1 & T_1 & M_{SP_1} & L_{SP_1} \\
M_2 & L_2 & T_2 & M_{SP_2} & L_{SP_2} \\
. & . & . & . & . \\
M_n & L_n & T_n & M_{SP_n} & L_{SP_n}
\end{bmatrix}
$$

to give the derivatives of hub and swashplate force and moments with respect to the swashplate pitch and roll angles.

The residuals $(M_i - M)$, $(L_i - L)$ etc., for each test point, and the root mean squares of the residuals for each set of test points, were then calculated. (See Appendix D.) These were helpful in detecting errors in the data, and also gave an indication of the suitability of the linear equations used to describe the model behavior.

To determine swashplate angles for trim it should be noted that in the foregoing analysis the following relationships have been determined

$$
\begin{Bmatrix} M \\ L \end{Bmatrix} = \begin{Bmatrix} M_o \\ L_o \end{Bmatrix} + \begin{bmatrix} \dfrac{\partial M}{\partial \theta} & \dfrac{\partial M}{\partial \phi} \\[2mm] \dfrac{\partial L}{\partial \theta} & \dfrac{\partial L}{\partial \phi} \end{bmatrix} \begin{Bmatrix} \theta \\ \phi \end{Bmatrix}
$$

For the hub moments to be trimmed, $M = L = 0$, hence the swashplate angles required to trim the rotor will be given by

$$
\begin{Bmatrix} \theta \\ \phi \end{Bmatrix} = - \begin{bmatrix} \dfrac{\partial M}{\partial \theta} & \dfrac{\partial M}{\partial \phi} \\[2mm] \dfrac{\partial L}{\partial \theta} & \dfrac{\partial L}{\partial \phi} \end{bmatrix}^{-1} \begin{Bmatrix} M_o \\ L_o \end{Bmatrix}
$$

Rotor
Trim

In a similar manner the swashplate angles required to make the swashplate moments (control moments) go to zero are found to be

$$
\begin{Bmatrix} \theta \\ \phi \end{Bmatrix} = - \begin{bmatrix} \dfrac{\partial M_{SP}}{\partial \theta} & \dfrac{\partial M_{SP}}{\partial \phi} \\[2mm] \dfrac{\partial L_{SP}}{\partial \theta} & \dfrac{\partial L_{SP}}{\partial \phi} \end{bmatrix} \begin{Bmatrix} M_{SP} \\ L_{SP} \end{Bmatrix}
$$

S.P. Trim

Rotor-gyroscope stability. - The stability of the free-gyroscope system
was determined experimentally by observing the period and time to decay of
transient oscillations of the control mode. The control mode was excited by
suddenly releasing a large steady-state moment applied to the swashplate.
The decaying oscillations were, therefore, centered about the zero moment
level. This procedure was used to ensure that large overshooting rotor forces
were not inadvertently applied.

The swashplate pitch and roll angular displacements were recorded con-
tinuously on the oscillograph until the transient oscillations had died away.
Figure 20 shows a typical recording.

From the figure the frequency, the time to half amplitude and the type of
stability mode may be deduced. The frequency is obtained by taking the recip-
rocal of the time between successive peaks of oscillation. The time to half
amplitude is obtained by fitting a smooth curve through the peaks
and noting the time taken for the peak to peak displacement to reduce to half
its amplitude. It is generally more-or-less independent of the starting time,
thereby indicating an exponential decay.

The direction of precession of the gyroscope and the circularity of the
mode is indicated by the phase and relative amplitude of the swashplate pitch
and roll displacements. Roll displacement leading the pitch displacement
indicates an advancing precessive motion. Equal amplitude of pitch and roll
indicates a circular mode. The teetering motion is indicated if the amplitude
of one displacement is much larger than the other.

Some transient responses exhibited a slight tendency to pulse during the
decay and this impaired the precision of determination of period and time to
half amplitude. This could have been caused by proximity to another mode,
possibly the rotor precessive.
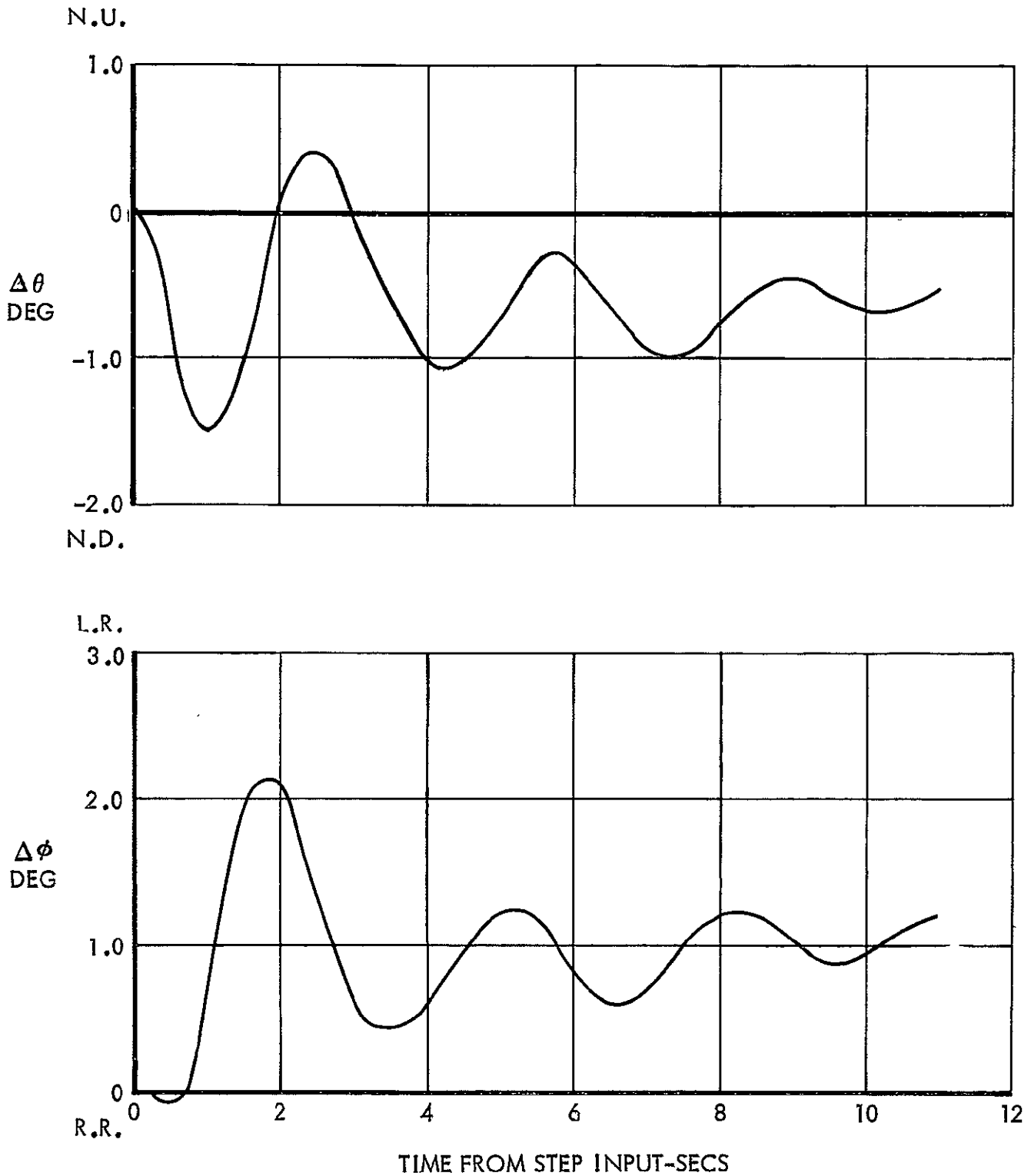
APPLIED MOMENT = 300 IN. LB. RIGHT ROLL

Figure 20.   Swashplate Angular Response To Swashplate
Roll Moment Step Input - 70 Knots, 154 RPM

THEORETICAL AND EXPERIMENTAL RESULTS

Aeroelastic Derivatives

Aeroelastic derivatives, which include the effects of structural deflec-tions, are determined from wind tunnel data by the least squares method. The test data are correlated with derivatives obtained from theory.

The derivatives which follow include the changes in hub moment, swash-plate moment, and thrust resulting from variations in blade cyclic and col-lective pitch, or rotor angle of attack. All derivatives are nondimensional-zied relative to angles in degrees. Data are given over a speed range of 50 to 120 knots and advance ratios range from about 0.4 to 2.0.

Hub moment derivatives due to blade cyclic pitch. - A summary of the theoretical hub moment derivative coefficients due to blade cyclic pitch is shown in Figure 2. Rolling and pitching moment coefficients due to either θ_{1c} or θ_{1s} are plotted along the ordinates and abscissas respectively. Intersecting curves for constant values of advance ratio "μ" and flap frequency ratio "P" are drawn for the value of Lock No. at nominal sea level air density. If divided by solidity "σ" the curves would be generally applicable to all motors.

The P $=\infty$ curve is a limit case where there are no structural deflections. Thus, points along this line represent aerodynamic derivative coefficients applicable to a rigid blade. To aid in correlating test and theoretical data, wind tunnel speed curves for the present tests are also plotted.

Relative phase and magnitude changes with forward speed and advance ratio are indicated on the plots. The derivative coefficients grow in magnitude along lines of constant forward speed in the direction of decreasing advance ratio, due to greater cyclic control effectivity resulting from both lower advance ratio and higher rotor speed.

The aeroelastic derivative coefficients increasingly deviate from the rigid blade condition along lines of constant forward speed in the direction

of decreasing advance ratio. This phenomenon is primarily due to increasing rotor rpm, whereby the ratio of rotor angular frequency to blade first natural flap frequency (1/P) increases, causing greater lag in blade response to inputs.

The theoretical derivative coefficients accompanied by the appropriate test data are shown on Figures 21 through 27. Each figure gives data for one forward speed. Test values of advance ratio approximate values of 0.4, 0.5, 0.8, 1.1, and 2.0; not all of which are shown at each forward speed. Tick lines on the theoretical curves relate to test values. The experimental data was taken in both the free and locked swashplate modes of operation.

Test and theory generally agree better at the lower forward speeds and the higher advance ratios. Some of the assumptions in the theoretical method (i.e., no downwash) are known to be inappropriate at low advance ratio. The test data is less valid at higher forward speeds because of the higher model vibration level.

Swashplate moment derivatives due to blade cyclic pitch. - The swashplate (or gyro) aeroelastic moment derivative coefficients due to either of the blade cyclic angles θ_{1c} and θ_{1s} are presented in a manner parallel to the corresponding hub derivative coefficients. The theoretical data are summarized on Figure 28.

The swashplate coefficients reflect the cant angle; thus, they are rotated about 60° relative to the hub coefficients, Figure 2.

The phase shifts and relative magnitude changes with velocity and advance ratio are very similar to the parallel changes on the hub moment plots. Swashplate moment sensitivities are increased with increasing rotor rpm and decreasing advance ratio, and the greater lag in blade response with increasing rotor speed is also reflected here.

The comparisons between theory and test are made on Figures 29 through 35. The figures display swashplate derivatives coefficients which are for the same conditions as the hub moment coefficients on Figures 21 through 27.

$\dfrac{\partial C_l}{\partial \theta_{1c}}$

$\dfrac{\partial C_m}{\partial \theta_{1c}}$

$\dfrac{\partial C_l}{\partial \theta_{1s}}$

$\dfrac{\partial c_m}{\partial \theta_{1s}}$

-.001
0
.001
.002
.003

-.006   -.005   -.004   -.003   -.002   -.001   0
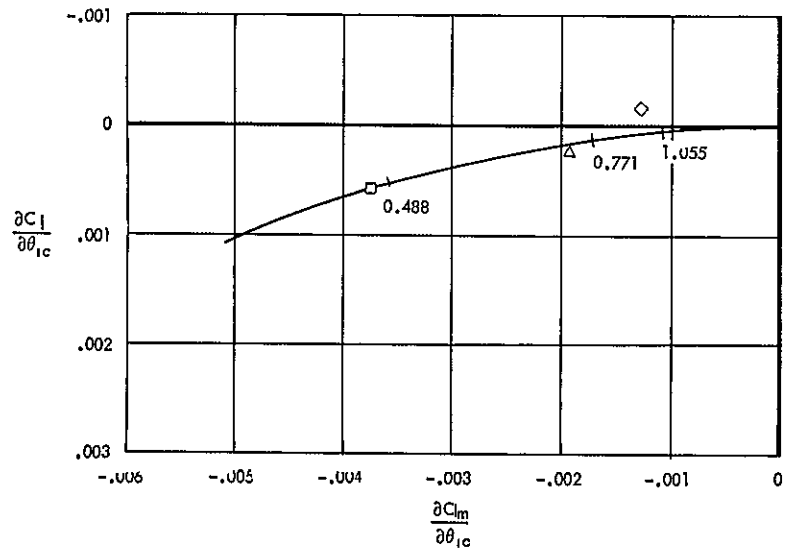
0.488
0.771
1.055

LOCKED SWASHPLATE

□ μ = 0.488
△   0.771
◇   1.055
LOCK NO. = 4.57

-.001
0
.001
.002
.003
.004
.005
.006
.007

0   .001   .002   .003   .004   .005

1.055
0.771
0.488
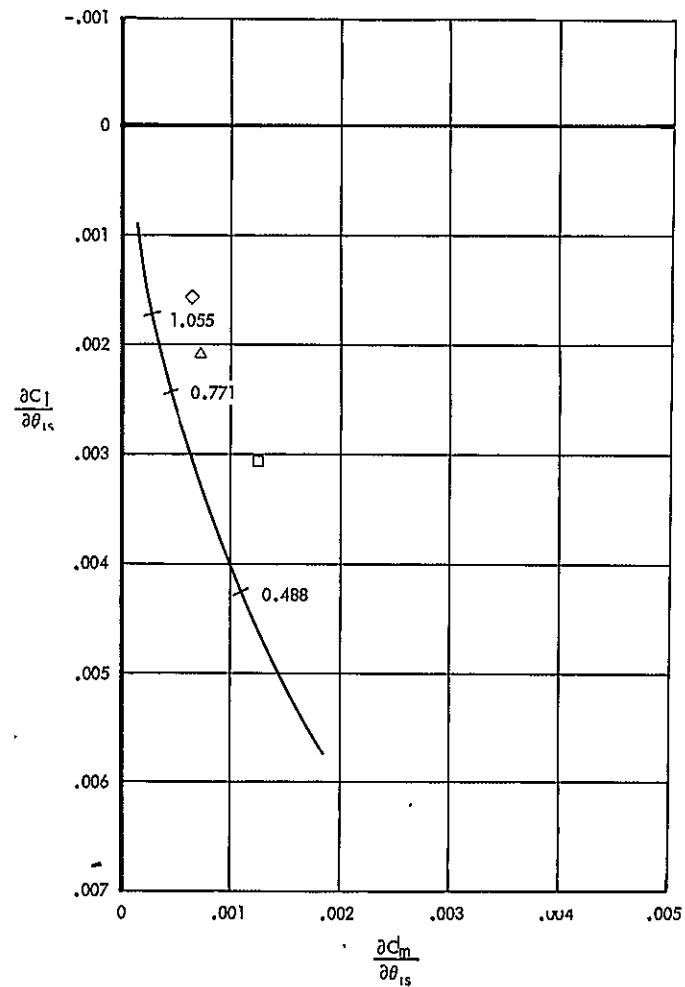
Figure 21.   Hub Moment Derivatives Due to Cyclic Pitch -50 Knots

Figure 22. Hub Moment Derivatives Due to Cyclic Pitch -60 Knots

Left graph:

$\frac{\partial C_l}{\partial \theta_{1c}}$

-.001

0

.001

.002

.003

-.006   -.005   -.004   -.003   -.002   -.001   0

$\frac{\partial C_m}{\partial \theta_{1c}}$

1.125 1.96

0.783

0.492

LOCKED SWASHPLATE

□ μ = 0.492
△   0.783
◇   1.125
▽   1.960

LOCK NO. = 4.57

Right graph:

$\frac{\partial C_l}{\partial \theta_{1s}}$

-.001

0

.001

.002

.003

.004

.005

.006

.007

0   .001   .002   .003   .004   .005

$\frac{\partial C_m}{\partial \theta_{1s}}$

1.96

1.125

0.783

0.492

Figure 23. Hub Moment Derivatives Due to Cyclic Pitch -70 Knots
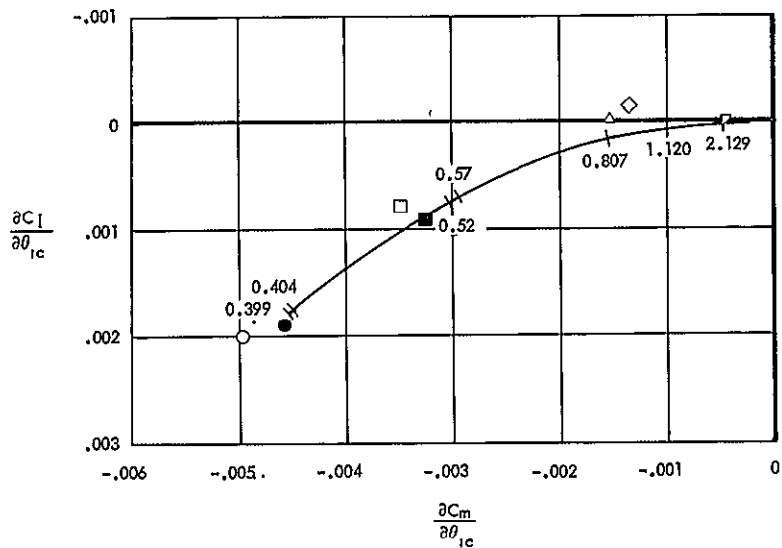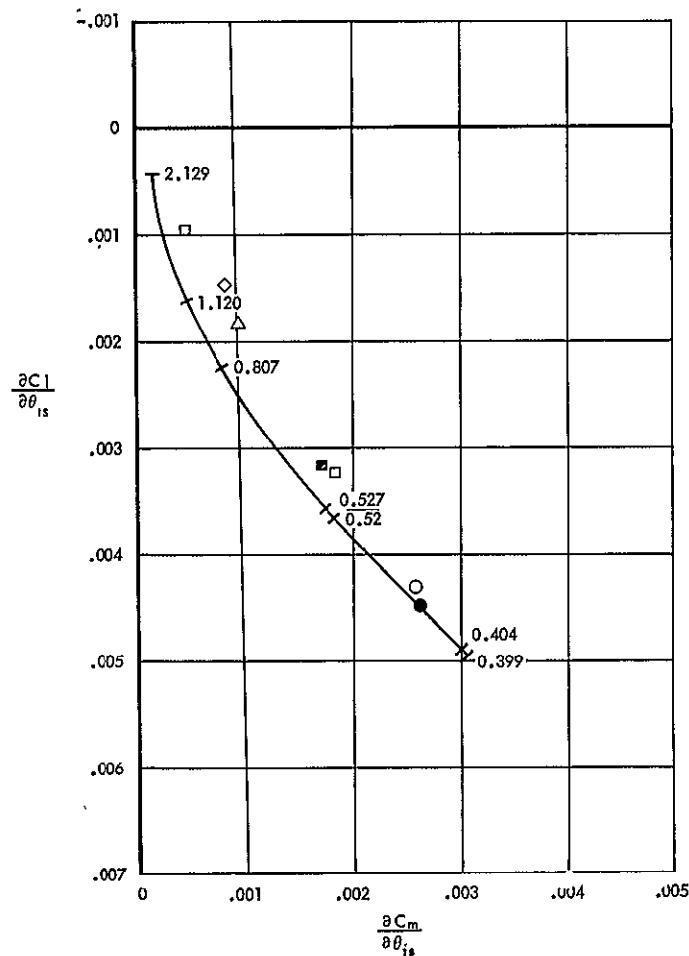
Figure 24. Hub Moment Derivatives Due to Cyclic Pitch -80 Knots
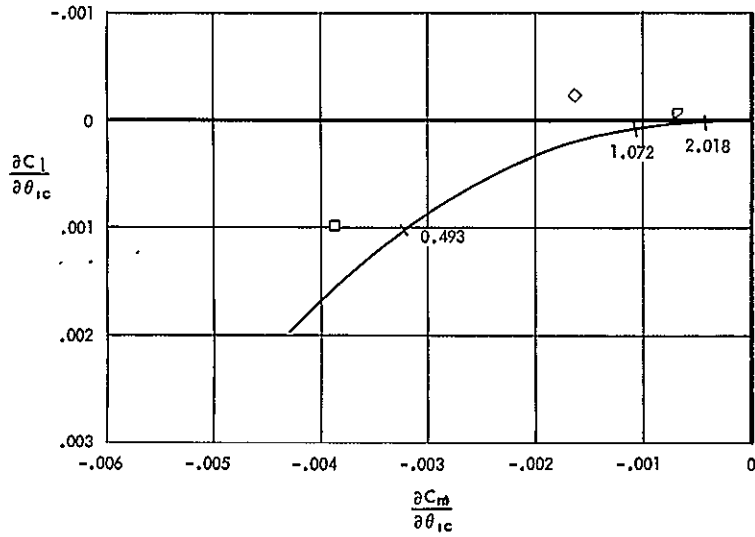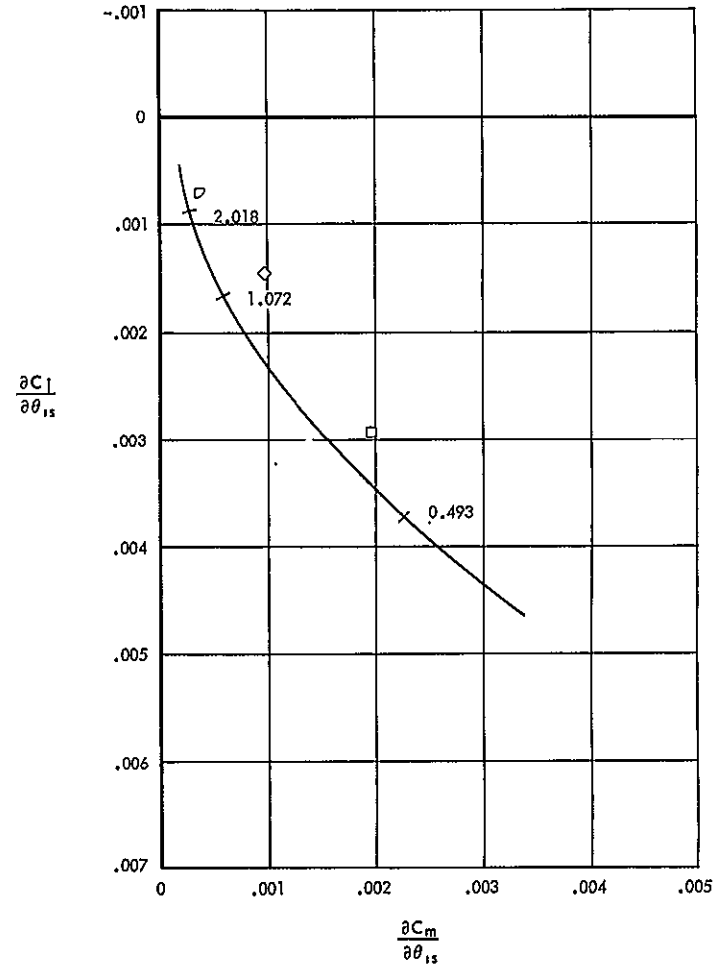
Figure 25. Hub Moment Derivatives Due to Cyclic Pitch -90 Knots
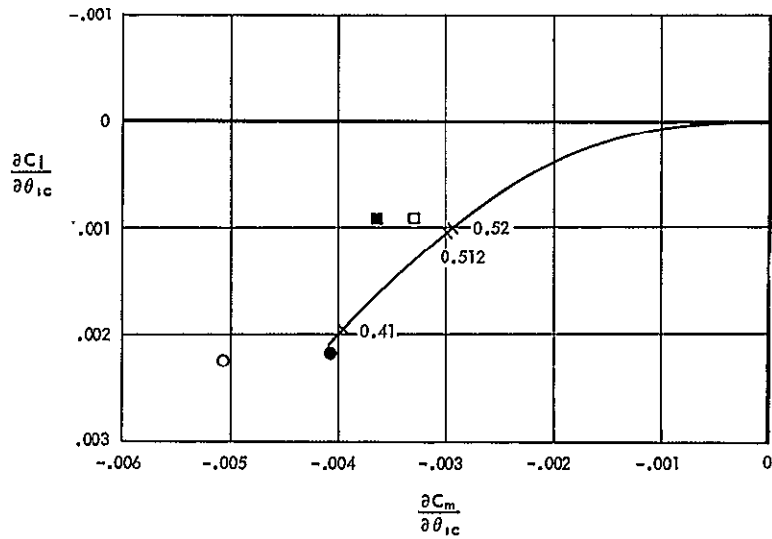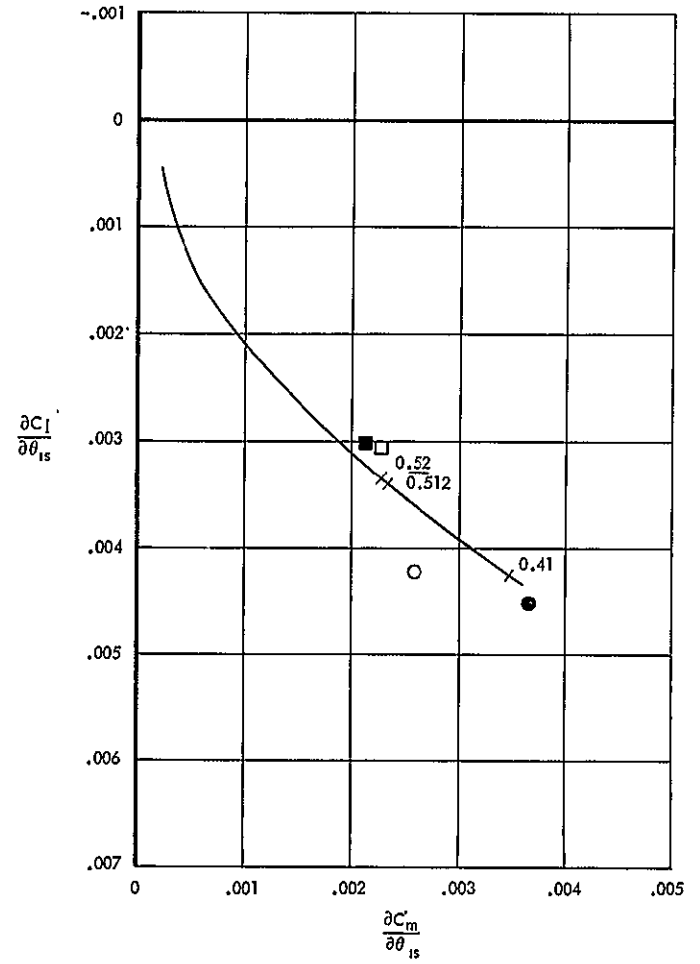
Figure 26. Hub Moment Derivatives Due to Cyclic Pitch -100 Knots
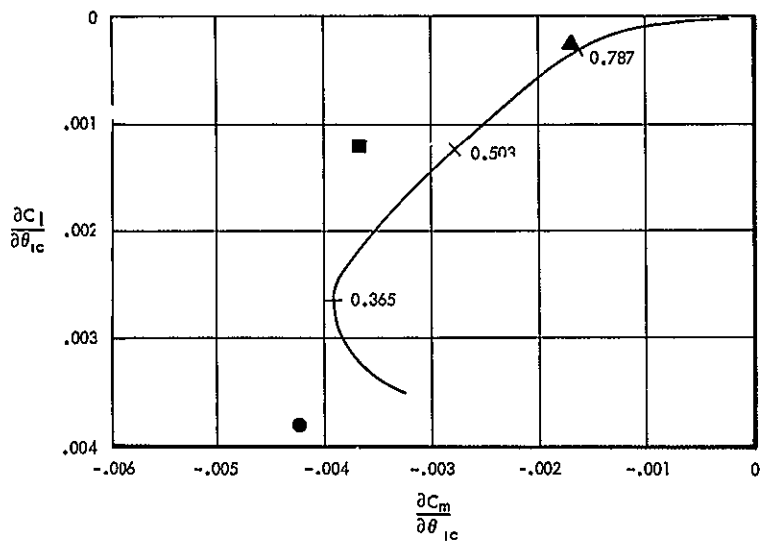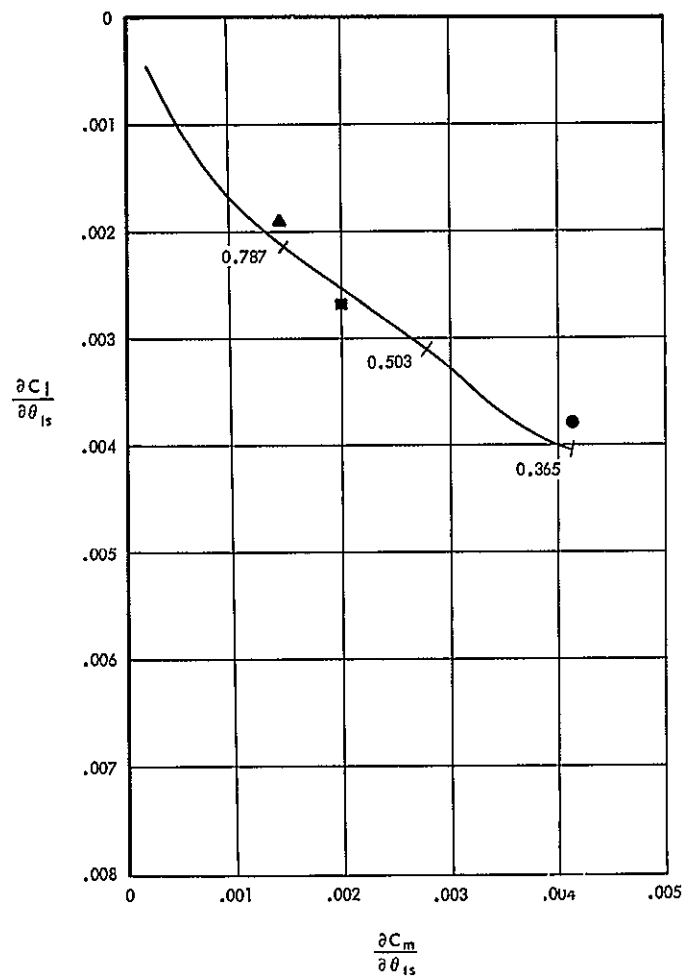
Figure 27. Hub Moment Derivatives Due to Cyclic Pitch -120 Knots
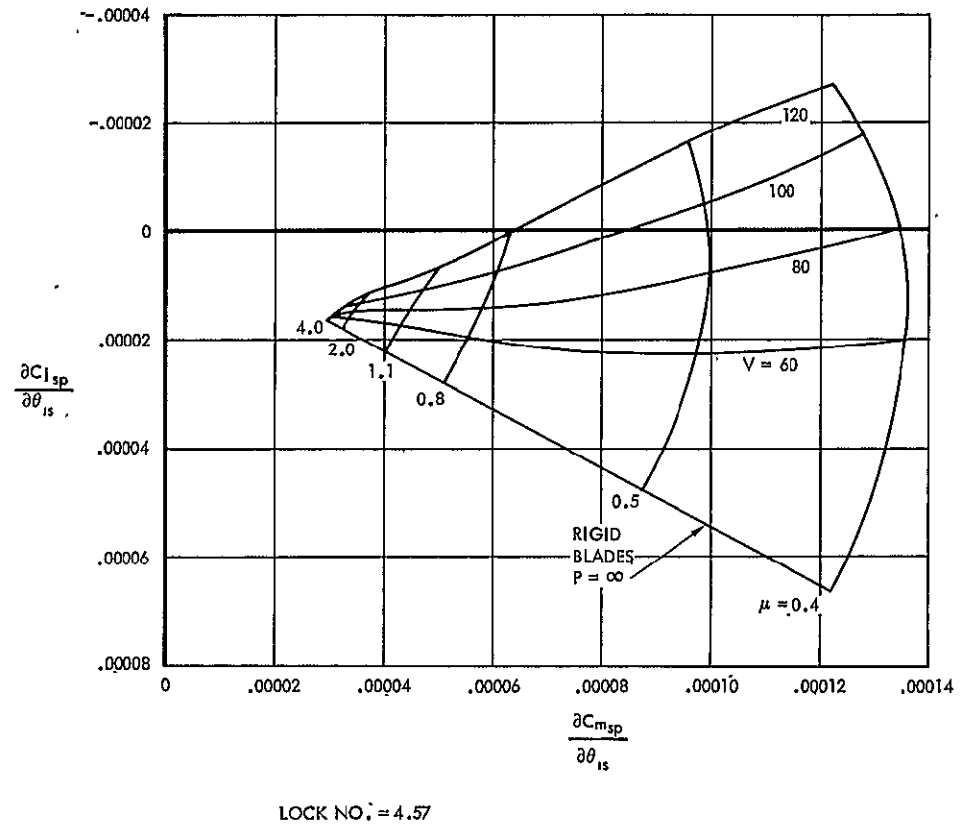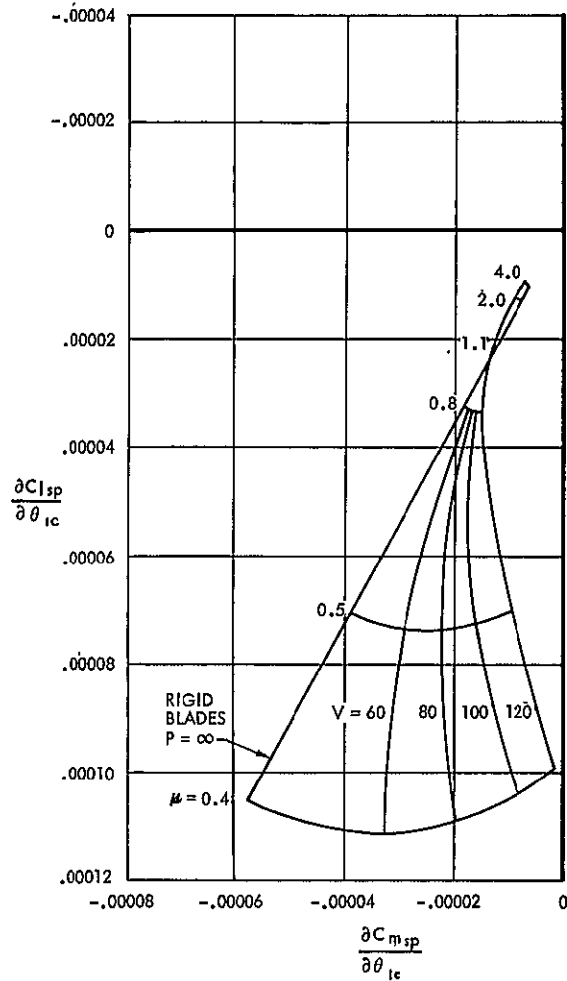
Figure 28. Theoretical Hub Moments Due to Cyclic Pitch
Effect of Flap Frequency Ratio and Velocity

Figure 29. Swashplate Moment Derivatives Due to Cyclic Pitch - 50 Knots

-.00002

0

.00002

.00004

.00006

.00008

.00010

.00012

.00014

$\dfrac{\partial C_{l_{sp}}}{\partial \theta_{lc}}$

1.112

0.799

0.402

-.00008   -.00006   -.00004   -.00002   0

$\dfrac{\partial C_{m_{sp}}}{\partial \theta_{lc}}$

-.00002

0

.00002

.00004

.00006

$\dfrac{\partial C_{l_{sp}}}{\partial \theta_{ls}}$

1.112   0.799

0.402

0   .00002   .00004   .00006   .00008   .00010   .00012   .00014

$\dfrac{\partial C_{m_{sp}}}{\partial \theta_{ls}}$
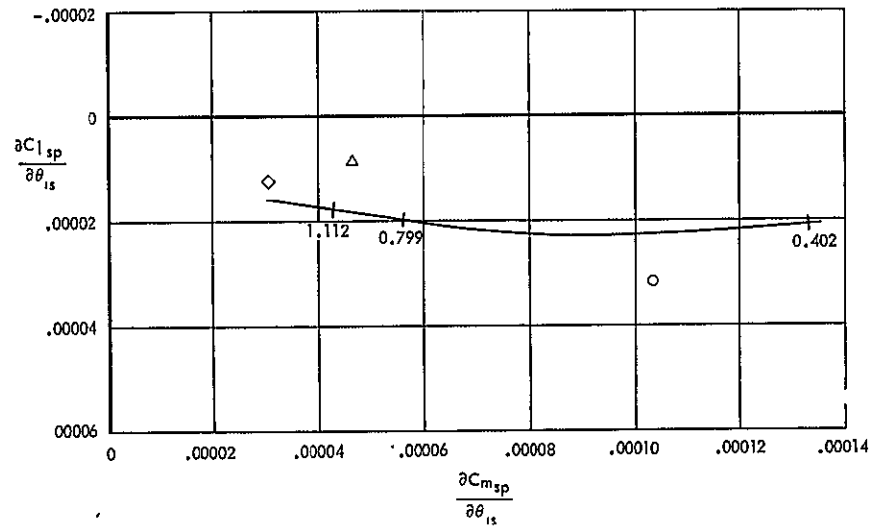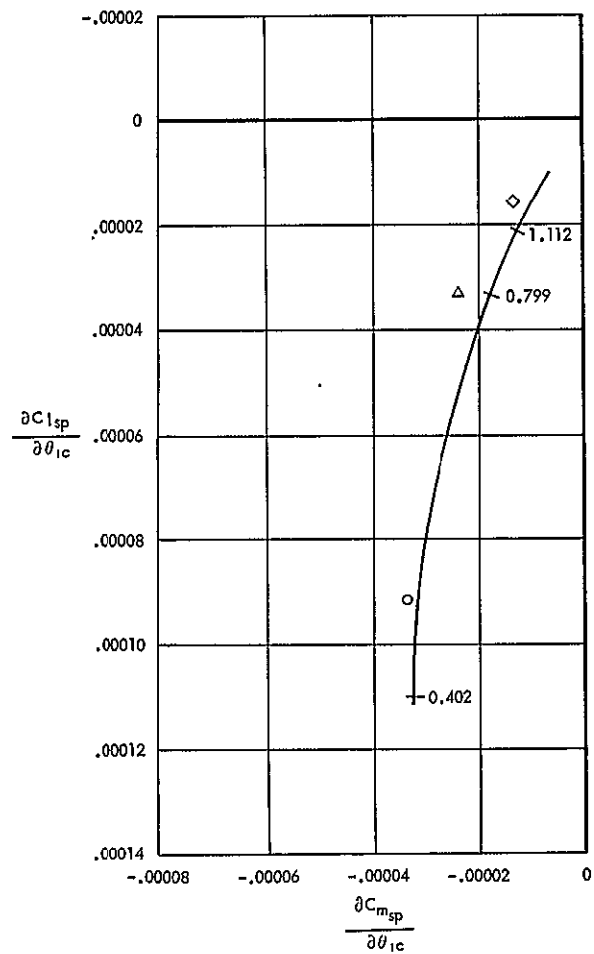
LOCKED SWASHPLATE
O $\mu = 0.402$
△   0.799
◇   1.112
LOCK NO. = 4.57

Figure 30. Swashplate Moment Derivatives Due to Cyclic Pitch - 60 Knots

$-.00002$

0

$.00002$

$.00004$

$.00006$

$.00008$

$.00010$

$.00012$

$.00014$

$\dfrac{\partial C_{l_{sp}}}{\partial \theta_{lc}}$

▽
1.96

1.125

△

0.783

□

0.492

$-.00008$ $-.00006$ $-.00004$ $-.00002$ 0

$\dfrac{\partial C_{m_{sp}}}{\partial \theta_{lc}}$

$-.00002$

0

$.00002$

$.00004$

$.00006$

$\dfrac{\partial C_{l_{sp}}}{\partial \theta_{ls}}$

◇
▽

△

1.96 — 1.125 — 0.783 — 0.492

□

0 $.00002$ $.00004$ $.00006$ $.00008$ $.00010$ $.00012$ $.00014$

$\dfrac{\partial C_{m_{sp}}}{\partial \theta_{ls}}$
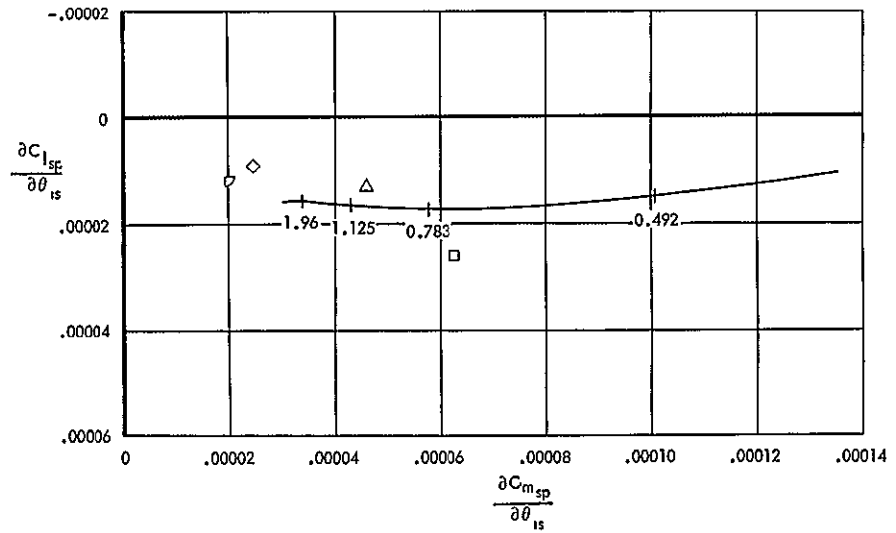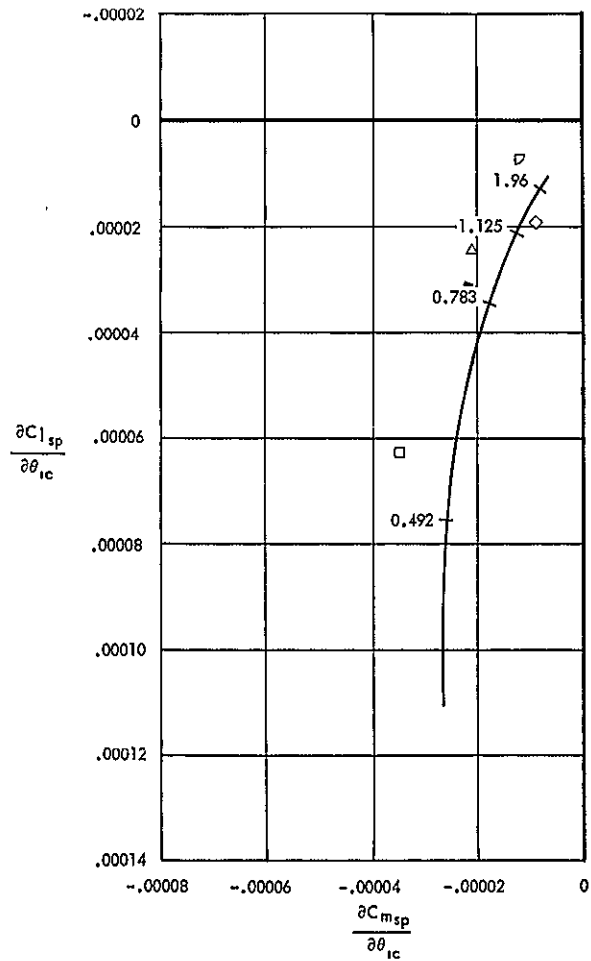
LOCKED SWASHPLATE

□ $\mu = 0.492$

△ 0.783

◇ 1.125

▽ 1.960

LOCK NO. $= 4.57$

Figure 31. Swashplate Moment Derivatives Due to Cyclic Pitch - 70 Knots
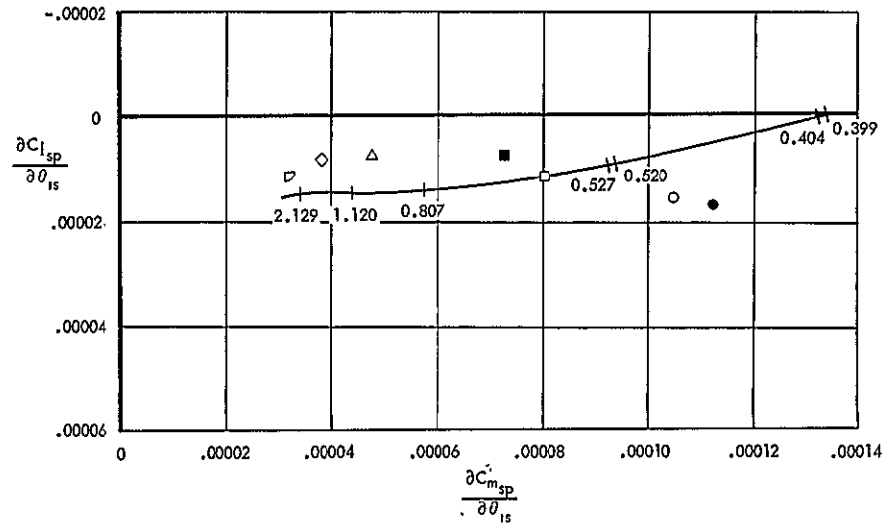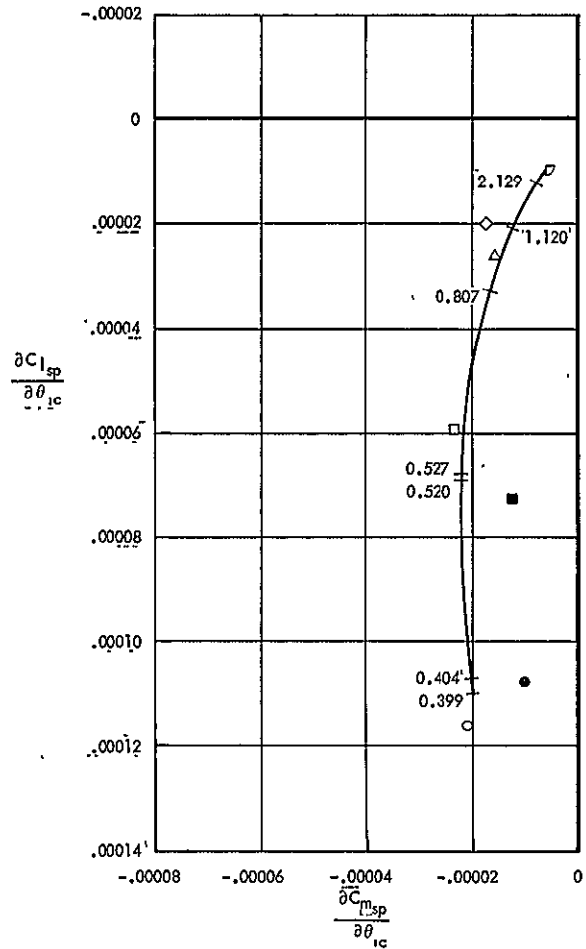
Figure 32. Swashplate Moment Derivatives Due to Cyclic Pitch - 80 Knots
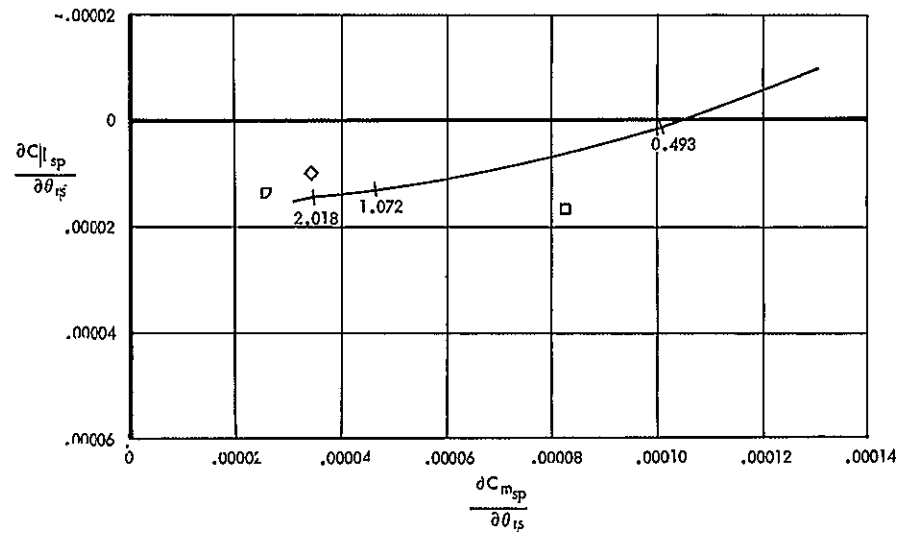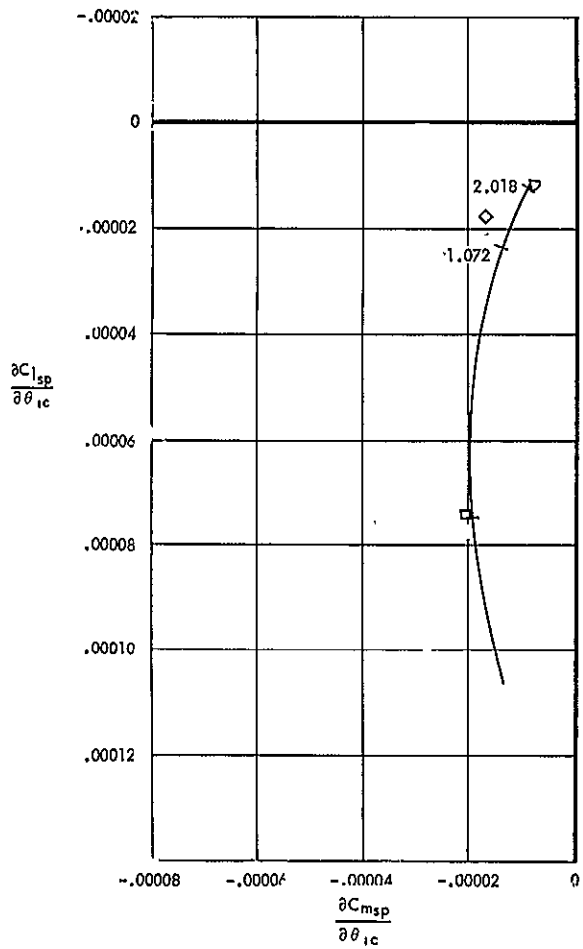
Figure 33. Swashplate Moment Derivatives Due to Cyclic Pitch - 90 Knots
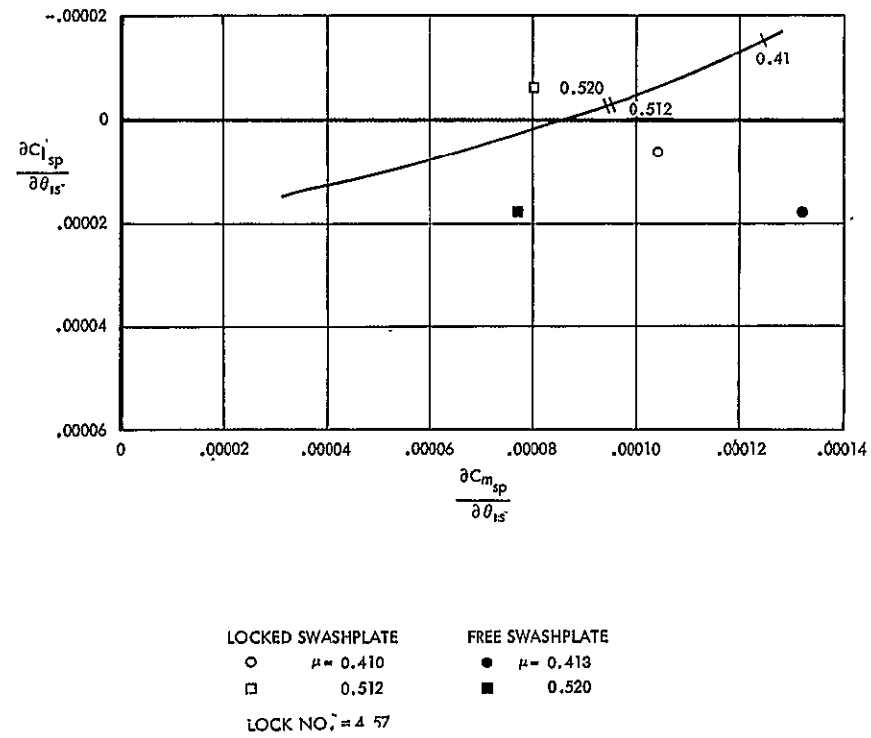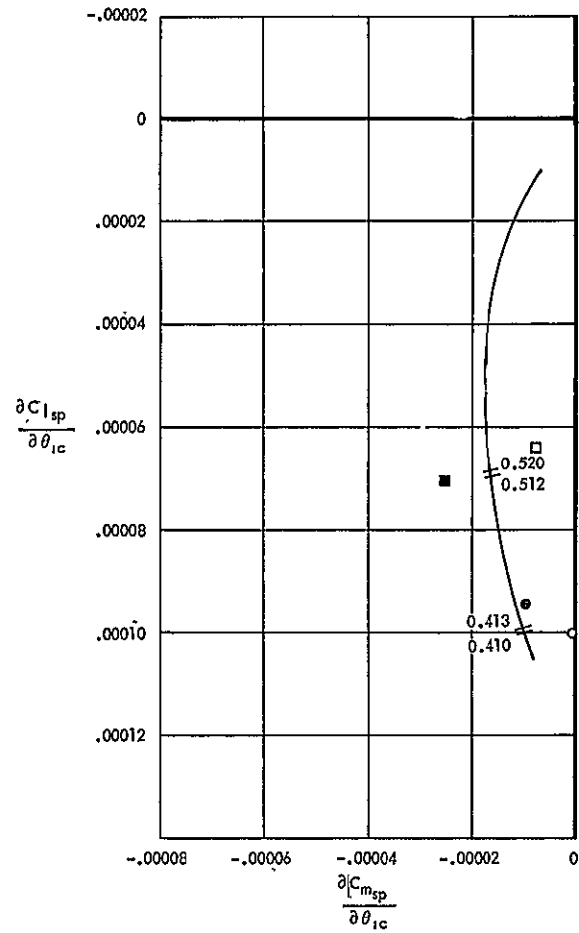
Figure 34.   Swashplate Moment Derivatives Due to Cyclic Pitch - 100 Knots
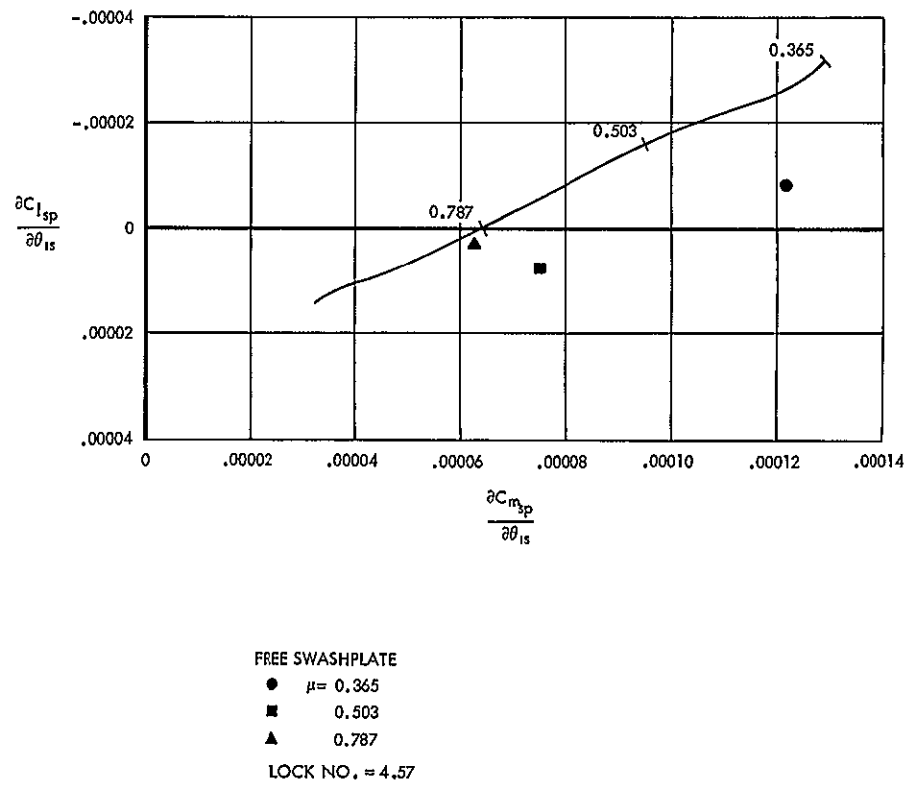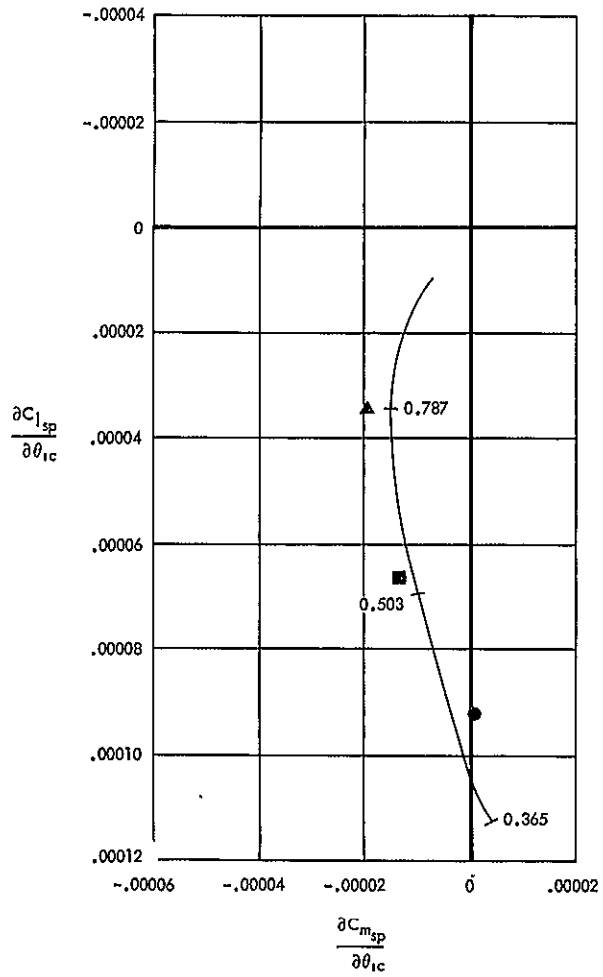
Figure 35. Swashplate Moment Derivatives Due to Cyclic Pitch - 120 Knots

The swashplate aeroelastic derivatives, in conjunction with the hub moment aeroelastic derivatives, determine the control moment effort required to apply pitch and roll moments and ultimately pitch and roll rates to the airframe.

The swashplate test data points display somewhat less regularity than the hub moment derivative data points, due in part to the smaller magnitude of the loads. The correlation is better at higher advance ratios and lower forward speeds.

The effects of rotating damping are not included in the theoretical swashplate derivatives of Figures 29 through 35, even though each of the four derivatives is influenced by rotating damping. However, if the derivatives are written in terms of the swashplate pitch and roll angles θ and ϕ, rotating damping appears in just two of the derivatives. The relationship between derivatives of swashplate tilt angles and derivatives of blade cyclic angles is:

$$
\begin{bmatrix}
\dfrac{\partial C_{m_{sp}}}{\partial \theta} & \dfrac{\partial C_{m_{sp}}}{\partial \phi} \\[2em]
\dfrac{\partial C_{l_{sp}}}{\partial \theta} & \dfrac{\partial C_{l_{sp}}}{\partial \phi}
\end{bmatrix}
=
\begin{bmatrix}
\dfrac{\partial C_{m_{sp}}}{\partial \theta_{1c}} & \dfrac{\partial C_{m_{sp}}}{\partial \theta_{1s}} \\[2em]
\dfrac{\partial C_{l_{sp}}}{\partial \theta_{1c}} & \dfrac{\partial C_{l_{sp}}}{\partial \theta_{1s}}
\end{bmatrix}
\begin{bmatrix}
\dfrac{\partial \theta_{1c}}{\partial \theta} & \dfrac{\partial \theta_{1c}}{\partial \theta} \\[2em]
\dfrac{\partial \theta_{1s}}{\partial \theta} & \dfrac{\partial \theta_{1s}}{\partial \phi}
\end{bmatrix}
$$

where:

$$
\begin{bmatrix}
\dfrac{\partial \theta_{1c}}{\partial \theta} & \dfrac{\partial \theta_{1c}}{\partial \phi} \\[2em]
\dfrac{\partial \theta_{1s}}{\partial \theta} & \dfrac{\partial \theta_{1s}}{\partial \phi}
\end{bmatrix}
=
\begin{bmatrix}
-.4347 & .7530 \\[2em]
.7530 & .4347
\end{bmatrix}
$$

Damping appears in the resultant off-diagonal derivatives, adding to $\partial C_{m_{sp}}/\partial \phi$ and subtracting from $\partial C_{l_{sp}}/\partial \theta$.
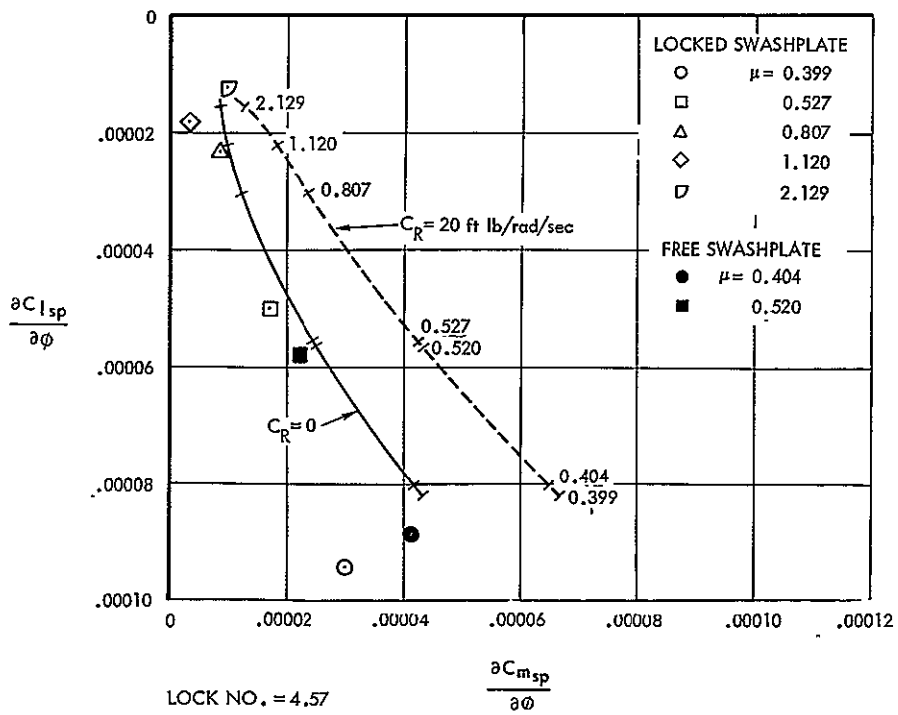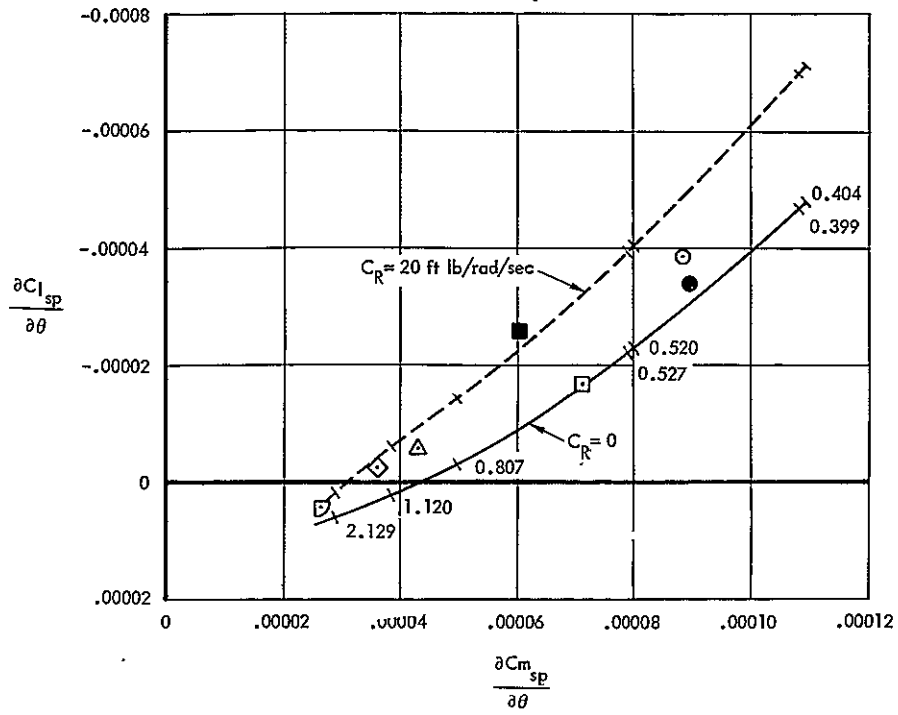
Figure 36.   Swashplate Moment Derivatives Due to Swashplate
Tilt Angles - 80 Knots, Lock No. - 4.57

The swashplate derivative coefficients in terms of swashplate tilt angles are shown on Figure 36 for the 80 knot forward speed condition. Curves with no rotating damping (relatable to Figure 32) and with 20 ft-lb/rad/sec of rotating damping are shown for illustrative purposes. The damping value chosen as representative of the tunnel model is 7 ft-lb/rad/sec.

The small value of rotating damping applicable to the tunnel model has little effect on the correlation between theory and test of the swashplate derivatives, in addition to being difficult to determine precisely. For these reasons, the rotating damping effect is ignored in the presentation of most of the swashplate moment derivatives.

Lift derivatives due to blade cyclic pitch. - Analytically determined lift coefficients, due to changes in the blade cyclic angles θ_{1c} and θ_{1s}, and plotted versus advance ratio and the square of its inverse, are shown in Figure 37. Coefficient curves are shown for various forward speeds.

Theoretical and experimental values are shown on Figures 38 through 40 at forward speeds of 50, 70, and 90 knots; also plotted as functions of advance ratio.

The test points tend to be slightly lower than the analytical curves for both derivatives. The correlation is about the same at all advance ratios.

Derivatives due to blade collective pitch and rotor angle of attack. - Analytical nondimensionalized derivatives of hub moment, swashplate moment, and thrust due to the collective blade angle are shown on Figures 41 through 43. Corresponding derivatives due to rotor angle of attack are given on Figures 44 through 46. Derivatives along lines of either constant forward speed or advance ratio are indicated. The thrust derivatives for various forward speeds are presented as the dependent variables of advance ratio and the square of its inverse.

Figure 41 shows analytical derivatives of hub rolling and pitching moments due to the blade collective feathering angle. At high advance ratio, collective angles produce mainly rolling moments. At the higher rotor speeds, attendant to high forward speeds and low advance ratios, collective angles
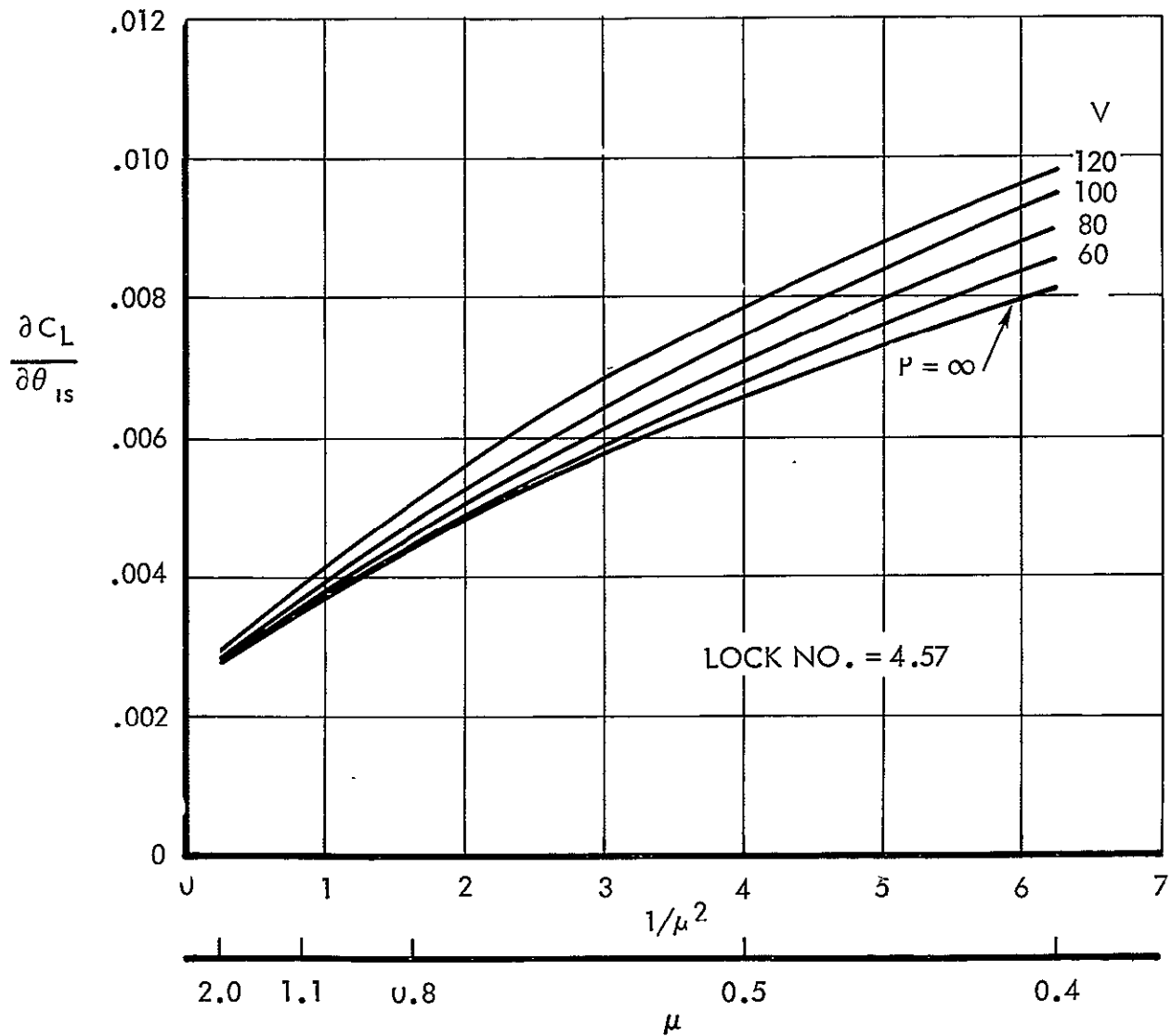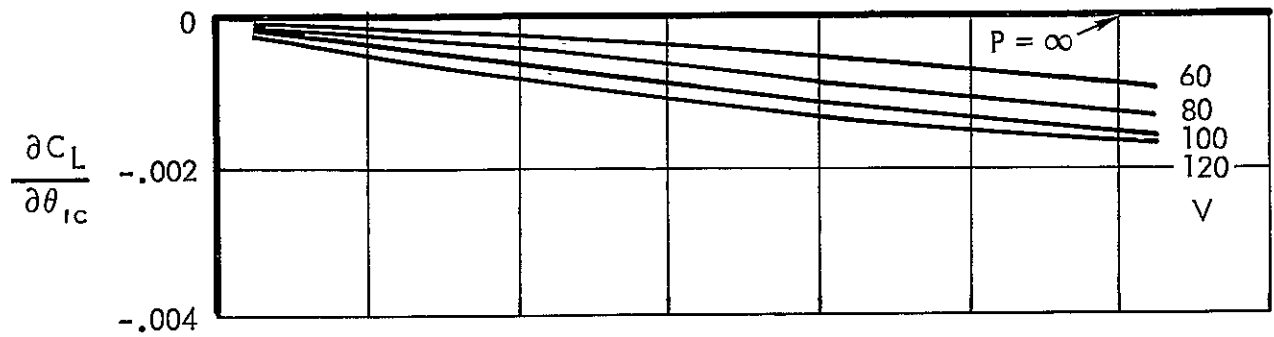
Figure 37. Theoretical Lift Derivatives Due to Cyclic Pitch
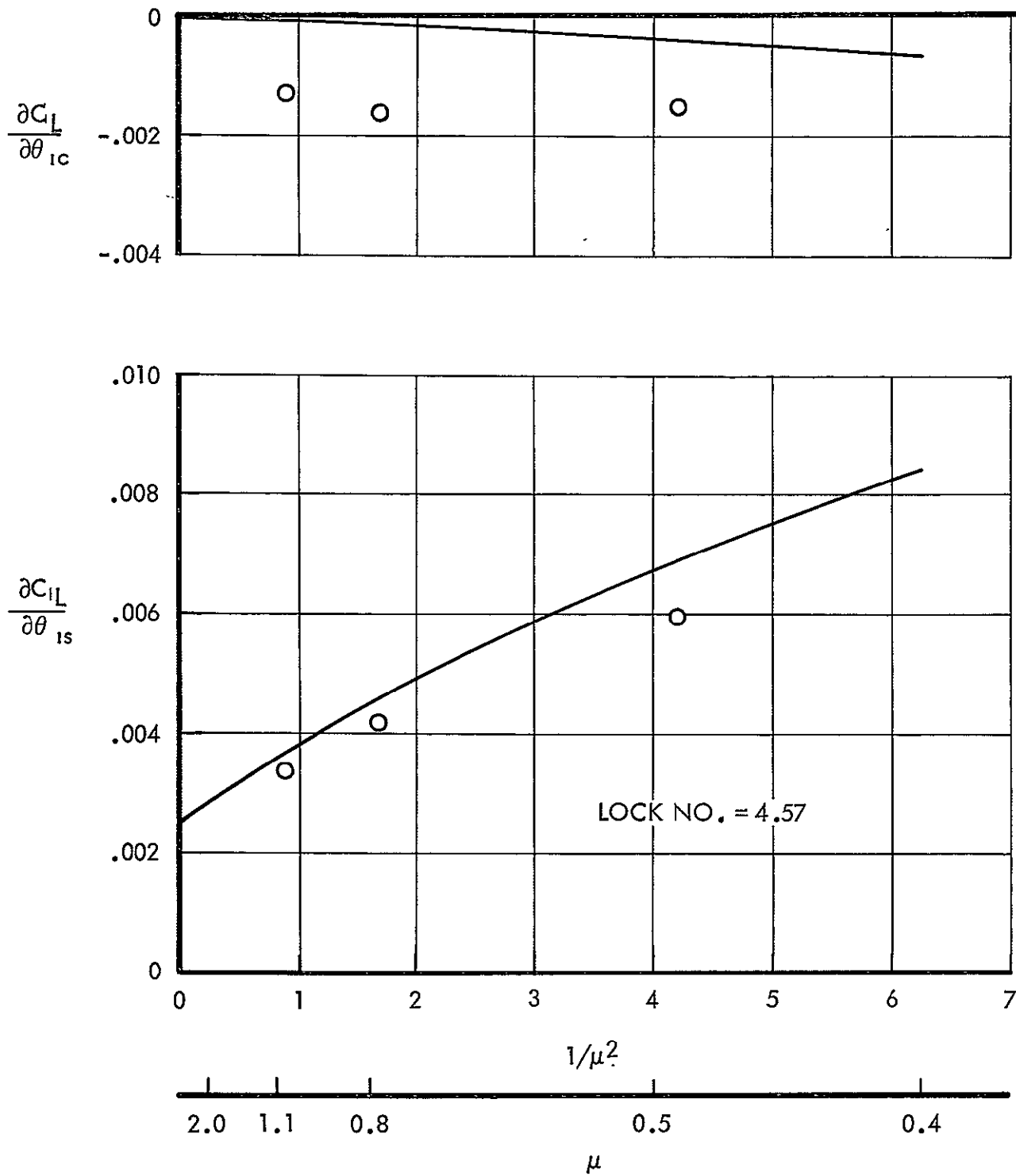
Figure 38. Lift Deriviatives Due to Cyclic Pitch, Test
and Analysis at 50 Knots, Locked Swashplate

111
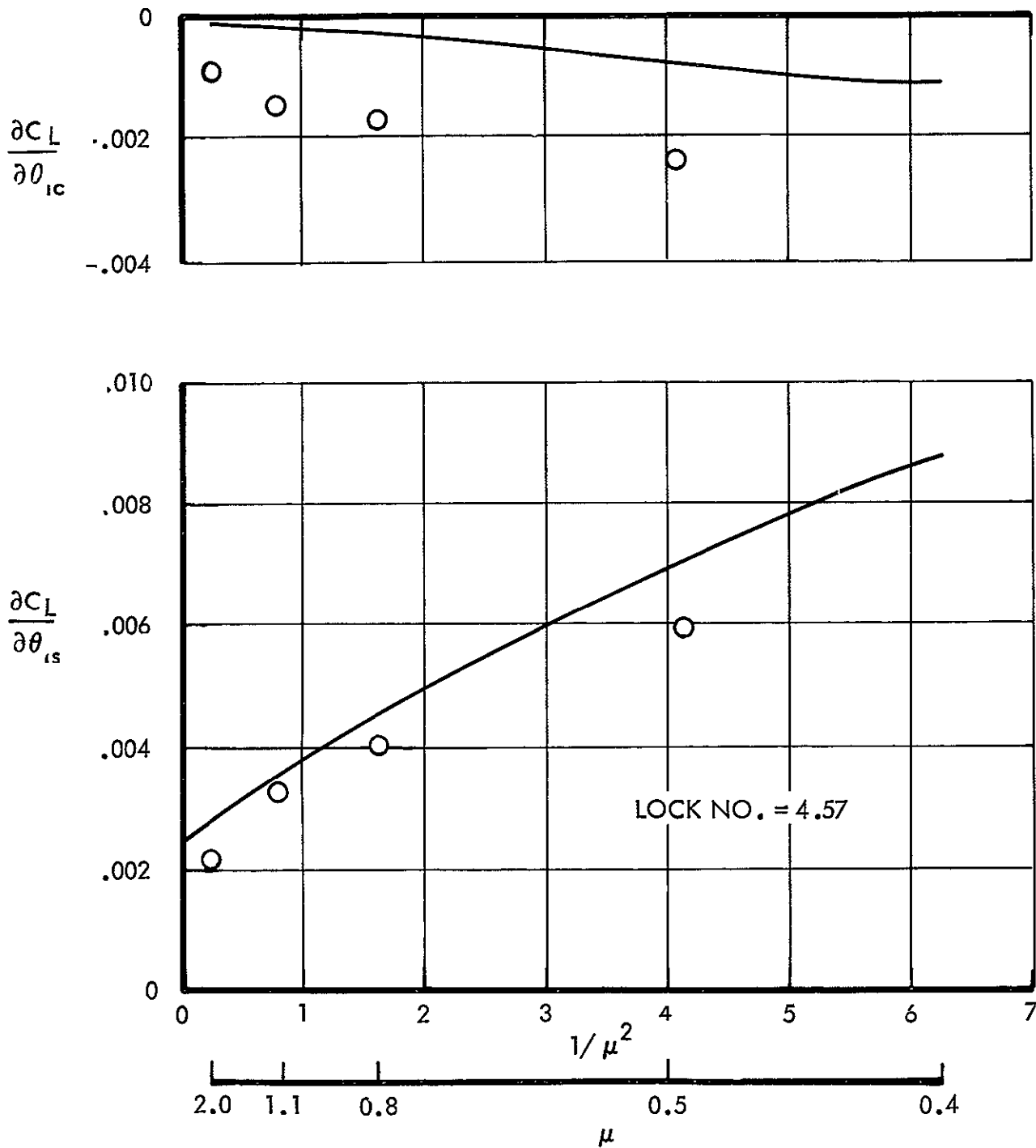
Figure 39.   Lift Derivatives Due to Cyclic Pitch Angles, Test
and Analysis at 70 Knots, Locked Swashplate
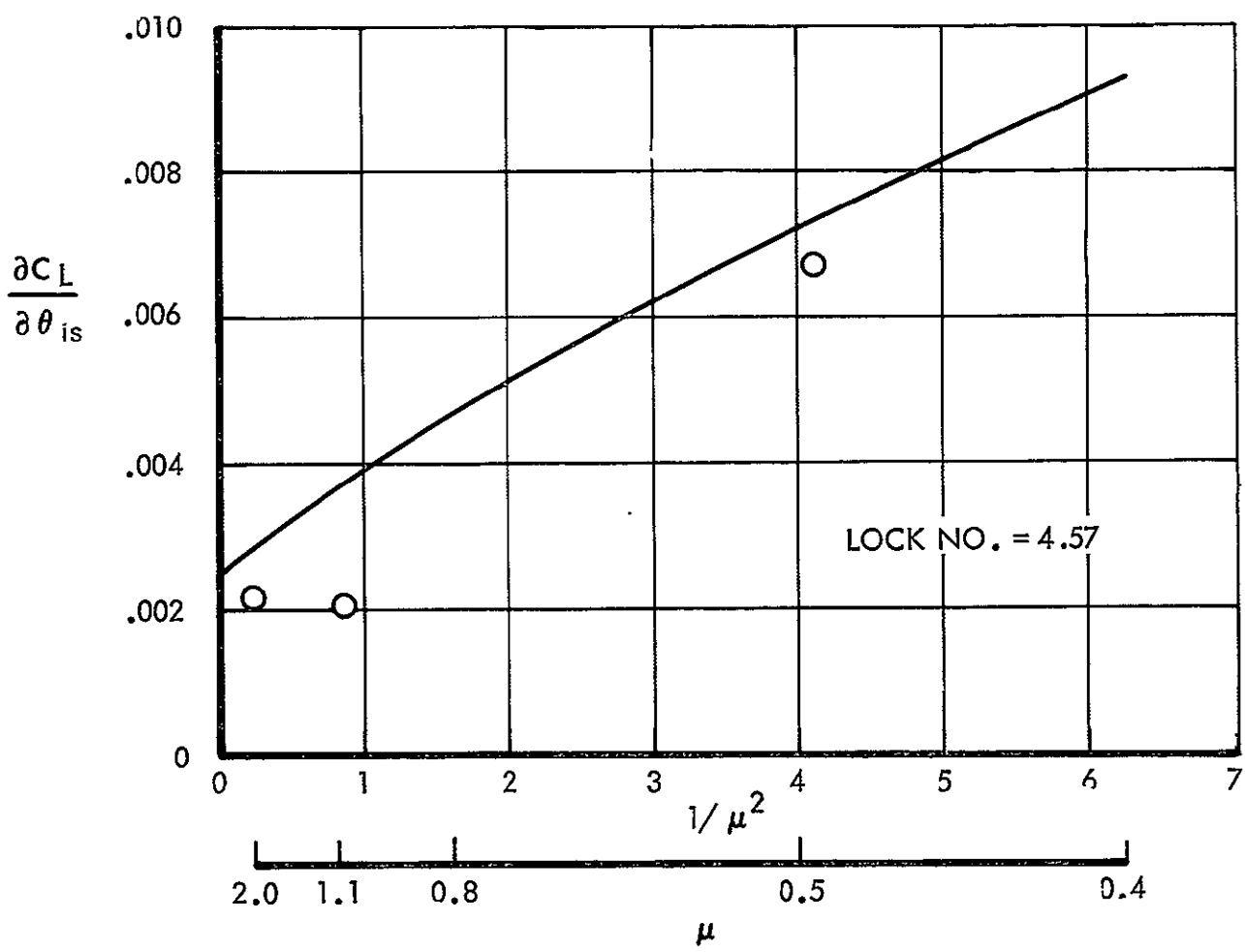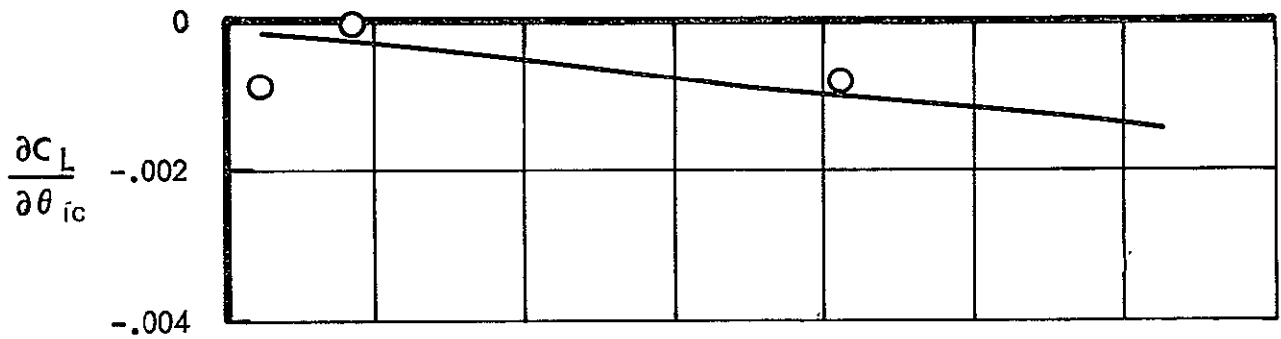
Figure 40. Lift Derivatives Due to Cyclic Pitch Angles, Test and Analysis at 90 Knots, Locked Swashplate
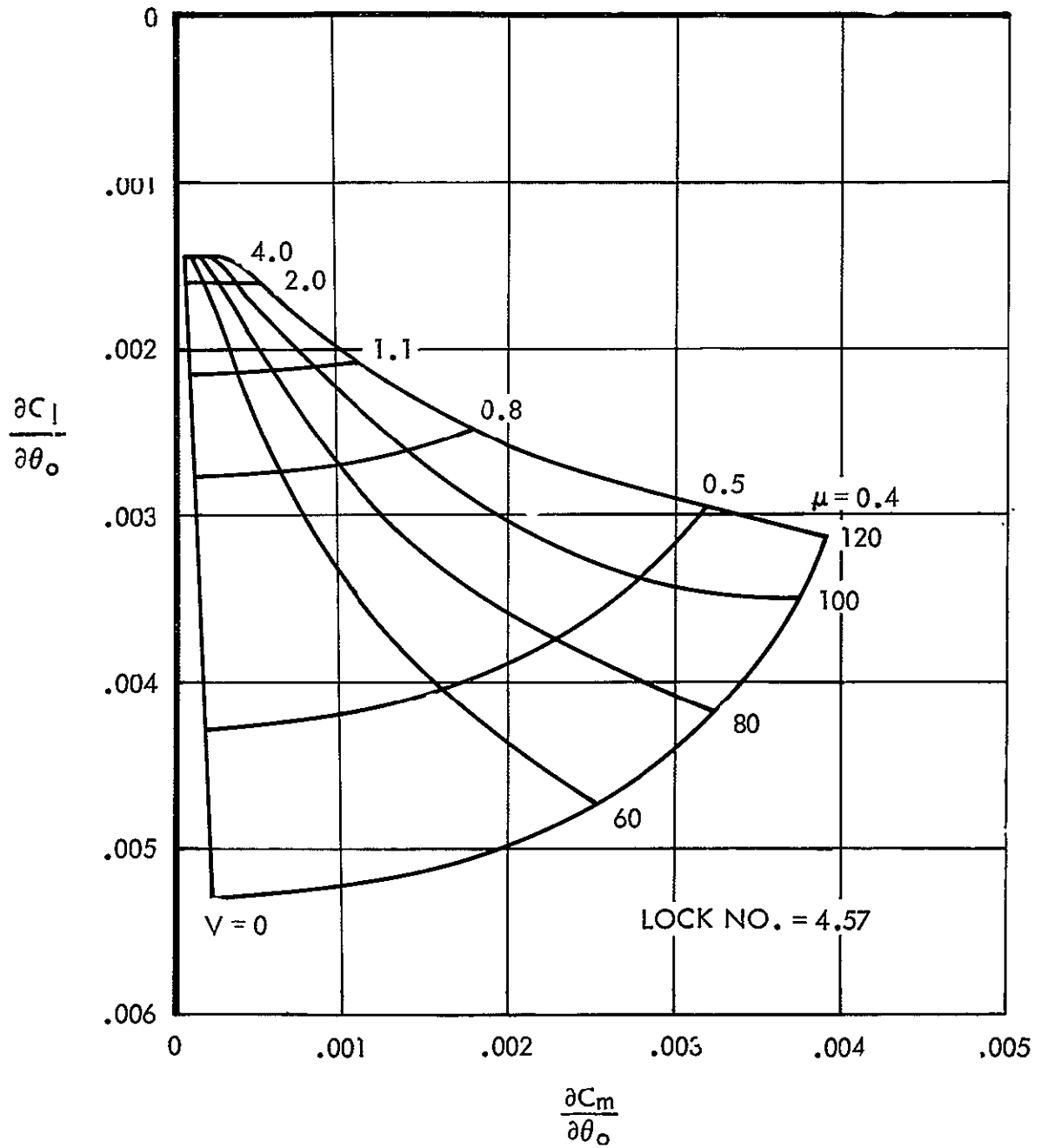
Figure 41. Analytically Derived Hub Moment Derivatives Due To Collective Pitch
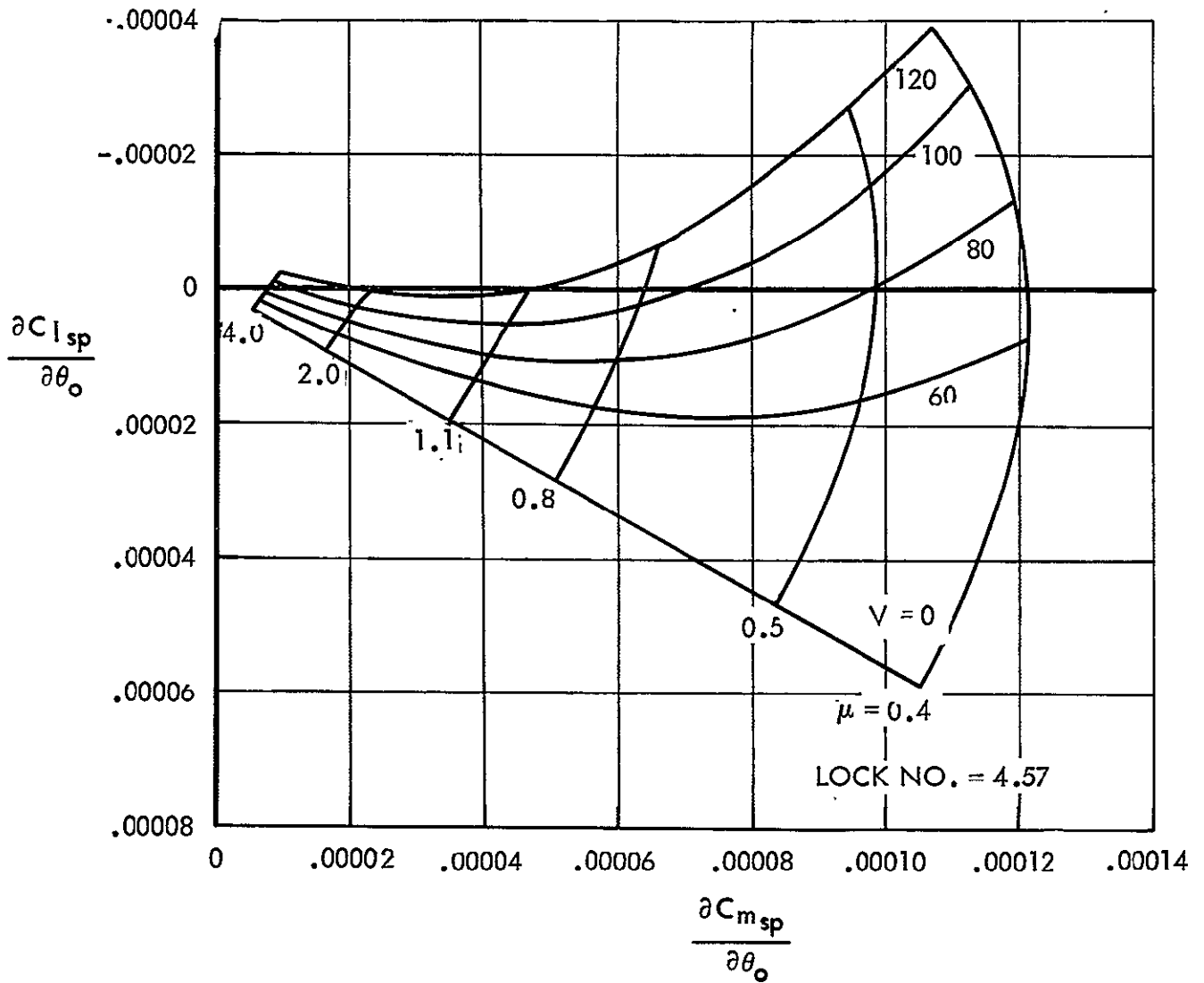
Figure 42. Analytically Derived Swashplate Moment Derivatives
Due To Collective Pitch
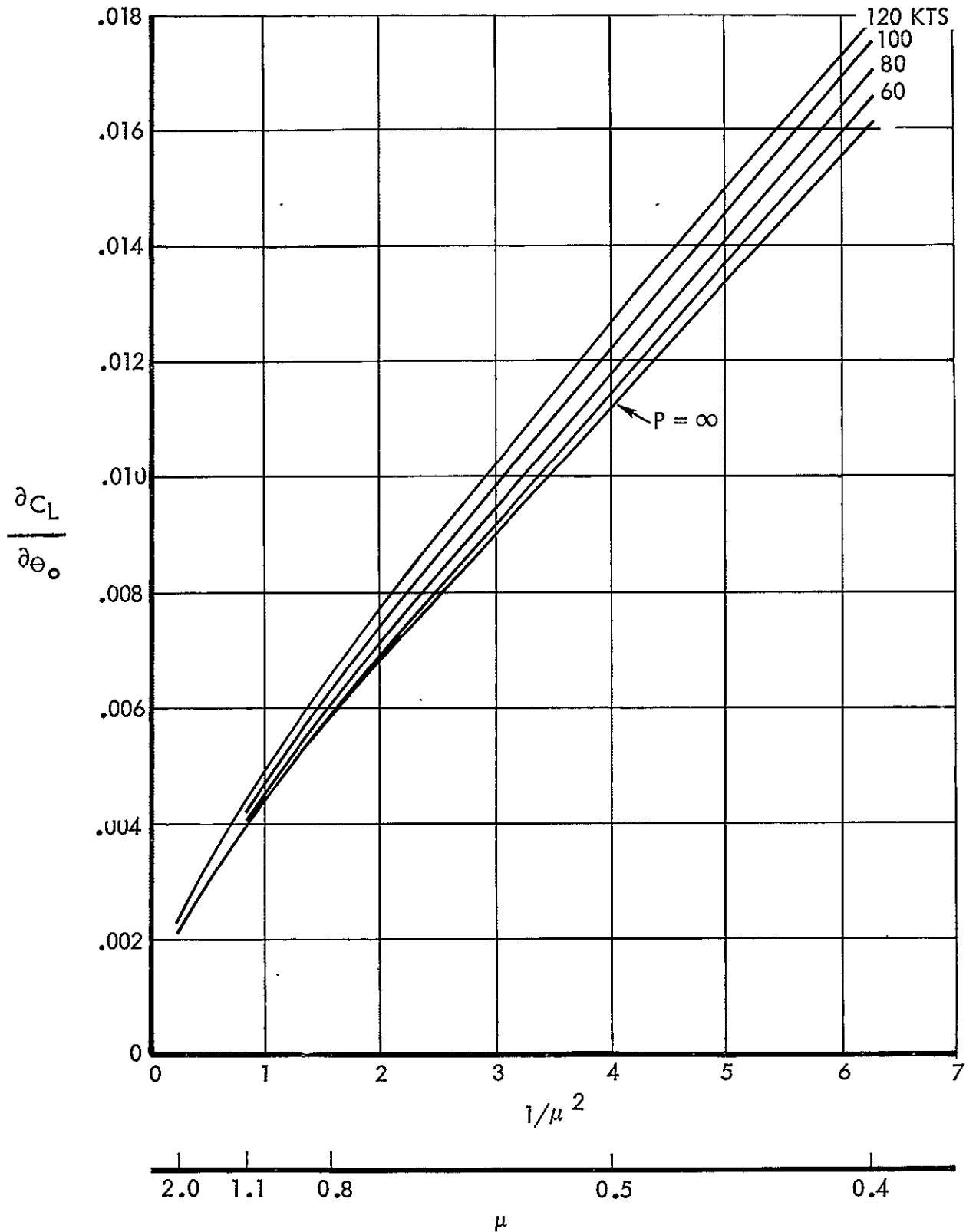
Figure 43. Analytically Derived Lift Derivatives Due To
Collective Pitch Angle
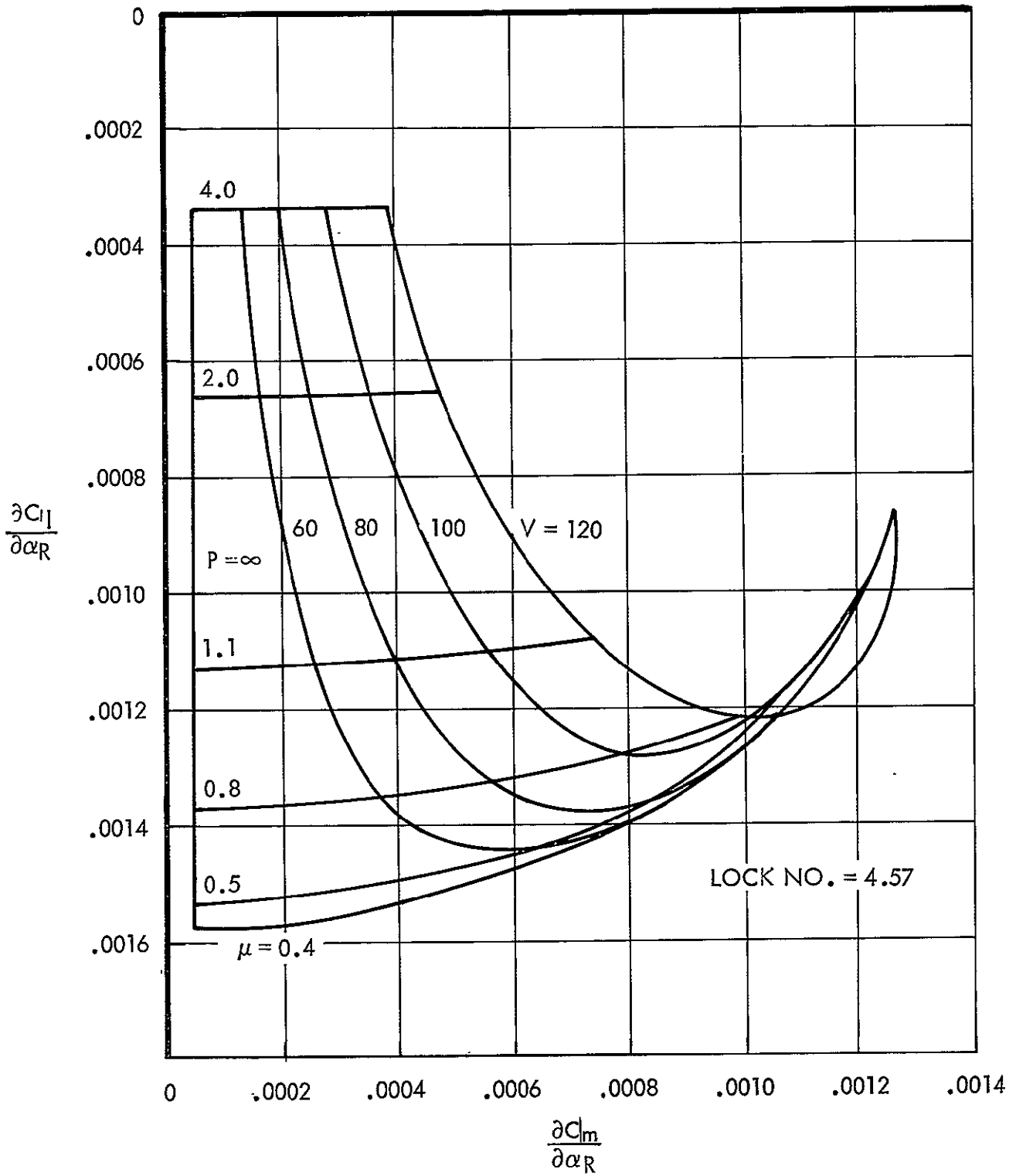
Figure 44. Analytically Derived Hub Moment Derivatives Due To Rotor Angle Of Attack

117
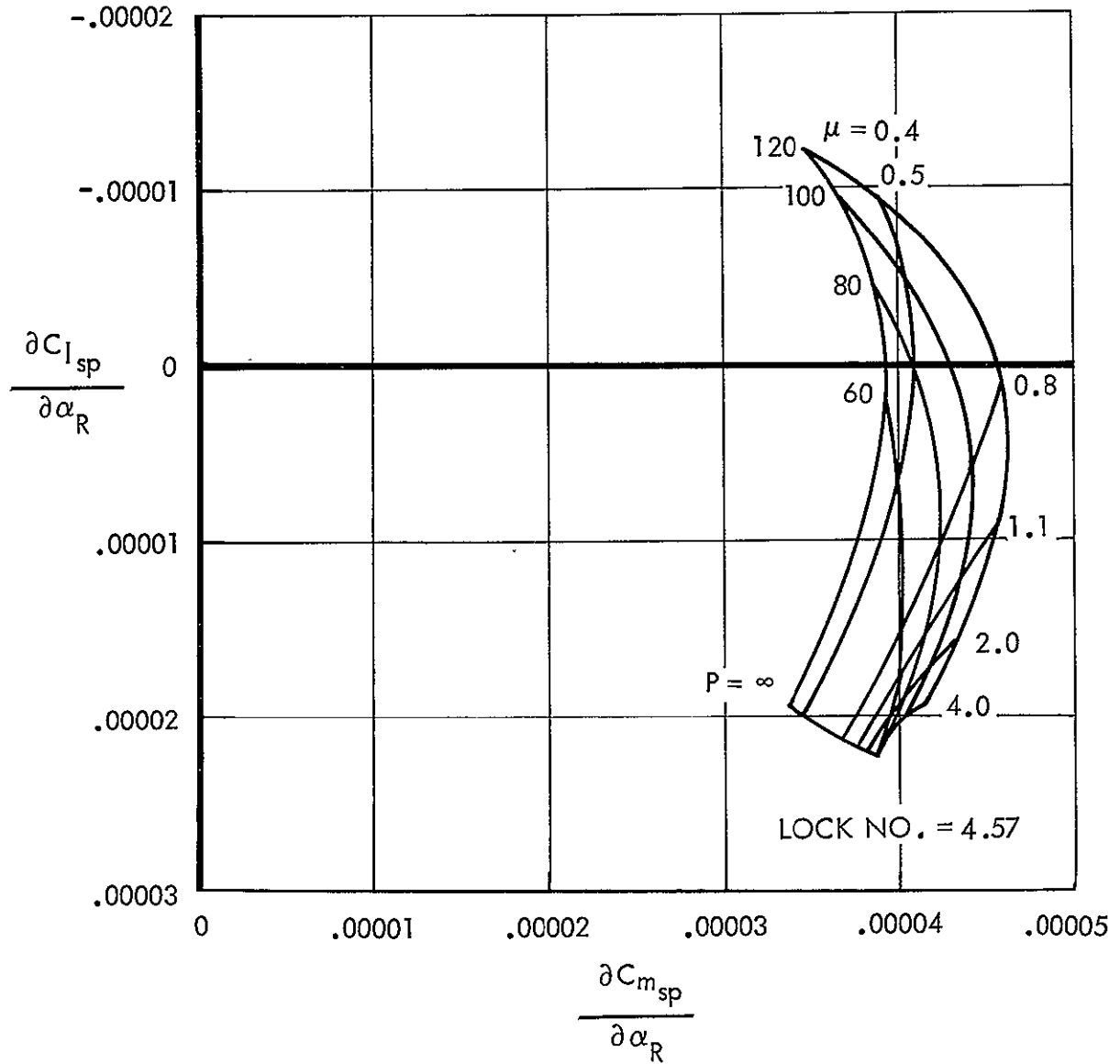
Figure 45. Analytically Derived Swashplate Moment Derivatives Due To Rotor Angle Of Attack

118
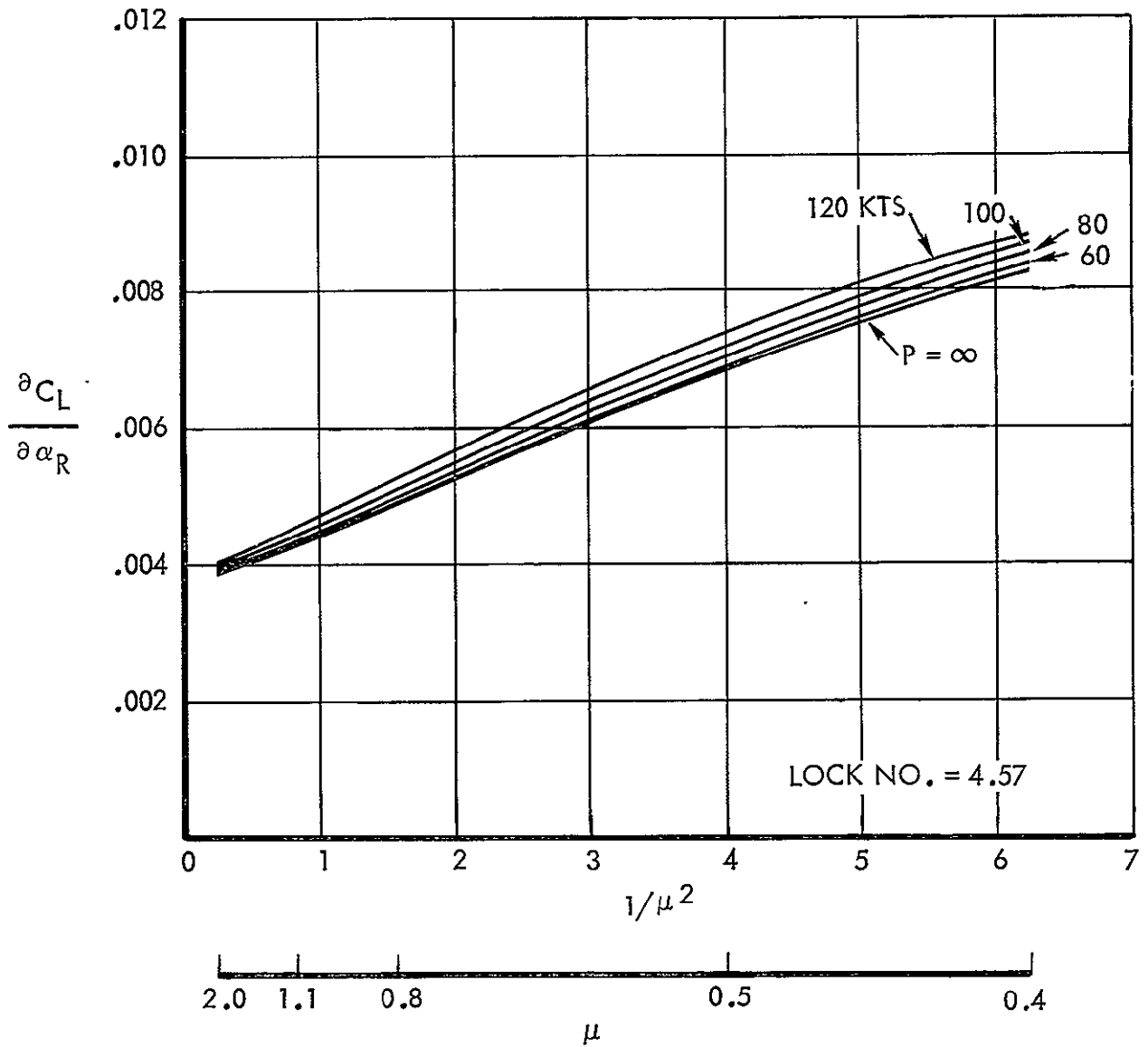
Figure 46. Analytically Derived Lift Derivatives Due to Rotor Angle Of Attack

mainly influence hub pitching moments. This figure is similar to that part of 2 which shows hub moments due to the blade cyclic angle θ_{1s}. At high advance ratios, collective angle is more effective in controlling hub rolling moments than is θ_{1s}.

The swashplate moment derivatives of blade collective angles are shown in Figure 42. The figure is rotated 60° relative to the hub moment derivatives plot (Figure 41) due to the cant angle Ψ_0 which rotates swashplate moments relative to hub moments.

The derivative of lift due to collective pitch is shown in Figure 43. This derivative varies little with forward speed but strongly with advance ratio. At advance ratios above about 1.0, the cyclic angle θ_{1s} is more effective in producing lift than is the collective angle. Figure 37 shows lift due to θ_{1s}.

Hub moments resulting from unit changes in rotor angle of attack are shown on Figure 44. The hub moments vary relatively little with advance ratio and forward speed compared with the loads produced by changes in blade feathering angles. Rolling moment is seen to increase with decreasing advance ratio at low rotor speeds. However, at high rotor speeds, a decrease in advance ratio lowers hub rolling moments.

The swashplate moments dependent on unit changes in rotor angle of attack are shown in Figure 45. Changes in moments with variations in forward speed and advance ratio are small when compared with the moments resulting from changes in blade feathering angles.

Lift produced by the rotor angle of attack is presented in Figure 46. Changes in forward speed have little effect on the nondimensionalized derivative. This derivative is similar to the lift derivative due to θ_{1s}, Figure 37.

Trim Cyclic Angles

The experimental trim angles presented here are based on conditions attained during testing. Since it was not practical to attain "flight trim" conditions in the wind tunnel, test "trim points" are calculated from test

data derivatives presented in preceding paragraphs in combination with calculated moments on hub and swashplate corresponding to blade cyclic angles equal to zero.

Hub trimmed cyclic angles. - The blade cyclic pitch angles that are required to produce zero mean hub moments during steady-state operation are defined as the hub trimmed cyclic angles. The applicable test conditions were attained in the locked-swashplate mode of operation, in which test control operator applied inputs necessary to determine a trimmed condition at the hub.

Analytically determined trim angles are shown in Figures 3, 47 and 48. The effect of varying forward speed at constant advance ratio, is shown on Figure 3 for a collective angle fixed at 1.5 degrees. Increase in forward speed at constant advance ratio causes reduction of the trim angle θ_{1c} with little effect on θ_{1s}; this effect is due to rotor centrifugal flattening. The lateral cyclic θ_{1s} is more a function of advance ratio.

Figure 47 illustrates the effect of the collective angle on the trim cyclic angles at a forward speed of 120 knots and a fixed rotor angle of attack. Changes in collective angle at constant advance ratio mainly influences the lateral trim angle θ_{1s}, as might be expected.

The effect on trim of changing rotor angle of attack is shown in Figure 48 , at 120 knots and at a collective feathering angle of 0 degrees. Changes in angle of attack mainly change the θ_{1s} cyclic angle.

Analytical and theoretical trim angles are compared in Figures 49 through 55. The figures show data for a forward speeds ranging from 50 to 120 knots. The test trim angles are based on both locked- and free-swashplate data, although the hub trim data used were obtained primarily in the locked mode of operation. A zero rotor angle of attack and 1.5 degree of collective angle are used.

The agreement between test and theory for the cyclic θ_{1s} is satisfactory. However, the test data is consistently higher than the analytical results, generally by about 2 to 3 degrees, for the θ_{1c} cyclic angles. Several reasons are suggested for the discrepancy. Blade spanwise flow was neglected in the analysis; also neglected was the deflection of the flow through the rotor caused
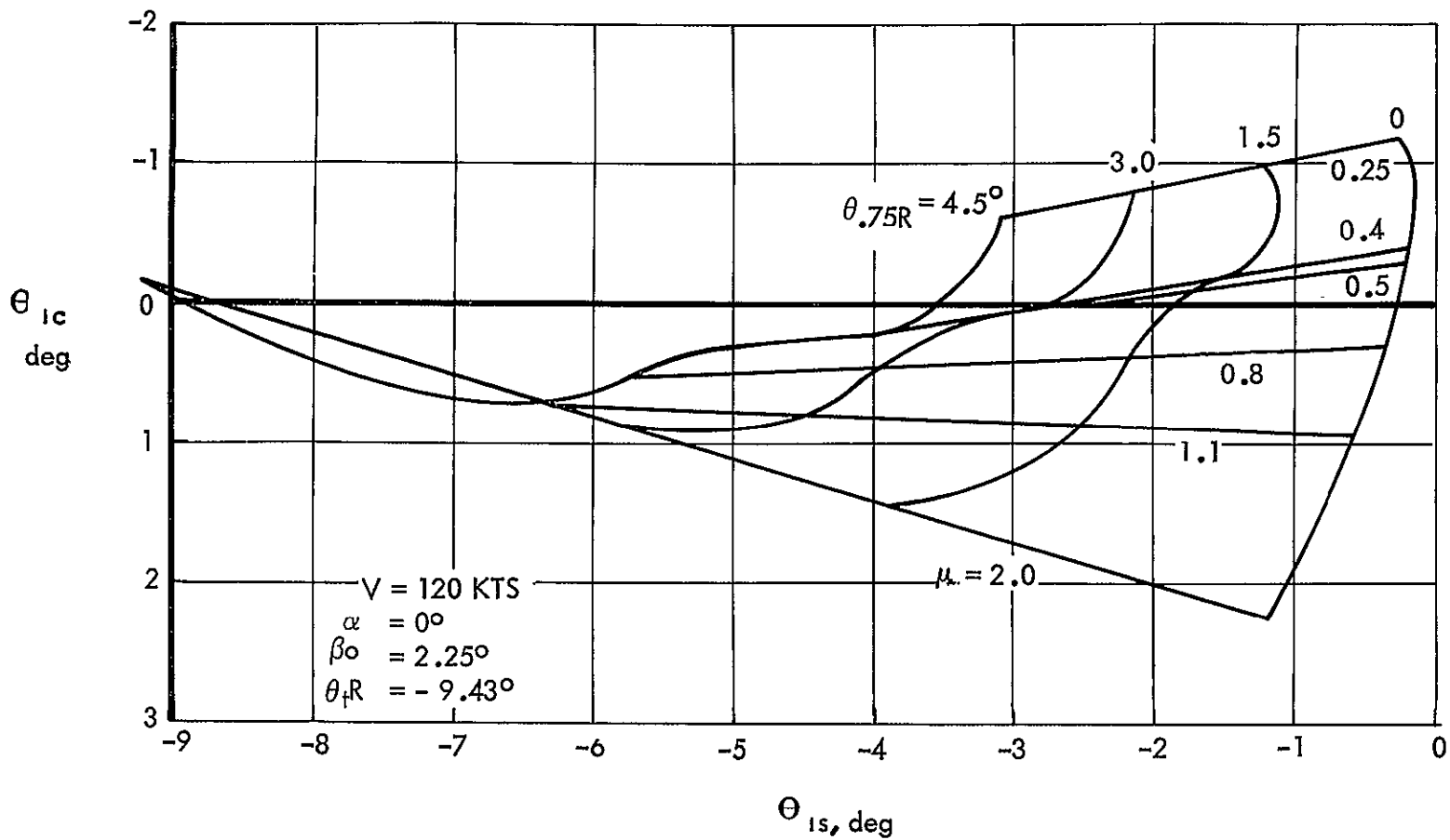
Figure 47. Analytically Derived Cyclic Pitch Angles For Hub Moment
Trimmed Condition, Effect Of Collective Angle
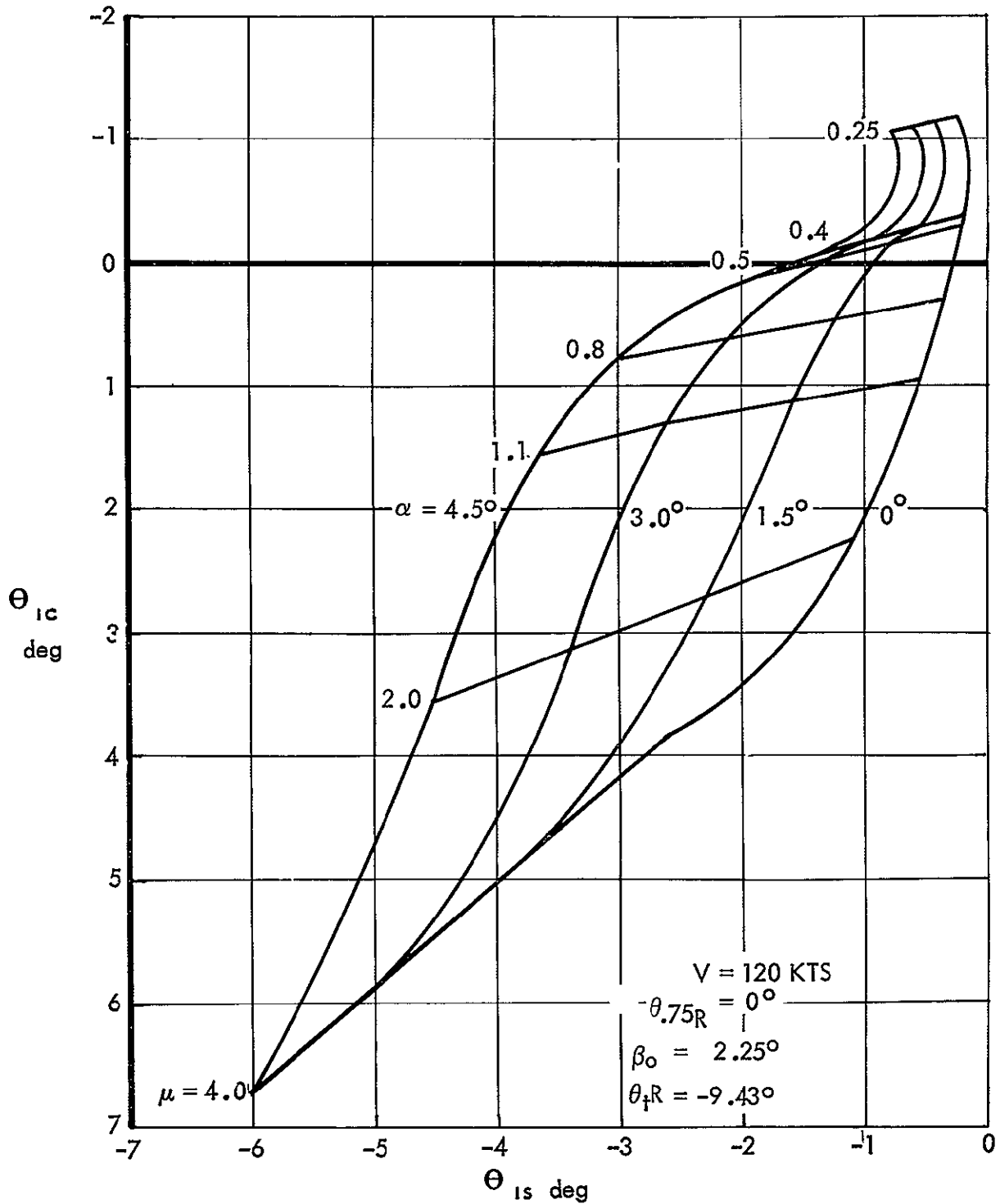
Figure 48. Analytically Derived Cyclic Pitch Angles For Hub Moment
Trimmed Conditions, Effect Of Rotor Angle Of Attack
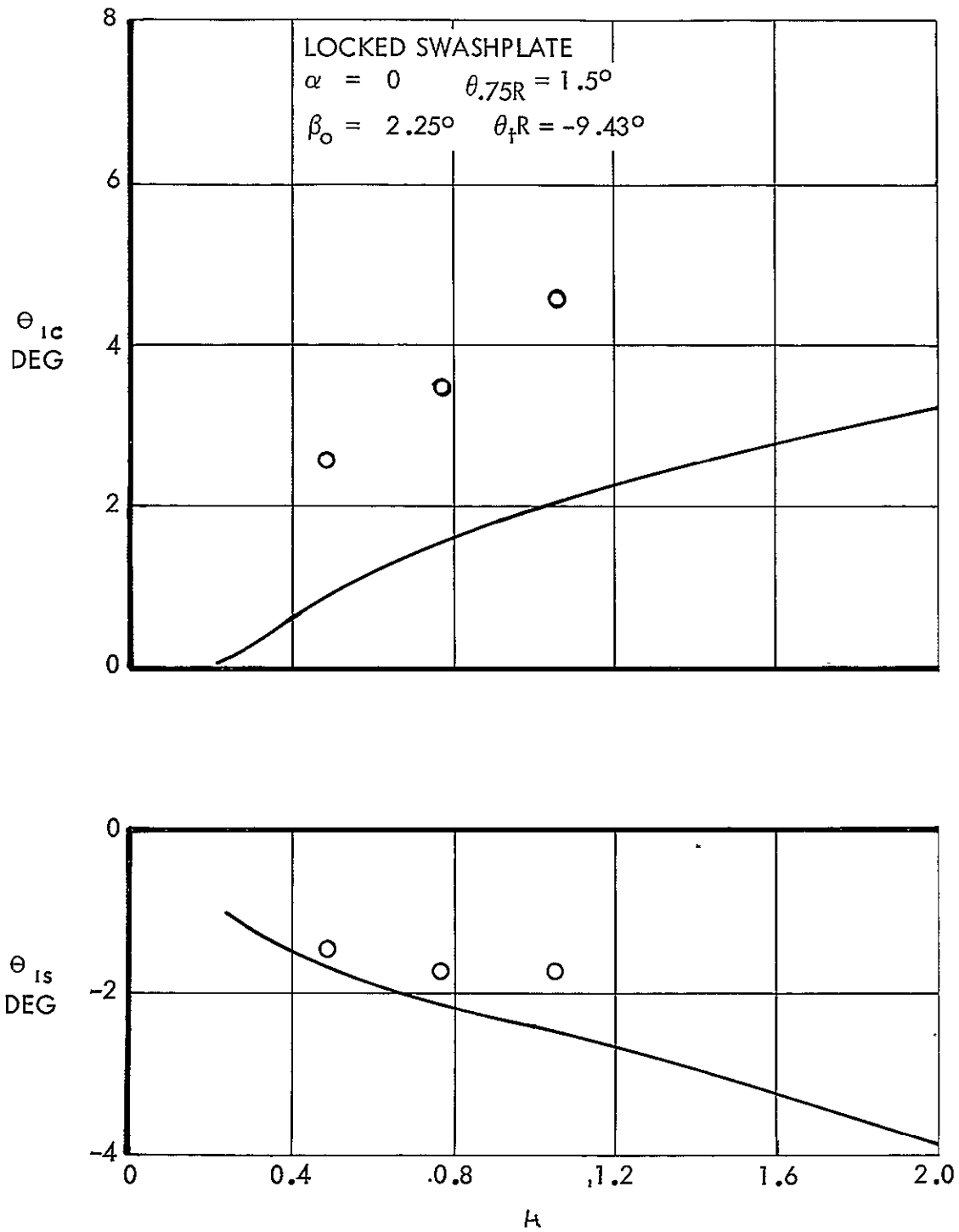
Figure 49. Cyclic Pitch Angles For Hub Moment Trimmed Condition - 50 Knots

LOCKED SWASHPLATE
$\alpha = 0$ $\theta_{.75R} = 1.5°$
$\beta_0 = 2.25°$ $\theta_1 R = -9.43°$
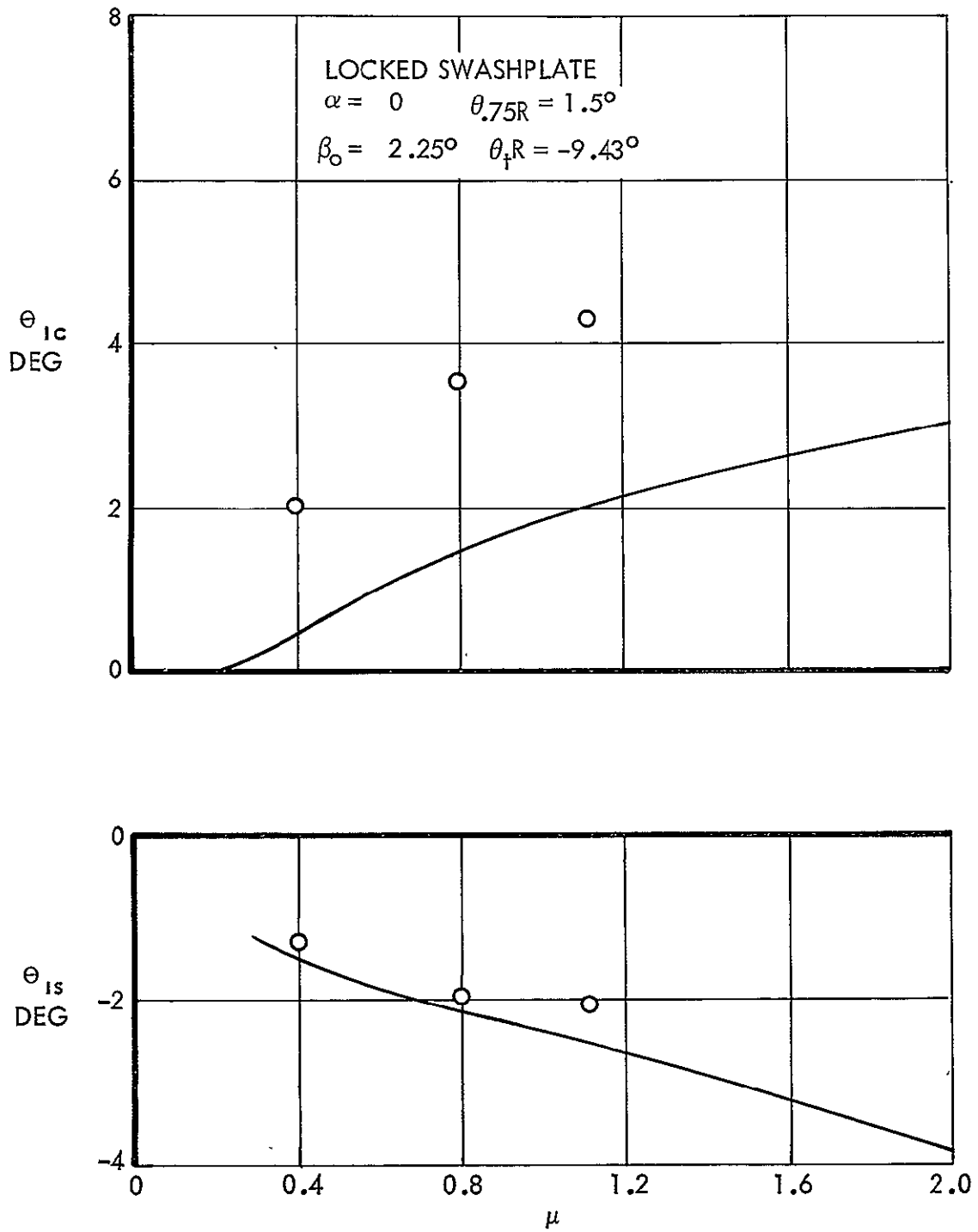
Figure 50. Cyclic Pitch Angles For Hub Moment Trimmed Condition - 60 Knots
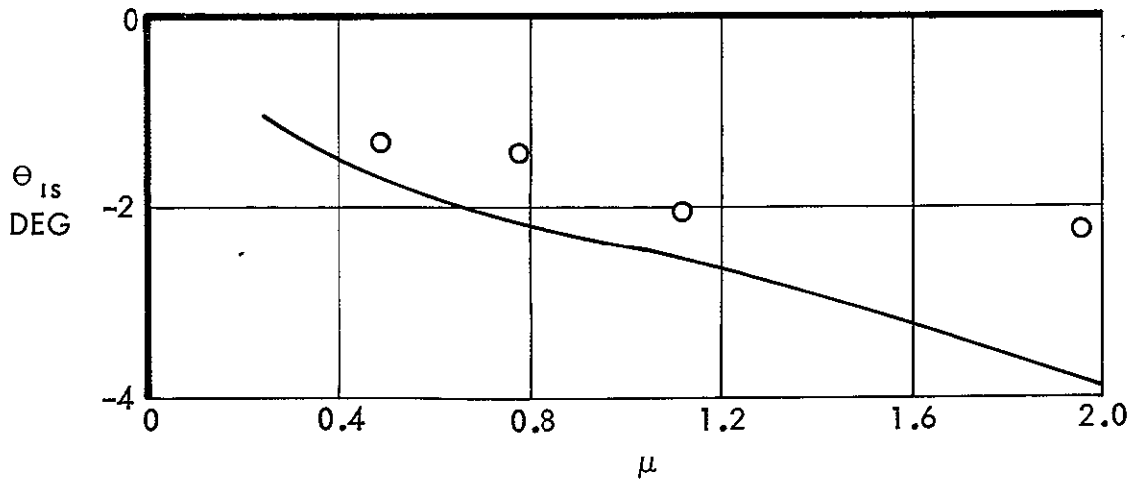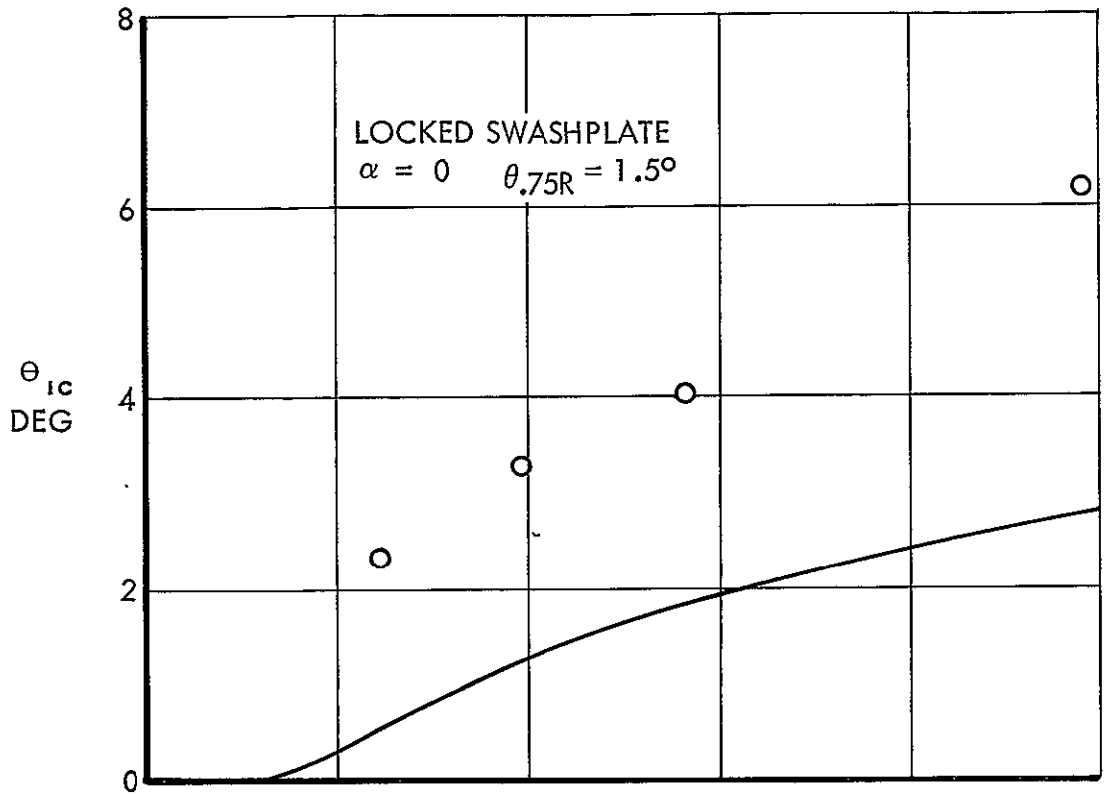
Figure 51. Cyclic Pitch Angles For Hub Moment Trimmed Condition - 70 Knots
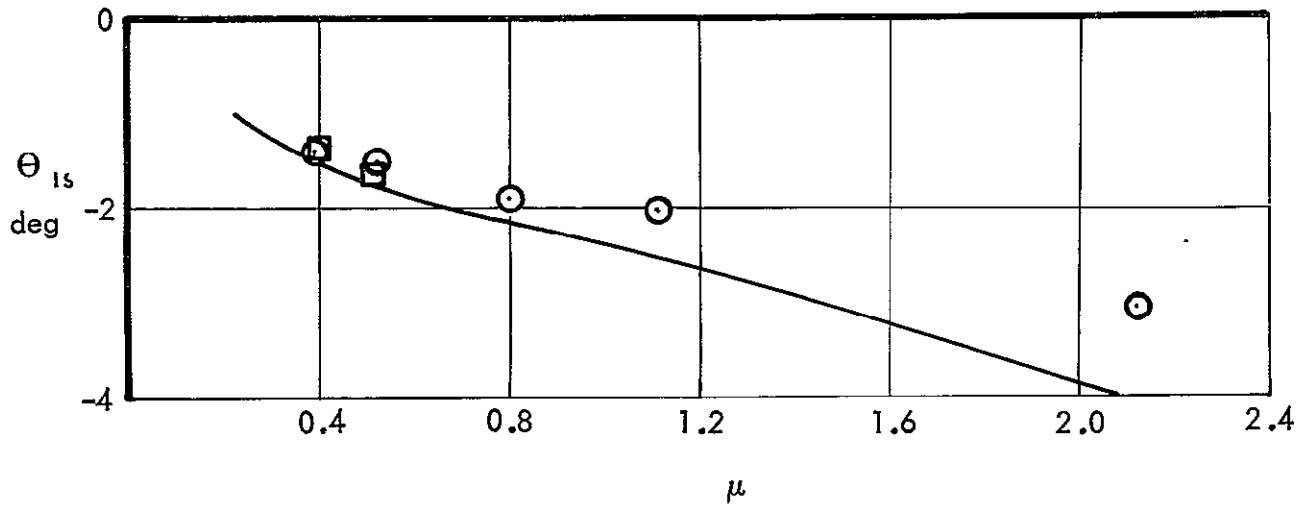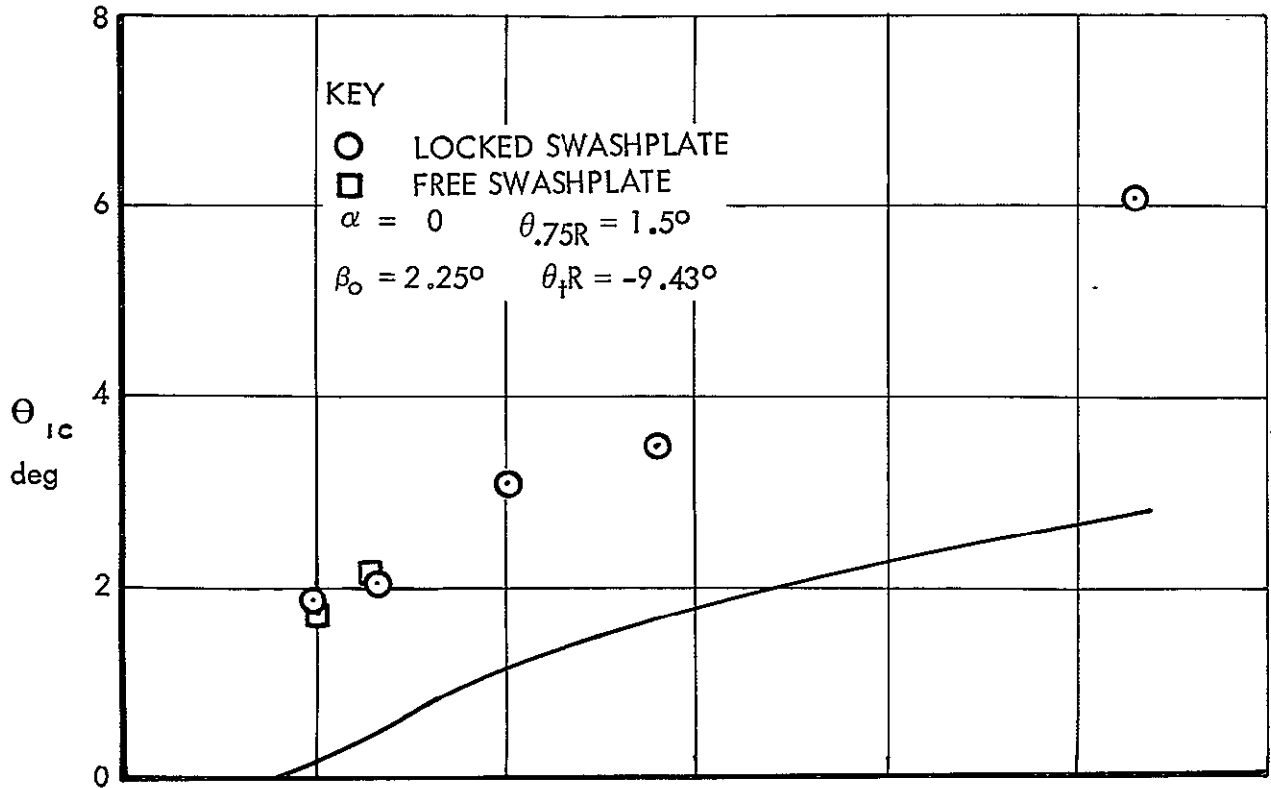
Figure 52. Cyclic Pitch Angles For Hub Moment Trimmed Condition - 80 Knots

127

LOCKED SWASHPLATE
$\alpha = 0$ $\theta_{.75R} = 1.5°$
$\beta_o = 2.25°$ $\theta_t R = -9.43°$
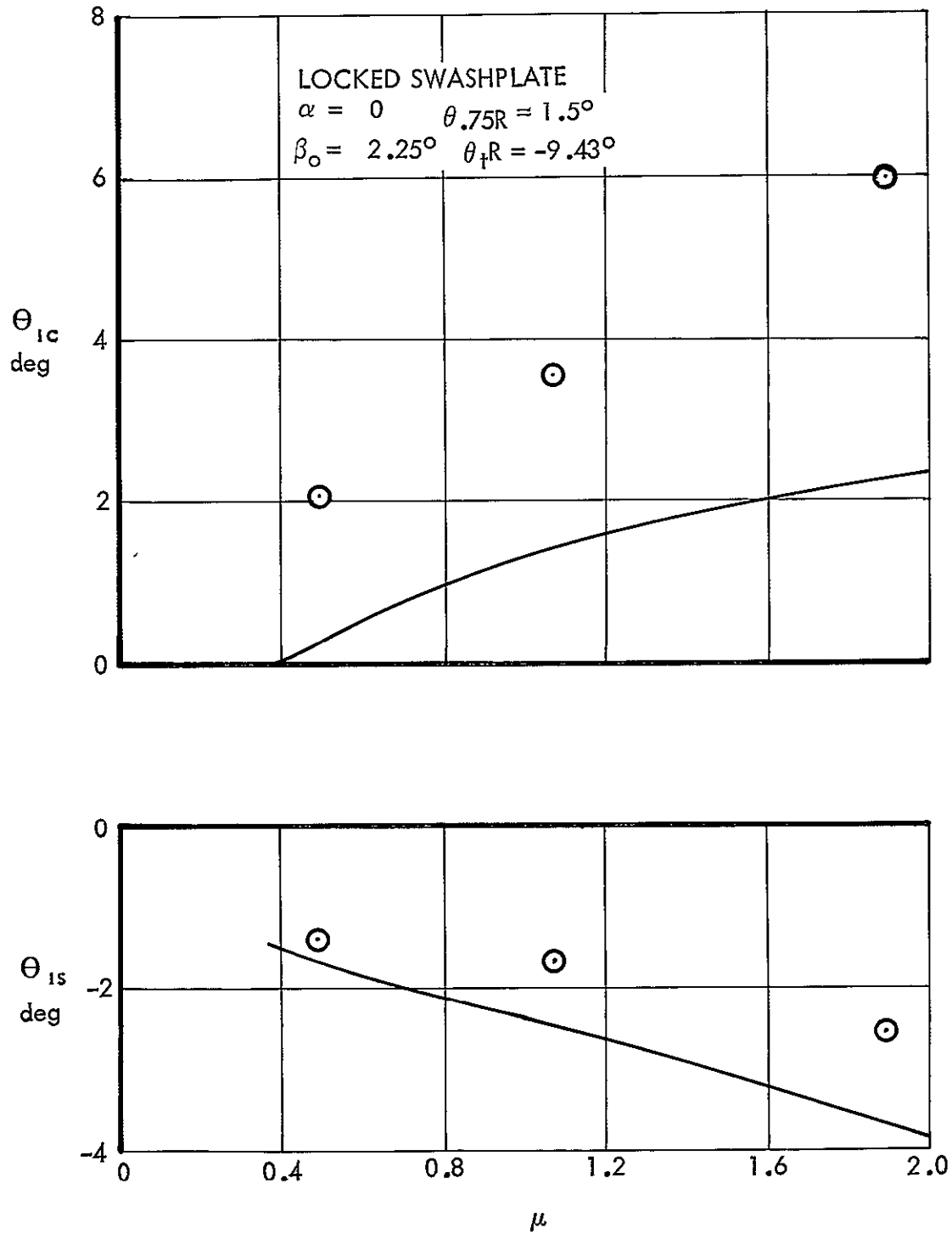
Figure 53. Cyclic Pitch Angles For Hub Moment Trimmed Condition - 90 Knots
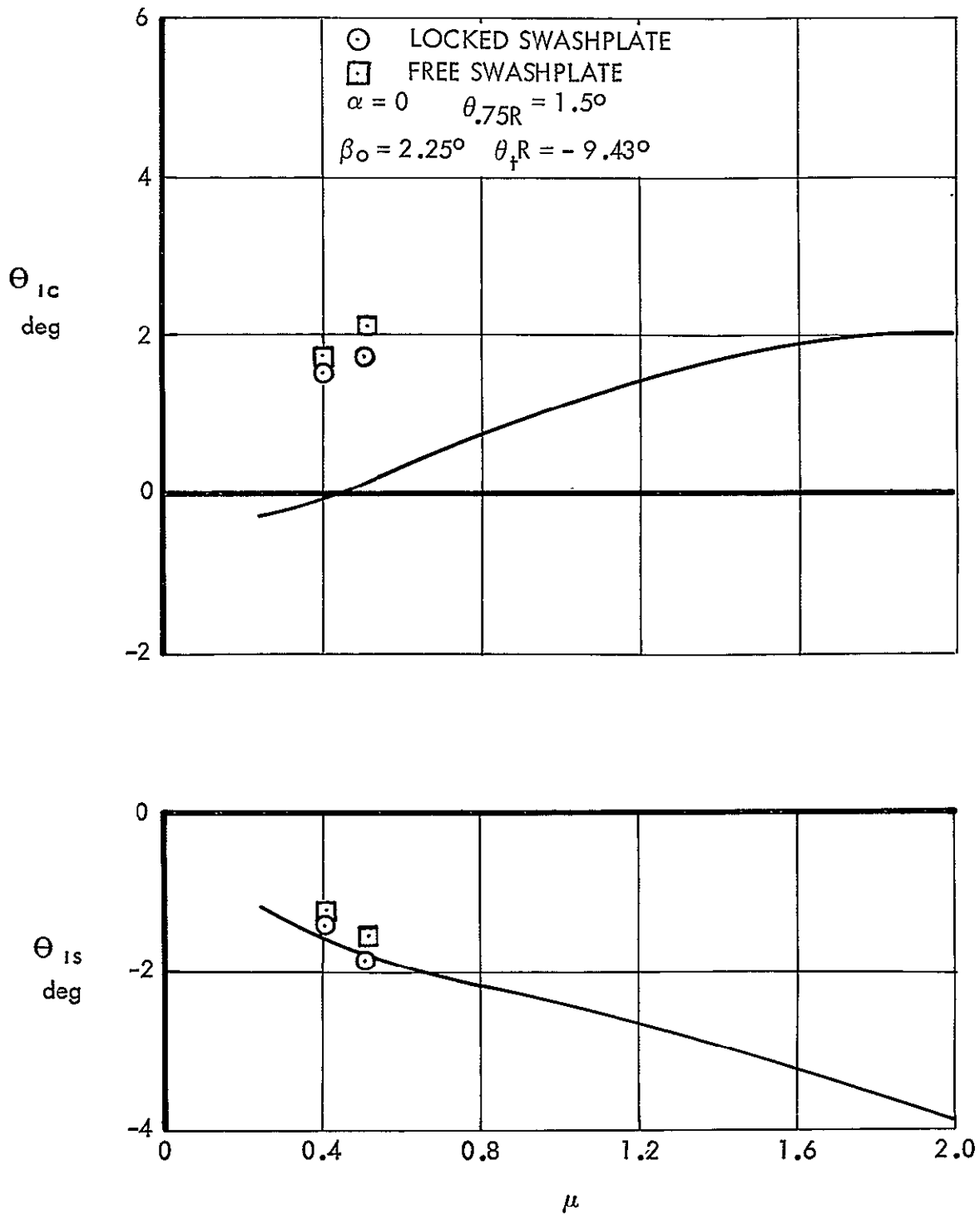
Figure 54. Cyclic Pitch Angles For Hub Moment Trimmed Condition - 100 Knots
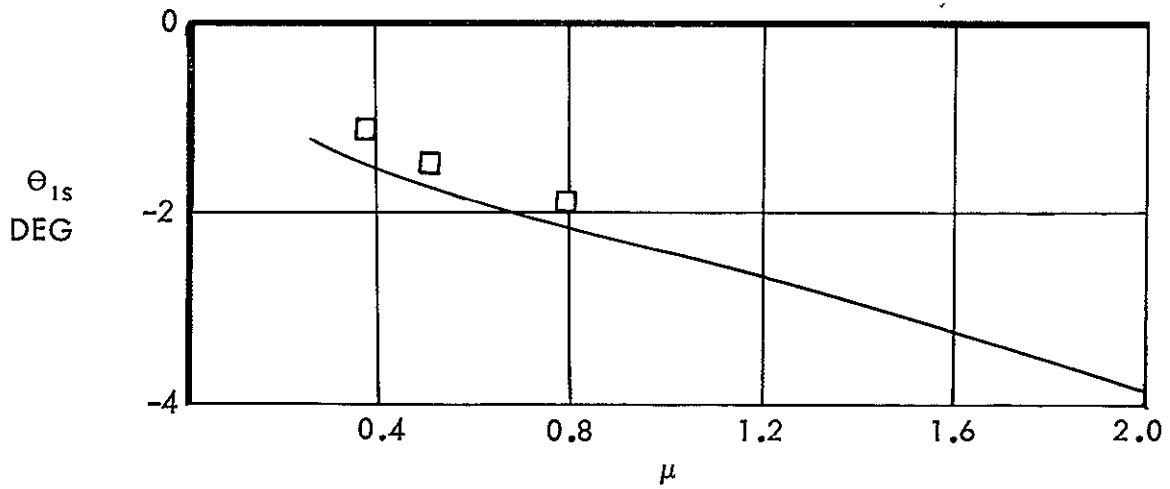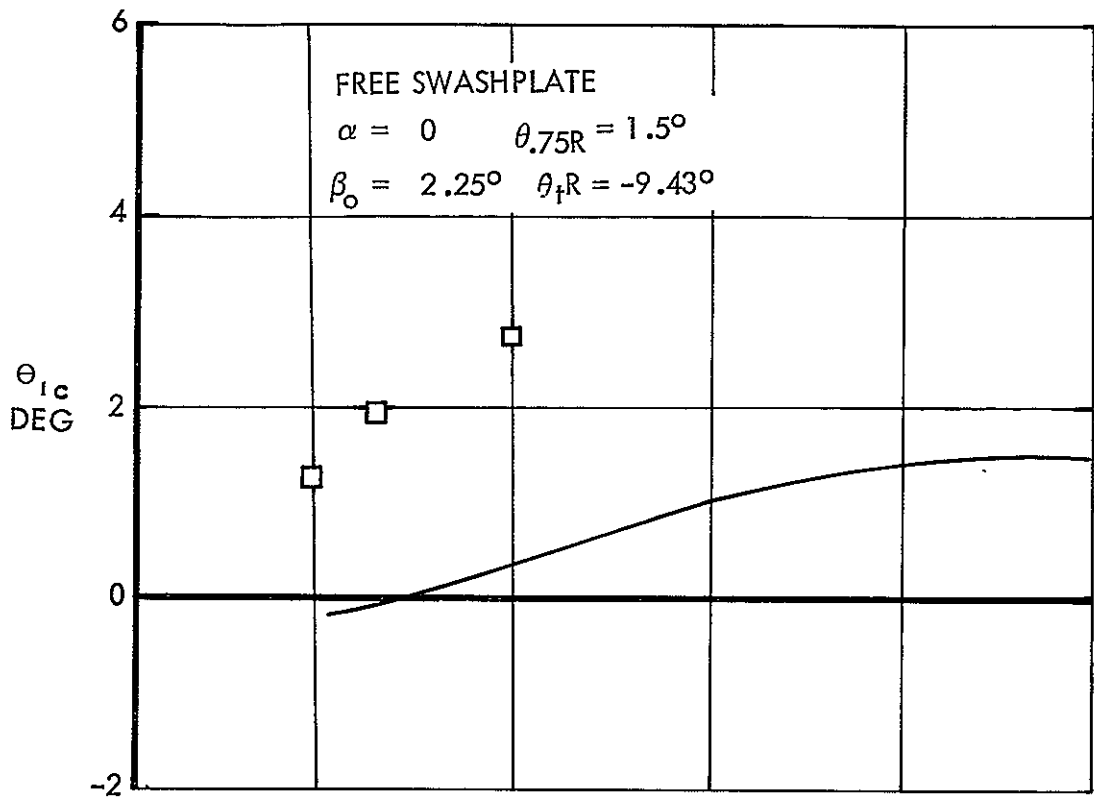
Figure 55. Cyclic Pitch Angles For Hub Moment Trimmed Condition - 120 Knots

130

by the fuselage. The inclusion of these factors in the analytical solution would probably improve the trim correlation.

Swashplate trimmed cyclic angles. - The cyclic feathering angles that produce zero mean swashplate moments are here referred to as the swashplate (or gyro) trim angles. The swashplate is normally trimmed in steady-state operation in the free-gyro mode in wind tunnel tests. This is in contrast to the hub trimmed condition, which can generally be produced only by operator manipulation of the controls.

It is important to note that the feathering moment feedback system operates so as to put the gyroscope into mean equilibrium. If the control moments applied to the swashplate are zero, then the gyroscope precesses to the mean steady position, which causes swashplate moment feedback from the rotor to become zero. The gyroscope and swashplate become trimmed.

If the advance ratio is such that the mean vector sum of the blade root bending moments also becomes zero, then the hub moments are also trimmed. At high advance ratio, swashplate trim is usually accompanied by small unbalanced hub moments.

Theoretical swashplate trim cyclic angles at fixed collective and rotor angle of attack at various forward speeds and advance ratios are shown in Figure 4. Swashplate damping is not included in this figure, or in subsequent figures, except where mentioned. This figure may be compared with Figure 3, the corresponding hub trimmed solution. At low advance ratio, the two figures agree fairly well. In other words, at low advance ratio, with only a small reverse velocity region, hub moment is a linear function of swashplate moment, i.e., with swashplate moment zero, the hub moment is zero. At the higher values of advance ratio, say at $\mu > .5$, the reverse velocity region becomes much greater in size, and the aerodynamic center shifts to the three-quarter chord location. The feathering moment per unit blade root bending moment changes sign. It is possible, therefore, that the net feathering moment vector applied to the swashplate then could become zero even while the rotor supports a significant hub moment. In this case, the cyclic pitch angles required to trim the swashplate moments to zero would be different from those

131

required to trim hub moments. Figure 3 and 4 show that at advance ratio less than, say $\mu = .5$, the cyclic pitch angles required to trim both hub and swashplate moments to zero are approximately the same.

Figures 56 and 57 show the effect of changing collective angle and rotor angle of attack, respectively, at 120 knots. Comparisons with the hub trimmed solutions of Figure 47 and 48 show the trim angles to be similar at low advance ratio, but dissimilar elsewhere.

Comparisons between analytical and experimental trim are shown in Figures 58 through 63 at forward speeds ranging from 60 to 120 knots. Confidence limits to the accuracy of the experimental data are not precisely known, but it is expected that anomalies in the rotating friction, for example, which would be more-or-less independent of the forward speed dynamic pressure, would cause larger and larger errors in swashplate trim cyclic pitch angles as the forward speed reduced at constant advance ratio. This may account for the increasingly poor agreement at the higher advance ratios as the forward speed is reduced.

The effects of rotating damping are shown on Figure 61 at 80 knots. A rotating damping value of 20 ft-lb/rad/sec is used for the data presented. The actual value of the model was later determined to be about 7 ft-lb/rad/sec.
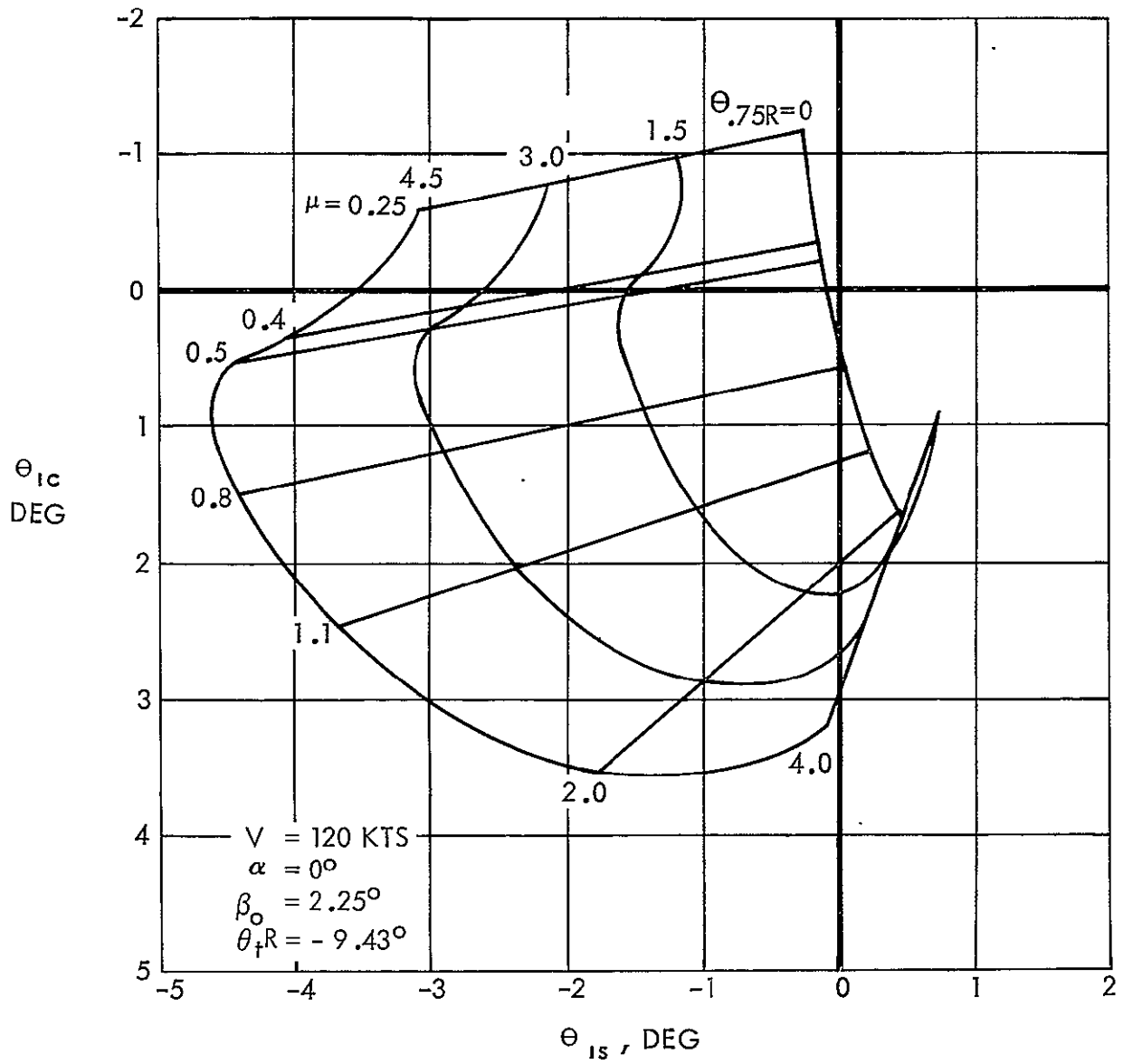
Figure 56. Analytically Derived Cyclic Angles For Swashplate Moment
Trimmed Condition - Effect Of Collective Pitch Angle
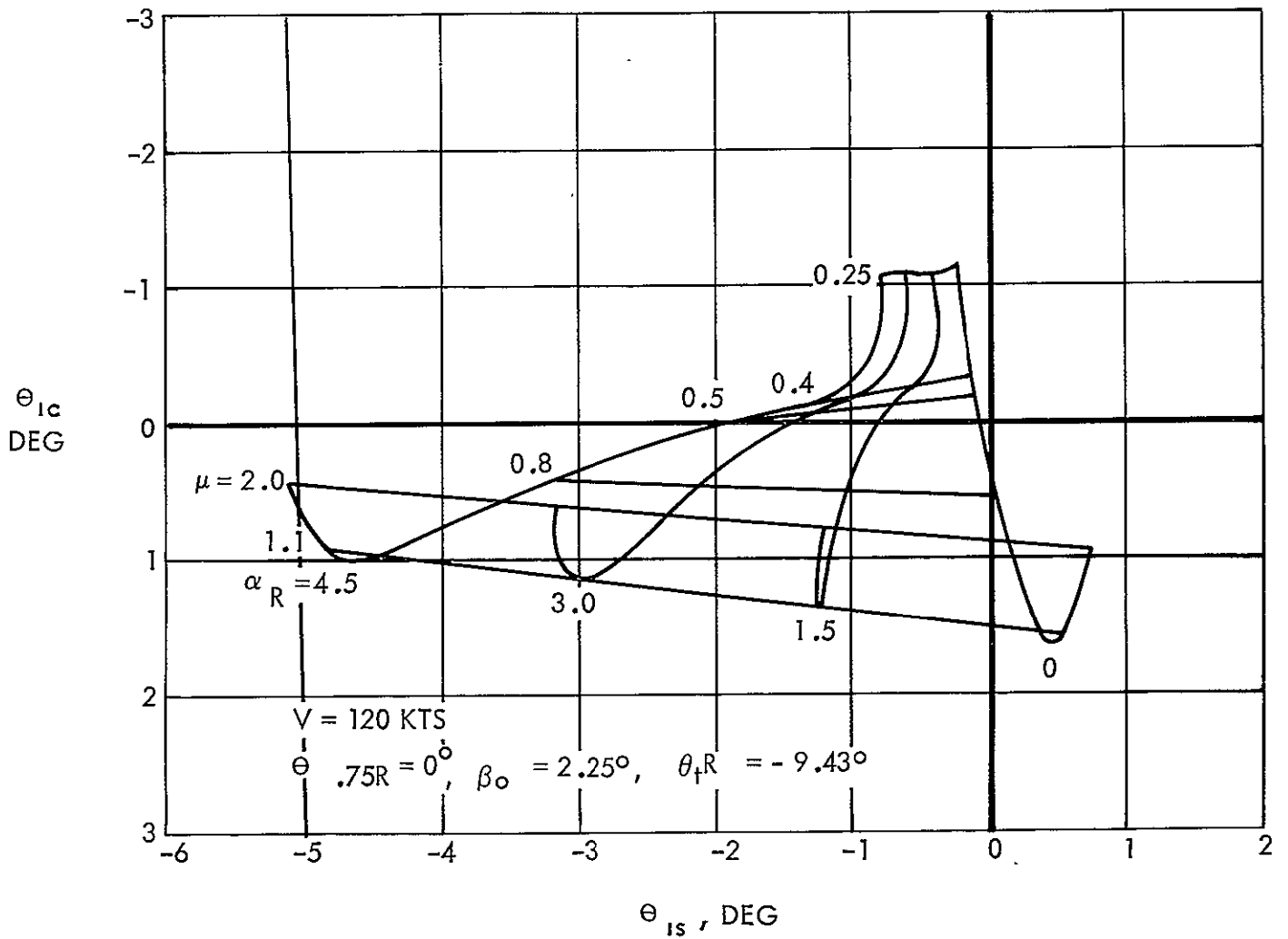
Figure 57. Analytically Derived Cyclic Pitch Angles For Swashplate Moment
Trimmed Condition - Effect Of Rotor Angle Of Attack

134
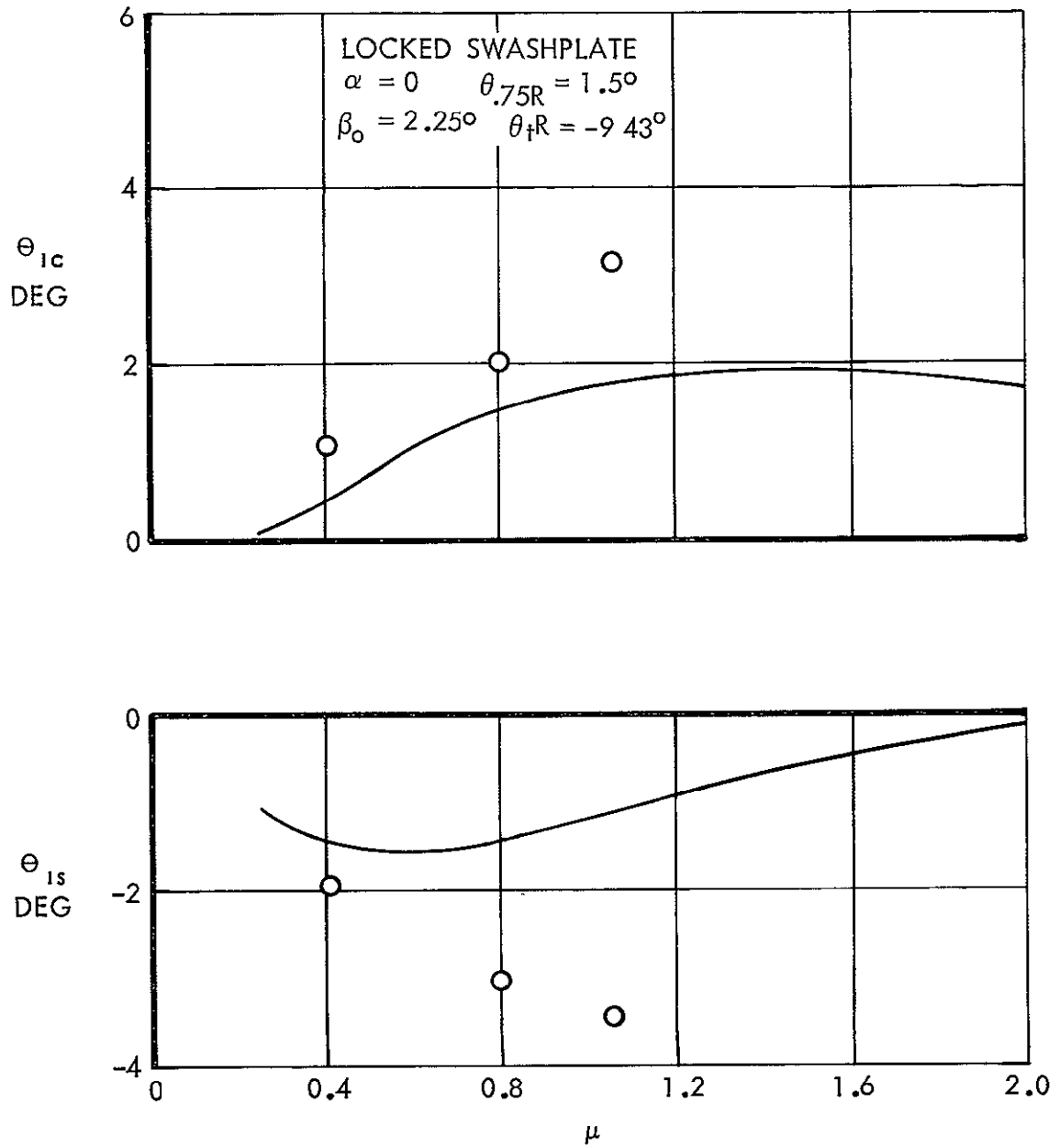
Figure 58. Cyclic Pitch Angles for Swashplate Moment
Trimmed Condition - 60 Knots

135
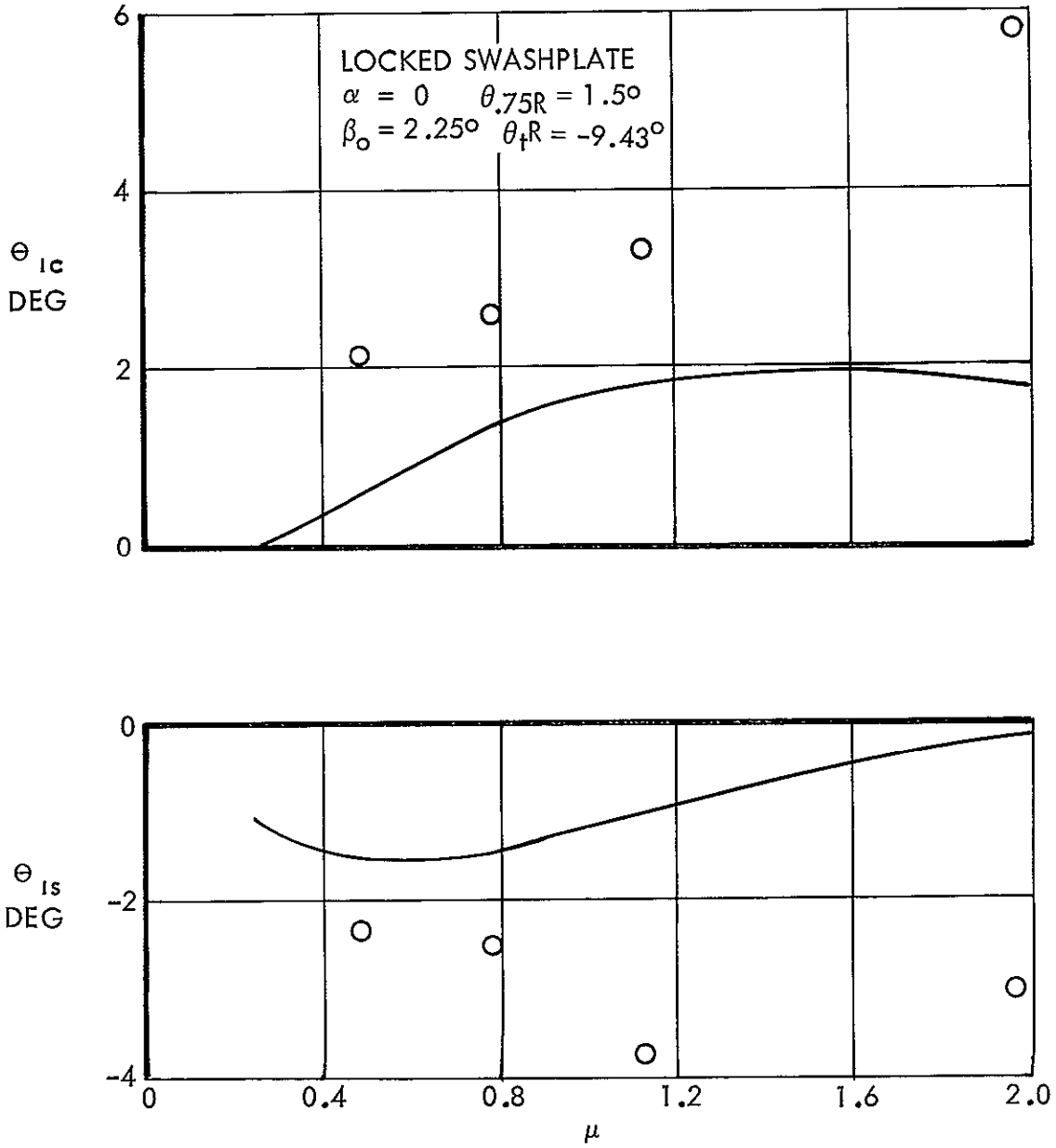
Figure 59. Cyclic Pitch Angles For Swashplate Moment
Trimmed Condition - 70 Knots

136
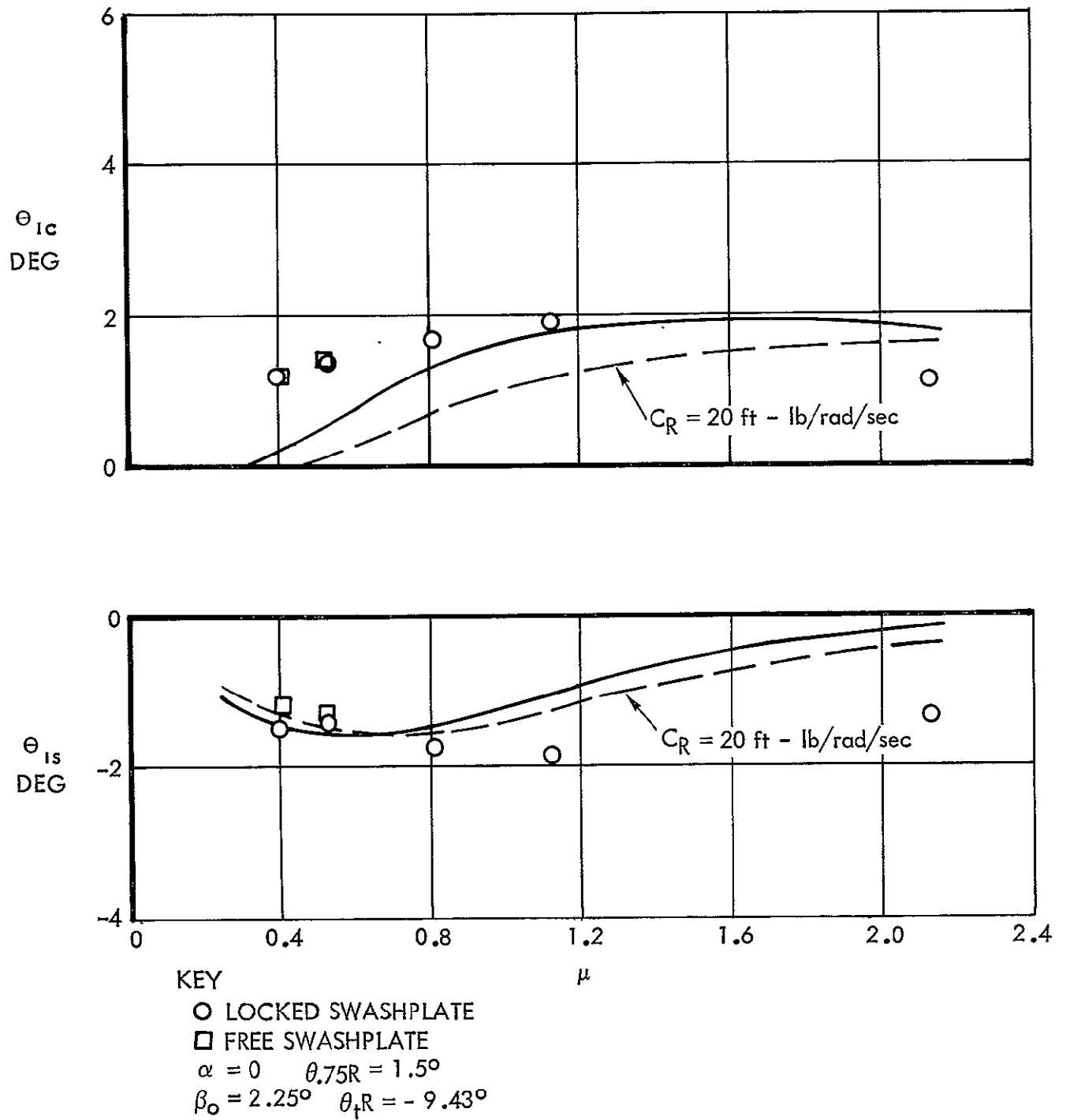
Figure 60. Cyclic Pitch Angles For Swashplate Moment
Trimmed Condition - 80 Knots

137
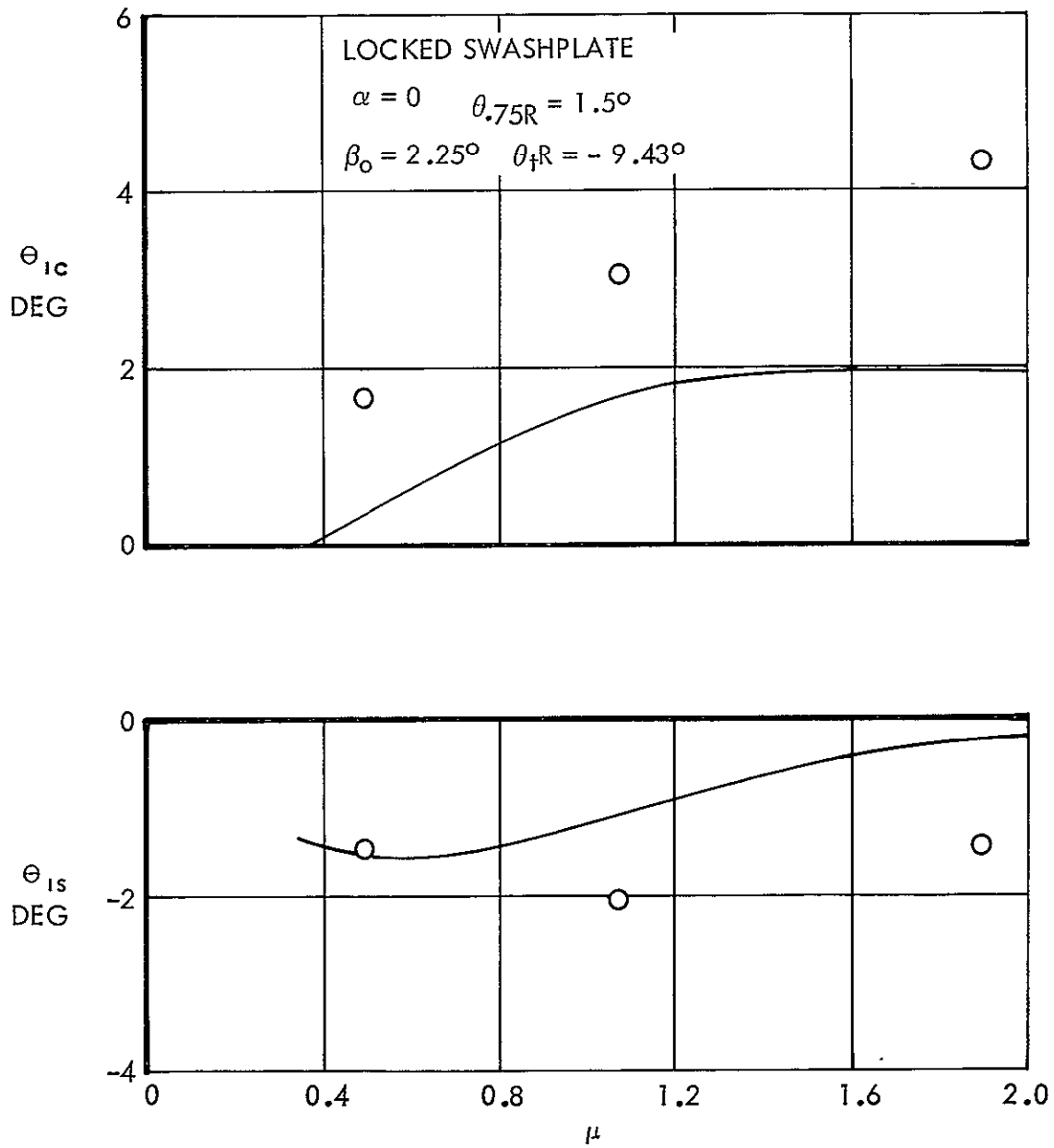
Figure 61. Cyclic Pitch Angles For Swashplate Moment
Trimmed Condition - 90 Knots
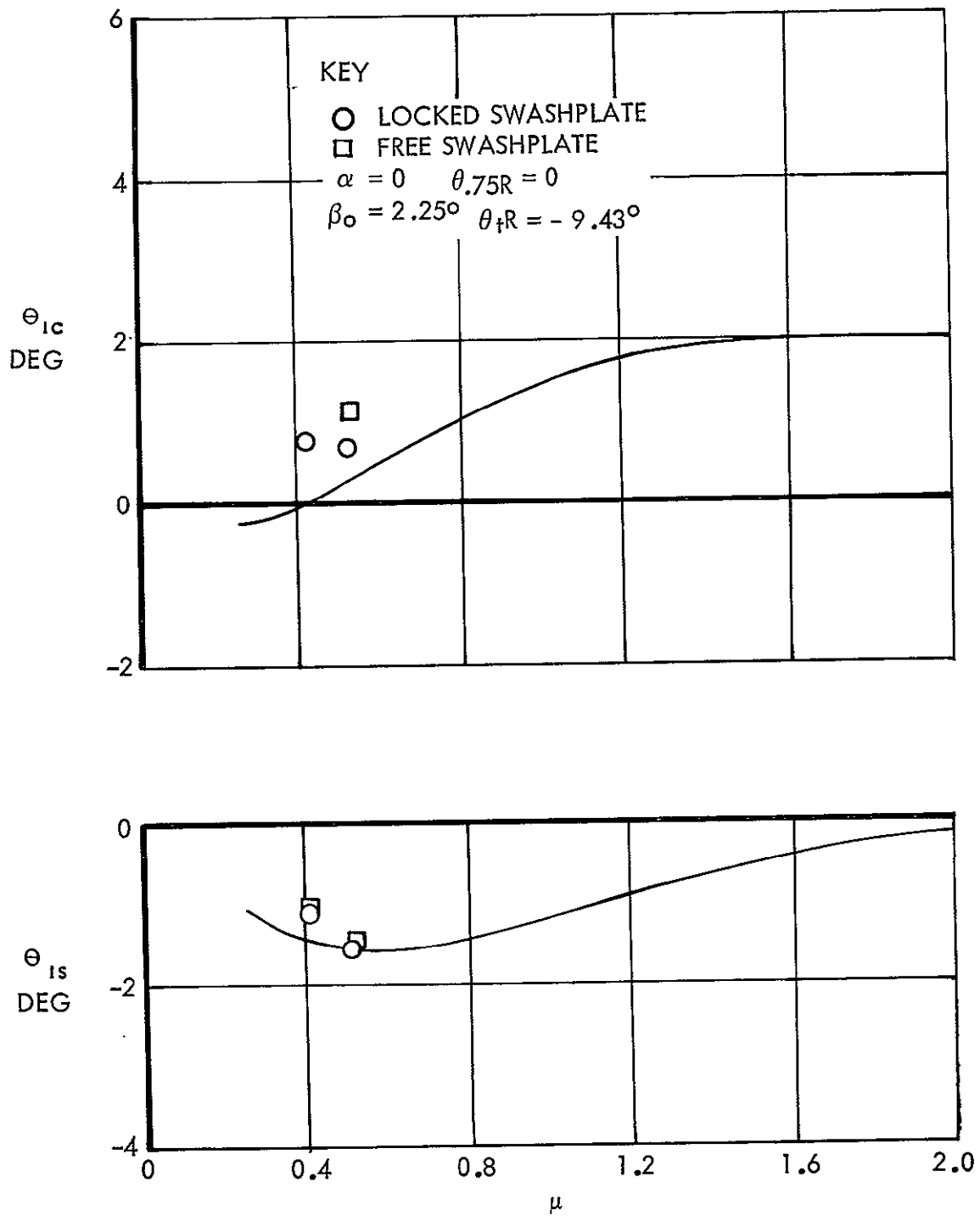
Figure 62. Cyclic Pitch Angles For Swashplate Moment
Trimmed Condition - 100 Knots
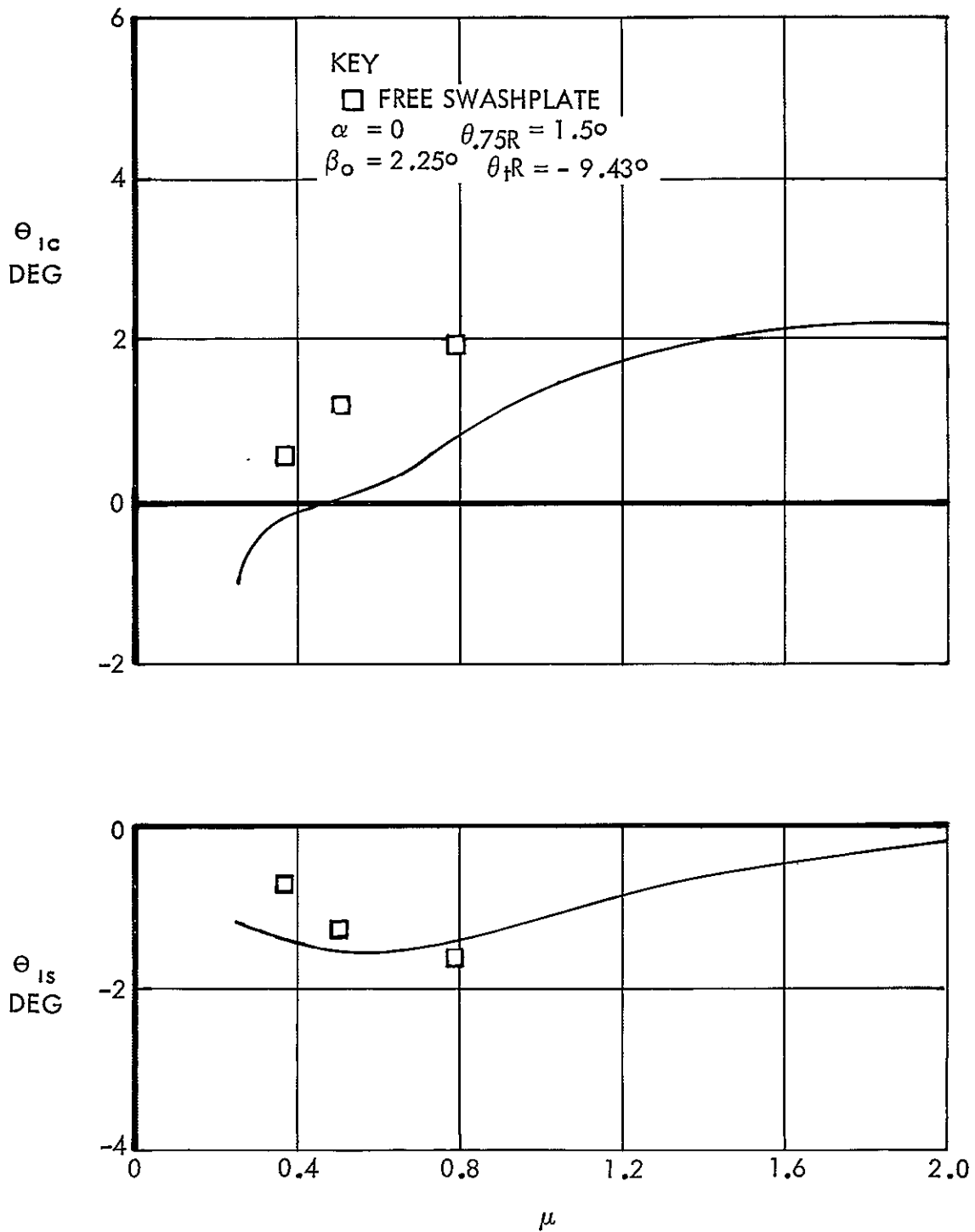
Figure 63. Cyclic Pitch Angles For Swashplate Moment
Trimmed Condition - 120 Knots

Control Effectiveness

The change in hub moment resulting from a change in swashplate moment is a measure of the control effectiveness of a rotor-gyro system. The control effectiveness derivatives are determined from test data by the method outlined in the preceding section. The theoretical method was described under "Theoretical Development."

The test and analytical results are compared in Figure 64 through 66, for forward speeds of 60, 80, and 120 knots. Rotating (feathering) damping is not included in the theoretical results, except at 80 knots where the effect of 20 ft-lb/rad/sec of rotating damping is shown. Rotating damping acts to reduce the rotor response to swashplate moments slightly and to shift the phase of the rotor response.

The control effectiveness test data appear to contain considerable scatter. This is likely caused by the combination of error from the two sets of data upon which it depends, namely the hub and swashplate moment cyclic pitch aeroelastic derivatives.

There does appear to be a trend toward poorer agreement at low forward speed and high advance ratio, i.e., low values of advancing tip dynamic pressure $\frac{\rho}{2} (\Omega R + V)^2$.

It should be noted before leaving the subject, however, that the method of plotting emphasizes the disagreement between experiment and theory. At the lower advance ratios, there is rarely a phase angle discrepancy greater than, say 5° or an amplitude error of more that 20 percent.

141
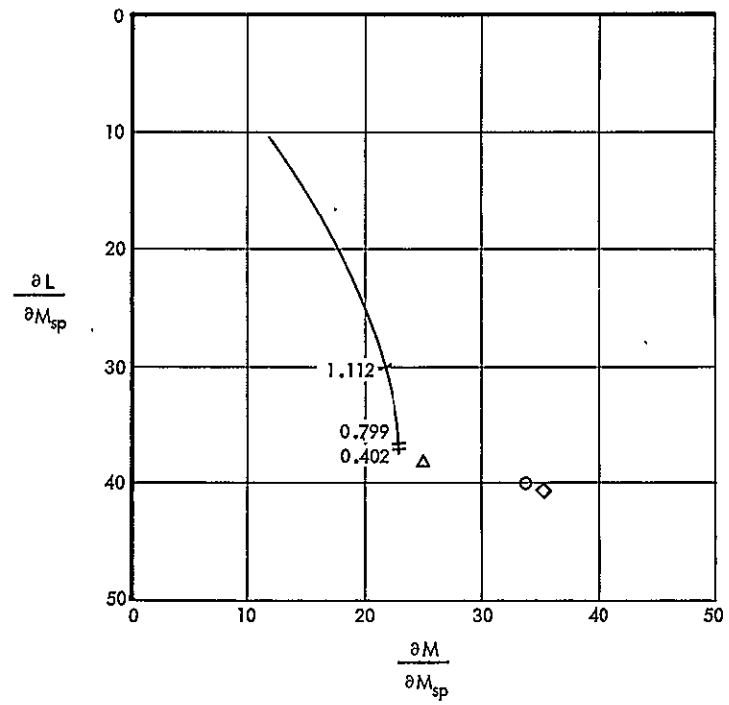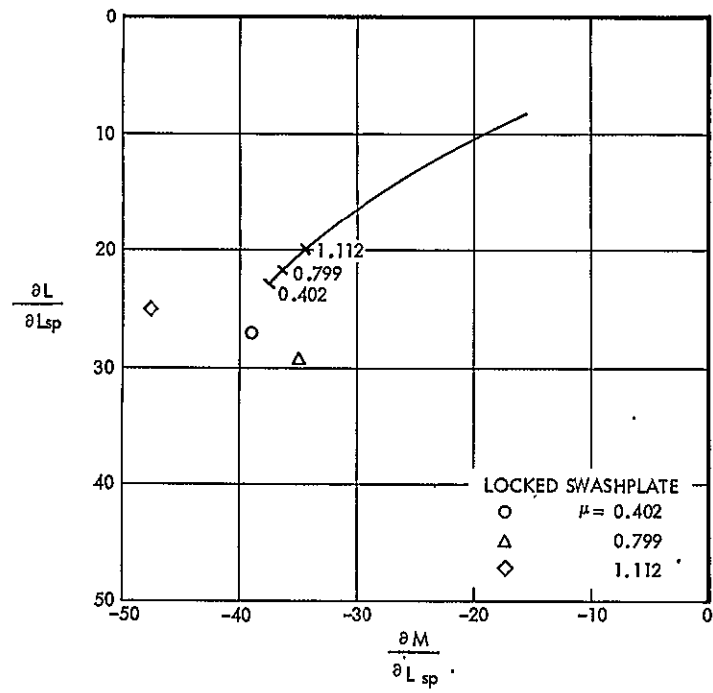
Figure 64. Hub Moments Due to Unit Swashplate Moments - 60 Knots
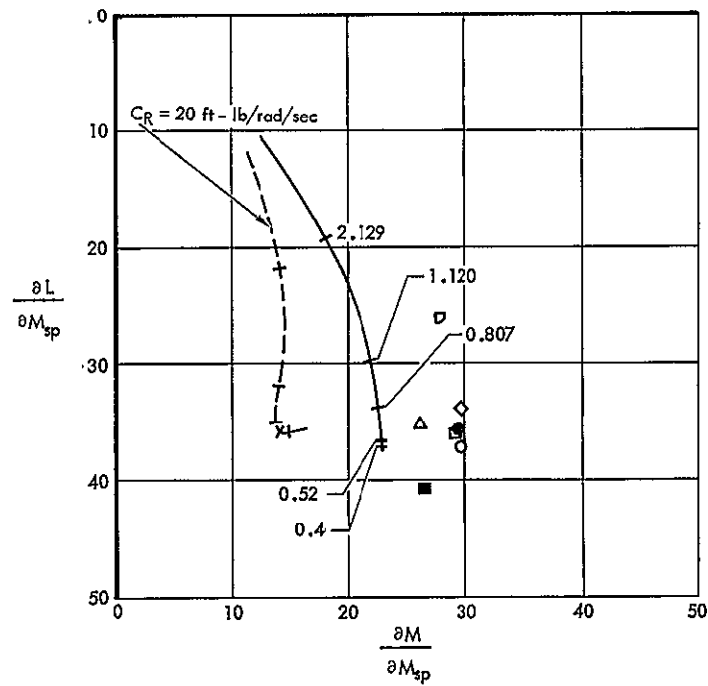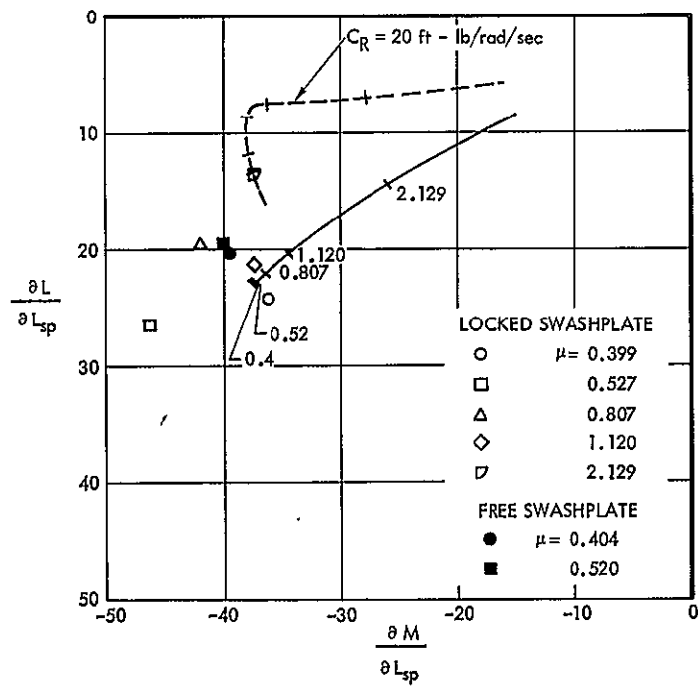
Figure 65. Hub Moments Due to Unit Swashplate Moments - 80 Knots
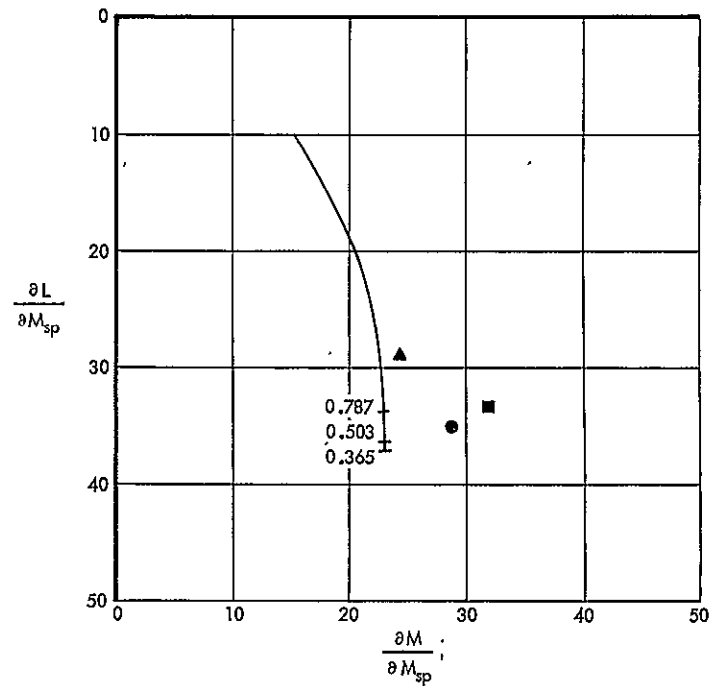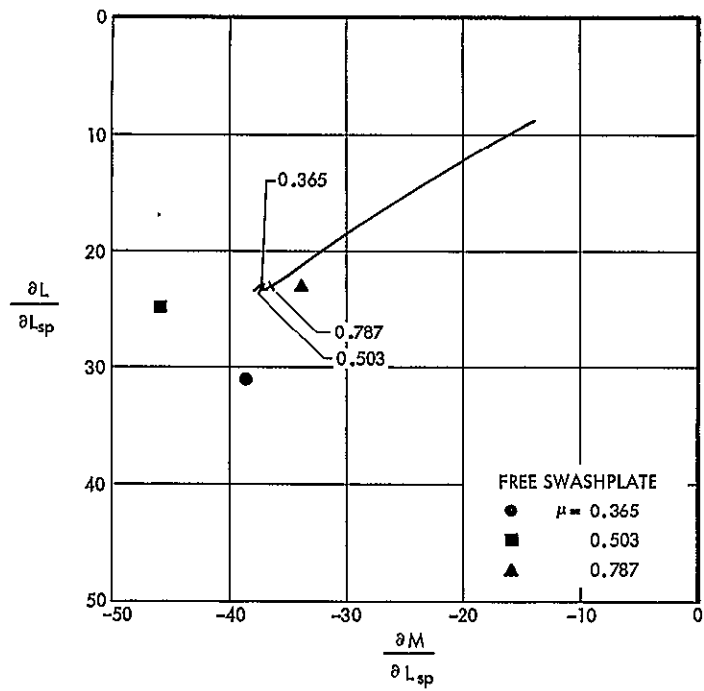
Figure 66.   Hub Moments Due to Unit Swashplate Moments - 120 Knots

Rotor-Gyroscope System Stability

The theoretical determination of rotor-gyroscope system stability characteristics (mode shape vectors, natural frequencies, and damping) and the experimental determination of the precessive character of the control mode, its natural damped frequency and the reciprocal of its time to half amplitude were discussed in preceding sections. This section displays the experimental values of the natural frequency and $1/T_{\frac{1}{2}}$ versus rotor speed on the same page for purposes of comparison; see Figures 67 through 72. The calculated characteristics shown on the plots are based on values of rotating damping (feathering friction) and stationary damping (swashplate dashpot) determined experimentally.

If the swashplate is viewed from a set of axes which rotates with the rotor, the feathering damping C_R is defined as the swashplate moment required to overcome blade feathering friction and aerodynamic feathering damping moment per unit angular velocity of the swashplate. Viewed relative to the earth fixed axis system, feathering damping becomes proportional to swashplate position (as well as velocity) and so becomes important in calculating swashplate (or gyro) aeroelastic derivatives.

The swashplate moments due to swashplate displacement in earth fixed axes may be shown by the matrix representation as:

$$
\begin{Bmatrix} M_\Theta \\ M_\phi \end{Bmatrix} = \begin{bmatrix} \dfrac{\partial M\Theta}{\partial \Theta} & \left(\dfrac{\partial M_\Theta}{\partial \phi} + \Omega C_R\right) \\ \left(\dfrac{\partial M\phi}{\partial \Theta} - \Omega C_R\right) & \dfrac{\partial M\phi}{\partial \phi} \end{bmatrix} \begin{Bmatrix} \Theta \\ \phi \end{Bmatrix}
$$

where the derivatives are aeroelastic.

An interesting observation is that the feathering damping only contributes to the cross swashplate displacement derivatives and should not, therefore, be evident in the diagonal elements of the matrix of experimental data. If good agreement between theoretical and experimental values of the on-diagonal elements are achieved it might be assumed that the off-diagonal elements due

145

to aerodynamics are similarly accurately predicated and the difference between theory and experiment would be the feathering damping. This technique was used in the study and it was learned that the feathering damping was very small and, therefore, could not be accurately determined.

The swashplate damping produced by the control force servos was calculated and checked by (bench) tests. The spring augmentation devices, which are parallel to the control servos, were also tested and modified to reduce damping to an acceptable value. The total damping from the two sources was deduced to be 53 ft lb/rad/sec. Stationary axis damping contributions from the bellcranks and links were expected to be negligibly small. The swashplate damping coefficient was also determined from the control moment sensor and swashplate angle data recorded in the wind tunnel. Small harmonic motions and some nonlinear action made interpretation difficult, but the general order of the swashplate damping appeared to be between 50 and 120 ft-lb/rad/sec from that experimental source.

The rotating damping C_R (feathering friction) chosen as representative was 7 ft-lb/rad/sec, much less than the value predicted earlier, 25 ft-lb/rad/sec, but compatible with the value deduced by comparing theoretical and experimental swashplate derivatives. The swashplate damping C_S was approximately 80 ft-lb/rad/sec, from inspection of experimental stability data. This was within the range expected from the bench and tunnel test data.

The frequency, in cps of the gyro advancing processive (or control mode and the reciprocal of its time to half amplitude were calculated over the entire rpm range at speeds of 60, 70, 80, 90, 100 and 120 knots, using best estimates of rotating and stationary axis damping deduced above:

$$C_R = 7 \text{ ft-lb/rad/sec}$$

$$C_S = 80 \text{ ft-lb/rad/sec}$$

and the results are plotted in Figure 67 through 72 where they are compared with experimental values.

The theoretical damped natural frequencies varied with rotor speed in the same manner as the experimental values but were approximately 30 percent

greater. The experimental $1/T_{\frac{1}{2}}$ was somewhat erratic but generally straddled the theoretical values. There was a tendency for the system to be two to three times more stable than predicted at 50 percent of the full rpm. The reason for this is not yet understood.

The tests were performed under near sea level air density conditions, and the results are compared with analyses using sea level air density. The stability results should depend on air density, or Lock Number, but a systematic investigation of the effects of density variation has not yet be undertaken.

AIRSPEED   60 KT

I_G .15 SLUG-FT^2

Ω_G 10,000 RPM

K_S 0

C_S 80 FT-LB/RAD/SEC

C_R 7 FT-LB/RAD/SEC

SEA LEVEL AIR DENSITY

1P

PERCENT
FULL RPM

UNSTABLE ◁   ▷ STABLE

FREQUENCY C.P.S.
1/SEC

RECIPROCAL OF TIME TO HALF AMP.
1/SEC
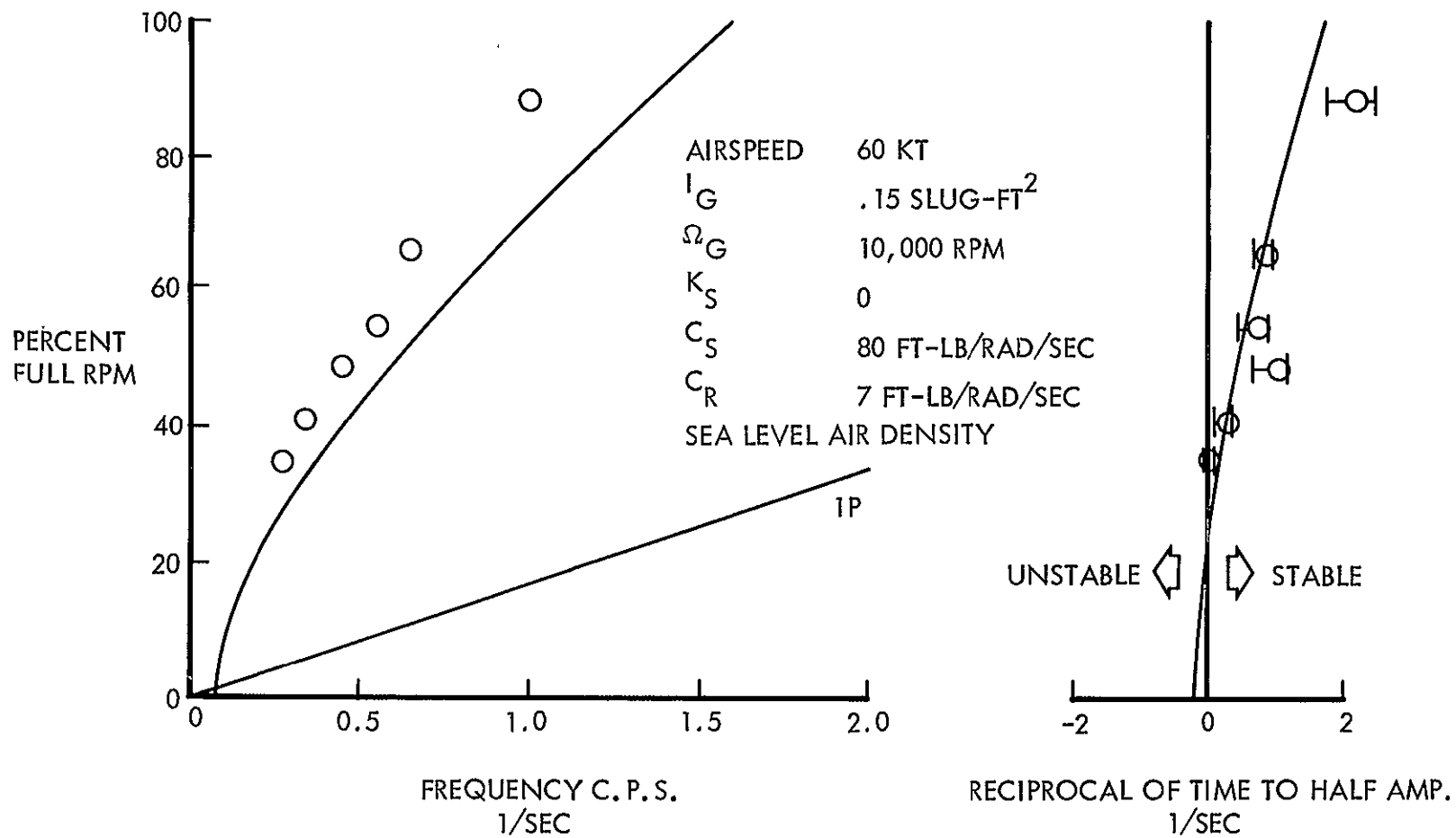
Figure 67.   Fixed-Shaft, Free-Gyro Stability By Theory And Test - 60 Knots

PERCENT
FULL RPM

AIRSPEED 70 KT

I_G .15 SLUG-FT^2

Ω_G 10,000 RPM

K_S 0

C_S 80 FT-LB/RAD/SEC

C_R 7 FT-LB/RAD/SEC

SEA LEVEL AIR DENSITY

1P

UNSTABLE ⇐ | ⇒ STABLE

FREQUENCY C.P.S.
1/SEC

RECIPROCAL OF TIME TO HALF AMP.
1/SEC
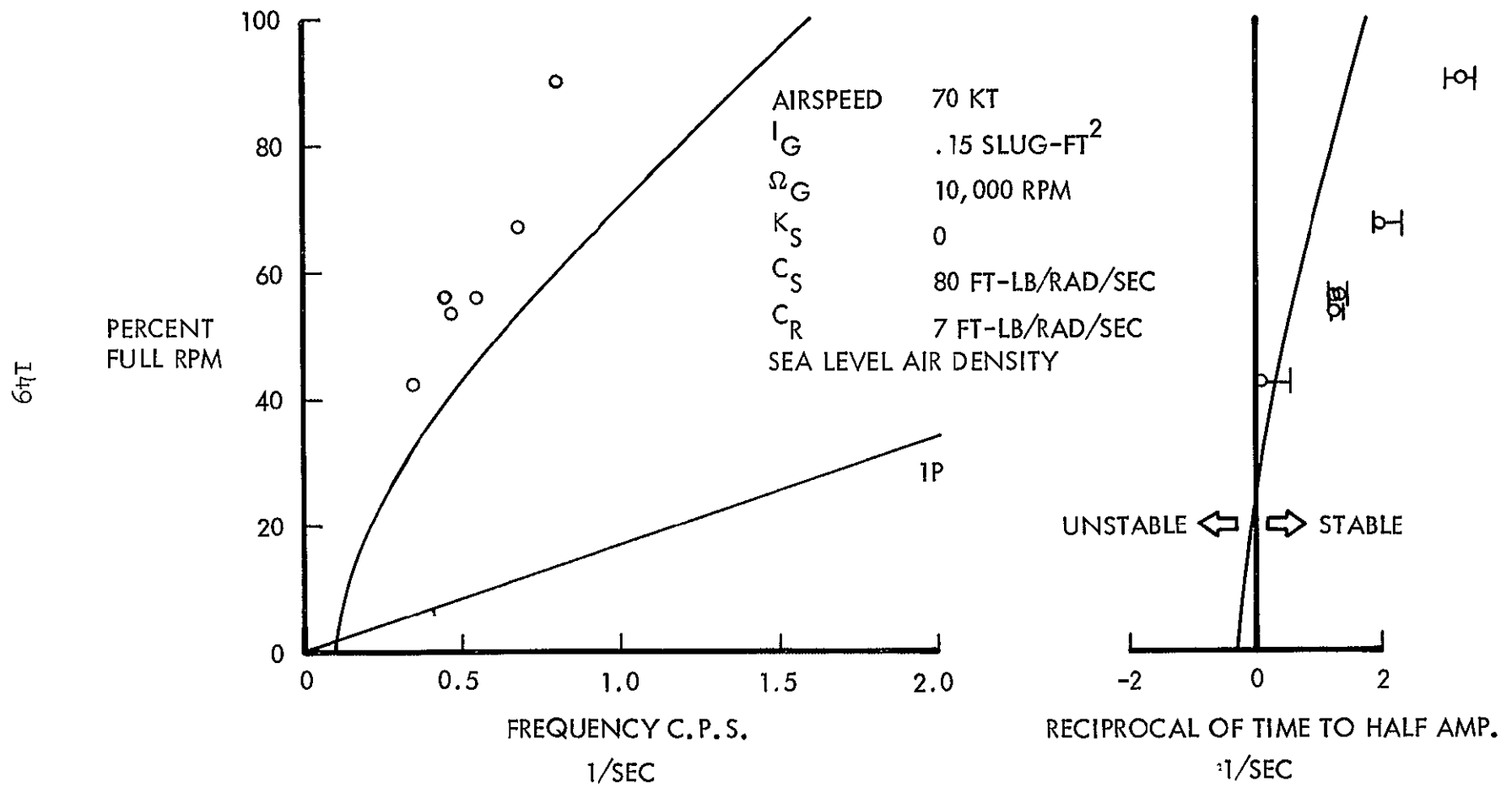
Figure 68. Fixed-Shaft, Free-Gyro Stability By Theory And Test - 70 Knots
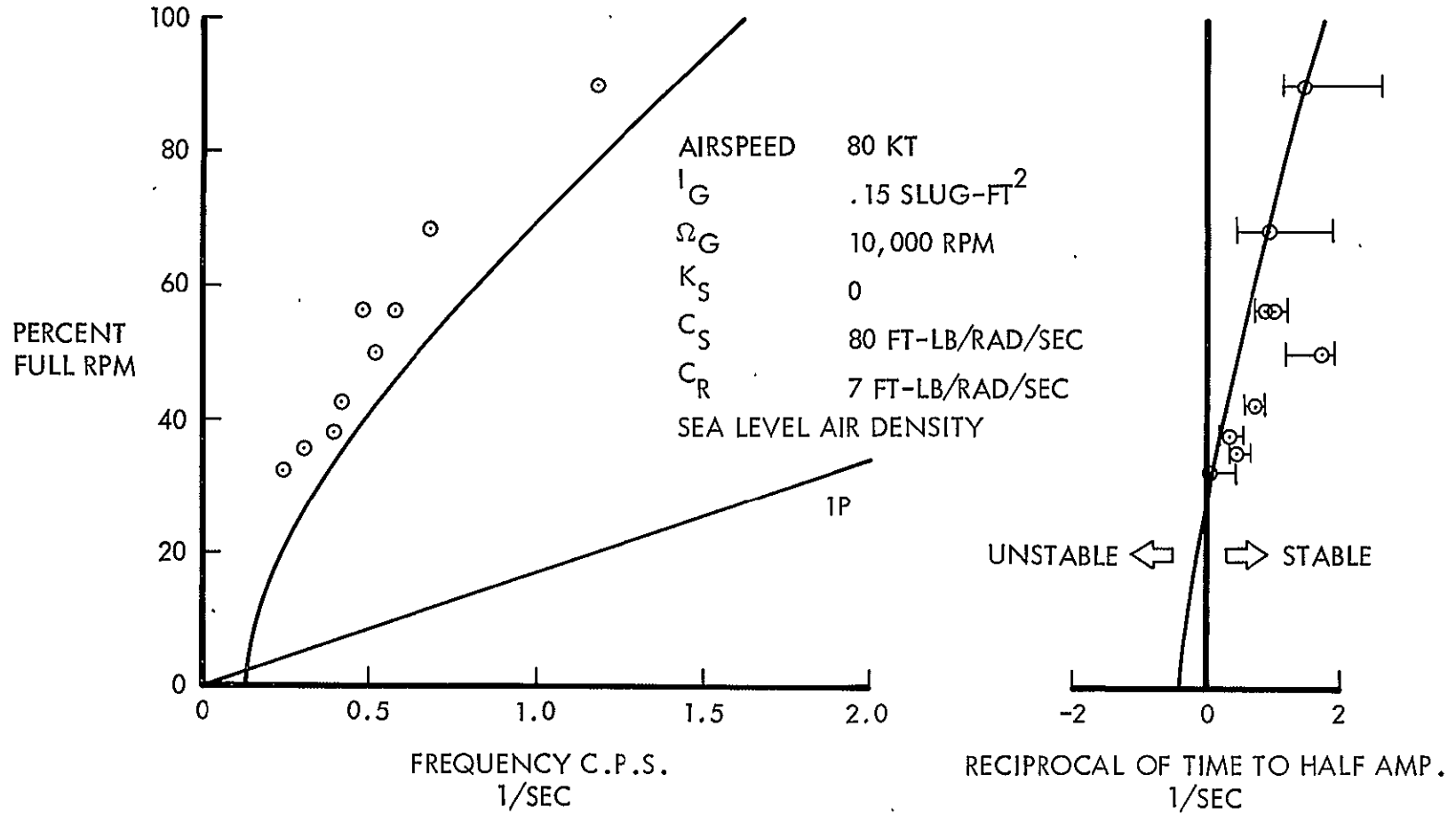
Figure 69. Fixed-Shaft, Free-Gyro Stability By Theory And Test - 80 Knots
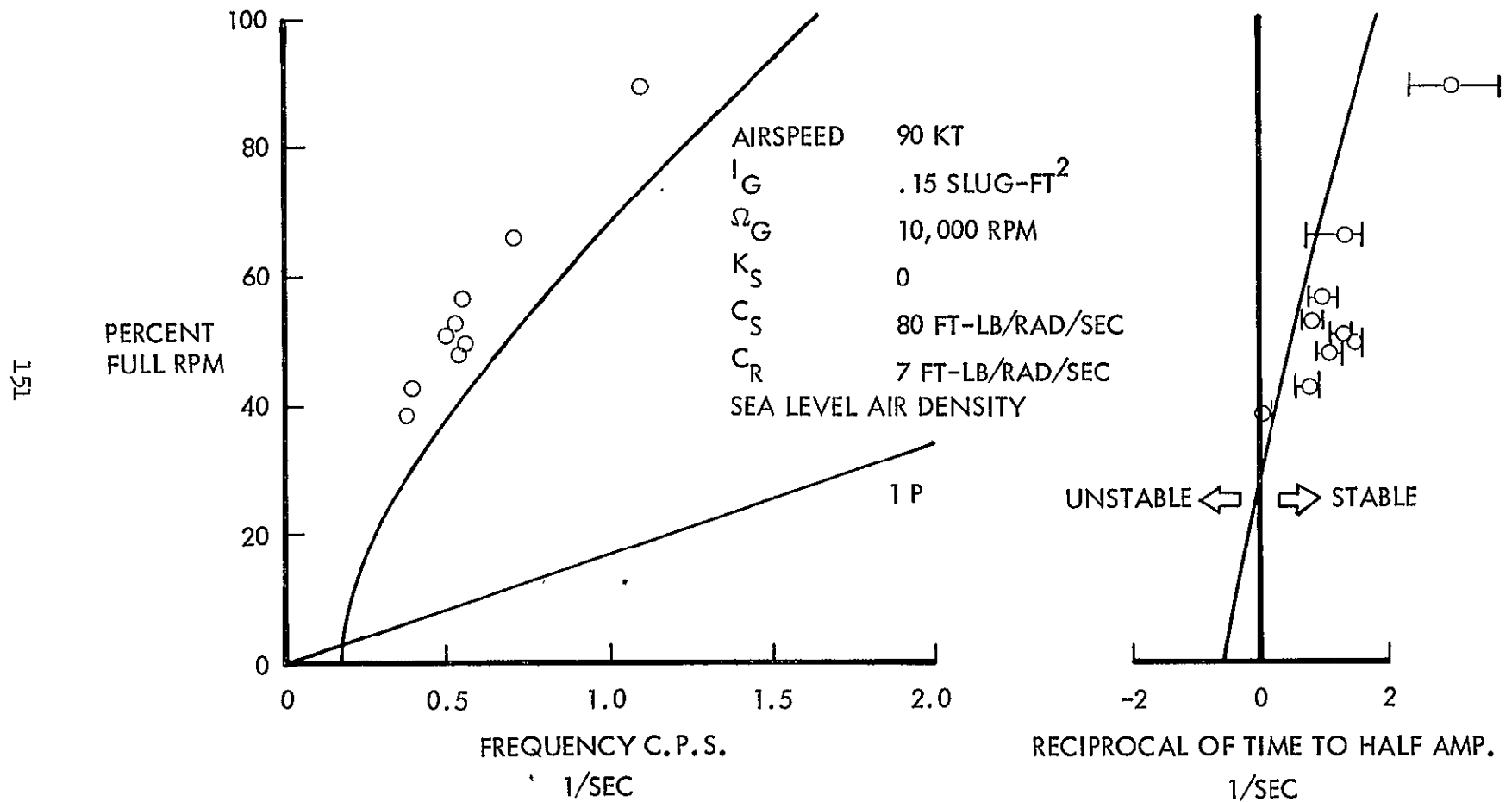
Figure 70. Fixed-Shaft, Free-Gyro Stability By Theory And Test - 90 Knots
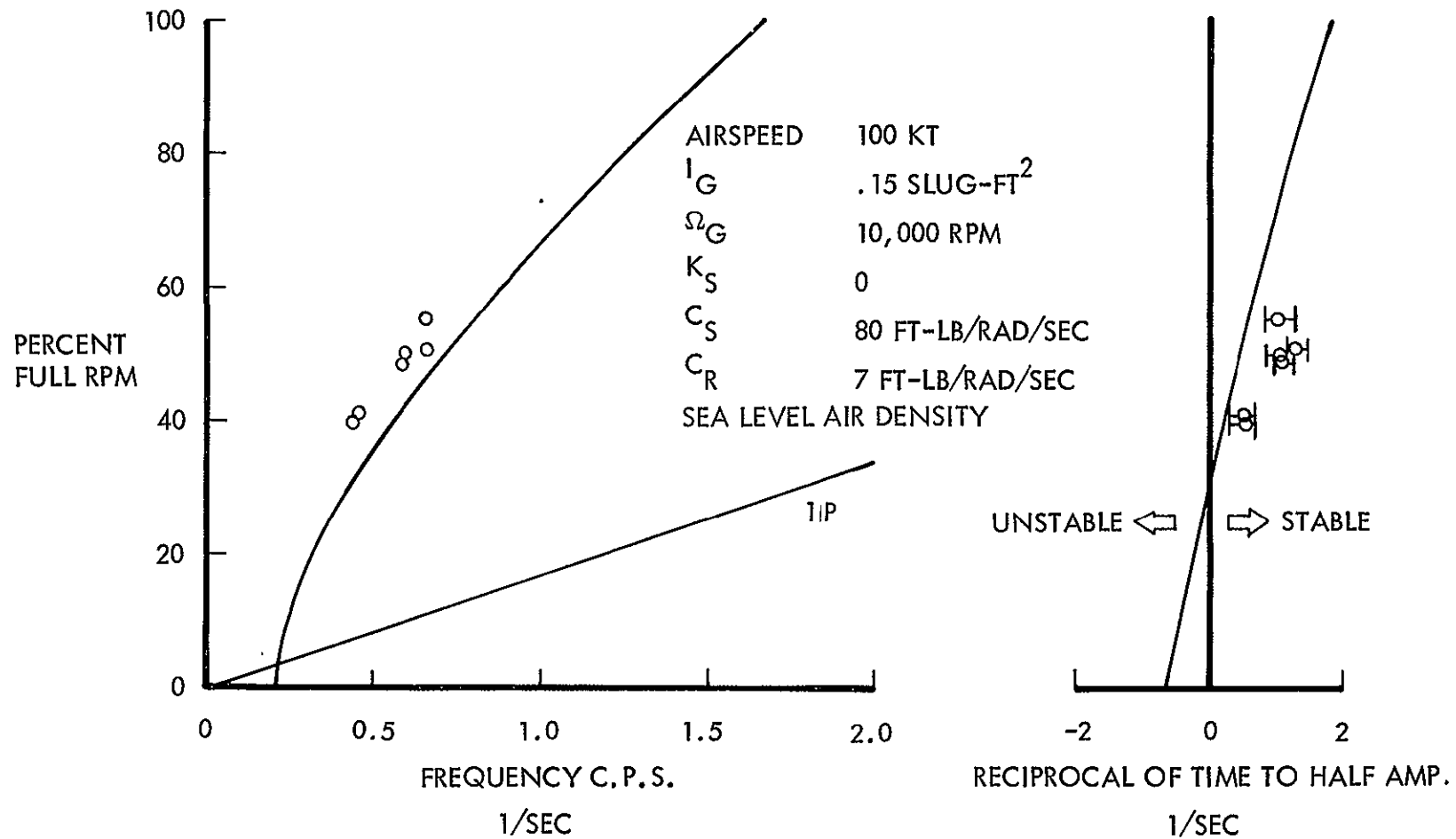
Figure 71. Fixed-Shaft, Free-Gyro Stability By Theory And Experiment - 100 Knots
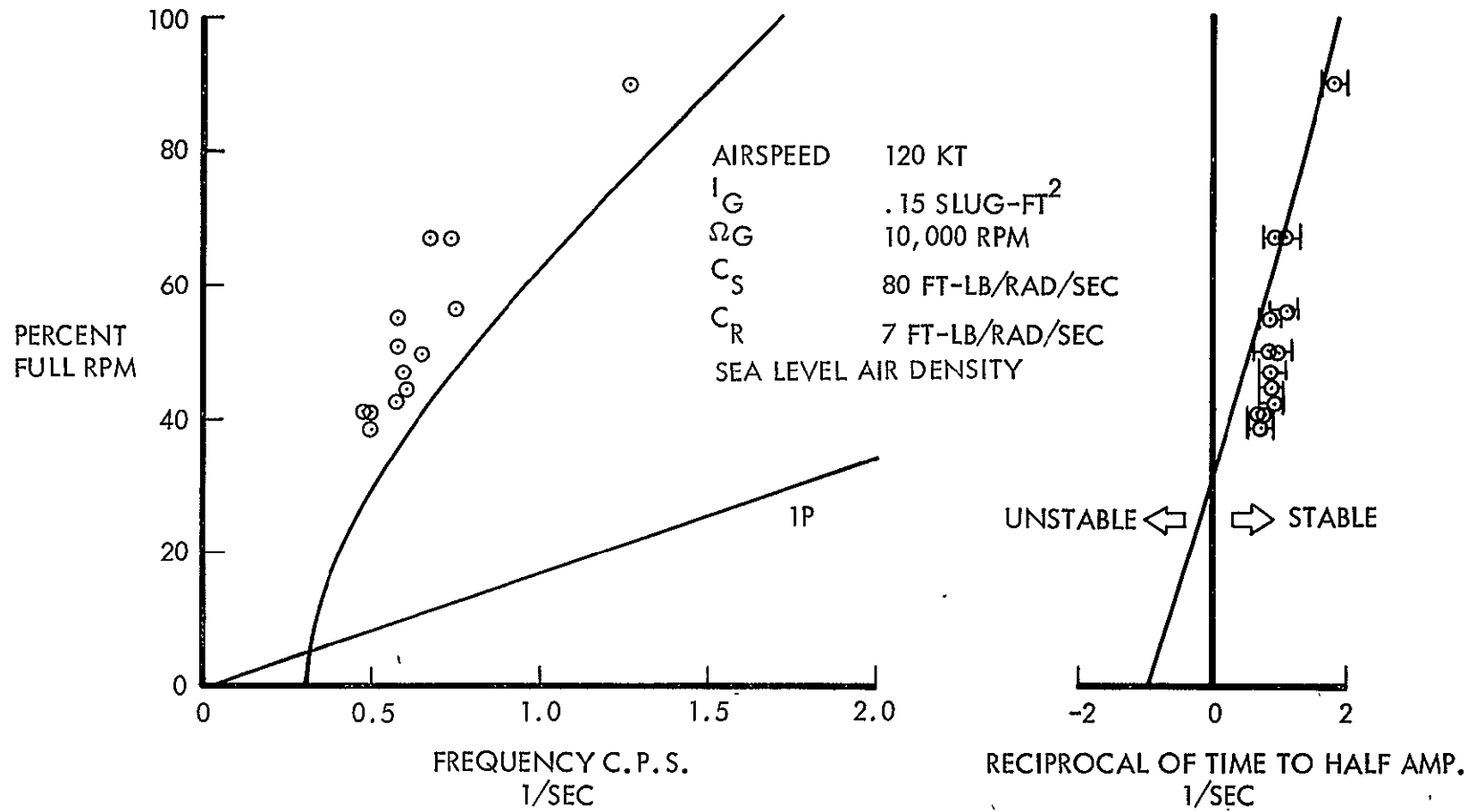
Figure 72. Fixed-Shaft, Free-Gyro Stability By Theory And Test - 120 Knots

TOPICS RELATED TO WIND
TUNNEL TESTS

Wind Tunnel Simulation of Free Flight

The stability of a fixed-shaft system during rotor starts/stops was extensively investigated theoretically and compared with test results; these are discussed earlier in this report. However, any of several body degrees of freedom can couple with rotor and gyro motions; namely body pitch, roll, and plunge. It is logical to question whether the stability of a free flying vehicle can be adequately represented by a fixed shaft system. Therefore, an 8 degree-of-freedom analysis was used to gain information about systems in which body motion is included.

Three configurations are compared: The fixed-shaft system, a gimballed inertia airframe suitable for tunnel testing, and a hypothetical airworthy vehicle. The gimballed inertia airframe is similar to the fixed-shaft model, except that body pitch and roll are permitted. The hypothetical airworthy vehicle is aerodynamically similar to the gimballed inertia airframe, a body plunge motion is included in addition to pitch and roll, and its mass and moments of inertia are more appropriate.

The analysis of the airworthy vehicle does not contain all possible motions. However, those omitted (body surge, sideslip, and yawing motions) would have second order effects on the rotor and gyro compared with those included. Thus, the 8 degree-of-freedom analysis is considered adequate for investigating the rotor-gyro stability of the flight article.

The gimballed inertia airframe is examined to determine whether it would yield more representative stability data than a fixed shaft airframe.

Stability root plots for the fixed-shaft case, the gimballed airframe, and the airworthy vehicle are shown on Figure 73 through 75 respectively. A forward speed of 120 knots was chosen as representative of conversion flight. (Conversion is the name applied to the operation of converting from a helicopter to an airplane in the case of a stoppable rotor composite aircraft.) The path of each root is plotted as it varies with rotor speed. Shown
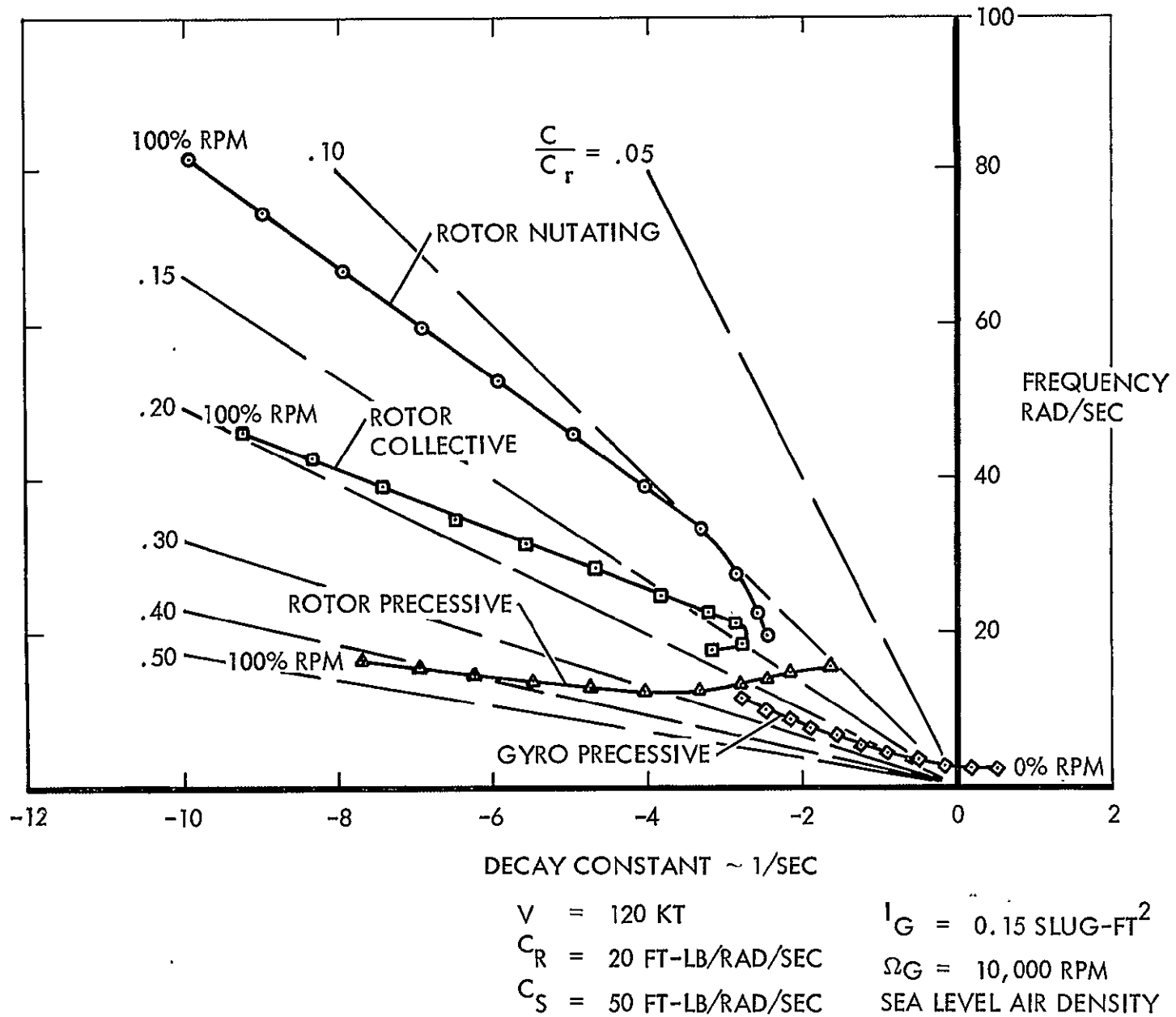
Figure 73. Fixed-Shaft, Free Gyro Stability - Effect Of Rotor Speed
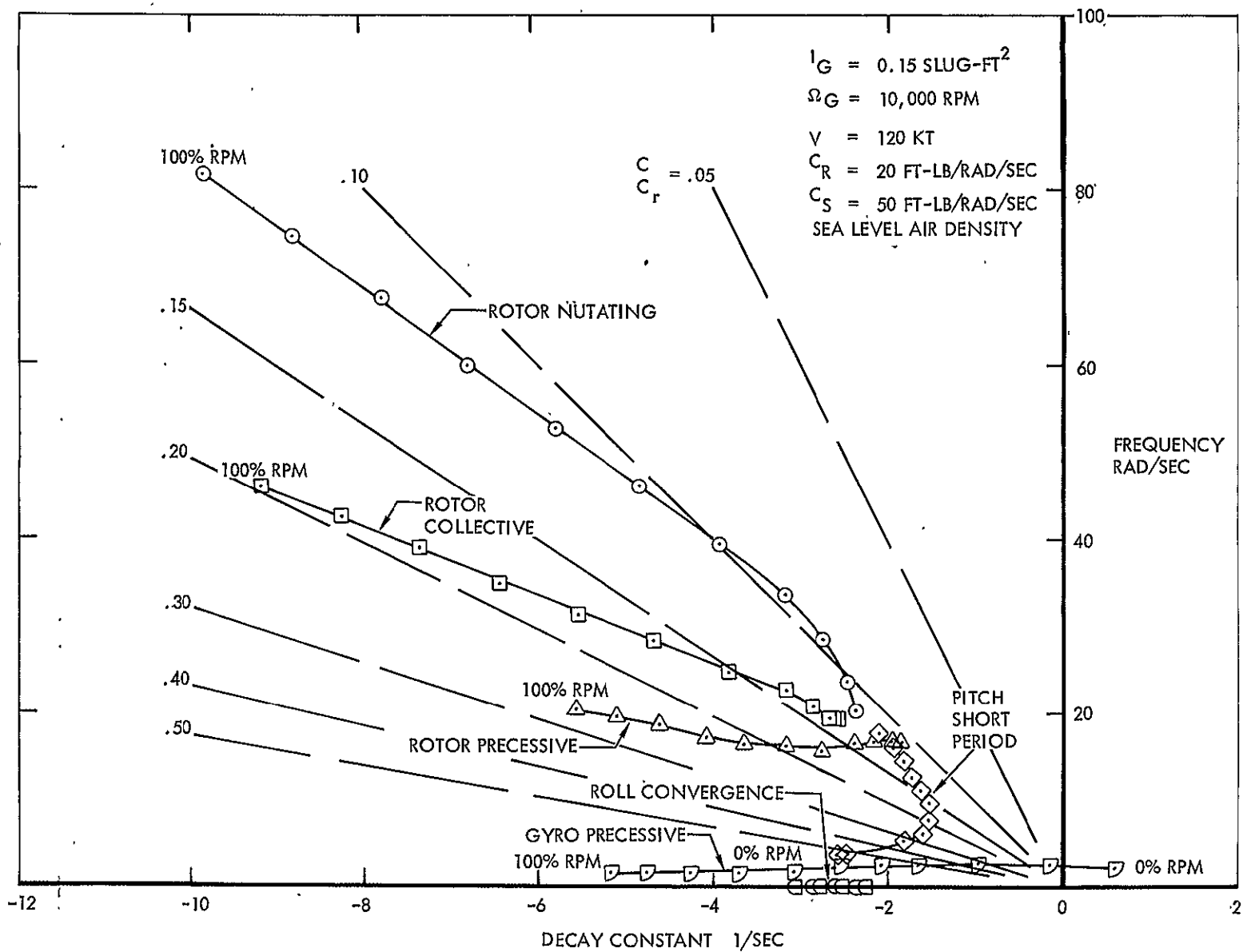
Figure 74. Gimbaled-Shaft, Free Gyro Stability - Effect Of Rotor Speed

Figure 75. Stability Of Airworthy Vehicle With Free-Gyro - Effect Of Rotor Speed

are roots for 10 rotor speeds from 355 rpm (100 percent normal rotor speed) in equal 35.5 rpm increments, down to 35.5 rpm; a root is also shown for 3.55 rpm. This range of rotor speeds covers that which the rotor would encounter during conversion.

Figures 73 through 75 show roots for configuration using a free gyro; no rotating or stationary mechanical stiffnesses are used. Rotating and stationary swashplate damping values of 20 and 50 ft-lb/rad/sec respectively are used, which do not differ greatly from the values determined for the fixed shaft vehicle. The airframe inertias and aerodynamic derivatives used here are those derived in Appendix A. The body aerodynamic derivatives used are identical for the gimballed airframe and the airworthy vehicle. However, the body inertias are necessarily larger for the gimballed existing model.

The calculated roots may be classified as belonging to rotor, gyro, or body modes. The rotor and gyro both have precessive and nutating modes. The rotor also has a collective mode. The pitch short period and the roll convergence modes result from the body degrees-of-freedom. The modes are named for the predominant motion they exhibit at either high or low rpm (low or high advance ratio respectively); the former for the rotor and gyro modes, and the latter for the body modes. The modal content varies considerably with changes in rotor speed.

The nutating and precessive natural frequencies of the classical free gyroscope would be twice the angular velocity and zero respectively, as viewed by a stationary observer. As the gyro and rotor (which is also a gyroscope) are damped, interconnected, and have different angular velocities, their natural frequencies are shifted from the above values.

The rotor modes display their least complicated behavior in a hover condition. The rotor, when vibrating in the nutating mode in hover, exhibits pure advancing motion of slightly over 2P. The collective mode in hover consists of a uniform vertical oscillation of the rotor, with frequency very close to that of the blade first natural flapping. The rotor flaps regressively in hover when vibrating in the precessive mode, which has the lowest frequency of the rotor modes.

158

At normal rotor speed ($\mu = 0.33$ at 120 knots), the rotor modal behavior as displayed in hover predominates. As rotor speed drops and advance ratio grows, the mode deviates from the relatively simple behavior it has in hover. With the rotor almost stopped, the modes are nearly unrecognizable.

The rotor modes of the fixed-shaft vehicle, not complicated by body motion, are easier to examine than corresponding modes of the other configurations. Rotor collective content increases with decreasing rotor speed in the nutating and precessing modes. Near zero rotor speed, the nutating mode degenerates to a combination of collective flapping and longitudinal teetering flapping. Up collective flapping coincides with pitch down teetering flapping. The precessive mode is similar to the nutating mode at near stopped rotor speeds, except that up collective flapping is coincident with pitch-up teetering flapping. Regressive flapping in the collective mode increases with decreasing rpm. At the lower rpm limit, the rotor motion in this mode is composed of lateral (rolling) teetering flapping with negligible collective flapping. The frequencies of each of these three modes approach the blade nonrotating first flap natural frequency at very low rpm. Gyro motion is present in all of the rotor modes at all rotor speeds.

Body motions are included in the rotor modes of the gimballed and airworthy systems at all rotor speeds. The rotor motions in the rotor modes of the gimballed model are similar to those of the fixed shaft system. However, body motion is pronounced and the rotor modes are more affected in the case of the flightworthy vehicle, with its attendant lower inertias and plunge degree-of-freedom. The flight vehicle rotor modes differ in the following respects at very low rotor speeds: the collective mode is still flapping regressively as well as collectively at 3.55 rpm, and the advancing flapping in the nutating mode remains evident at this rotor speed.

Of all the modes, the gyro nutating mode is the least affected by changes in the configuration or rotor speed, since it is of much higher frequency than the other modes. This mode is virtually the same for all three configurations. The frequency is about 810 rad/sec at full rotor speed and decreases to about 760 rad/sec at zero rotor speed. The decay constant stays at about -170/sec, or better than 20% of critical. It is an advancing mode. The roots of this mode are not shown.

Of more importance is the gyro precessive mode, which is the mode most responsive to control moment inputs. The plots of the root paths show that this mode is unstable at low rotor speeds. The onset of instability of the fixed shaft system occurs at about 50 rpm. For the configurations with body degrees of freedom, instability is delayed until down to about 30 rpm.

Vector plots of the gyro displacements in the gyro precessive mode for the three configurations are shown in Figure 76. The gyro precesses in an advancing manner at all rotor speeds when the shaft is fixed. With body motion allowed, the mode is regressive above about 30 precent of normal rotor speed. At lower rotor speeds, the mode advances, as with the fixed-shaft system. Although not shown on Figure 76 the rotor generally follows the gyro except at very low rotor speeds. At 1 percent of normal rpm, the rotor diverges in a teetering fashion.

Whether the gyro is advancing or regressing in the precessive mode is important in connection with some of the system parameters presented in Appendix D for a fixed-shaft vehicle. However, the general discussions of the effects on system stability of varying gyro inertia, damping, and stiffnesses apply to vehicles with body degrees-of-freedom.

When comparing fixed and free shaft system stabilities, swashplate stationary damping is a most important consideration. Rotating damping is stabilizing for both precessively advancing and regressing gyros, except at near stopped rotor speeds. However, increased stationary swashplate damping will tend to destabilize an advancing gyro mode and stabilize a regressing gyro mode. This is illustrated in Appendix C, in which the gyro precessive mode has been driven regressively below about 50 percent of normal rpm by a swashplate spring. Therefore, in conclusion, the free-shaft configurations are inherently more stable than the fixed-shaft system for other than very low rotor speeds; because of the regressive character of the gyro precessive mode as opposed to the advancing free gyro of the fixed shaft system.

Further evidence of the greater stability of this mode with body degrees-of-freedom present is indicated by comparing the gyro precessive roots of Figure 73 with those of Figures 74 and 75. Except in the
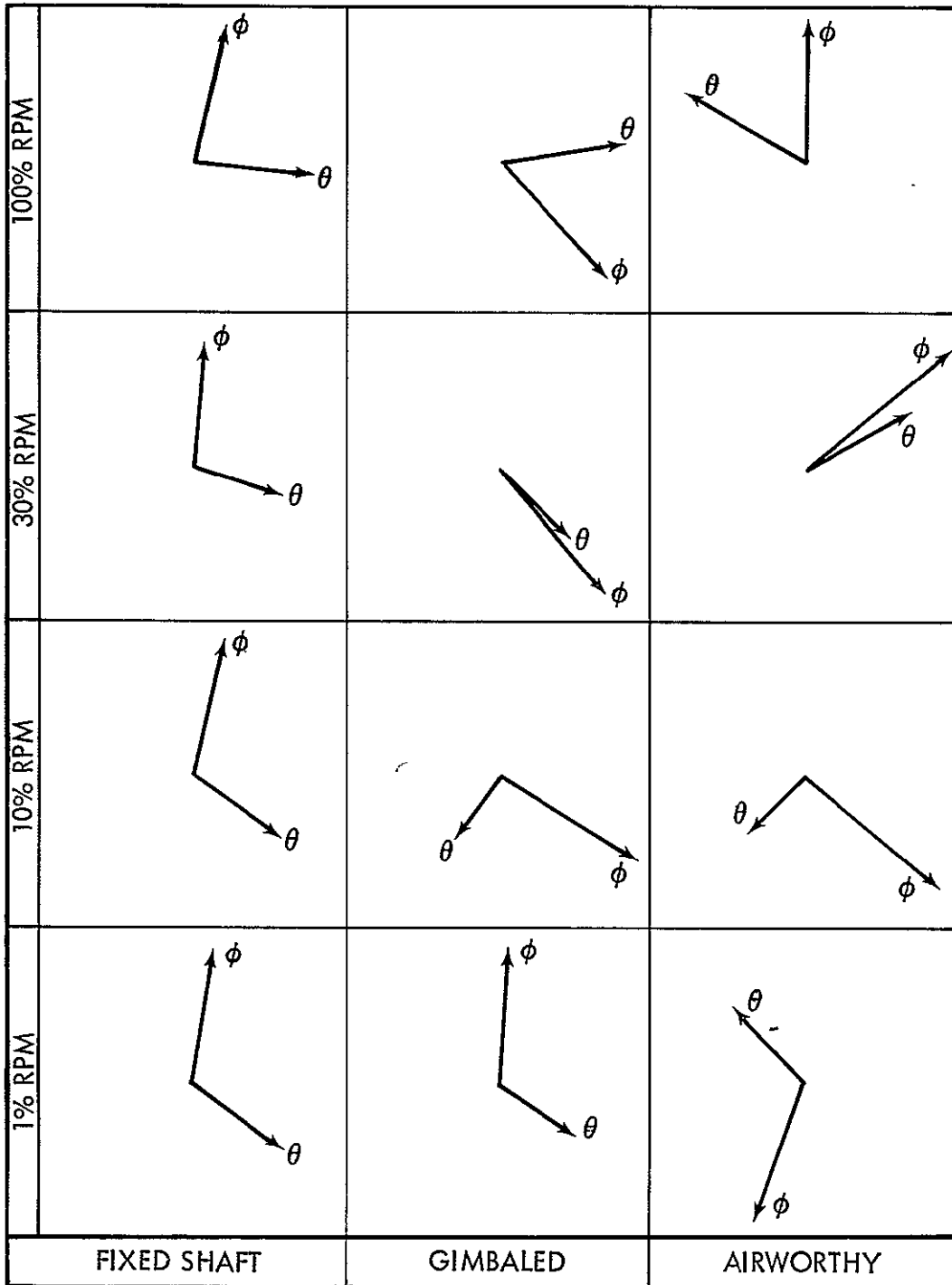
Figure 76. Gyro Precessive Mode - Gyro Modal Vectors

161

unstable region, damping is significantly greater with the inclusion of body motions; and the onset of instability is delayed.

The last group of modes herein considered are the body modes. At low rotor speed these modes may be roughly approximated by neglecting the rotor and gyro and solving the remaining body equations. The gimballed model yields the following non-zero roots from the uncoupled equations:

$$\lambda = -1.31 \pm 1.07i \qquad \text{(pitch equation)}$$

$$\lambda = -1.45 \qquad \text{(roll equation)}$$

The corresponding non-zero roots for the airworthy vehicle are:

$$\lambda = -5.38 \pm 4.51i \qquad \text{(coupled pitch and plunge equations)}$$

$$\lambda = -2.65 \qquad \text{(roll equation)}$$

The two complex pairs of roots are those of the pitch short-period modes. These roots are approximated at low rpm on Figures 74 and 75 . At low rotor speed the mode is composed mainly of body pitch motion. Body roll and rotor advancing flapping motions increase with increasing rotor speed. The amplitude of body pitch motion is about the same as that of the body roll motion at near normal rotor speeds. This mode is quite similar for both the gimballed model and the airworthy vehicle.

The non-oscillating roots obtained from the roll equations belong to the roll convergence mode. These roots are also critically damped with the rotor included, Figures 74 and 75 . The mode is composed mainly of body roll motion at low rotor speed. Body pitch motion increases with rotor speed. The magnitude of body pitch and roll is similar at high rpm. The behavior of this body mode is very similar for both configurations.

A comparison of the fixed-shaft airframe with the systems with body motion allowed has pointed out some of the limitations of applying fixed-shaft stability data to a flight vehicle. The behavior of the gyro control mode

162

is different at most rotor speeds; thus the resultant fixed-shaft data are overly pessimistic. However, the gimballed inertia airframe appears to very adequately represent an airworthy vehicle, except for the absence of the long period body modes. The lack of a plunge degree-of-freedom using the gimballed model does not appear to be a serious limitation.

Since the gimballed model modes are similar to those of the free flying aircraft, and the gyro precessive modes of the two exhibit behavior, at high rpm, quite different from that of the fixed-shaft rotor (being regressive in the former and advancing in the latter), and inasmuch as the body short period pitch and roll modes do not exist in the fixed-shaft case, and further; since mechanization of the gimballed model for operation at rpm greater than 50 percent of nominal does not appear to present any extrodinary difficulty, it is recommended that a gimballed model be employed to study the stability of a modelled slowed-rotor compound helicopter.

Rotor Performance

The slowed/stopped rotor vehicle when operating in the helicopter mode, and during the conversion operation requires power to:

(1) Provide a propulsive force, to overcome rotor and fuselage drag
(2) Provide torque to overcome blade profile and induced drag.

In this section the power requirements of the rotor, in terms of effective drag, are discussed for the zero lift conversion condition. The relative magnitudes of the propulsive and torque contributions to the total power required are examined.

The total effective drag is defined as:

$$\text{EFFECTIVE DRAG} = \text{ROTOR DRAG} + \frac{\text{ROTOR POWER}}{\text{VELOCITY}}$$

Rotor drag was measured by the tunnel balance (tare corrections were made). Rotor power was obtained from the output of the shaft torque strain gages.

The test data was corrected to a zero-lift condition by treating the rotor as an elliptical wing having the geometric properties

$$\text{wing area,} \quad S_w = \pi R^2$$

$$\text{wing span,} \quad b = 2R$$

$$\text{wing aspect ratio,} \quad A = \frac{b^2}{S_w} = \frac{4}{\pi}$$

For an elliptical wing the induced drag coefficient

$$C_{D_i} = \frac{C_L^2}{\pi A}$$

hence

$$D_i = q \, S_w \, C_{D_i} = \frac{q \, S_w}{\pi A} \left[\frac{L}{q \, S_w} \right]^2 = \frac{L^2}{\pi q \, A \, S_w} = \frac{L^2}{4 \, \pi \, R^2 \, q}$$

thus for $L = 0$

$$D_{eff} = D + \frac{P}{V} - \frac{L^2}{4 \, \pi \, R^2 \, q}$$

At the low values of lift experienced in the test program this analytical correction is considered adequate.

The rotor performance is discussed in terms of drag coefficient rather than power coefficient because according to the usual definitions, drag coefficient is non-dimensionalized by forward speed, and power by rotor angular velocity. For normal helicopter operation, where forward speed is varied at essentially constant rpm, power coefficient is preferred. However the conversion maneuver involves rpm change at constant forward speed, thus drag coefficient is more meaningful for describing rotor performance, and relating propulsive and torque contributions.

In non-dimensional form

$$C_{D_{eff}} = \frac{1}{q \, (\pi R^2)} \left[D \right] + \frac{1}{q \, (\pi R^2)} \left[\frac{P}{V} - \frac{L^2}{4 \pi R^2 \, q} \right]$$

which may be expressed

$$C_{D_{eff}} = C_D \text{ propulsion} + C_D \text{ torque} - C_{D_i}$$

Figures 77 and 78 present the variation of

$$\frac{C_D \text{ propulsion}}{\sigma} \text{ and } \frac{C_D \text{ torque}}{\sigma}$$

for advance ratios for three forward speeds. The data points shown represent test conditions at nominal hub moment trim; no attempt was made to correct the data to exactly zero hub moment. As a consequence, while the total rotor lift is zero, the blades experience lift variations around the azimuth and induced drag is thus present, which probably contributes to the data scatter.

Figure 79 presents the torque and propulsive contributions to the total rotor effective drag. As would be expected, both terms decrease with reducing rpm. Above an advance ratio of 1.5 the rotor torque is negligible, and the total effective drag is equal to the rotor drag.

The data indicated that the part of the effective drag due to rotor torque became slightly negative at advance ratio greater than $\mu = 1.7$. This was probably due to the greater drag of the blades in the reverse velocity region than in the advancing flow region.
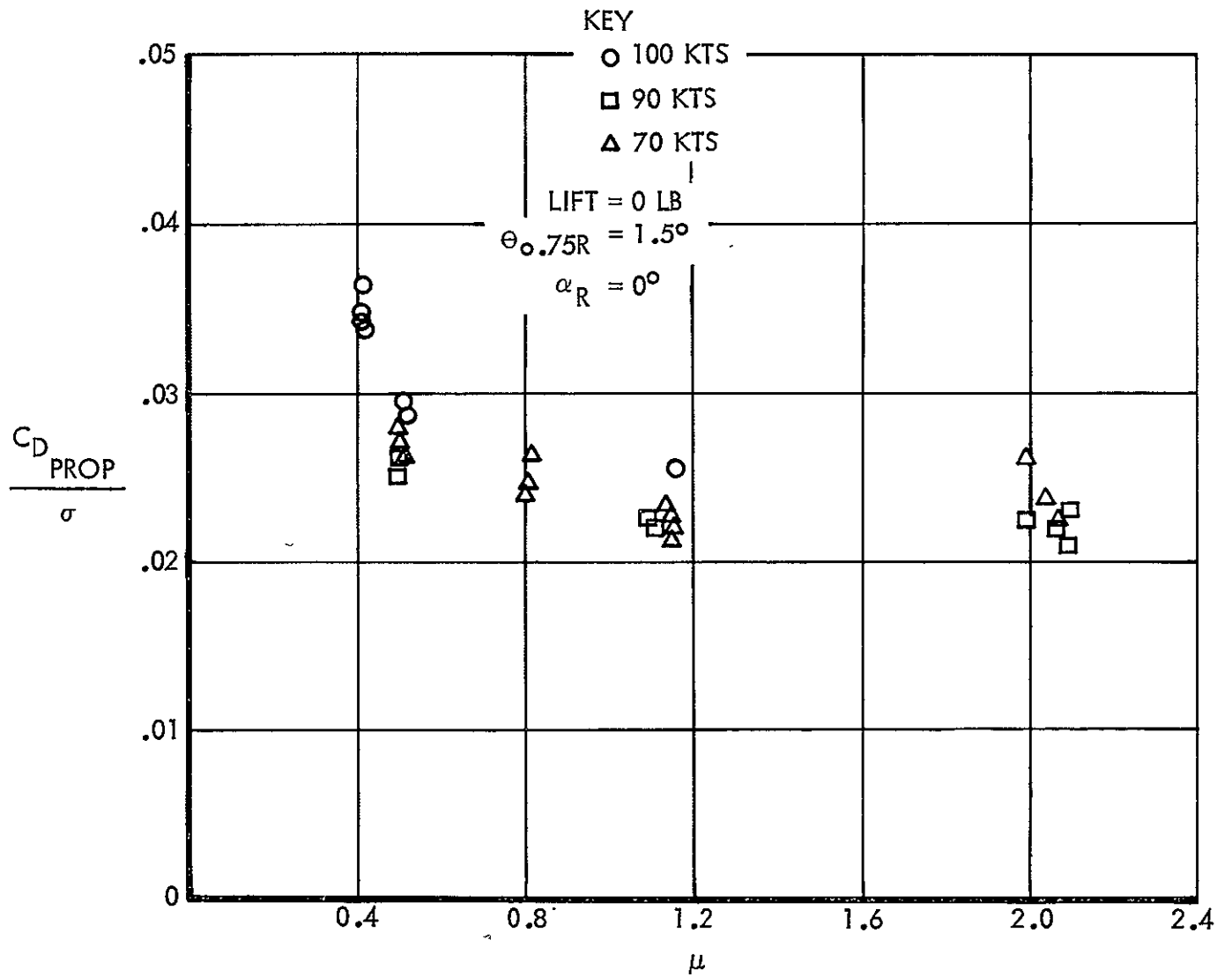
Figure 77. Rotor Drag Coefficient Versus Advance Ratio

167
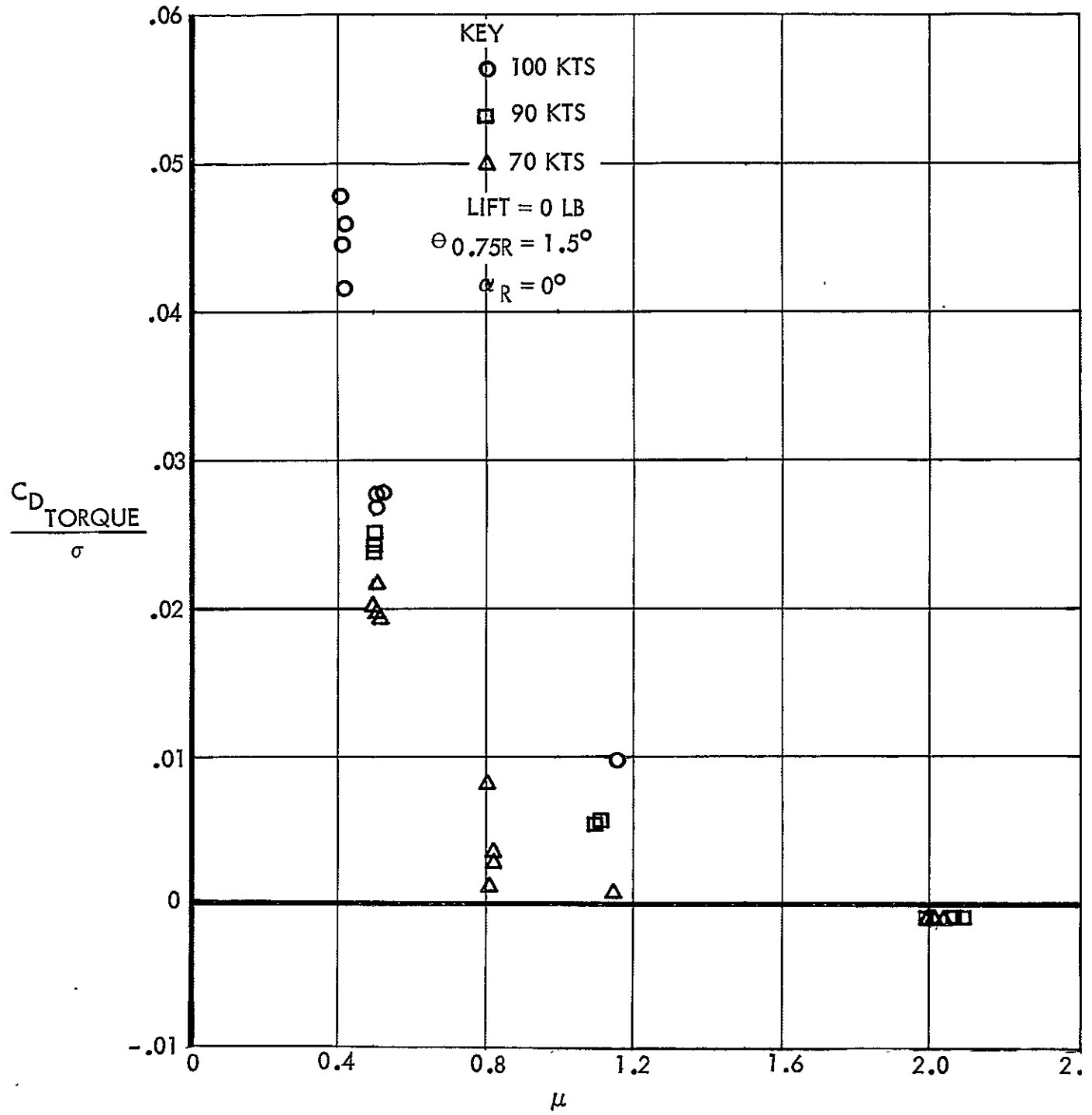
Figure 78.   Rotor Power Expressed As Effective Drag
Coefficient Versus Advance Ratio
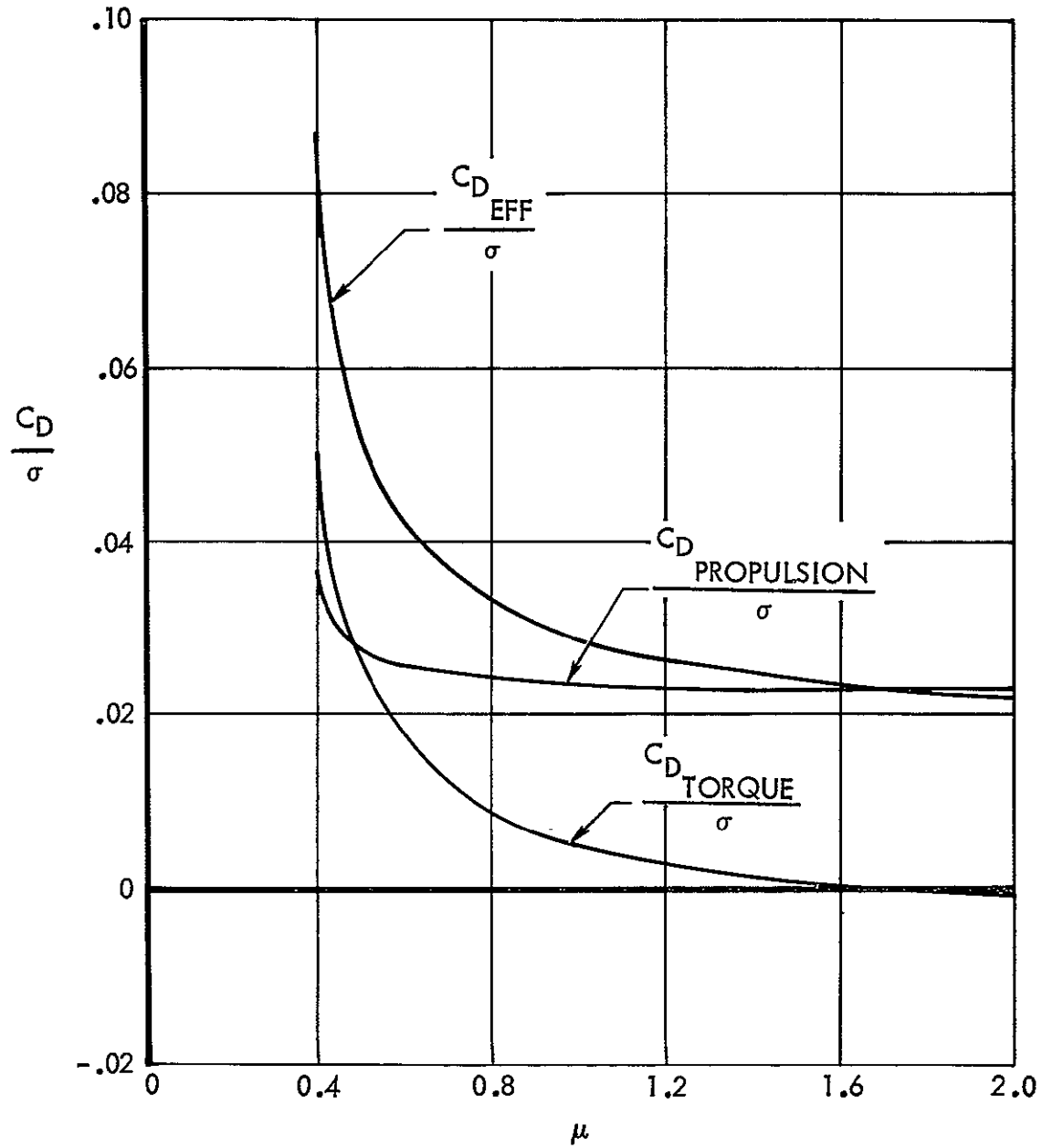
Figure 79.   Rotor Total Effective Drag Coefficient Versus Advance Ratio

CONCLUSIONS

The basic objectives of the study, "...to develop analyses directed at predicting the rotor model behavior and to measure the rotor model characteristics in various regions of interest.", were accomplished. The body of data on slowed/stopped hingeless rotors which had accrued in the decade preceding this study has been expanded by developing trim, control, and stability data over a range of rotor speeds from 8.5 to 90 percent of nominal rpm at flight speeds ranging from 50 to 120 knots; these data were developed both theoretically and experimentally. Some noteworthy conclusions are:

o A high-speed, constant-speed, gyro control system was demonstrated to be stable, to automatically trim swashplate moments to zero, and to produce hub moments in response to operator applied control moments which varied only slightly in magnitude and azimuth over a wide range of rotor speed and advance ratio.

o Feathering divergence at low rotor speed, discovered in earlier testing, was reconfirmed and explained by analysis. Analysis also showed that swashplate damping aggravated feathering divergence but that its effect could be ameliorated by feathering friction.

o Expository methods, developed to give insight into the behavior of rotor systems, led to the correct prediction of aeroelastic derivative trends over the advance ratio range $.4 < \mu < 2.0$; and the correct prediction of control mode stability trends over the full "conversion" advance ratio range.

- Studies of the practicality of testing the CL-870 model gimballed in the wind tunnel concluded that sufficient differences exist between fixed-shaft and free-flight stability to warrant the experimental study of the latter, but only at rotor speeds greater than 50 percent of nominal. At lower rotor speeds, the fixed-shaft case appeared to adequately represent free-flight.

  The studies also showed that gimballed model stability resembled free-flight stability in all essential features.

  The mechanization of the gimballed model should not be difficult since elevators and aileron and a special rotor control system would not be needed at the higher rotor speeds.

  For the above reasons, gimballed model tests at high rotor speed are recommended.

- Performance of compound helicopters is greatly improved by slowing the rotor. The torque required to maintain rotor speed on a non-lifting rotor decreases rapidly with decreasing rotor speed and becomes negligible at an advance ratio $\mu = 1.5$. The drag decreases somewhat with decreasing rotor speed to a constant value at an approximate advance ratio of $\mu = 1.1$. As a result of the reduced drag and torque, the total power required by the unloaded rotor reduces to about 1/3 that required at 0.4 advance ratio.

APPENDIX A
DERIVATION OF THE DIFFERENTIAL EQUATIONS
OF MOTION OF THE FREE FLYING AIRCRAFT

Differential equations of motion of the free-flying, retractable-rotor aircraft, during the period of conversion from the helicopter to the stopped-rotor condition, are derived. The aircraft, rotor and stabilizing gyroscope are represented by eight degrees of freedom:

- aircraft pitch, roll, and plunge (3 DOF)
- rotor pitch, roll, and coning flapping (3 DOF)
- gyroscope pitch and roll (2 DOF)

Scope and Procedure

A set of linear ordinary differential equations is derived to represent a gyro-controlled, hingeless rotor and airframe with sufficient accuracy to permit all significant modes of motion to be determined and their stabilities to be assessed. The rotor speed (rpm) is allowed to vary from a nominal value for a helicopter (100 percent rpm) to zero. The degrees of freedom employed in this analysis are those expected to be significant; illustrated in Figures A-1, A-2, and A-3. They are:

Airframe	pitch	Θ
Airframe	roll	Φ
Airframe	plunge	z
Gyro	pitch	θ
Gyro	roll	ϕ
Rotor flap	collective	δ_o
Rotor flap	pitch	δ_θ
Rotor flap	roll	δ_ϕ

The gyro angles θ and ϕ, illustrated in Figure A-2, are measured relative to the airframe. The absolute tilt angle of the gyro in space is therefore $\theta + \Theta$ and $\phi + \Phi$. The rotor flapping modes shown in Figure A-3 represent motions which are measured relative to the rotor shaft. Lateral, fore and aft, and yaw degrees of freedom are not used because the very low frequency dutch roll, spiral and phugoid modes are not expected to deviate much from those computed

Pitch, Roll and Plunge (of the complete
vehicle)

Shaft Pitch Θ

Shaft Roll Φ

Shaft Plunge z
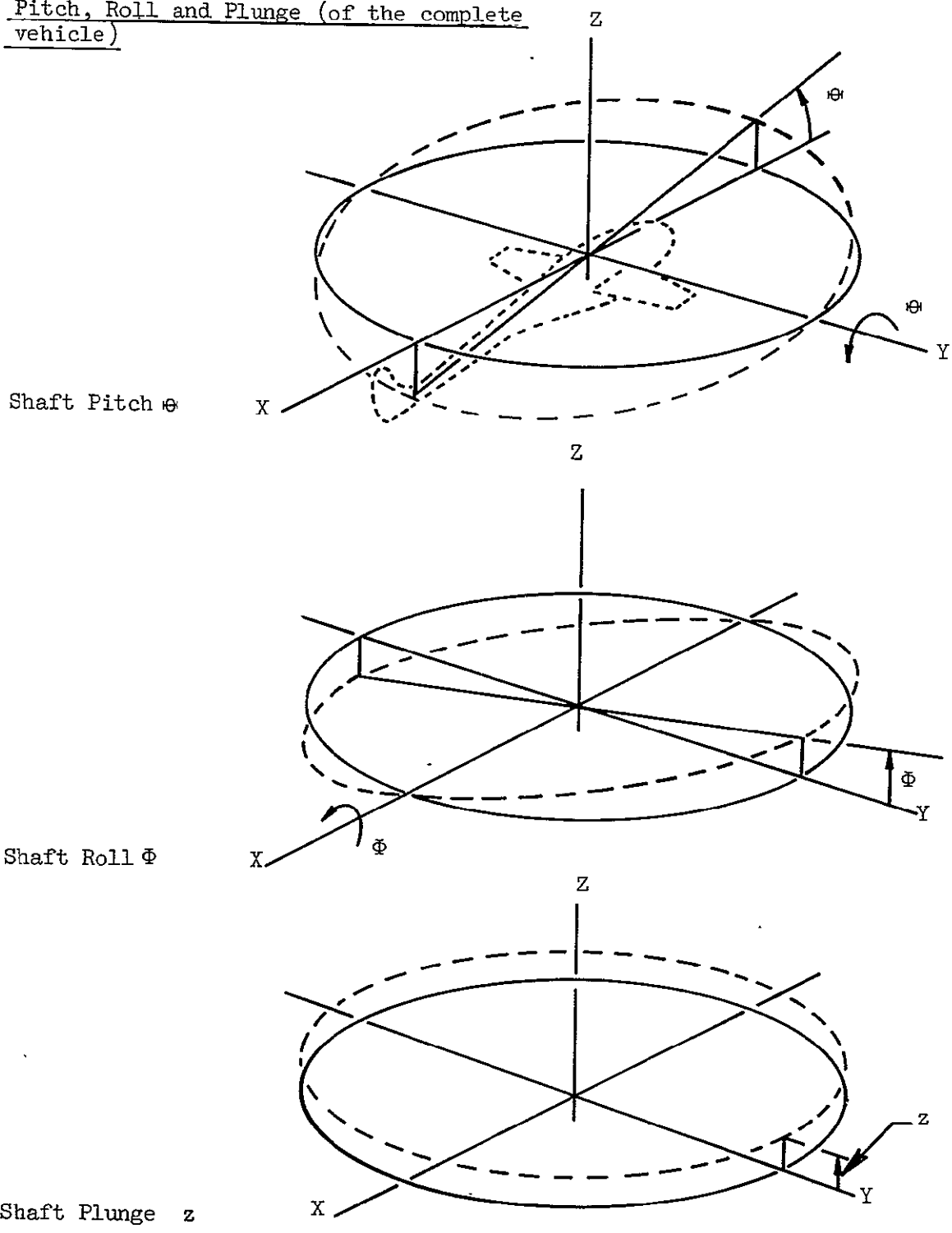
Figure A-1.   Degrees of Freedom in Stationary Axes; Pitch,
Roll, and Plunge of the Complete Aircraft

173

Gyro Pitch

$\Psi_o = 60°$
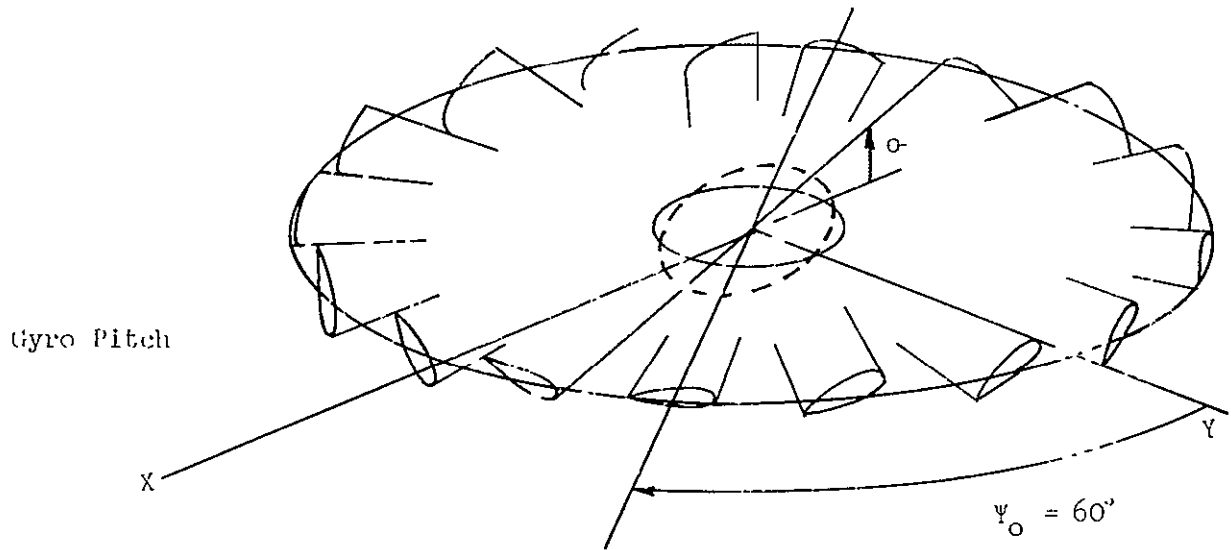
Note: Blade feathering displacements accompanying gyro tilt angles show effect of cant angle Ψ_o.

Gyro Roll

$\Psi_o = 60°$
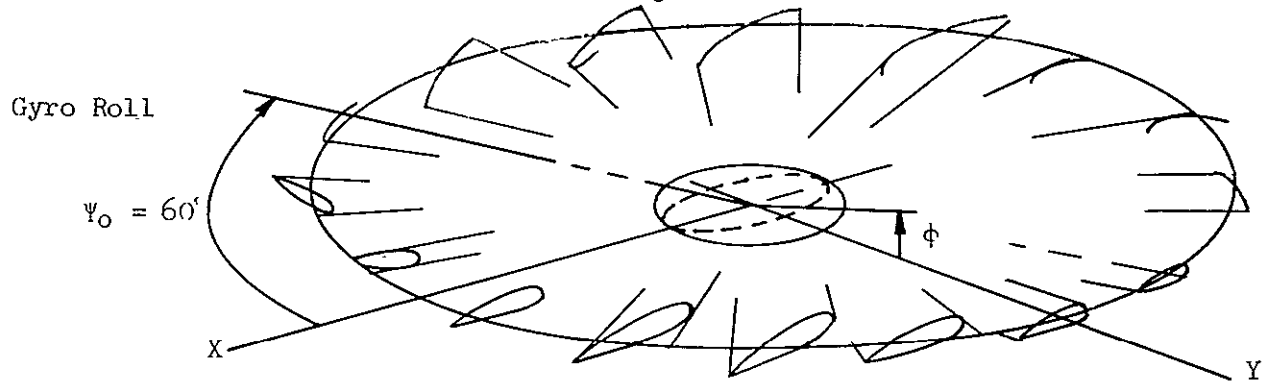
Figure A-2. Degrees of Freedom in Stationary Axes; Gyro (or Swashplate) Motion

Collective
Flapping δ_0

Pitch
Flapping δ_θ

Roll
Flapping δ_ϕ

$\Psi_0 = 60°$

$\Psi_0 = 60°$
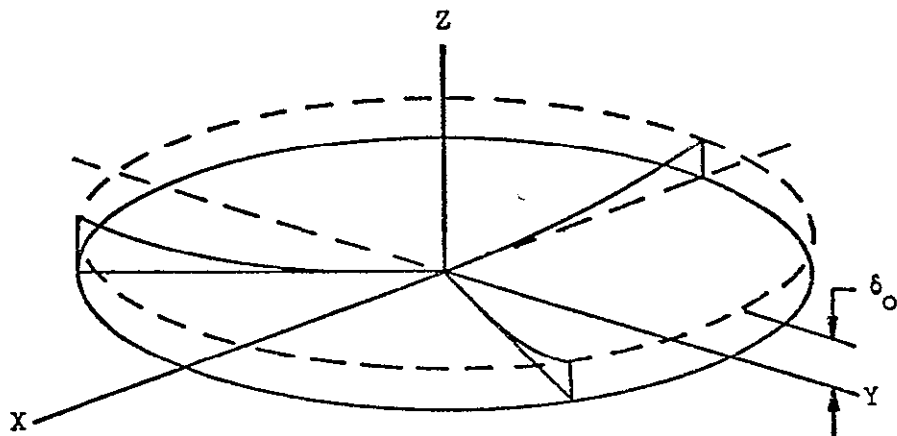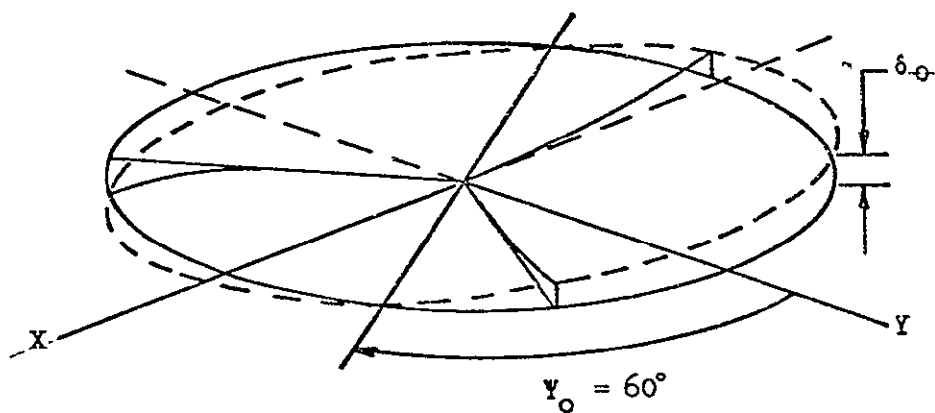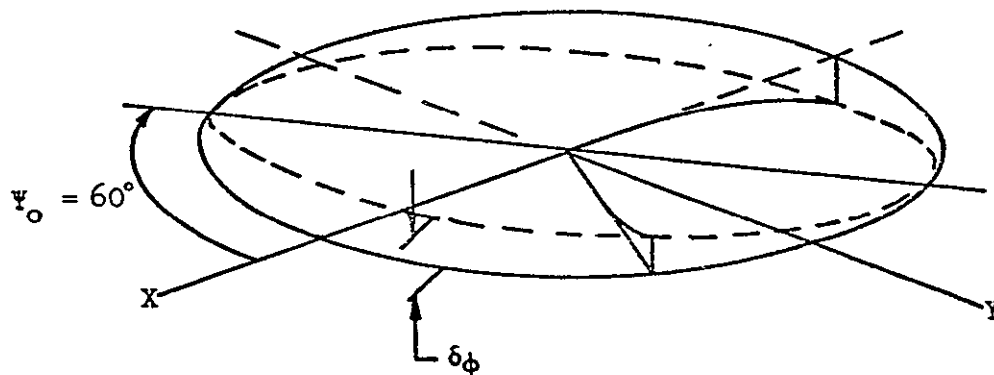
Note: Position of the blades is arbitrary. The modes maintain the same
position relative to the earth-fixed axes shown. Pitch and roll
flapping modes lag by the cant angle.

Figure A-3.   Degrees of Freedom in Stationary Axes;
Rotor Flapping Modes

175

by considering mean rotor aeroelastic and airframe derivatives. It is expected that these motions could be easily stabilized and controlled in designing an aircraft, therefore study of them is left for another time.

An additional objective of the study was to determine the practicality of wind tunnel tests in which the rotor would be attached to a rolling and pitching framework. In-plane motions of the blades were not admitted in the analysis and this is recognized as a possible shortcoming. However, since only small loads are applied in tests, due to structural limitations little nonlinear action is expected.

The equations and their coefficients are determined in a general enough way so that this work can be used as a basis for assessing the effects of periodically varying coefficients. However, a study of the effects of the periodic coefficients on stability, steady-state response, and transient response is beyond the scope of the work undertaken to date.

A five degree of freedom version of the equations (pitch, roll, and plunge are locked out) represents the rotor in the wind-tunnel-test configuration. This version is investigated first. Later, body inertia and aerodynamic derivatives are added and the stability of the whole free flight vehicle system is determined.

The differential equations are first derived in an axis system rotating with the rotor. The equations consisting of inertia, centrifugal, damping, spring, gyroscope, structural, and aerodynamic terms are then transformed to stationary axes. The equations are derived in the following sequence:

(1) Rotor Inertia terms
(2) Rotor Centrifugal and structural terms and rotating spring
(3) Rotor structural damping terms and gyro rotating damping
(4) Gyroscope terms
(5) Aerodynamic terms
(6) Collection of terms in rotating axes
(7) Transformation to stationary axes
(8) Swashplate springs and dampers
(9) Body terms

The derivation is preceded by descriptions of the rotor and gyroscope system and of rotor system motions.

Geometry of the Rotor System

Blades. - Each of three blades has a constant 14-in. (1.17 ft) chord, from 15 percent of the rotor radius to the tip. The rotor radius (R) is 16.5 ft. The feathering hinge axis and the quarter chord locus intersect at the center of rotation and are separated by a sweep-forward angle of the quarter chord (Λ) of 1.5 deg (0.0262 rad). The blades are preconed to an angle β_o from the disk plane of 2.25 deg (0.0393 rad). Each blade twisted linearly, leading edge down (washout), from zero at the center of rotation to 9.43 deg (-0.1645 rad) at the tip ($\theta_t R$). These dimensions are illustrated in Figure A-4.

The twist and coning angles are not degrees of freedom in the present formulation of the problem; these angles are fixed at all times.

Blades to gyroscope (and swashplate). - The feathering horns on the blades are connected to the gyroscope housing by a system of walking beams and linkages. In turn the housing is attached to the swashplate by three rods which constrain it to remain parallel to the swashplate. Angular displacements of the swashplate and gyroscope are therefore assumed to be identical (elastic distortion and joint tolerances are ignored).

In a simplified representation, the three blades are linked to the swashplate as shown in Figure A-5.

Blade feathering angles occur at azimuth angles different from the azimuth angle of the gyro tilt. This angle, called the cant angle (ψ_o) does not affect the basic behavior of the system so long as the shaft is prevented from pitching and rolling. In addition, the gyro arm is shorter than the blade feathering horn arm so that the gyro tilt angle is greater than the feathering displacement; this feature provides the mechanical advantage illustrated in Figure A-6.

$$k = \text{mechanical advantage} = \frac{\text{horn arm}}{\text{gyro arm}} = 1.15 \text{ for the rotor system tested}$$

in the present study.
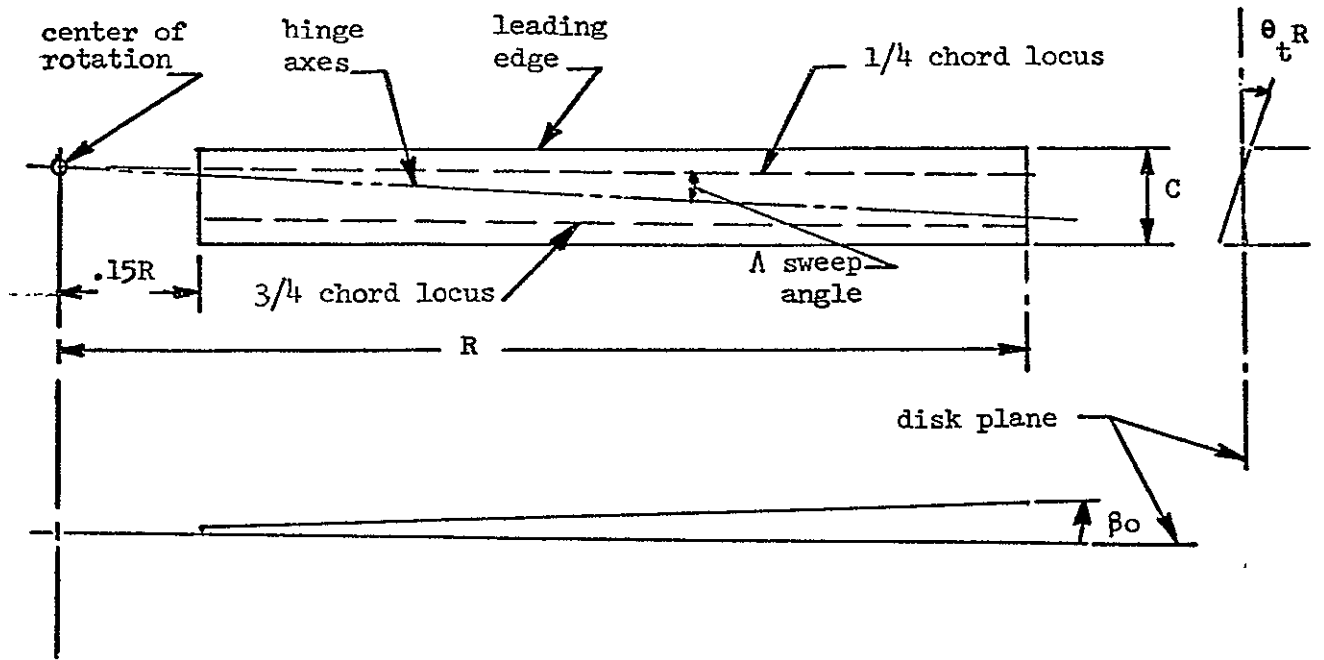
Figure A-4. Rotor Blade Geometry
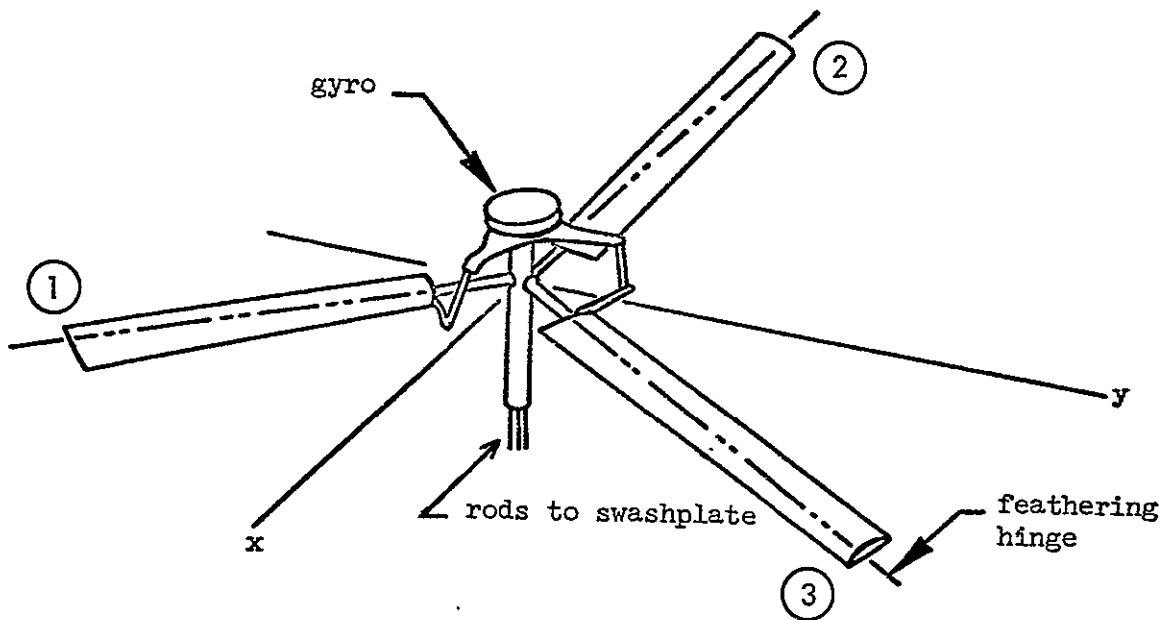
Figure A-5. Linkages Between Blade(s) Feathering
Motion and Swashplate Tilt

178

$$k = \frac{\text{HORN ARM}}{\text{GYRO ARM}} = \text{MECHANICAL ADVANTAGE} = 1.15 \text{ FOR THE PRESENT EXAMPLE.}$$
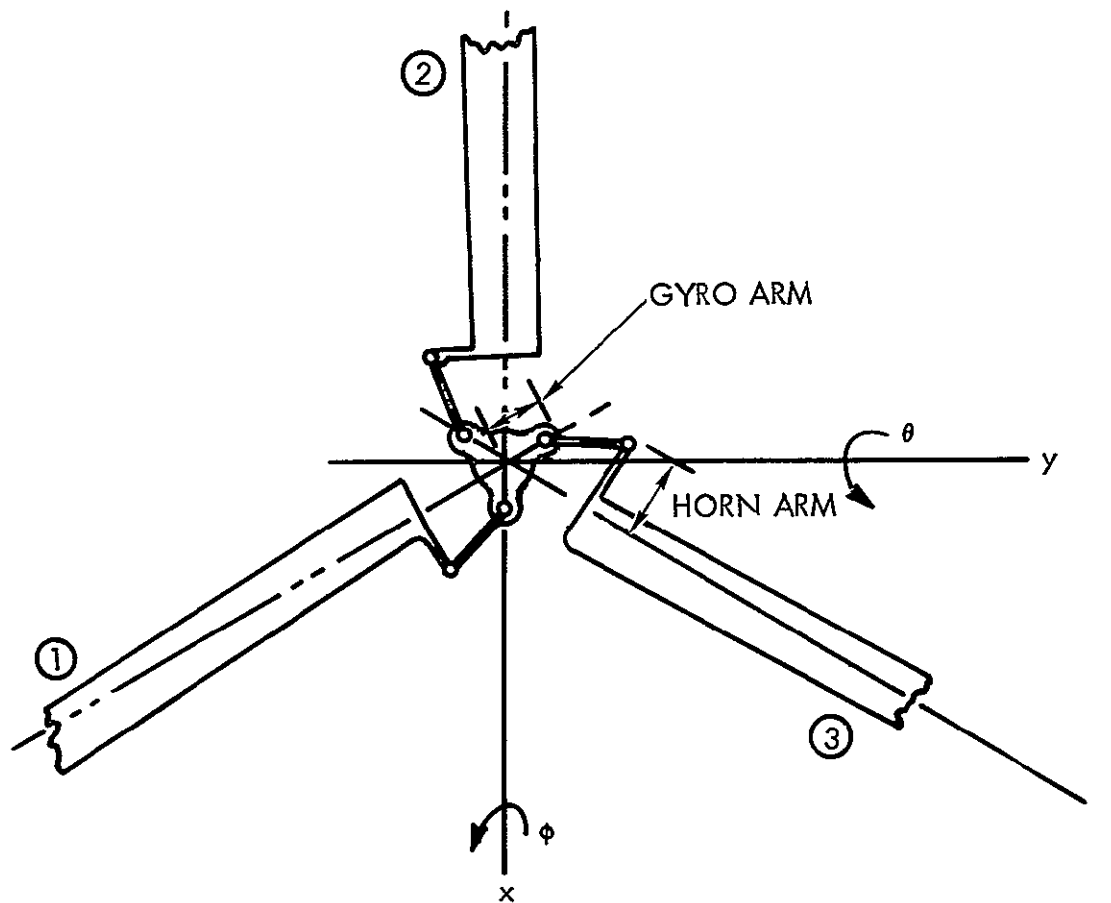
x , y AXES ROTATE WITH ROTOR,
PITCH AND ROLL ANGLES OF GYRO
ARE RELATIVE TO THE ROTATING AXES

Figure A-6.   Linkages Between Blade Feathering and Gyro Tilt
Angles, Showing Mechanical Advantage

Single blade motions. - The motions of the rotor are made up of the motions of single blades. The individual blades are assumed to move in four different modes:

(1) Feathering
(2) Linear Flapping (used to represent rotor pitch and roll motions)
(3) Parabolic Flapping (structural elastic deformations)
(4) Vertical Displacement

The motions, which are illustrated in Figure A-7, consist of displacements and their derivatives with respect to time.

Although the above four modes of motion comprise all the blade motions used in the derivations, it must be recognized that there are two "shape parameters" which cause two of the forcing derivatives: the rotor precone angle will cause aerodynamic loads due to linear flap displacement; and the twist shape will also cause aerodynamic loads.

Rotor pitch, roll, and plunge motions are now described relative to axes rotating with the rotor in terms of motions of the blades. As the rotor pitches or rolls, an equivalent motion is seen by letting the blades flap and feather. Considering a rotor with a number of blades b, a cant angle ψ_o, and the number ① blade located ψ_o behind the x axis of the rotating system,
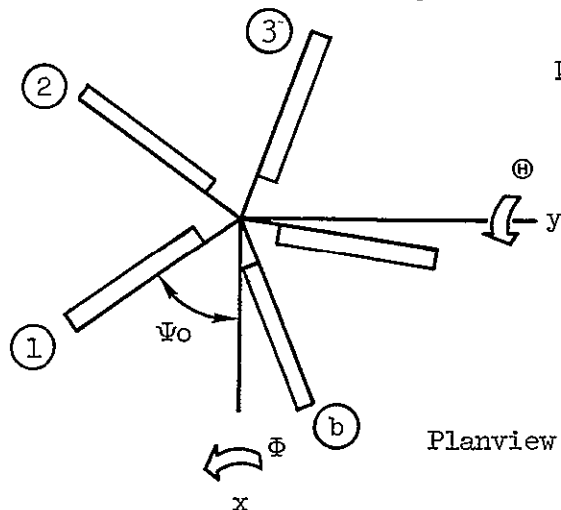
Notes: 1. Numbers in circles in this and in subsequent sketches identify particular rotor blades in the discussion and in the derivations which follow.

2. x and y axes shown are rotating axes.

Planview of rotor

FEATHERING MOTION

θ_f + nose up

feathering axis

undistorted disk plane

LINEAR FLAPPING

$\beta, \dot{\beta}$ tip up +

disk plane

$\mathcal{C}_L$ rotation

PARABOLIC FLAPPING

$\mathcal{C}_L$ rotation

$\delta, \dot{\delta}$ tip up +

disk plane

VERTICAL DISPLACEMENT

+ $\dot{z}$ flow

$z, \dot{z}$ up +

disk plane

plunge velocity is + upward
therefore relative flow is downwash
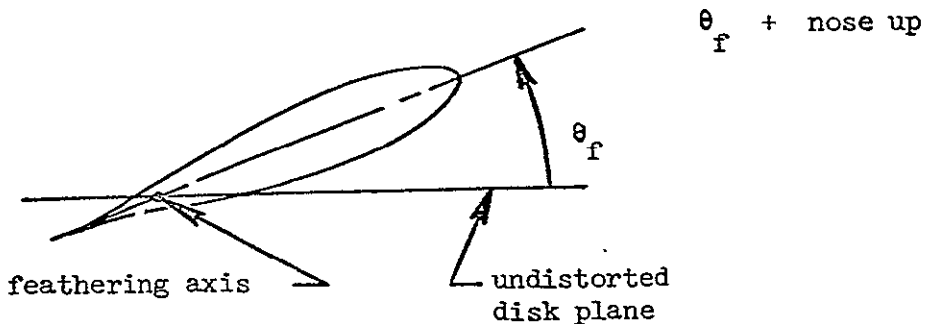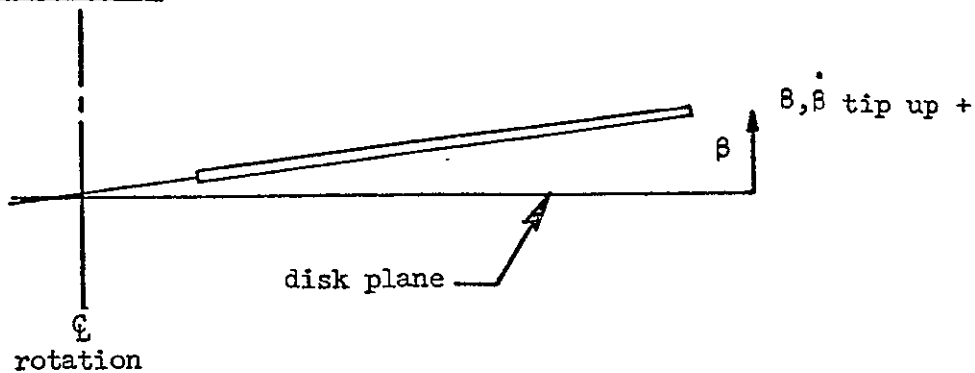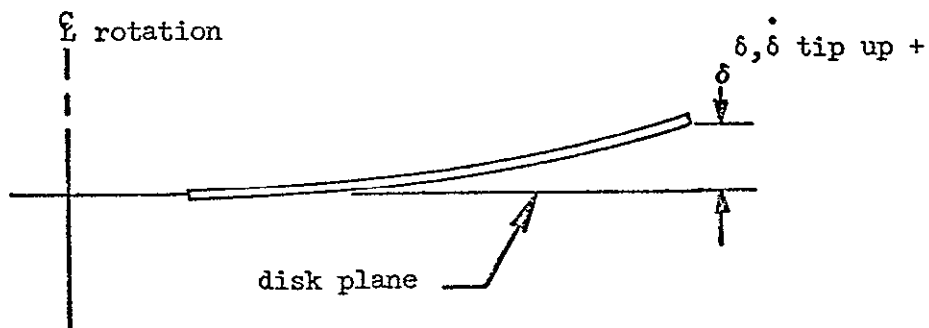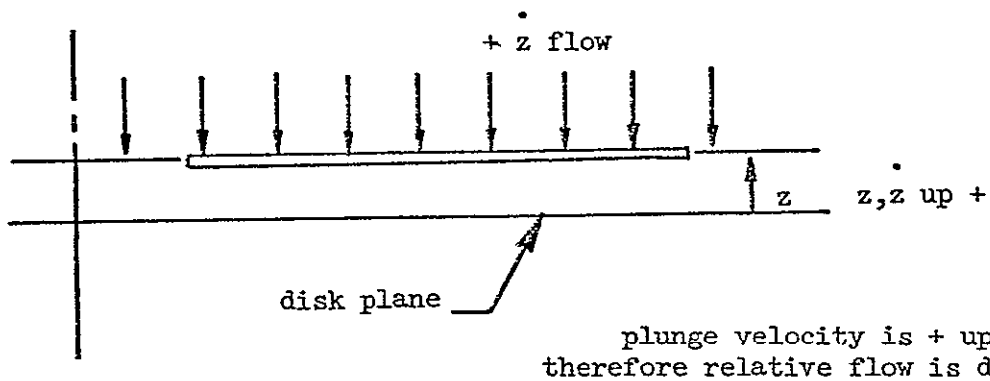
Figure A-7. The Four Modes of Motion

the flapping motion, for any blade which is identified as blade p, is given by

$$\dot{\beta}_{\textcircled{p}} = - \left\{ \text{Cos} \left[\psi_0 + (p\text{-}1) \frac{2\pi}{b} \right] \right\} \oplus - \left\{ \text{Sin} \left[\psi_0 + (p\text{-}1) \frac{2\pi}{b} \right] \right\} \Phi$$

which, for each blade of a three-bladed rotor, where the rotor cant angle, becomes $\psi_0 = 60°$

$$\beta_1 = -0.5 \oplus -0.866 \, \Phi$$

$$\beta_2 = 1.0 \oplus +0 \, \Phi$$

$$\beta_3 = -0.5 \oplus +0.866 \, \Phi$$

Feathering angles for the three blades are deduced by resolving $\oplus$ and Φ into flapping and feathering components:
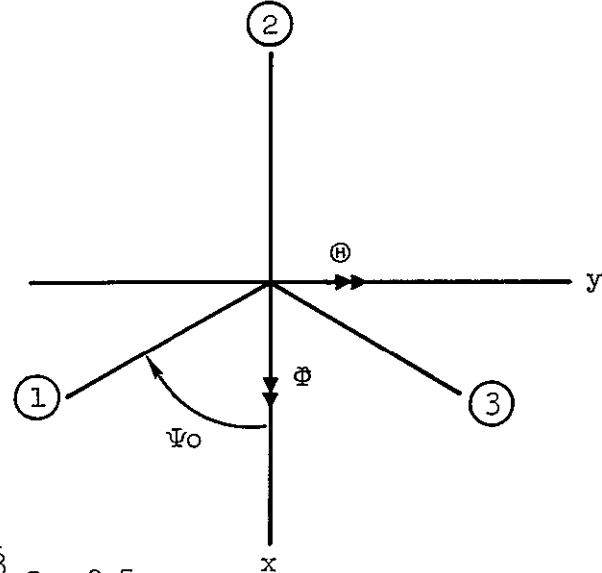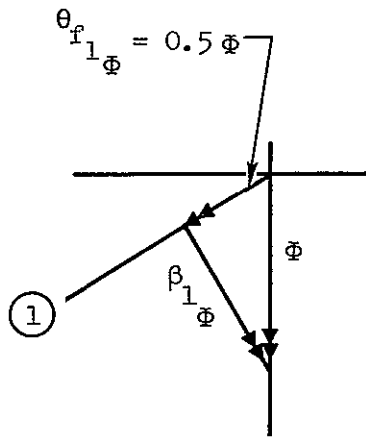
$$\theta_{f_1} = - \frac{\sqrt{3}}{2} \oplus + 0.5 \, \Phi$$

$$\theta_{f_2} = 0 - 1.0 \, \Phi$$

$$\theta_{f_3} = \frac{\sqrt{3}}{2} \oplus + 0.5 \, \Phi$$

182

In matrix notation, the flapping and feathering motions of the blades, in terms of rotor pitching and rolling motions, are:

$$
\begin{Bmatrix} \beta_1 \\ \theta_{f_1} \\ \beta_2 \\ \theta_{f_2} \\ \beta_3 \\ \theta_{f_3} \end{Bmatrix}
=
\begin{bmatrix}
-\frac{1}{2} & -\frac{\sqrt{3}}{2} \\
-\frac{\sqrt{3}}{2} & +\frac{1}{2} \\
1.0 & 0 \\
0 & -1.0 \\
-\frac{1}{2} & \frac{\sqrt{3}}{2} \\
\frac{\sqrt{3}}{2} & \frac{1}{2}
\end{bmatrix}
\begin{Bmatrix} \Theta \\ \Phi \end{Bmatrix}
$$

Plunge motions of the blades are

$$
\begin{Bmatrix} z_1 \\ z_2 \\ z_3 \end{Bmatrix}
=
\begin{Bmatrix} 1.0 \\ 1.0 \\ 1.0 \end{Bmatrix} z
$$

Swashplate tilt in rotating axes. - Where it is easy to generalize, generalization is made and the particular case of the 33-ft diameter rotor system is abstracted. Blade feathering angles due to swashplate tilt in pitch and roll are written for a rotor with "b" blades where "b" is any integer greater than 2; the generalized rotor used for this discussion is illustrated in the following sketch. The number (1) blade lags the x axis by the cant angle ψ_0, and therefore always possesses maximum negative feathering angle due to positive gyro pitch angle and zero feathering angle due to gyro roll; the lag is accomplished through pitch link geometry as illustrated in

Figure A-6. Because of this orientation of the axes the expression for blade feathering angle is independent of the gyro cant angle.
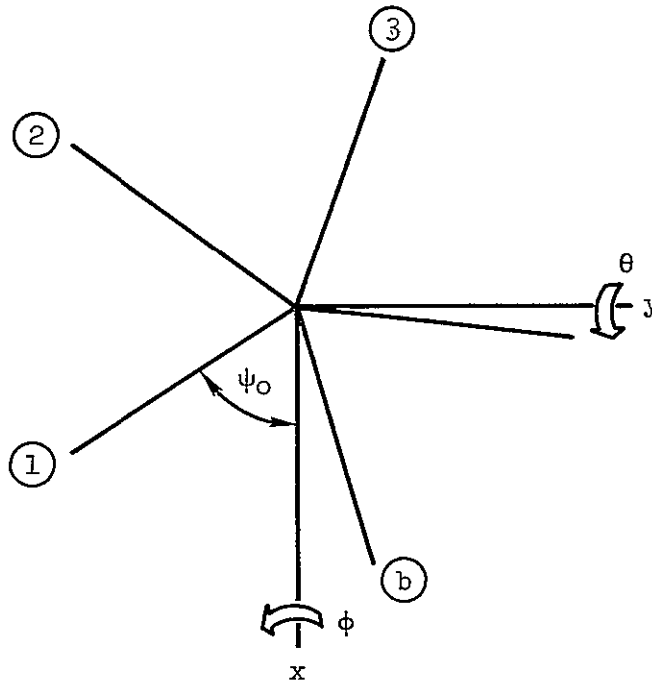
Since swashplate pitch tilt is lagged through the cant angle to blade ① directly, the blade feathering tilt due to swashplate tilt is

$$\theta_{f_{\textcircled{p}}} = -\frac{1}{k}\left\{\text{Cos}\left[(p\text{-}1)\frac{2\pi}{b}\right]\right\}\theta - \frac{1}{k}\left\{\text{Sin}\left[(p\text{-}1)\frac{2\pi}{b}\right]\right\}\phi$$

where p identifies the particular blade, any of ① through ⓑ, to which the expression applies. For each of 3 blades of a three-bladed rotor,

$$\theta_{f_1} = -\frac{1}{k}\theta + 0\,\phi$$

$$\theta_{f_2} = \frac{0.5}{k}\theta - \frac{0.866}{k}\phi$$

$$\theta_{f_3} = \frac{0.5}{k}\theta + \frac{0.866}{k}\phi$$

which is denoted thus in matrix form:

$$\left\{ \begin{array}{c} \theta_{f_1} \\ \\ \theta_{f_2} \\ \\ \theta_{f_3} \end{array} \right\} = \left[\begin{array}{cc} -\dfrac{1}{k} & 0 \\ \\ \dfrac{0.5}{k} & -\dfrac{0.866}{k} \\ \\ \dfrac{0.5}{k} & \dfrac{0.866}{k} \end{array} \right] \left\{ \begin{array}{c} \theta \\ \\ \phi \end{array} \right\}$$

Rotor flapping modes in rotating axes. - The number of modes in a complete set of rotor flapping modes (corresponding to the first flap mode of a single blade as in the case shown) equals the number of blades. For three-bladed rotors, the three modes are: collective flapping, pitch flapping, and roll flapping; these are illustrated in Figure A-8. For more than three blades, modes that would exist in addition to the above three modes would be self-balancing; that is, they would produce no net vertical inertia force or pitching or rolling inertia moments. For example, the modes of a four-bladed rotor would be as shown in Figure A-9.

The transformation relating tip deflections to rotor modal deflections for the four-bladed rotor is given by the following expressions:

$$\delta_1 = \delta_o - \delta_\theta + 0 + \delta_s$$

$$\delta_2 = \delta_o + 0 - \delta_\phi - \delta_s$$

$$\delta_3 = \delta_o + \delta_\theta + 0 + \delta_s$$

$$\delta_4 = \delta_o + 0 + \delta_\phi - \delta_s$$

$$\left\{ \begin{array}{c} \delta_1 \\ \\ \delta_2 \\ \\ \delta_3 \\ \\ \delta_4 \end{array} \right\} = \left[\begin{array}{cccc} 1 & -1 & 0 & 1 \\ \\ 1 & 0 & -1 & -1 \\ \\ 1 & 1 & 0 & 1 \\ \\ 1 & 0 & 1 & -1 \end{array} \right] \left\{ \begin{array}{c} \delta_o \\ \\ \delta_\theta \\ \\ \delta_\phi \\ \\ \delta_s \end{array} \right\}$$
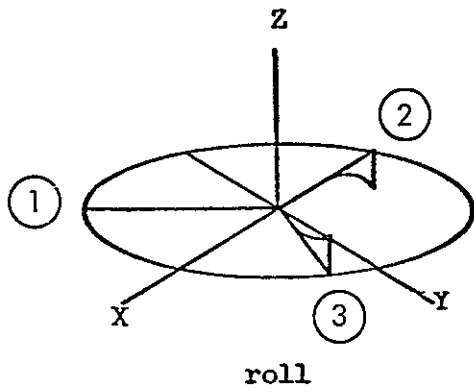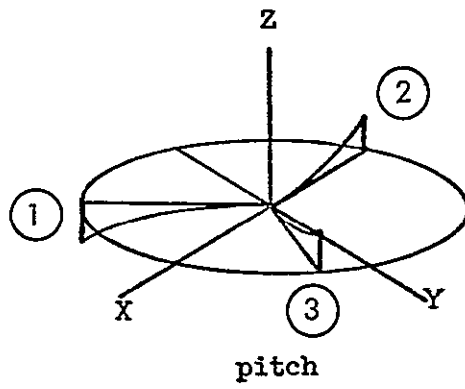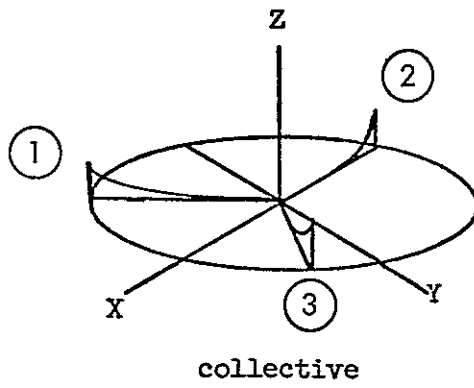
Figure A-8. Flapping Modes of a Three-Blade Rotor

airflow

collective

pitch

roll

self-balancing
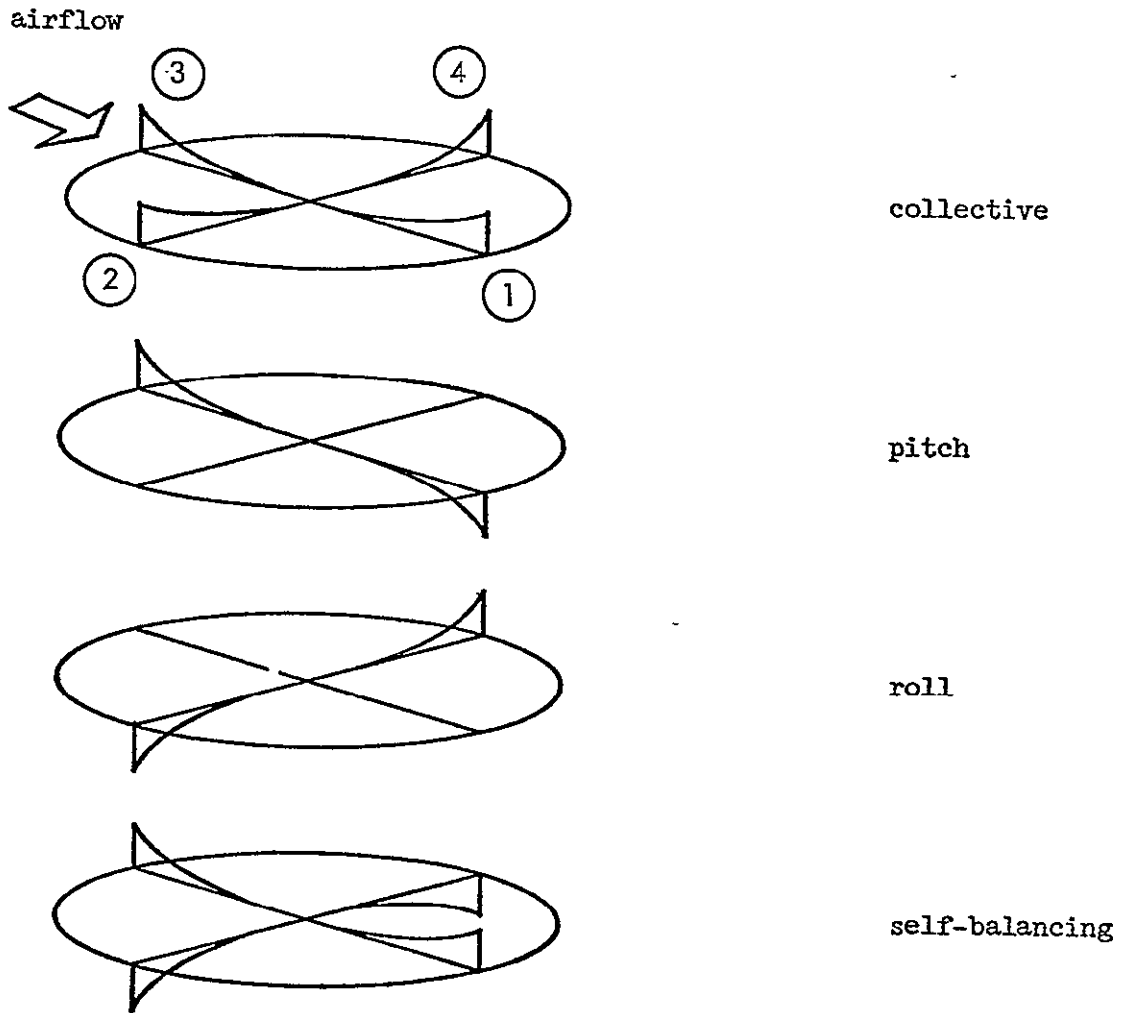
Figure A-9. Flapping Modes for a Four-Blade Rotor

For the three-bladed rotor locations of flapping modes relative to the rotating axes must be identified. The resulting relationship for tip deflections is:

$$\delta_1 = \delta_o - \delta_\theta$$

$$\delta_2 = \delta_o + \frac{1}{2}\delta_\theta - \frac{\sqrt{3}}{2}\delta_\phi$$

$$\delta_3 = \delta_o + \frac{1}{2}\delta_\theta + \frac{\sqrt{3}}{2}\delta_\phi$$

$$\begin{Bmatrix} \delta_1 \\ \delta_2 \\ \delta_3 \end{Bmatrix} = \begin{bmatrix} 1 & -1 & 0 \\ 1 & .5 & -.866 \\ 1 & .5 & .866 \end{bmatrix} \begin{Bmatrix} \delta_o \\ \delta_\theta \\ \delta_\phi \end{Bmatrix}$$

It is important to note that the pitch and roll flapping axes are not coincident with the pitch and roll rotating axes but lag behind by the cant angle.

Summary of motion in rotating axes. - Let the fundamental rotor degrees of freedom, in rotating axes, be arrayed in a column vector called $\{\beta\}$,

$$\{\beta\} = \begin{Bmatrix} \oplus \\ \Phi \\ z \\ \theta \\ \phi \\ \delta_o \\ \delta_\theta \\ \delta_\phi \end{Bmatrix} = \text{a vector of degrees of freedom.}$$

188

and let the displacements of the blades (shown for a three-blade rotor) be arrayed into a column vector called $\{\eta\}$,

$$\{\eta\} = \begin{Bmatrix} \beta_1 \\ z_1 \\ \theta_1 \\ \delta_1 \\ \beta_2 \\ z_2 \\ \theta_2 \\ \delta_2 \\ \beta_3 \\ z_3 \\ \theta_3 \\ \delta_3 \end{Bmatrix} \quad = \text{a vector of blade motions.}$$

The relationship between blade motions and rotor motions is a single-valued nonsquare matrix, denoted $\begin{bmatrix} D \end{bmatrix}$. The combined expressions are

$$\{\eta\} = [D] \{\beta\}$$

$$
\begin{Bmatrix} \beta_1 \\ z_1 \\ \theta_1 \\ \delta_1 \\ \beta_2 \\ z_2 \\ \theta_2 \\ \delta_2 \\ \beta_3 \\ z_3 \\ \theta_3 \\ \delta_3 \end{Bmatrix}
=
\begin{bmatrix}
-.5 & -.866 & 0 & 0 & 0 & 0 & 0 & 0 \\
0 & 0 & 1.0 & 0 & 0 & 0 & 0 & 0 \\
-.866 & .5 & 0 & \frac{-1}{k} & 0 & 0 & 0 & 0 \\
0 & 0 & 0 & & 0 & 1.0 & -1.0 & 0 \\
1.0 & 0 & 0 & 0 & 0 & 0 & 0 & 0 \\
0 & 0 & 1.0 & 0 & 0 & 0 & 0 & 0 \\
0 & -1.0 & 0 & \frac{.5}{k} & \frac{-.866}{k} & 0 & 0 & 0 \\
0 & 0 & 0 & 0 & 0 & 1.0 & .5 & -.866 \\
-.5 & .866 & 0 & 0 & 0 & 0 & 0 & 0 \\
0 & 0 & 1.0 & 0 & 0 & 0 & 0 & 0 \\
.866 & .5 & 0 & \frac{.5}{k} & \frac{-.866}{.k} & 0 & 0 & 0 \\
0 & 0 & 0 & 0 & 0 & 1.0 & .5 & .866
\end{bmatrix}
\begin{Bmatrix} \Theta \\ \Phi \\ z \\ \theta \\ \phi \\ \delta_o \\ \delta_\theta \\ \delta_\phi \end{Bmatrix}
$$

190

<u>Rotor inertia terms in rotating axes.</u> - Each rotor blade is assumed to have all mass concentrated in its chord plane (i.e., blade has no thickness or twist, although twist aerodynamic forces are considered).

The relationships between the motions of the degrees of freedom and motions of the blades are as follows:

$$\{\eta\} = [D]\{\theta\}$$
$$\{\dot{\eta}\} = [D]\{\dot{\beta}\}$$
$$\{\ddot{\eta}\} = [D]\{\ddot{\beta}\}$$

which show the motions of the blades due to changes in displacement, velocity, or acceleration as related to the degrees of freedom. Therefore, blade accelerations are related to degree-of-freedom accelerations by:

$$
\begin{Bmatrix} \ddot{\beta}_1 \\ \ddot{z}_1 \\ \ddot{\theta}_1 \\ \ddot{\delta}_1 \\ \ddot{\beta}_2 \\ \ddot{z}_2 \\ \ddot{\theta}_2 \\ \ddot{\delta}_2 \\ \ddot{\beta}_3 \\ \ddot{z}_3 \\ \ddot{\theta}_3 \\ \ddot{\delta}_3 \end{Bmatrix}
=
\begin{bmatrix}
-.5 & -.866 & 0 & 0 & 0 & 0 & 0 & 0 \\
0 & 0 & 1.0 & 0 & 0 & 0 & 0 & 0 \\
-.866 & .5 & 0 & \frac{-1}{k} & 0 & 0 & 0 & 0 \\
0 & 0 & 0 & 0 & 0 & 1.0 & -1.0 & 0 \\
1.0 & 0 & 0 & 0 & 0 & 0 & 0 & 0 \\
0 & 0 & 1.0 & 0 & 0 & 0 & 0 & 0 \\
0 & -1.0 & 0 & \frac{.5}{k} & \frac{-.866}{k} & 0 & 0 & 0 \\
0 & 0 & 0 & 0 & 0 & 1.0 & .5 & -.866 \\
-.5 & .866 & 0 & 0 & 0 & 0 & 0 & 0 \\
0 & 0 & 1.0 & 0 & 0 & 0 & 0 & 0 \\
.866 & .5 & 0 & \frac{.5}{k} & \frac{.866}{k} & 0 & 0 & 0 \\
0 & 0 & 0 & 0 & 0 & 1.0 & .5 & .866
\end{bmatrix}
\begin{Bmatrix} \ddot{\Theta}_R \\ \ddot{\Phi}_R \\ \ddot{z} \\ \ddot{\theta}_R \\ \ddot{\phi}_R \\ \ddot{\delta}_o \\ \ddot{\delta}\theta_R \\ \ddot{\delta}\phi_R \end{Bmatrix}
$$

The next step is to develop a matrix which relates generalized forces on the blades to accelerations of the blades. The generalized forces are root shear (V), root bending moment (bm), feathering moment (fm), and flapping generalized force (H). In this analysis the elements of mass in the blades are assumed to move only normal to the rotor disk (no radial or tangential motions). Therefore, there are no inertia forces, relative to axes which rotate with the rotor, due to velocity. The only inertia forces are those due to acceleration, which is interpreted to mean that the blade generalized forces are related to blade motions by the blade inertia matrix,

$$\left\{ GF_b \right\} = - \left[I_b \right] \left\{ \ddot{\eta} \right\}$$

the vehicle degree-of-freedom generalized forces are related to the blade generalized forces by:

$$\left\{ GF \right\} = \left[D \right]^T \left\{ GF_b \right\}$$

Therefore, the vehicle degree-of-freedom generalized forces are related to vehicle degree-of-freedom motions by

$$\left\{ GF \right\} = - \left[D \right]^T \left[I_b \right] \left[D \right] \left\{ \ddot{\beta} \right\}$$

The terms of the differential equation due to acceleration of the degrees of freedom of the vehicle are therefore

$$- \left[D \right]^T \left[I_b \right] \left[D \right]$$

The minus sign makes them inertia reaction forces which puts them in the right hand side (RHS) of the differential equations.

192

The $[I_b]$ matrix for the three-blade rotor consists of 12x12 elements, two thirds of which are zero. The non-zero elements are arranged in three 4x4 sub-matrices, and since the blades are identical, the three sub-matrices are also identical.

$$
\begin{Bmatrix} bm_① \\ V_① \\ fm_① \\ H_① \\ bm_② \\ V_② \\ fm_② \\ H_② \\ bm_③ \\ V_③ \\ fm_③ \\ H_③ \end{Bmatrix}
=
\left[
\begin{array}{cccc|cccc|cccc}
\frac{dbm}{d\ddot\beta} & \frac{dbm}{d\ddot z} & \frac{dbm}{d\ddot\theta} & \frac{dbm}{d\ddot\delta} & & & & & & & & \\
\frac{dV}{d\ddot\beta} & \frac{dV}{d\ddot z} & \frac{dV}{d\ddot\theta} & \frac{dV}{d\ddot\delta} & & & & & & & & \\
\frac{dfm}{d\ddot\beta} & \frac{dfm}{d\ddot z} & \frac{dfm}{d\ddot\theta} & \frac{dfm}{d\ddot\delta} & & & & & & & & \\
\frac{dH}{d\ddot\beta} & \frac{dH}{d\ddot z} & \frac{dH}{d\ddot\theta} & \frac{dH}{d\ddot\delta} & & & & & & & & \\
\hline
 & & & & \frac{dbm}{d\ddot\beta} & \frac{dbm}{d\ddot z} & \frac{dbm}{d\ddot\theta} & \frac{dbm}{d\ddot\delta} & & & & \\
 & & & & \frac{dV}{d\ddot\beta} & \frac{dV}{d\ddot z} & \frac{dV}{d\ddot\theta} & \frac{dV}{d\ddot\delta} & & & & \\
 & & & & \frac{dfm}{d\ddot\beta} & \frac{dfm}{d\ddot z} & \frac{dfm}{d\ddot\theta} & \frac{dfm}{d\ddot\delta} & & & & \\
 & & & & \frac{dH}{d\ddot\beta} & \frac{dH}{d\ddot z} & \frac{dH}{d\ddot\theta} & \frac{dH}{d\ddot\delta} & & & & \\
\hline
 & & & & & & & & \frac{dbm}{d\ddot\beta} & \frac{dbm}{d\ddot z} & \frac{dbm}{d\ddot\theta} & \frac{dbm}{d\ddot\delta} \\
 & & & & & & & & \frac{dV}{d\ddot\beta} & \frac{dV}{d\ddot z} & \frac{dV}{d\ddot\theta} & \frac{dV}{d\ddot\delta} \\
 & & & & & & & & \frac{dfm}{d\ddot\beta} & \frac{dfm}{d\ddot z} & \frac{dfm}{d\ddot\theta} & \frac{dfm}{d\ddot\delta} \\
 & & & & & & & & \frac{dH}{d\ddot\beta} & \frac{dH}{d\ddot z} & \frac{dH}{d\ddot\theta} & \frac{dH}{d\ddot\delta}
\end{array}
\right]
\begin{Bmatrix} \ddot\beta_1 \\ \ddot z \\ \ddot\theta_1 \\ \ddot\delta_1 \\ \ddot\beta_2 \\ \ddot z_2 \\ \ddot\theta_2 \\ \ddot\delta_2 \\ \ddot\beta_3 \\ \ddot z_3 \\ \ddot\theta_3 \\ \ddot\delta_3 \end{Bmatrix}
$$

In Appendix B, where flapping characteristics of the three-blade rotor of the wind tunnel model are discussed the mass distribution on each blade is divided into two parts:

o one part representing the distribution of mass between the blade tip
and the root, but excluding any mass concentrated at the tip

o a second part which represents only the tip mass.

Each of the submatrices in the preceding 12x12 matrix is therefore composed of two parts: one due to distributed mass and one due to tip mass. Those elements due to distributed mass are derived for each of the four accelerations as follows:

Due to $\ddot{\beta}$, for $+\ddot{\beta}$ (tip moving up) the inertia forces will act in the down direction. Using signs corresponding to RHS of equations,

$$d\ell = -\ddot{\beta}r \frac{dm}{dr} dr$$

$$\frac{dbm}{d\ddot{\beta}} = - \int_{.15R}^{R} r^2 \frac{dm}{dr} dr$$

$$\frac{dV}{d\ddot{\beta}} = - \int_{.15R}^{R} r \frac{dm}{dr} dr$$

$$\frac{dfm}{d\ddot{\beta}} = \Lambda \frac{dbm}{d\ddot{\beta}}$$

$$\frac{dH}{d\ddot{\beta}} = - \int_{.15R}^{R} \left(\frac{r}{R}\right)^2 r \frac{dm}{dr} dr$$

Due to $\ddot{z}$, for $+\ddot{z}$ (whole blade moving up) inertia force will act in the down direction, and terms corresponding to RHS of equations are

$$d\ell = -\ddot{z} \frac{dm}{dr} dr$$

$$\frac{dbm}{d\ddot{z}} = - \int_{.15R}^{R} r \frac{dm}{dr} dr$$

$$\frac{dV}{d\ddot{z}} = - \int_{.15R}^{R} \frac{dm}{dr} dr$$

$$\frac{dfm}{d\ddot{z}} = \Lambda \frac{dbm}{d\ddot{z}}$$

$$\frac{dH}{d\ddot{z}} = -\int_{.15R}^{R} \left(\frac{r}{R}\right)^2 \frac{dm}{dr} dr$$

Due to $\ddot{\theta}$, for $+\ddot{\theta}_f$ (blade nose moving up) inertia forces will act in the down direction, and terms corresponding to RHS of equations are

$$d\ell = -\ddot{\theta}_f \Lambda r \frac{dm}{dr} dr$$

$$\frac{dbm}{d\ddot{\theta}_f} = -\Lambda \int_{.15R}^{R} r^2 \frac{dm}{dr} dr$$

$$\cdot \frac{dV}{d\ddot{\theta}_f} = -\Lambda \int_{.15R}^{R} r \frac{dm}{dr} dr$$

$$\frac{dfm}{d\ddot{\theta}_f} = -\Lambda^2 \int_{.15R}^{R} r^2 \frac{dm}{dr} dr$$

$$\frac{dH}{d\ddot{\theta}_f} = -\Lambda \int_{.15R}^{R} r\left(\frac{r}{R}\right)^2 \frac{dm}{dr} dr$$

Due to $\ddot{\delta}$, for $+\ddot{\delta}$ (blade tip moving up) inertia forces will act in the down direction, and terms corresponding to RHS of equations are

$$d\ell = -\left(\frac{r}{R}\right)^2 \frac{dm}{dr} dr$$

$$\frac{dbm}{d\ddot{\delta}} = -\int_{.15R}^{R} \left(\frac{r}{R}\right)^2 r \frac{dm}{dr} dr$$

195

$$\frac{dV}{d\ddot{\delta}} = - \int_{.15R}^{R} \left(\frac{r}{R}\right)^2 \frac{dm}{dr}\, dr$$

$$\frac{dfm}{d\ddot{\delta}} = \Lambda\, \frac{dbm}{d\ddot{\delta}}$$

$$\frac{dH}{d\ddot{\delta}} = - \int_{.15R}^{R} \left(\frac{r}{R}\right)^4 \frac{dm}{dr}\, dr$$

The $\left[I_b\right]$ matrix for the distributed mass part is expressed as follows when the preceding expressions are included:

$$
-\left[I_b\right] =
\begin{bmatrix}
-\int_{.15R}^{R} r^2 \frac{dm}{dr}\, dr & -\int_{.15R}^{R} r\, \frac{dm}{dr}\, dr & -\Lambda\int_{.15R}^{R} r^2 \frac{dm}{dr}\, dr & -\int_{.15R}^{R}\left(\frac{r}{R}\right)^2 r\, \frac{dm}{dr}\, dr \\[2ex]
-\int_{.15R}^{R} r\, \frac{dm}{dr}\, dr & -\int_{.15R}^{R} \frac{dm}{dr}\, dr & -\Lambda\int_{.15R}^{R} r\, \frac{dm}{dr}\, dr & -\int_{.15R}^{R}\left(\frac{r}{R}\right)^2 \frac{dm}{dr}\, dr \\[2ex]
-\Lambda\int_{.15R}^{R} r^2 \frac{dm}{dr}\, dr & -\Lambda\int_{.15R}^{R} r\, \frac{dm}{dr}\, dr & -\Lambda^2\int_{.15R}^{R} r^2 \frac{dm}{dr}\, dr & -\Lambda\int_{.15R}^{R}\left(\frac{r}{R}\right)^4 \frac{dm}{dr}\, dr \\[2ex]
-\int_{.15R}^{R}\left(\frac{r}{R}\right)^2 r\frac{dm}{dr}\, dr & -\int_{.15R}^{R}\left(\frac{r}{R}\right)^2 \frac{dm}{dr}\, dr & -\Lambda\int_{.15R}^{R} r\left(\frac{r}{R}\right)^2 \frac{dm}{dr}\, dr & -\int_{.15R}^{R}\left(\frac{r}{R}\right)^4 \frac{dm}{dr}\, dr
\end{bmatrix}
$$

It is noted that the matrix is symmetrical, and that it includes only five different integrals.

The weight and stiffness distributions of each rotor blade of the 33-ft diameter rotor of the wind tunnel model are given in Figures 9 and 12 in the body of this report. An algebraic approximation of the weight distribution, dwt./dr is shown in Figure 9. Converting this expression to represent units of mass gives

$$\frac{dm}{dr} = 0.44 - 0.0478r + 0.001823r^3 \text{ slugs/ft}$$

Numerical values for each of the elements due to distributed mass can therefore be determined for the wind tunnel model rotor, as follows:

$$\int_{.15R}^{R} \left(\frac{dm}{dr}\right) dr = 2.53 \text{ slugs}$$

$$\int_{.15R}^{R} r \left(\frac{dm}{dr}\right) dr = 20.8 \text{ slugs/ft}$$

$$\int_{.15R}^{R} r^2 \left(\frac{dm}{dr}\right) dr = 219.0 \text{ slugs/ft}^2$$

$$\int_{.15R}^{R} r^3 \left(\frac{dm}{dr}\right) dr = 2590 \text{ slugs/ft}^3$$

$$\int_{.15R}^{R} r^4 \left(\frac{dm}{dr}\right) dr = 33,700 \text{ slugs/ft}^4$$

To derive equations of the elements for the tip mass part of the equations, the same logic used for the distributed mass part is used, except that m_{tip} replaces $\frac{dm}{dr}$ dr, and R replaces r. The equivalent of the 6.0 lb tip mass shown in Figure 9 is 0.1862 slugs, and R determined from the figure is 16.25 ft. Therefore, to each of the five integrals another term, representing the concentrated tip mass, is added:

$$\text{to} \quad \int_{.15R}^{R} \left(\frac{dm}{dr}\right) dr \qquad \text{add} \quad .1862 \text{ slugs}$$

$$\text{to} \quad \int_{.15R}^{R} r \left(\frac{dm}{dr}\right) dr \qquad \text{add} \quad (16.25)(.1862) = 3.03 \text{ slugs/ft}$$

to $\displaystyle\int_{.15R}^{R} r^2 \left(\frac{dm}{dr}\right) dr$ add $(16.25)^2 (.1862)$ $= 49.2$ slugs/ft^2

to $\displaystyle\int_{.15R}^{R} r^3 \left(\frac{dm}{dr}\right) dr$ add $(16.25)^3 (.1862)$ $= 800$ slugs/ft^3

to $\displaystyle\int_{.15R}^{R} r^4 \left(\frac{dm}{dr}\right) dr$ add $(16.25)^4 (.1862)$ $= 13,000$ slugs/ft^4

The resulting numerical values of the integrals are

$$\int \left(\frac{dm}{dr}\right) dr + m_{tip} = 2.72 \text{ slugs}$$

$$\int r \left(\frac{dm}{dr}\right) dr + m_{tip} R = 23.8 \text{ slugs/ft}$$

$$\int r^2 \left(\frac{dm}{dr}\right) dr + m_t R^2 = 268 \text{ slugs/ft}^2$$

$$\int r^3 \left(\frac{dm}{dr}\right) dr + m_t R^3 = 3390 \text{ slugs/ft}^3$$

$$\int r^4 \left(\frac{dm}{dr}\right) dr + m_t R^4 = 46,700 \text{ slugs/ft}^4$$

Another contribution to the inertia matrix occurs if the mass is actually not located along the blade's quarter-chord. It adds to the feathering moment of inertia and affect only the 3,3 element of the matrix. Therefore, to make the inertia matrix more correctly represent the wind tunnel model rotor, increment of local moment of pitch inertia about the 1/4 chord, 0.216 slug/ft^2, will be added to the 3,3 element.

To complete the inertia matrix, the following constants (applicable to the wind tunnel model rotor) are to be combined with the integrals:

$$\Lambda = .0262$$

$$\Lambda^2 = .000686$$

$$\frac{1}{R^2} = .003675$$

$$\frac{\Lambda}{R^2} = .0000962$$

$$\frac{1}{R^4} = .0000135$$

Combining the preceding items appropriately results in the numerical value of the inertia matrix as follows:

$$-\left[I_b \right] = - \begin{bmatrix} 268 & 23.8 & 7.01 & 12.46 \\ 23.8 & 2.72 & .623 & .985 \\ 7.01 & .623 & .400 & .326 \\ 12.46 & .985 & .326 & .631 \end{bmatrix}$$

Note $I_o = 0.216$ slug/ft^2 was added to the 3,3 element.

The inertia matrix for a single blade $\left[I_b \right]$ evaluated is now introduced into the expression for the inertia matrix for the entire rotor $\left[D \right]^T \left[I_b \right] \left[D \right]$. The following page shows the completed inertia matrix for the rotor.

Rotor centrifugal and structural terms and rotating spring. - The elements of mass of the rotor are subjected to constant centrifugal inertia forces. These forces produce moments and generalized forces on the degrees of freedom proportional to displacements. These forces are similar to forces induced by structural deflection except that they couple degrees of freedom whereas structural forces do not. Because, in this formulation of the differential equations of motion, it was chosen to couple dynamic inertia forces (i.e., acceleration inertia forces) the structural forces are not coupled between degrees of freedom.

Since the blade deflections are related to deflections of the degrees of freedom by

$$\left\{ \eta \right\} = \left[D \right] \left\{ \beta \right\}$$

and the generalized forces due to centrifugal forces on the blades are given by

$$\left\{ GF_b \right\} = \left[CF \right] \left\{ \eta \right\}$$

and rotor generalized forces are related to blade generalized forces by

$$\left\{ GF \right\} = \left[D \right]^T \left\{ GF_b \right\}$$

the rotor centrifugal forces are related to rotor deflections as follows:

$$\left\{ GF \right\} = \left[D \right]^T \left[CF \right] \left[D \right] \left\{ \beta \right\}$$

The centrifugal force matrix for a single blade is

$$\left[CF_b \right] = \begin{bmatrix} \dfrac{\partial\,bm}{\partial\beta} & \dfrac{\partial\,bm}{\partial z} & \dfrac{\partial\,bm}{\partial\theta} & \dfrac{\partial\,bm}{\partial\delta} \\[2ex] \dfrac{\partial V}{\partial\beta} & \dfrac{\partial V}{\partial z} & \dfrac{\partial V}{\partial\theta} & \dfrac{\partial V}{\partial\delta} \\[2ex] \dfrac{\partial fm}{\partial\beta} & \dfrac{\partial fm}{\partial z} & \dfrac{\partial fm}{\partial\theta} & \dfrac{\partial fm}{\partial\delta} \\[2ex] \dfrac{\partial H}{\partial\beta} & \dfrac{\partial H}{\partial z} & \dfrac{\partial H}{\partial\theta} & \dfrac{\partial H}{\partial\delta} \end{bmatrix}$$

and the [CF] matrix for the entire rotor is formed by three identical single blade matrices along a diagonal, similar to the inertia matrix.

The elements of the centrifugal force matrix for a single blade consist of the change in root bending moment (bm), shear (V), feathering moment (fm), and generalized force (H) due to linear flap deflection (β), vertical displacement (z), feathering angle (θ), and parabolic flapping deflection (δ).

$$\frac{dbm}{d\beta} = -\Omega^2 \int r^2 \frac{dm}{dr}\,dr = -\Omega^2\,I_b$$

where the negative sign denotes RHS of the differential equations.

$$\frac{dV}{d\beta} = 0$$

$$\frac{dfm}{d\beta} = -\Omega^2 \Lambda \int r^2 \frac{dm}{dr}\,dr = -\Omega^2 \Lambda\,I_b$$

204
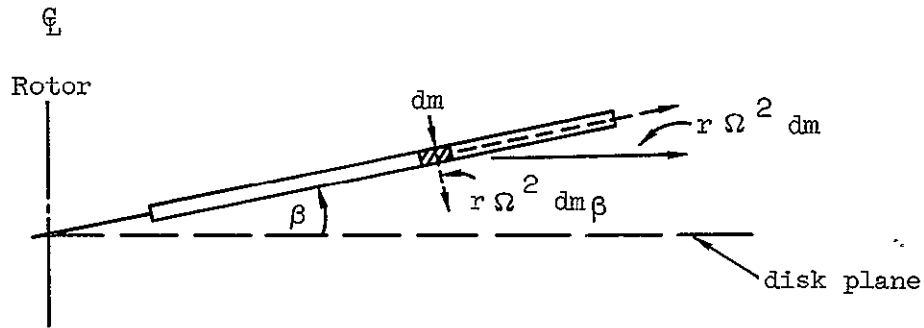
$$\frac{dH}{d\beta} = -\left(\frac{r}{R}\right)^2 r\,\Omega^2\,dm = -\frac{\Omega 2}{R^2}\int r^3\,\frac{dm}{dr}\,dr$$

The centrifugal forces due to vertical displacement z are all zero

$$\frac{dbm}{dz} = \frac{dV}{dz} = \frac{dfm}{dz} = \frac{dH}{dz} = 0$$

The centrifugal force terms due to feathering angle are as follows:

$$\frac{dbm}{d\theta_f} = -\Omega^2 \Lambda \int r^2\,\frac{dm}{dr}\,dr = -\Omega^2 \Lambda\,I_b$$

$$\frac{dV}{d\theta_f} = 0$$

$$\frac{dfm}{d\theta_f} = -\Omega^2\left(\Lambda^2 \int r^2\,\frac{dm}{dr}\,dr + I_o\right) = -\Omega^2\left(\Lambda I_b + I_o\right)$$

$$\frac{dH}{d\theta_f} = -\Lambda\frac{\Omega^2}{R^2}\int r^3\,\frac{dm}{dr}\,dr;$$

this term comes from flapping due to feathering.

205

The centrifugal force terms due to parabolic flapping deflection (δ) are as follows:

$$\frac{dbm}{d\delta} = -\frac{\Omega^2}{R^2} \int r^3 \frac{dbm}{dr} \, dr$$

$$\frac{dV}{d\delta} = 0$$

$$\frac{dfm}{d\delta} = -\Lambda \frac{\Omega^2}{R^2} \int r^3 \frac{dm}{dr} \, dr$$

$$\frac{dH}{d\delta} = -\frac{\Omega^2}{R^4} \int r^4 \frac{dm}{dr} \, dr = -\Omega^2 M_\delta$$

where

$$M_\delta = \int \left(\frac{r}{R}\right)^4 \frac{dm}{dr} \, dr = \text{blade flapping generalized mass}$$

If the centrifugal force and structural stiffness are combined in the latter term, it becomes

$$\frac{dH}{d\delta} = -\omega_\delta^2 M_\delta$$

where ω_δ^2 is the flapping frequency of the blades in rotating axes under the combined influences of centrifugal and structural forces.

In summary, the blade centrifugal force matrix, including the effects of blade structural bending stiffness is written as follows:

$$
\left[CF_b\right] =
\begin{bmatrix}
\dfrac{dbm}{d\beta} & \dfrac{dbm}{dz} & \dfrac{dbm}{d\theta_f} & \dfrac{dbm}{d\delta} \\[2ex]
\dfrac{dV}{d\beta} & \dfrac{dV}{dz} & \dfrac{dV}{d\theta_f} & \dfrac{dV}{d\delta} \\[2ex]
\dfrac{dfm}{d\beta} & \dfrac{dfm}{dz} & \dfrac{dfm}{d\theta_f} & \dfrac{dfm}{d\delta} \\[2ex]
\dfrac{dH}{d\beta} & \dfrac{dH}{dz} & \dfrac{dH}{d\theta_f} & \dfrac{dH}{d\delta}
\end{bmatrix}
$$

$$
=
\begin{bmatrix}
-\Omega^2 \displaystyle\int r^2 \frac{dm}{dr}\, dr & 0 & -\Omega^2 \Lambda \displaystyle\int r^2 \frac{dm}{dr} & -\dfrac{\Omega^2}{R^2}\displaystyle\int r^3 \frac{dm}{dr}\, dr \\[3ex]
0 & 0 & 0 & \\[3ex]
-\Omega^2 \Lambda \displaystyle\int r^2 \frac{dm}{dr}\, dr & 0 & -\Omega^2\left(\Lambda^2 \displaystyle\int r^2 \frac{dm}{dr}\, dr + I_o\right) & -\Lambda\dfrac{\Omega^2}{R^2}\displaystyle\int r^3 \frac{dm}{dr}\, dr \\[3ex]
-\dfrac{\Omega^2}{R^2}\displaystyle\int r^3 \frac{dm}{dr}\, dr & 0 & -\Lambda\dfrac{\Omega^2}{R^2}\displaystyle\int r^3 \frac{dm}{dr}\, dr & -\dfrac{\omega_\delta^2}{R^4}\displaystyle\int r^4 \frac{dm}{dr}\, dr
\end{bmatrix}
$$

Notes: (1) The (4,4) element contains flapping structural stiffness as well as centrifugal stiffness.

(2) the $\left[CF_b\right]$ matrix can be obtained from the $-\left[I_b\right]$ matrix by factoring by Ω^2, deleting the second row and column, and adding

$$-\frac{\left(\omega_\delta^2 - \Omega^2\right)}{R^4}\int r^4 \frac{dm}{dr}\, dr$$

to the (4,4) element; or more concisely, by factoring the generalized mass by ω_δ^2 instead of Ω^2.

207

The numerical value of the single-blade centrifugal force matrix becomes

$$
\left[CF_b\right] = -\begin{bmatrix} 268\,\Omega^2 & 0 & 7.01\,\Omega^2 & 12.46\,\Omega^2 \\ 0 & 0 & 0 & 0 \\ 7.01\,\Omega^2 & 0 & .400\,\Omega^2 & .326\,\Omega^2 \\ 12.46\,\Omega^2 & 0 & .326\,\Omega^2 & .631\,\Omega^2 \end{bmatrix}
$$

which is used to relate the generalized forces on the degrees of freedom due to centrifugal forces and blade bending stiffness to deflections in the degrees of freedom, per the expression

$$
\left[D\right]^T \left[CF_b\right] \left[D\right]
$$

The operations combining these matrices are shown on the following page.

Any feathering spring that might exist in the blade system (in the rotating axes), for example due to the feathering spring effect of a tension-torsion pack, is not included in the centrifugal force matrices shown on these pages. If a value of the feathering spring coefficient K_R is available, and is considered significant, the matrix can be modified to include the effects of the feathering spring by adding K_R values to elements 4,4 and 5,5.

208

Rotor structural damping and gyro rotating damping. - Structural damping
is proportional to and in phase with blade structural deflection velocities.
Therefore, to include the effects of damping of the structural modes, a gen-
eralized force which opposes the velocity of each mode is added. This force
is given in terms of the fraction of critical damping (γ). It is expressed
in terms of a damping coefficient, $2\gamma\omega M$, and is applied to the three flapping
modes as shown in the following matrix.

Blade feathering motions are opposed by mechanical friction (viscous
friction in this linear analysis). In the matrix it becomes swashplate
moments due to swashplate tilt velocities. These terms are considered to
represent feathering (rotating) damping, denoted by the symbol C_R.

Relative to axes which rotate with the rotor, the mechanical damping
terms are written in matrix form as follows:

$$
\begin{Bmatrix} M \\ L \\ T \\ M_\theta \\ M_\phi \\ H_{\delta_0} \\ H_{\delta_\theta} \\ H_{\delta_\phi} \end{Bmatrix} = -
\begin{bmatrix}
0 & & & & & & & \\
& 0 & & & & & & \\
& & 0 & & & & & \\
& & & C_R & & & & \\
& & & & C_R & & & \\
& & & & & 2\gamma_{\delta_0}\omega_{\delta_0}M_{\delta_0\delta_0} & & \\
& & & & & & 2\gamma_{\delta_\theta}\omega_{\delta_\theta}M_{\delta_\theta\delta_\theta} & \\
& & & & & & & 2\gamma_{\delta_\phi}\omega_{\delta_\phi}M_{\delta_\phi\delta_\phi}
\end{bmatrix}
\begin{Bmatrix} \dot{\oplus} \\ \dot{\Phi} \\ \dot{z} \\ \dot{\theta} \\ \dot{\phi} \\ \dot{\delta}_0 \\ \dot{\delta}_\theta \\ \dot{\delta}_\phi \end{Bmatrix}
$$

Rotating Axes   Rotating Axes

The minus sign indicates that the terms are meant to fall on the right
hand side of the differential equations.

High-speed gyroscope terms in rotating axes - The equations of motion
of an unrestrained undamped gyroscope relative to its own rotating axes
are

$$
\begin{bmatrix} I_G & 0 \\ 0 & I_G \end{bmatrix}
\begin{Bmatrix} \ddot{\theta} \\ \ddot{\phi} \end{Bmatrix}
+ \Omega^2_G
\begin{bmatrix} I_G & 0 \\ 0 & I_G \end{bmatrix}
\begin{Bmatrix} \theta \\ \phi \end{Bmatrix}
= \begin{Bmatrix} \text{Forcing} \\ \text{Moments} \end{Bmatrix}
$$

The two axes of tilt are not coupled and each has its own natural
frequency Ω_G.

211

The equations of the gyroscope relative to axes rotating with the rotor are obtained by transforming the above equations from gyro axes to rotor axes. Absolute tilt angles of the gyro in rotor coordinates are composed of the body tilt angles $\oplus$, Φ and the tilt of the gyro relative to the body θ, ϕ. Therefore the gyro and rotor axes are related as follows:

$$\left\{ \begin{array}{c} \theta \\ \phi \end{array} \right\}_{\substack{Gyro \\ axes}} = \left[\; T \; \right] \left\{ \left\{ \begin{array}{c} \oplus \\ \Phi \end{array} \right\} + \left\{ \begin{array}{c} \theta \\ \phi \end{array} \right\} \right\}_{Rotor \; Axes}$$

where $\left[\; T \; \right]$ is the sine, cosine transformation

$$\left[\; T \; \right] = \begin{bmatrix} \cos \; (\Omega_G - \Omega) \; t & -\sin \; (\Omega_G - \Omega) \; t \\ \sin \; (\Omega_G - \Omega) \; t & \cos \; (\Omega_G - \Omega) \; t \end{bmatrix}$$

The transformation relationship can also be written

$$\left\{ \begin{array}{c} \theta \\ \phi \end{array} \right\}_{\substack{gyro \\ axes}} = \left[\; T \; \vdots \; T \; \right] \left\{ \begin{array}{c} \oplus \\ \Phi \\ \theta \\ \phi \end{array} \right\} \; rotor \; axes$$

and its time derivative can be written

$$\left\{ \begin{array}{c} \dot{\theta} \\ \dot{\phi} \end{array} \right\}_{\substack{gyro \\ axes}} = \left[\; \dot{T} \; \vdots \; \dot{T} \; \right] \left\{ \begin{array}{c} \oplus \\ \Phi \\ \theta \\ \phi \end{array} \right\}_{\substack{rotor \\ axes}} + \left[\; T \; \vdots \; T \; \right] \left\{ \begin{array}{c} \dot{\oplus} \\ \dot{\Phi} \\ \dot{\theta} \\ \dot{\phi} \end{array} \right\}_{\substack{rotor \\ axes}}$$

The second derivative with respect to time is

$$\left\{ \begin{array}{c} \ddot{\theta} \\ \ddot{\phi} \end{array} \right\}_{\substack{gyro \\ axes}} = \left[\; \ddot{T} \; \vdots \; \ddot{T} \; \right] \left\{ \begin{array}{c} \oplus \\ \Phi \\ \theta \\ \phi \end{array} \right\}_{\substack{rotor \\ axes}} + 2 \left[\; \dot{T} \; \vdots \; \dot{T} \; \right] \left\{ \begin{array}{c} \dot{\oplus} \\ \dot{\Phi} \\ \dot{\theta} \\ \dot{\phi} \end{array} \right\}_{\substack{rotor \\ axes}} + \left[\; T \; \vdots \; T \; \right] \left\{ \begin{array}{c} \ddot{\oplus} \\ \ddot{\Phi} \\ \ddot{\theta} \\ \ddot{\phi} \end{array} \right\}_{\substack{rotor \\ axes}}$$

The transformation and its time derivatives for rotational symmetry are

$$[T \mid T] = \begin{bmatrix} 1 & 0 & | & 1 & 0 \\ 0 & 1 & | & 0 & 1 \end{bmatrix}$$

$$[\dot{T} \mid \dot{T}] = (\Omega_G - \Omega) \begin{bmatrix} 0 & -1 & | & 0 & -1 \\ 1 & 0 & | & 1 & 0 \end{bmatrix}$$

$$[\ddot{T} \mid \ddot{T}] = (\Omega_G - \Omega)^2 \begin{bmatrix} -1 & 0 & -1 & 0 \\ 0 & -1 & 0 & -1 \end{bmatrix}$$

Substituting in the initial equations in this subsection yields

$$\begin{bmatrix} T \\ -- \\ T \end{bmatrix} \begin{bmatrix} I_G & 0 \\ 0 & I_G \end{bmatrix} \left\{ [\ddot{T} \mid \ddot{T}] \begin{Bmatrix} \oplus \\ \Phi \\ \theta \\ \phi \end{Bmatrix} + 2 [\dot{T} \mid \dot{T}] \begin{Bmatrix} \dot{\oplus} \\ \dot{\Phi} \\ \dot{\theta} \\ \dot{\phi} \end{Bmatrix} + [T \mid T] \begin{Bmatrix} \ddot{\oplus} \\ \ddot{\Phi} \\ \ddot{\theta} \\ \ddot{\phi} \end{Bmatrix} \right\}$$

$$+ \Omega_G^2 \begin{bmatrix} T \\ -- \\ T \end{bmatrix} \begin{bmatrix} I_G & 0 \\ 0 & I_G \end{bmatrix} [T \mid T] \begin{Bmatrix} \oplus \\ \Phi \\ \theta \\ \phi \end{Bmatrix} = \begin{bmatrix} T \\ -- \\ T \end{bmatrix} \begin{Bmatrix} \text{Forcing} \\ \text{Moments} \end{Bmatrix}$$

The terms of the equation are now examined one at a time. Expanding the first term gives

$$(\Omega_G - \Omega)^2 \begin{bmatrix} 1 & 0 \\ 0 & 1 \\ 1 & 0 \\ 0 & 1 \end{bmatrix} \begin{bmatrix} I_G & 0 \\ 0 & I_G \end{bmatrix} \begin{bmatrix} -1 & 0 & -1 & 0 \\ 0 & -1 & 0 & -1 \end{bmatrix} \begin{Bmatrix} \oplus \\ \Phi \\ \theta \\ \phi \end{Bmatrix}$$

Note: $(\Omega_G - \Omega)^2 = \Omega_G^2 - 2\Omega_G \Omega + \Omega^2$

Therefore, the first term of matrix equation, in rotor axes, becomes

$$(\Omega_G - \Omega)^2 \begin{bmatrix} -I_G & 0 & -I_G & 0 \\ 0 & -I_G & 0 & -I_G \\ -I_G & 0 & -I_G & 0 \\ 0 & -I_G & 0 & -I_G \end{bmatrix} \begin{Bmatrix} \oplus \\ \Phi \\ \theta \\ \phi \end{Bmatrix}$$

Expanding the second term gives

$$2(\Omega_G - \Omega) \begin{bmatrix} 1 & 0 \\ 0 & 1 \\ 1 & 0 \\ 0 & 1 \end{bmatrix} \begin{bmatrix} I_G & 0 \\ 0 & I_G \end{bmatrix} \begin{bmatrix} 0 & -1 & 0 & -1 \\ 1 & 0 & 1 & 0 \end{bmatrix} \begin{Bmatrix} \dot{\oplus} \\ \dot{\Phi} \\ \dot{\theta} \\ \dot{\phi} \end{Bmatrix}$$

Therefore, the second term of matrix equation, in rotor axes, becomes

$$2(\Omega_G - \Omega) \begin{bmatrix} 0 & -I_G & 0 & -I_G \\ I_G & 0 & I_G & 0 \\ 0 & -I_G & 0 & -I_G \\ I_G & 0 & I_G & 0 \end{bmatrix} \begin{Bmatrix} \dot{\oplus} \\ \dot{\Phi} \\ \dot{\theta} \\ \dot{\phi} \end{Bmatrix}$$

The third term in the gyro matrix equation can be written

$$\begin{bmatrix} T \\ \overline{T} \end{bmatrix} \begin{bmatrix} I_G & 0 \\ 0 & I_G \end{bmatrix} \begin{bmatrix} T \mid T \end{bmatrix} \begin{Bmatrix} \ddot{\oplus} \\ \ddot{\Phi} \\ \ddot{\theta} \\ \ddot{\phi} \end{Bmatrix}$$

which, in rotor axes, becomes

$$\begin{bmatrix} I_G & 0 & I_G & 0 \\ 0 & I_G & 0 & I_G \\ I_G & 0 & I_G & 0 \\ 0 & I_G & 0 & I_G \end{bmatrix} \begin{Bmatrix} \ddot{\oplus} \\ \ddot{\Phi} \\ \ddot{\theta} \\ \ddot{\phi} \end{Bmatrix}$$

The fourth term can be written in rotor axes,

$$\Omega_G^2 \begin{bmatrix} I_G & 0 & I_G & 0 \\ 0 & I_G & 0 & I_G \\ I_G & 0 & I_G & 0 \\ 0 & I_G & 0 & I_G \end{bmatrix} \begin{Bmatrix} \Theta \\ \Phi \\ \theta \\ \phi \end{Bmatrix}$$

Regrouping all terms gives the following matrix equation:

$$\begin{bmatrix} I_G & 0 & I_G & 0 \\ 0 & I_G & 0 & I_G \\ I_G & 0 & I_G & 0 \\ 0 & I_G & 0 & I_G \end{bmatrix} \begin{Bmatrix} \ddot{\Theta} \\ \ddot{\Phi} \\ \ddot{\theta} \\ \ddot{\phi} \end{Bmatrix}_{\substack{\text{Rotor} \\ \text{axes}}} + 2(\Omega_G - \Omega) \begin{bmatrix} 0 & -I_G & 0 & -I_G \\ I_G & 0 & I_G & 0 \\ 0 & -I_G & 0 & -I_G \\ I_G & 0 & I_G & 0 \end{bmatrix} \begin{Bmatrix} \dot{\Theta} \\ \dot{\Phi} \\ \dot{\theta} \\ \dot{\phi} \end{Bmatrix}_{\substack{\text{Rotor} \\ \text{axes}}}$$

$$+(2\Omega_G\Omega - \Omega^2) \begin{bmatrix} I_G & 0 & I_G & 0 \\ 0 & I_G & 0 & I_G \\ I_G & 0 & I_G & 0 \\ 0 & I_G & 0 & I_G \end{bmatrix} \begin{Bmatrix} \Theta \\ \Phi \\ \theta \\ \phi \end{Bmatrix}_{\substack{\text{Rotor} \\ \text{axes}}} = \begin{Bmatrix} M_\Theta \\ M_\Phi \\ M_\theta \\ M_\phi \end{Bmatrix}_{\text{forcing functions}}$$

Aerodynamic terms in rotating axes. -

The aerodynamic coefficients in the differential equations were
calculated in rotating axes and transferred to stationary.

In axes rotating with the rotor, the aerodynamic terms were calculated
in a manner similar to the way in which the inertia and centrifugal terms
were calculated. The displacements and velocities of individual blades were
first defined in terms of displacements and velocities of the degrees of freedom:

$$\eta = [D]\, \beta$$
$$\eta = [D]\, \dot{\beta}$$

215

Then the generalized forces on each blade, due to its displacements, velocities, and fixed geometric shapes, were calculated at closely spaced intervals around the azimuth with the effects of advance ratio accounted for.

$$\left\{GF_b\right\} = \left[\frac{\partial F_b}{\partial \eta}\right]\left\{\eta\right\} + \left[\frac{\partial F_b}{\partial \dot{\eta}}\right]\left\{\dot{\eta}\right\} + \left[\frac{\partial F_b}{\partial \begin{subarray}{c}fixed\\geom.\end{subarray}}\right]\left\{\begin{subarray}{c}fixed\\geom\end{subarray}\right\}$$

The generalized forces on the three blades due to their individual motions were combined to yield the matrices of areodynamic terms in rotating axes.

$$\left\{GF_\beta\right\} = \left[D\right]^T\left[\frac{\partial F_b}{\partial \eta}\right]\left[D\right]\left\{\beta\right\} + \left[D\right]^T\left[\frac{\partial F_b}{\partial \dot{\eta}}\right]\left[D\right]\left\{\dot{\beta}\right\} + \left[D\right]^T\left[\frac{\partial F_b}{\partial \begin{subarray}{c}fixed\\geom\end{subarray}}\right]\left\{\begin{subarray}{c}fixed\\geom\end{subarray}\right\}$$

The rotating axes matrices were called

aerodynamic stiffness

$$\left[D\right]^T\left[\frac{\partial F_b}{\partial \eta}\right]\left[D\right] = \left[A\right]$$

and

aerodynamic damping

$$\left[D\right]^T\left[\frac{\partial F_b}{\partial \dot{\eta}}\right]\left[D\right] = \left[A_R\right]$$

These were later transformed to stationary axes for use in the final equations of motion. The forcing terms were transformed to stationary axes as follows:

$$\left[T\right]^T\left[D\right]^T\left[\frac{\partial F_b}{\partial \begin{subarray}{c}fixed\\geom\end{subarray}}\right]\left\{\begin{subarray}{c}fixed\\geom\end{subarray}\right\}$$

where $\left[T\right]$ is the sine-cosine transformation of the degrees of freedom from stationary to rotating axes:

$$\beta_R = \left[T\right]\beta_S$$

The column matrix of fixed geometry parameters consisted of:

$$
\begin{Bmatrix} \text{fixed} \\ \text{geom} \end{Bmatrix} = \begin{Bmatrix} \beta_o \\ \theta_o \\ \theta_t \\ \dot{z} \end{Bmatrix}
$$

where:

β_o = precone angle

θ_o = collective pitch

θ_t = twist rate

$\dot{z}$ = vertical gust air velocity

The aerodynamic matrices were based on a tip loss factor $B = .97$ and a section lift curve slope $c_{l_\alpha} = .95\,(2\pi)$.

Collection of terms in rotating axes.-

Matrices are now combined (on the next page) into a matrix equation representing the equations of motion in the rotating axes system. Numerical or symbolic values are shown for all but aerodynamic terms.

217

Transformation to stationary axes.- The equations of motion of the rotor and gyro in 8 degrees of freedom are written in rotating coordinates in the preceding pages. They will now be transformed to stationary axes, and effects of the rigid airframe will be added thereto.

The pitch and roll of the rotor $(\oplus, \Phi)$ and of the gyro (θ, ϕ) were developed relative to the same rotating axes. The flapping mode pitch and roll deflections are lagged 60 degrees behind the rotating axes, therefore the blade axes are allowed to lag behind the gyro axes so that the standard transformation is valid.

The relationship between generalized coordinates (degrees of freedom) in rotating axes (subscript R) and in stationary axes (subscript S) is as follows:

$$
\begin{Bmatrix} \oplus \\ \Phi \\ z \\ \theta \\ \phi \\ \delta_O \\ \delta_\theta \\ \delta_\phi \end{Bmatrix}_R =
\begin{bmatrix}
\cos\Omega t & -\sin\Omega t & 0 & 0 & 0 & 0 & 0 & 0 \\
\sin\Omega t & \cos\Omega t & 0 & 0 & 0 & 0 & 0 & 0 \\
0 & 0 & 1.0 & 0 & 0 & 0 & 0 & 0 \\
0 & 0 & 0 & \cos\Omega t & -\sin\Omega t & 0 & 0 & 0 \\
0 & 0 & 0 & \sin\Omega t & \cos\Omega t & 0 & 0 & 0 \\
0 & 0 & 0 & 0 & 0 & 1.0 & 0 & 0 \\
0 & 0 & 0 & 0 & 0 & 0 & \cos\Omega t & -\sin\Omega t \\
0 & 0 & 0 & 0 & 0 & 0 & \sin\Omega t & \cos\Omega t
\end{bmatrix}
\begin{Bmatrix} \oplus \\ \Phi \\ z \\ \theta \\ \phi \\ \delta_O \\ \delta_\theta \\ \delta_\phi \end{Bmatrix}_S
$$

and in abbreviated notation:

$$ \{\beta\}_R = [T] \{\beta\}_S $$

and

$$ \{\dot{\beta}\}_R = [T] \{\dot{\beta}\}_S + [\dot{T}] \{\beta\}_S $$

and

$$ \{\ddot{\beta}\}_R = [T] \{\ddot{\beta}\}_S + 2[\dot{T}] \{\dot{\beta}\}_S + [\ddot{T}] \{\beta\}_S $$

Submatrices of $[T]$ involving $\Theta\Phi$, $\theta\phi$ and $\delta_\theta\,\delta_\Phi$ are uncoupled, from each other and from z and δ_0 elements. Therefore, each submatrix is handled independently. For rotationally symmetric terms, the matrices and their time derivatives become:

$$[T] = \begin{bmatrix} 1 & & & & & & & \\ & 1 & & & & & & \\ & & 1 & & & & & \\ & & & 1 & & & & \\ & & & & 1 & & & \\ & & & & & 1 & & \\ & & & & & & 1 & \\ & & & & & & & 1 \end{bmatrix}$$

$$[\dot{T}] = \Omega \begin{bmatrix} & -1 & & & & & & \\ 1 & & & & & & & \\ & & & -1 & & & & \\ & & 1 & & & & & \\ & & & & & & & \\ & & & & & & & \\ & & & & & & 1 & -1 \\ & & & & & & 1 & \end{bmatrix}$$

$$[\ddot{T}] = -\Omega^2 \begin{bmatrix} 1 & & & & & & & \\ & 1 & & & & & & \\ & & & & & & & \\ & & 1 & & & & & \\ & & & 1 & & & & \\ & & & & & & & \\ & & & & & & 1 & \\ & & & & & & & 1 \end{bmatrix}$$

222

For terms which are not rotationally symmetric, or which vary with azimuth, the full transformations and their derivatives must be used. For example, the first time derivative of $[T]$ is

$$[\dot{T}] = \Omega \begin{bmatrix} -\sin\Omega t & -\cos\Omega t & 0 & 0 & 0 & 0 & 0 & 0 \\ \cos\Omega t & -\sin\Omega t & 0 & 0 & 0 & 0 & 0 & 0 \\ 0 & 0 & 0 & 0 & 0 & 0 & 0 & 0 \\ 0 & 0 & 0 & -\sin\Omega t & -\cos\Omega t & 0 & 0 & 0 \\ 0 & 0 & 0 & \cos\Omega t & -\sin\Omega t & 0 & 0 & 0 \\ 0 & 0 & 0 & 0 & 0 & 0 & 0 & 0 \\ 0 & 0 & 0 & 0 & 0 & 0 & -\sin\Omega t & -\cos\Omega t \\ 0 & 0 & 0 & 0 & 0 & 0 & \cos\Omega t & -\sin\Omega t \end{bmatrix}$$

The rotor equations in rotating coordinates are repeated here,

$$[I]\{\ddot{\beta}\}_R + [D]\{\dot{\beta}\}_R + [S]\{\dot{\beta}\}_R - [A_R]\{\dot{\beta}\}_R - [A]\{\beta\}_R = 0$$

These equations are transformed to apply to stationary axes in two steps:

1. The transformation equations for $\{\beta\}_R$, $\{\dot{\beta}\}_R$ and $\{\ddot{\beta}\}_R$ are substituted for the differential equations (in the matrix equations).

2. The differential equations generalized forces are transformed from rotating to stationary axes by premultiplying by the transpose of the transformation matrix $[T]^T$.

The equations become:

$$[T]^T [I] \left[[T]\{\ddot{\beta}\}_S + 2[\dot{T}]\{\dot{\beta}\}_S + [\ddot{T}]\{\beta\}_S \right]$$

$$+ [T]^T [D] \left[[T]\{\dot{\beta}\}_S + [\dot{T}]\{\beta\}_S \right] + [T]^T [S] [T]\{\beta\}_S$$

$$+ [T]^T [A_R] \left[[T]\{\dot{\beta}\}_S + [\dot{T}]\{\beta\}_S \right] + [T]^T [A] [T]\{\beta\}_S = 0$$

$$\uparrow \qquad\qquad \uparrow \qquad\qquad \uparrow \qquad\qquad \uparrow \qquad\qquad \uparrow$$

Full transformations, indicated by arrows, must be used for aerodynamic derivative matrices. In all other places the abbreviated matrices for rotational symmetry are used. For the rotationally symmetric matrices

$$[T]^T = [T] = [1]$$

Expanding the matrix equation and keeping the aerodynamic terms separated from the mechanical terms, the equations become

$$[I] \, [T] \left\{ \ddot{\beta} \right\}_S \; + \; 2 \, [I] \, [\dot{T}] \left\{ \dot{\beta} \right\}_S \; + \; [I] \, [\ddot{T}] \left\{ \beta \right\}_S$$

$$+ \; [D] \, [T] \left\{ \dot{\beta} \right\}_S \; + \; [D] \, [\dot{T}] \left\{ \beta \right\}_S \; + \; [S] \left\{ \beta \right\}_S$$

$$+ \; [T]^T \, \underset{\text{Full}}{[A_R]} \, [T] \left\{ \dot{\beta} \right\}_S + [T]^T \, \underset{\text{Full}}{[A_R]} \, [\dot{T}] \left\{ \beta \right\}_S + [T]^T \, \underset{\text{Full}}{[A]} \, [T] \left\{ \beta \right\}_S \; = \; 0$$

The mechanical terms are grouped as follows:

$$[I] \left\{ \ddot{\beta} \right\}_S \; + \; \Big[2[I] \, [\dot{T}] \; + \; [D] \Big] \left\{ \dot{\beta} \right\}_S \; + \; \Big[[I] \, [\ddot{T}] + [D] \, [\dot{T}] + [S] \Big] \left\{ \beta \right\}_S$$

The individual transformed matrices $2[I] \, [\dot{T}]$, $[I] \, [\ddot{T}]$, and $[D] \, [\dot{T}]$ are calculated next and then the combined mechanical terms in stationary axes are assembled.

$2 \, [I] \, [\dot{T}]$ is as follows:

$$2\,\Omega \begin{bmatrix} 0 & -402.75 & 0 & -7.658 & -5.174 & 0 & -15.942 & -9.768 \\ 402.75 & 0 & 0 & 5.174 & -7.658 & 0 & 9.768 & -15.942 \\ 0 & 0 & 0 & 0 & 0 & 0 & 0 & 0 \\ 7.658 & -5.174 & 0 & 0 & -.604 & 0 & 0 & -.4252 \\ 5.174 & 7.658 & 0 & .604 & 0 & 0 & .4252 & 0 \\ 0 & 0 & 0 & 0 & 0 & 0 & 0 & 0 \\ 15.942 & -9.768 & 0 & 0 & -.4252 & 0 & 0 & -.9465 \\ 9.768 & 15.942 & 0 & .4252 & 0 & 0 & .9465 & 0 \end{bmatrix}$$

$[I] \, [\ddot{T}]$ is as follows:

$$-\Omega^2 \begin{bmatrix} 402.75 & 0 & 0 & 5.174 & -7.658 & 0 & 9.768 & -15.942 \\ 0 & 402.75 & 0 & 7.658 & 5.174 & 0 & 15.942 & 9.768 \\ 0 & 0 & 0 & 0 & 0 & 0 & 0 & 0 \\ 5.174 & 7.658 & 0 & .604 & 0 & 0 & .4252 & 0 \\ -7.658 & 5.174 & 0 & 0 & .604 & 0 & 0 & .4252 \\ 0 & 0 & 0 & 0 & 0 & 0 & 0 & 0 \\ 9.768 & 15.942 & 0 & .4252 & 0 & 0 & .9465 & 0 \\ -15.942 & 9.768 & 0 & 0 & .4252 & 0 & 0 & .9465 \end{bmatrix}$$

$[D]\,[\dot{T}]$ is as follows:

$$\Omega \begin{bmatrix} -.3(\Omega_G-\Omega) & 0 & 0 & -.3(\Omega_G-\Omega) & 0 & 0 & 0 & 0 \\ 0 & -.3(\Omega_G-\Omega) & 0 & 0 & -.3(\Omega_G-\Omega) & 0 & 0 & 0 \\ 0 & 0 & 0 & 0 & 0 & 0 & 0 & 0 \\ -.3(\Omega_G-\Omega) & 0 & 0 & -.3(\Omega_G-\Omega) & -C_R & 0 & 0 & 0 \\ 0 & -.3(\Omega_G-\Omega) & 0 & +C_R & -.3(\Omega_G-\Omega) & 0 & 0 & 0 \\ 0 & 0 & 0 & 0 & 0 & 0 & 0 & 0 \\ 0 & 0 & 0 & 0 & 0 & 0 & 0 & -1.893\,\gamma_{\delta_\theta}\omega_{\delta_\theta} \\ 0 & 0 & 0 & 0 & 0 & 0 & 1.893\,\gamma_{\delta_\phi}\omega_{\delta_\phi} & 0 \end{bmatrix}$$

$[2\,[I]\,[\dot{T}] + [D]]$ is as follows:

$$\begin{bmatrix} 0 & \begin{matrix}-.3\Omega_G\\-805.2\Omega\end{matrix} & 0 & -15.316\Omega & \begin{matrix}-.3\Omega_G\\-10.048\Omega\end{matrix} & 0 & -31.88\Omega & -19.54\Omega \\ \begin{matrix}+.3\Omega_G\\805.2\Omega\end{matrix} & 0 & 0 & \begin{matrix}+.3\Omega_G\\10.048\Omega\end{matrix} & -15.316\Omega & 0 & 19.54\Omega & -31.88\Omega \\ 0 & 0 & 0 & 0 & 0 & 0 & 0 & 0 \\ 15.316\Omega & \begin{matrix}-10.348\Omega\\-.3(\Omega_G-\Omega)\end{matrix} & 0 & C_R & \begin{matrix}-1.208\Omega\\-.3(\Omega_G-\Omega)\end{matrix} & 0 & 0 & -.8504\Omega \\ \begin{matrix}10.348\Omega\\.3(\Omega_G-\Omega)\end{matrix} & 15.316\Omega & 0 & \begin{matrix}1.208\Omega+\\.3(\Omega_G-\Omega)\end{matrix} & C_R & 0 & .8504\Omega & 0 \\ 0 & 0 & 0 & 0 & 0 & 3.786\gamma_{\delta_0}\gamma_{\delta_0} & 0 & 0 \\ 31.88\Omega & -19.54\Omega & 0 & 0 & -.8504\Omega & 0 & 1.893\gamma_{\delta_\theta}\omega_{\delta_\theta} & -1.893\Omega \\ 19.54\Omega & 31.88\Omega & 0 & .8504\Omega & 0 & 0 & 1.893\Omega & 1.893\gamma_{\delta_\phi}\omega_{\delta_\phi} \end{bmatrix}$$

Swashplate springs and dampers. - Springs and dampers are inserted
between the stationary ring of the swashplate and the airframe (body). The
springs produce swashplate moments proportional to swashplate tilt displace-
ments and the dampers produce moments proportional to the tilt velocities. In
this study both are considered to be rotationally symmetric or have equal
diagonal elements and zero off-diagonal elements.

Swashplate moments due to springs are given by:

$$
\begin{Bmatrix} M_\theta \\ M_\phi \end{Bmatrix} = - \begin{bmatrix} K_S & 0 \\ 0 & K_S \end{bmatrix} \begin{Bmatrix} \theta \\ \phi \end{Bmatrix}
$$

Swashplate moments due to dampers are given by:

$$
\begin{Bmatrix} M_\theta \\ M_\phi \end{Bmatrix} = - \begin{bmatrix} C_S & 0 \\ 0 & C_S \end{bmatrix} \begin{Bmatrix} \dot\theta \\ \dot\phi \end{Bmatrix}
$$

The minus signs indicate that matrices apply to RHS of differential
equations.

Body terms. - The rigid body terms are added directly to the rotor terms,
which were derived relative to earth-fixed axes. The rotor equations relate
the generalized forces acting on the rotor degrees of freedom to the motions
of the same degrees of freedom - in fact, they describe the free flight motion
of a rotor alone. Adding the body terms completes the description of the
motion of the entire vehicle.

The rotor equations with swashplate springs and dampers are:

$$
\begin{bmatrix} I \end{bmatrix} \ddot\beta + \left[2\begin{bmatrix} I \end{bmatrix}\begin{bmatrix} \dot T \end{bmatrix} + \begin{bmatrix} D \end{bmatrix} \right] \dot\beta + \left[\begin{bmatrix} I \end{bmatrix}\begin{bmatrix} \ddot T \end{bmatrix} + \begin{bmatrix} D \end{bmatrix}\begin{bmatrix} \dot T \end{bmatrix} + \begin{bmatrix} S \end{bmatrix} \right] \beta
$$

$$
- \begin{bmatrix} B_R \end{bmatrix} \dot\beta - \begin{bmatrix} B \end{bmatrix} \beta + \begin{bmatrix} C_S \end{bmatrix} \dot\beta + \begin{bmatrix} K_S \end{bmatrix} \beta = 0
$$

The body (aircraft type) equations of motion are also written relative to the earth-fixed axes.

Perkins & Hage (reference 6) give the rigid-body equations of motion relative to axes rotating with the body and aligned with the mean wind vector. They are:
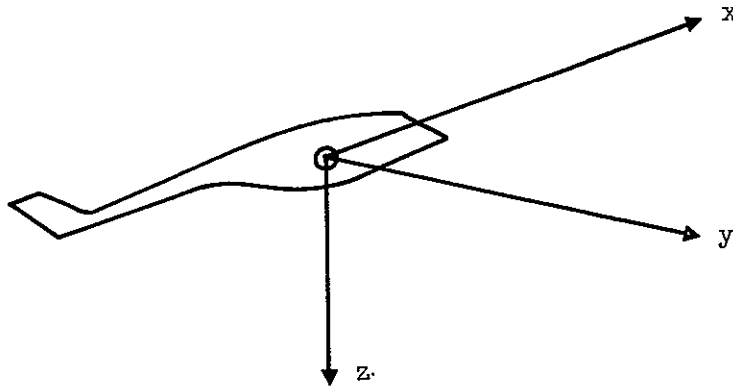
$$\frac{\partial M}{\partial \alpha} \, \Delta\alpha \; + \; \frac{\partial M}{\partial \dot{\theta}} \, \dot{\theta} \; + \; \frac{\partial M}{\partial \dot{\alpha}} \, \dot{\alpha} \; = \; m \, ky^2 \cdot \ddot{\theta}$$

$$\frac{\partial F_z}{\partial \alpha} \, \Delta\alpha \; = \; mV \, (\dot{\theta} - \dot{\alpha})$$

Substituting the following:

$$m \, k_y^2 \; = \; I_{yy}$$

$$\alpha \; = \; \frac{\dot{z}}{V}$$

$$\dot{\alpha} \; = \; \frac{\ddot{z}}{V}$$

the equations are written:

$$I_{yy}\,\ddot{\Theta} - \frac{1}{V}\,\frac{\partial M}{\partial\dot\alpha}\,\ddot{z} - \frac{\partial M}{\partial\dot\Theta}\,\dot{\Theta} - \frac{1}{V}\,\frac{\partial M}{\partial\alpha}\,\dot{z} = 0$$

$$m\ddot{z} - mV\,\dot{\Theta} - \frac{1}{V}\,\frac{\partial F_Z}{\partial\alpha}\,\dot{z} = 0$$

and in matrix form are:

$$\begin{bmatrix} I_{yy} & -\frac{1}{V}\frac{\partial M}{\partial\dot\alpha} \\ 0 & m \end{bmatrix}\begin{Bmatrix} \ddot{\Theta} \\ \ddot{z} \end{Bmatrix} + \begin{bmatrix} -\frac{\partial M}{\partial\dot\theta} & -\frac{1}{V}\frac{\partial M}{\partial\alpha} \\ -mV & -\frac{1}{V}\frac{\partial F_Z}{\partial\alpha} \end{bmatrix}\begin{Bmatrix} \dot{\Theta} \\ \dot{z} \end{Bmatrix} = 0$$

The aerodynamic derivatives are derived as though they are forcing functions (on RHS of equations). For axes fixed in the body (airplane axes),

$$\begin{bmatrix} I_{yy} & -\frac{1}{V}M_{\dot\alpha} \\ 0 & M \end{bmatrix}\begin{Bmatrix} \ddot{\Theta} \\ \ddot{z} \end{Bmatrix} + \begin{bmatrix} -Mq & -\frac{1}{V}M_{\alpha} \\ -MV & -\frac{1}{V}Z_{\alpha} \end{bmatrix}\begin{Bmatrix} \dot{\Theta} \\ \dot{z} \end{Bmatrix} = 0$$

For earth-axes the equations become

$$\begin{bmatrix} I_{yy} & -\frac{1}{V}M_{\dot\alpha} \\ 0 & M \end{bmatrix}\begin{Bmatrix} \ddot{\Theta} \\ \ddot{z} \end{Bmatrix} + \begin{bmatrix} -(M_q+M_{\dot\alpha}) & -\frac{1}{V}M_{\alpha} \\ 0 & -\frac{1}{V}Z_{\alpha} \end{bmatrix}\begin{Bmatrix} \dot{\Theta} \\ \dot{z} \end{Bmatrix} + \begin{bmatrix} -M_{\alpha} & 0 \\ -Z_{\alpha} & 0 \end{bmatrix}\begin{Bmatrix} \Theta \\ z \end{Bmatrix} = 0$$

For body-axes the dynamic determinant becomes

$$\begin{vmatrix} I_{yy}\lambda^2 - M_q\lambda & -\frac{1}{V}M_{\dot\alpha}\lambda^2 - \frac{1}{V}M_{\alpha}\lambda \\ -MV\lambda & M\lambda^2 - \frac{1}{V}Z_{\alpha}\lambda \end{vmatrix}$$

233

which expands to

$$I_{yy} M\lambda^4 - (MM_q + I_{yy} \frac{Z_\alpha}{V} + MM_{\dot\alpha})\lambda^3 + (M_q \frac{Z_\alpha}{V} - MM_\alpha)\lambda^2$$

For earth-axes the dynamic determinant becomes

$$\begin{vmatrix} I_{yy}\lambda^2 - (M_q + M_{\dot\alpha})\lambda - M_\alpha & -\frac{M_{\dot\alpha}}{V}\lambda^2 - \frac{M_\alpha}{V}\lambda \\ -Z_\alpha & M\lambda^2 - \frac{Z_\alpha}{V}\lambda \end{vmatrix}$$

which expands to

$$I_{yy} M\lambda^4 - (MM_q + I_{yy} \frac{Z_\alpha}{V} + MM_{\dot\alpha})\lambda^3 + (M_q \frac{Z_\alpha}{V} - MM_\alpha)\lambda^2$$

Since the two representations have the same characteristic equation they yield the same roots, frequency and damping, or, the two equations can be said to represent the same physical situation.

The earth-fixed representation is used in conjunction with the rotor equations; axes are selected to coincide with the rotor axis convention. The equations of the body relative to aircraft axes are

$$
\begin{bmatrix}
I_{yy} & 0 & -\dfrac{1}{V}M_{\dot\alpha} \\[6pt]
0 & I_{xx} & 0 \\[6pt]
0 & 0 & M
\end{bmatrix}
\begin{Bmatrix}
\ddot\Theta \\[6pt]
\ddot\Phi \\[6pt]
\ddot z
\end{Bmatrix}
+
\begin{bmatrix}
-(M_q + M_{\dot\alpha}) & 0 & -\dfrac{1}{V}M_\alpha \\[6pt]
0 & -L_p & 0 \\[6pt]
0 & 0 & -\dfrac{1}{V}Z_\alpha
\end{bmatrix}
\begin{Bmatrix}
\dot\Theta \\[6pt]
\dot\Phi \\[6pt]
\dot z
\end{Bmatrix}
$$

$$
+
\begin{bmatrix}
-M_\alpha & 0 & 0 \\[6pt]
0 & 0 & 0 \\[6pt]
-Z_\alpha & 0 & 0
\end{bmatrix}
\begin{Bmatrix}
\Theta \\[6pt]
\Phi \\[6pt]
z
\end{Bmatrix}
= 0
$$

where

$$
M_{\dot\alpha} = C_{m_{\dot\alpha}}\left(\frac{\overline{c}}{2V}\right) qS\overline{c}
$$

$$
M_q = C_{m_q}\left(\frac{\overline{c}}{2V}\right) qS\overline{c}
$$

$$
M_\alpha = C_{m_\alpha} qS\overline{c}
$$

$$
Z_\alpha = -C_{L_\alpha} qS
$$

$$
L_p = C_{\ell_p}\ \frac{b}{2V}\ qSb
$$

and:

$$
C_{m_{\dot\alpha}} = \frac{\partial C_m}{\partial \dfrac{\dot\alpha c}{2V}}\ ,\qquad
C_{m_q} = \frac{\partial C_m}{\partial \dfrac{qc}{2V}}
$$

$$
C_{\ell_p} = \frac{\partial C_\ell}{\partial \dfrac{pb}{2V}}
$$

235

Now the equations are rewritten in the helicopter axis system
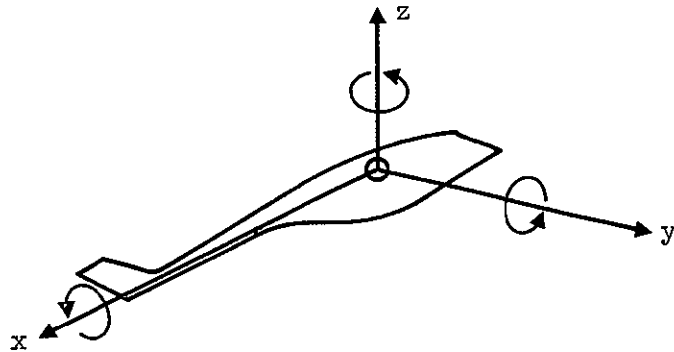
The Y axis is common to both systems, so signs of pitching moment and θ do not change. The helicopter Z axis is the negative of the airplane Z axis, so z displacements and z forces are of opposite signs to those of the airplane; the sign of the vertical force $-\frac{1}{V} Z_\alpha$ and of M remain unchanged. Since the roll axis is reversed, and roll forces and matrices are not coupled with the others, their signs do not change. Examining the cross terms:

- The sign of $-\frac{1}{V} M_{\dot\alpha}$ changes to $\frac{1}{V} M_{\dot\alpha}$
- The sign of $-\frac{1}{V} M_\alpha$ changes to $\frac{1}{V} M_\alpha$
- The sign of $- Z_\alpha$ changes to Z_α

The final equations of the body in rotor earth fixed axes system are as follows:

$$
\begin{bmatrix} I_{yy} & 0 & \frac{1}{V} M_{\dot\alpha} \\ 0 & I_{xx} & 0 \\ 0 & 0 & M \end{bmatrix}
\begin{Bmatrix} \ddot\Theta \\ \ddot\Phi \\ \ddot z \end{Bmatrix} +
\begin{bmatrix} -(M_q + M_{\dot\alpha}) & 0 & \frac{1}{V} M_\alpha \\ 0 & -L_p & 0 \\ 0 & 0 & -\frac{1}{V} Z_\alpha \end{bmatrix}
\begin{Bmatrix} \dot\Theta \\ \dot\Phi \\ \dot z \end{Bmatrix} +
\begin{bmatrix} -M_\alpha & 0 & 0 \\ 0 & 0 & 0 \\ Z_\alpha & 0 & 0 \end{bmatrix}
\begin{Bmatrix} \Theta \\ \Phi \\ z \end{Bmatrix} = 0
$$

These equations are based on the previously defined values of derivatives. It would be proper to redefine the derivatives in terms of the new axis system, but the system of derivatives is selected so that existing airplane-type derivatives can be used.

Aerodynamic derivatives of the wind tunnel model configuration are now estimated. A tail-plane of the proper general size is assumed to be added to stabilize the vehicle in free flight. Mass and inertia data appropriate to an equivalent flight vehicle are also estimated. Mass and inertia data of the actual wind tunnel model are also approximated so that dynamic modes of the model mounted in the wind tunnel could be calculated for comparison with hypothetical free-flight calculations.

The equations of motion of the airframe contain the aerodynamic and inertia terms needed for the analysis of vehicle stability. They are as follows:

$$M_\alpha \, , \; M_{\dot\alpha} \, , \; M_q$$
$$L_p$$
$$Z_\alpha$$

Inertia data required are

$$I_{yy} \, , \; I_{xx} \quad \text{and} \quad M$$

In the analyses discussed in this report, interference between the rotor and body is ignored; in other words, rotor derivatives assume absence of the airframe, and airframe derivatives assume absence of the rotor. It is expected that interference between an essentially unloaded rotor and a body are small and do not affect the basic form of the dynamic modes.

Geometry of the wing-body tail of the model with an assumed horizontal tail is shown in Figure A-10.

The pitching moment about the center of gravity due to a unit angle of attack (M_α) is caused by the body and tail. The wing is located so that its aerodynamic center is at the aircraft center of gravity and on the shaft axis. This location causes the wing to produce no moments about the center of gravity. Wing downwash has an effect on the tail contribution to moments.

$$M_\alpha = C_{m_\alpha} \, q \, S\bar{c}$$

$$= M_{\alpha_{body}} - C_{\ell_{\alpha_t}} \frac{\alpha t}{\alpha} \, q \, S_t \ell_t$$

where

$C_{\ell_{\alpha_t}}$ = lift curve slope of the tail

α_t = net angle of attack of the tail including downwash from the wing

q = dynamic pressure

S = wing area

S_t = tail area

ℓ_t = tail moment arm

$\bar{c}$ = mean aerodynamic chord of wing

The pitching moment due to a body angle of attack is proportional to the volume of the body (slender body theory),

$$M_{\alpha_{body}} = \frac{dM}{d\alpha} = 2 \text{ Volume } q$$

and the tail angle of attack is reduced by downwash from the wing,
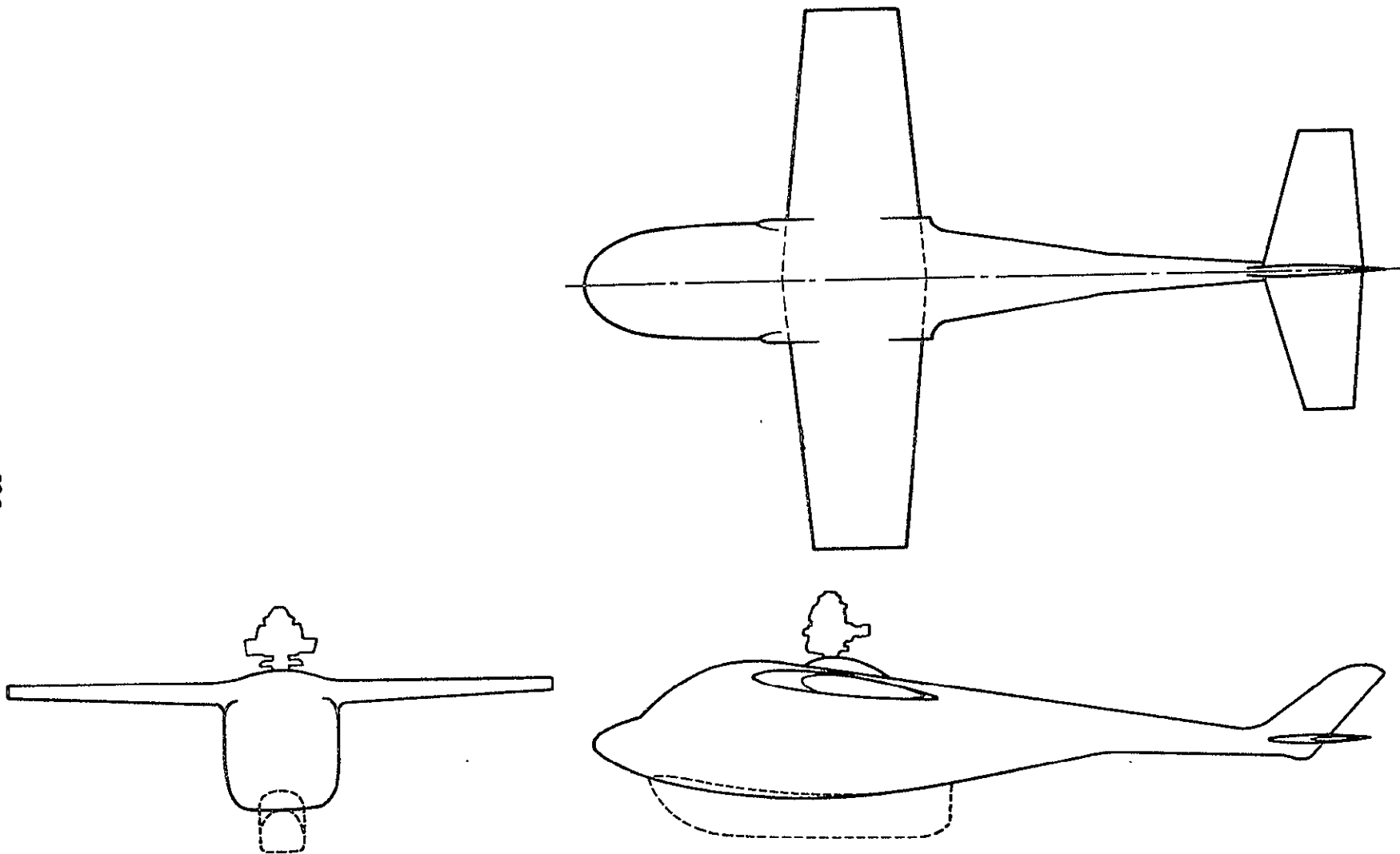
Figure A-10. Wing-Body-Tail Geometry Of The Gimballed Model And The Free-Flight Vehicle

$$\alpha_t = \alpha \left(1 - \frac{\partial \epsilon}{\partial \alpha} \right)$$

where

ϵ = downwash angle

α = wing angle of attack

Therefore, the nondimensional derivative is

$$C_{m_\alpha} = \frac{2\,\text{Vol}}{S\bar{c}} - C_{\ell_{\alpha_t}} \frac{S_t}{S} \frac{\ell_t}{\bar{c}} \left(1 - \frac{\partial \epsilon}{\partial \alpha} \right)$$

Physical dimensions of the model are

Fuselage volume	Vol	= 225 ft^3
Wing area	S	= 95 ft^2
Wing MAC	$\bar{c}$	= 4.58 ft
Tail moment arm	ℓ_t	= 18.3 ft
Tail area	S_t	= 33.3 ft^2

The wing and tail geometries are

	Area, S ft^2	Span, b ft	Aspect Ratio	Taper Ratio	C_{ℓ_α}
Wing	95	20.8	4.55	.62	4.0
Tail	33.3	11.0	3.60	.5	3.6

Downwash at the tail is obtained from page 224 of Reference 6, knowing the position of the tail relative to the wing, and the wing geometry. The value determined for this vehicle is

$$\frac{\partial \epsilon}{\partial \alpha} \approx .3$$

Therefore,

$$C_{m_\alpha} = \frac{2 \times 225}{95 \times 4.58} - 3.6 \times \frac{33.3}{95} \times \frac{18.3}{4.58} \times (1 - .30) = -2.51$$

and

$$M_\alpha = -2.51 \, q \, Sc$$

The pitching moment due to $\dot{\alpha}$ is

$$M_{\dot{\alpha}} = C_m \left(\frac{\dot{\alpha}\bar{c}}{2V}\right) \frac{c}{2V} \, q \, S\bar{c}$$

or

$$M_{\dot{\alpha}} = C_{m_{\dot{\alpha}}} \, q \, S\bar{c}$$

$$C_{m_{\dot{\alpha}}} = -C_{l_t} \frac{St}{S} \frac{lt}{\bar{c}} \frac{lt}{V} \frac{d\epsilon}{d\alpha}$$

Substituting values for the model, at a flight speed of 120 knots,

$$C_{m_{\dot{\alpha}}} = -3.6 \frac{33.3}{95} \frac{18.3}{4.58} \frac{18.3}{203} (.30) = -0.136$$

and

$$M_{\dot{\alpha}} = -.136 \, q \, S\bar{c}$$

The pitching moment coefficient due to q is

$$C_{m_q} = c_{l_{\alpha_t}} \frac{St}{S} \frac{lt}{\bar{c}} \frac{lt}{V}$$

Substituting-value for the model, at a flight speed of 120 knots,

$$C_{m_q} = 3.6 \times \frac{33.3}{95} \times \frac{18.3}{4.58} \times \frac{18.3}{203} = -.4\,54$$

and

$$M_q = -.454 \, q \, S\bar{c}$$

The damping in roll derivative at a selected flight speed depends only on the aspect ratio and taper ratio of the wing,

$$AR = 4.55$$

$$T.R. = .62$$

$$L_p = C_{\ell_{\left(\frac{pb}{2V}\right)}} \left(\frac{b}{2V}\right) q \, Sb$$

Using geometry of the model and a 120 knot flight speed, a value is obtained from page 357 of Reference 9,

$$C_{\ell_{\left(\frac{pb}{2V}\right)}} = -.43$$

Therefore,

$$L_p = -.022 \, q \, Sb$$

The vertical force due to angle of attack comes from the wing and tail.

$$Z_\alpha = -C_{L_\alpha} q \, S$$

where

C_{L_α} is for the airplane

$$C_{L_{\alpha_{airplane}}} = C_{L_{\alpha_{wing}}} + C_{l_{\alpha_t}} \frac{St}{S} \left(1 - \frac{\partial \epsilon}{\partial \alpha}\right)$$

242

Substituting values for the model,

$$C_{L_{\alpha_{airplane}}} = 4.0 + 3.6 \times \frac{33.3}{95}(1 - .3) = 4.88$$

Therefore,

$$Z_\alpha = -4.88 \; q \; S$$

In summary then the aerodynamic derivatives are

$$M_\alpha = -2.51 \; q \; S\bar{c}, \text{ (at any speed)} = -2.51 \; q \; S\bar{c} \text{ (at 120 knots)}$$

$$M_{\dot{\alpha}} = -\frac{27.6}{V} \; q \; S\bar{c}, \text{ (at any speed)} = -.136 \; q \; S\bar{c} \text{ (at 120 knots)}$$

$$M_q = -\frac{92}{V} \; q \; S\bar{c}, \text{ (at any speed)} = -.454 \; q \; S\bar{c} \text{ (at 120 knots)}$$

$$L_p = -\frac{4.46}{V} \; q \; Sb, \text{ (at any speed)} = -.022 \; q \; Sb \text{ (at 120 knots)}$$

$$Z_\alpha = -4.88 \; q \; S, \text{ (at any speed)} = -4.88 \; q \; S \text{ (at 120 knots)}$$

The moments of inertia are determined separately for the free flying vehicle and the wind tunnel model. Estimated distributions of the masses are used. The flying weight of the free vehicle is based on the actual weight of a helicopter similar to the wind tunnel model: 3500 lb. The wind tunnel model weighs approximately 6000 lb. Inertia data for the body and hub are needed to complete the required data items. The mass and inertia of the rotor blades are included in the rotor equations of motion. A summary of this additional inertia data is as follows:

INERTIA DATA SUMMARY

	Free Flight Vehicle	Wind Tunnel Model
Gross weight, lb	3500	6000
Body and Hub weight, lb	3220	5200
Pitch moment of inertia, I_{YY}, slug ft^2	1300	2400
Roll moment of inertia, I_{xx}, slug ft^2	800	1500
Mass, M, slugs	100	177

APPENDIX B
DISCUSSION OF BLADE FLAPPING

Each of the three blades of the rotor is assumed to flap normal to the rotor disk only. This assumption implies that as far as the flapping degree of freedom is concerned, the blades have no twist, no collective, and no cyclic pitch. It further implies no radiuswise and no in-plane motions of the blades. This assumption eliminates coriolis forces and in-plane to feathering coupling. The blade 1st flapping mode, only, is considered; its mode shape changes only slightly when rotor rotational speed is varied from zero to full rpm; so, a single mean shape is used for all values of rpm. Since there are three blades, there are three rotor elastic modes associated with the blade 1st flapping mode. These three modes are shown in Figure A-8.

It would be expected that the two modes which bend the shaft, pitch and roll, should have the same frequency, and that this frequency would be slightly lower than that for the colletive motion. It becomes evident upon investigation, however, that the shaft is so stiff that deflections in the modes are almost entirely due to the blades. Therefore, the three rotor modes have effectively the same frequency.

The three rotor modes can be used to formulate a complete description of all first flapping displacements. This can be visualized by a plane passing through the three blade tips; a plane can only translate vertically and tilt in pitch and roll.

<div align="center">

Summary of General Observations Applicable to
Blade Flapping Motion
</div>

1. There are three rotor modes corresponding to the blade 1st flapping mode of a three-blade rotor. These are shown on Figure A-8.
2. The shape of the blade 1st flapping mode is adequately described by

$$\frac{\delta}{\delta_{tip}} = \left(\frac{r}{R}\right)^2$$

3. The three rotor modes are orthogonal to each other and are the complete set of 1st flapping modes.

4. The rotor shaft bending contribution to the rotor pitch and roll modes is negligible, so the natural frequency of these two modes (in vacuo) equals the frequency of the collective mode.

5. The principles involved in finding the rotor blade natural flapping frequencies at zero rpm in vacuo and with centrifugal effects included for any rpm are illustrated with a rudimentary model. The results approximate those which were obtained with a more comprehensive model.

Notation Used in Appendix B

EI	Bending Stiffness, lb in.^{2}
f	Natural vibration frequency, cps
F	Force applied at lumped mass, lb
k_θ	Spring stiffness, in. lb/radian
m	Mass, slugs $\div$ 12
r	Distance from center of rotation, in.
R	Tip radius, in.
$[S]$	Blade bending structural influence matrix, in/lb
δ	Blade flapping deflection, in.
θ	Root spring deflection angle, rad
ω	Natural vibration frequency, rad/sec
Ω	Rotor rotation rate, rad/sec

Subscripts:

$1,2,\ldots$	Mass node number; vibration mode number
δ	Structural deflection
i,n,p	Lumped mass number
tip	tip of blade

Blade Frequencies and Mode Shapes as Influenced by Centrifugal Forces and Shaft Stiffness

A simple example is used to illustrate the effects of blade stiffness, mass distribution, shaft stiffness, and centrifugal forces on natural frequencies and mode shapes of a blade relative to axes which rotate with the rotor. Although it would probably be necessary to use at least 3 or 4 lumped masses to adequately represent the blade mass distribution (also a stiffness matrix based on linear variation of EI between lumps would be more accurate than a constant EI), the example uses only 2 lumped masses and a constant EI. The results of this relatively crude representation have been shown to be close to results obtained by analyses using up to 30 lumps.

The shaft bending stiffness is represented by a spring attached to the blade root as shown below. The blade deformations under the action of forces applied at the mass nodes are also shown below

$$\left\{ \begin{array}{c} \delta_{s_1} \\ \\ \delta_{s_2} \end{array} \right\} = \left[\quad S \quad \right] \left\{ \begin{array}{c} F_1 \\ \\ F_2 \end{array} \right\}$$
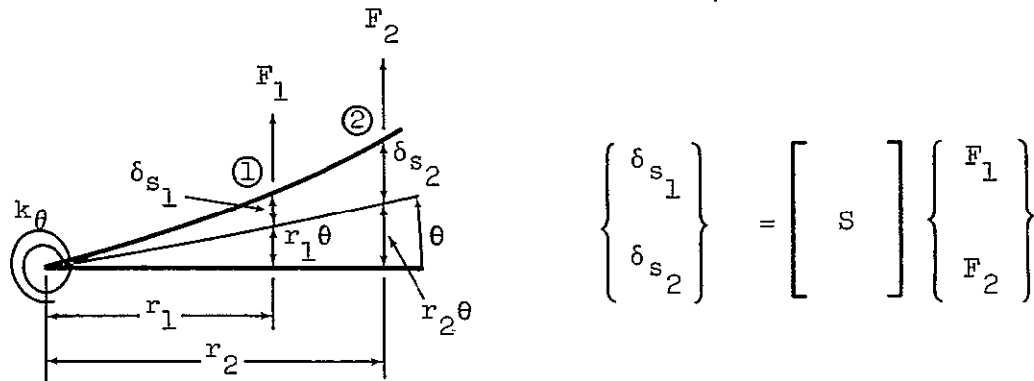
The part of the deflection due to bending of the blade is denoted by δ_s and that due to the root spring by $r\theta$. The square matrix $[S]$ relates the bending deflection to the node point forces. The root spring angular deflection θ is

$$\theta = \frac{r_1 F_1 + r_2 F_2}{k_\theta}$$

which is written in matrix notation as

$$\theta = \begin{bmatrix} \dfrac{r_1}{k_\theta} & \dfrac{r_2}{k_\theta} \end{bmatrix} \begin{Bmatrix} F_1 \\ F_2 \end{Bmatrix}$$

The total deflection then is given by:

$$\begin{Bmatrix} \delta_1 \\ \delta_2 \end{Bmatrix} = \begin{Bmatrix} \delta_{1s} \\ \delta_{2s} \end{Bmatrix} + \begin{Bmatrix} r_1 \\ r_2 \end{Bmatrix} \theta$$

$$= \begin{Bmatrix} \delta_{1s} \\ \delta_{2s} \end{Bmatrix} + \begin{Bmatrix} r_1 \\ r_2 \end{Bmatrix} \begin{bmatrix} \dfrac{r_1}{k_\theta} & \dfrac{r_2}{k_\theta} \end{bmatrix} \begin{Bmatrix} F_1 \\ F_2 \end{Bmatrix}$$

$$= \begin{bmatrix} S \end{bmatrix} \begin{Bmatrix} F_1 \\ F_2 \end{Bmatrix} + \frac{1}{k_\theta} \begin{bmatrix} r_1^2 & r_1 r_2 \\ r_1 r_2 & r_2^2 \end{bmatrix} \begin{Bmatrix} F_1 \\ F_2 \end{Bmatrix}$$

$$\begin{Bmatrix} \delta_1 \\ \delta_2 \end{Bmatrix} = \begin{bmatrix} \begin{bmatrix} S \end{bmatrix} + \frac{1}{k_\theta} \begin{bmatrix} r_1^2 & r_1 r_2 \\ r_1 r_2 & r_2^2 \end{bmatrix} \end{bmatrix} \begin{Bmatrix} F_1 \\ F_2 \end{Bmatrix} \quad - - - - - - - - - - \quad (1)$$

To evaluate the vibration modes and frequencies, all aerodynamic forces are assumed to be zero and the applied forces

$$\begin{Bmatrix} F_1 \\ F_2 \end{Bmatrix}$$

are due to inertia and vertical components of blade tension forces induced by centrifugal forces. The inertia forces in a vibrating system are given by $\omega^2 m \delta$. Centrifugal force produces tension in the blades, which increases

as each lumped mass is passed on the way from the tip to the root. Blade
tension immediately inboard of any station, n, is

$$\text{Tension} = \Omega^2 \sum_{i=n}^{p} r_i m_i$$

where p identifies the most outboard mass. The vertical reaction at station
n depends on the deflection of the blade at n, n+1, and n-1
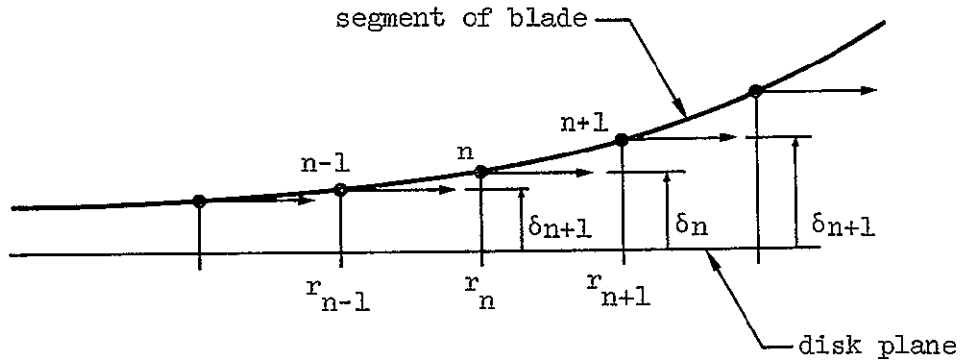
$$V_{cf_n} = \left(\frac{\delta_{n+1} - \delta_n}{r_{n+1} - r_n}\right) \Omega^2 \sum_{i=n+1}^{p} r_i m_i - \left(\frac{\delta_n - \delta_{n-1}}{r_n - r_{n-1}}\right) \Omega^2 \sum_{i=n}^{p} r_i m_i$$

The net vertical force due to inertia and centrifugally induced force is

$$F_n = \omega^2 m_n \delta_n + \Omega^2 \left[\left(\frac{\delta_{n+1} - \delta_n}{r_{n+1} - r_n}\right) \sum_{i=n+1}^{p} r_i m_i - \left(\frac{\delta_n - \delta_{n-1}}{r_n - r_{n-1}}\right) \sum_{i=n}^{p} r_i m_i\right]$$

and, in the two-mass representation of the example,

$$F_1 = \omega^2 m_1 \delta_1 + \Omega^2 \left[\left(\frac{\delta_2 - \delta_1}{r_2 - r_1}\right)\left(r_2 m_2\right) - \frac{\delta_1}{r_1}\left(r_1 m_1 + r_2 m_2\right)\right]$$

$$F_2 = \omega^2 m_2 \delta_2 + \Omega^2 \left[-\left(\frac{\delta_2 - \delta_1}{r_2 - r_1} \right) (r_2 m_2) \right]$$

and, in matrix form,

$$\left\{ \begin{matrix} F_1 \\ F_2 \end{matrix} \right\} = \omega^2 \begin{bmatrix} m_1 & 0 \\ 0 & m_2 \end{bmatrix} \left\{ \begin{matrix} \delta_1 \\ \delta_2 \end{matrix} \right\} + \Omega^2 \left[\frac{r_2 m_2}{r_2 - r_1} \begin{bmatrix} -1 & 1 \\ 1 & -1 \end{bmatrix} - \begin{bmatrix} m_1 + \dfrac{r_2}{r_1} m_2 & 0 \\ 0 & 0 \end{bmatrix} \right] \left\{ \begin{matrix} \delta_1 \\ \delta_2 \end{matrix} \right\}$$

From equations (1), regarding the structural deflection due to vertical forces,

$$\left\{ \begin{matrix} F_1 \\ F_2 \end{matrix} \right\} = \left[[S] + \frac{1}{k_\theta} \begin{bmatrix} r_1^2 & r_1 r_2 \\ r_1 r_2 & r_2^2 \end{bmatrix} \right]^{-1} \left\{ \begin{matrix} \delta_1 \\ \delta_2 \end{matrix} \right\}$$

Equating structural forces with inertia and centrifugally induced

$$\left[[S] + \frac{1}{k_\theta} \begin{bmatrix} r_1^2 & r_1 r_2 \\ r_1 r_2 & r_2^2 \end{bmatrix} \right]^{-1} \left\{ \begin{matrix} \delta_1 \\ \delta_2 \end{matrix} \right\} = \left[\omega^2 \begin{bmatrix} m_1 & 0 \\ 0 & m_2 \end{bmatrix} + \Omega^2 \left[\frac{r_2 m_2}{r_2 - r_1} \begin{bmatrix} -1 & 1 \\ 1 & -1 \end{bmatrix} \right. \right.$$

$$\left. \left. - \begin{bmatrix} m_1 + \dfrac{r_2}{r_1} m_2 & 0 \\ 0 & 0 \end{bmatrix} \right] \right] \left\{ \begin{matrix} \delta_1 \\ \delta_2 \end{matrix} \right\}$$

To determine the natural frequencies and mode shapes of the two-mass-represented blade relative to rotating axes, which include the effects of blade stiffness, mass distribution, centrifugal forces and root hinge stiffness, the two roots of the characteristics equation of the following equations are evaluated.

$$\left[\left[[S] + \frac{1}{k_\theta}\begin{bmatrix} r_1^2 & r_1 r_2 \\ r_1 r_2 & r_2^2 \end{bmatrix}\right]^{-1} - \left[\omega^2\begin{bmatrix} m_1 & 0 \\ 0 & m_2 \end{bmatrix} + \Omega^2\frac{r_2 m_2}{r_2 - r_1}\begin{bmatrix} -1 & 1 \\ 1 & -1 \end{bmatrix}\right]\right.$$

$$\left.- \begin{bmatrix} m_1 + \dfrac{r_2}{r_1} m_2 & 0 \\ 0 & 0 \end{bmatrix}\right]\begin{Bmatrix} \delta_1 \\ \delta_2 \end{Bmatrix} = 0 \tag{2}$$

A simple check of the equation is available. If the structural matrix is zero and the shaft spring is zero (this in effect makes the system a string with two weights, swinging around a pylon) then one of the natural frequencies would equal the rotational velocity; i. e., a root would be $\omega = \Omega$:

Substituting $\omega = \Omega$ and dividing by Ω^2 yields:

$$\left|\begin{bmatrix} m_1 & 0 \\ 0 & m_2 \end{bmatrix} + \frac{r_2 m_2}{r_2 - r_1}\begin{bmatrix} -1 & 1 \\ 1 & -1 \end{bmatrix} - \begin{bmatrix} m_1 + \dfrac{r_2}{r_1} m_2 & 0 \\ 0 & 0 \end{bmatrix}\right| = 0$$

$$\left|\begin{matrix} -\dfrac{r_2 m_2}{r_2 - r_1} - \dfrac{r_2 m_2}{r_1} & \dfrac{r_2 m_2}{r_2 - r_1} \\[3ex] \dfrac{r_2 m_2}{r_2 - r_1} & m_2 - \dfrac{r_2 m_2}{r_2 - r_1} \end{matrix}\right| = 0$$

The determinant equals zero when expanded.

The natural frequencies and mode shapes are found from the eigenvalues and eigenfunctions of the equations.

$$\left\| \left[[S] + \frac{1}{k_\theta} \begin{bmatrix} r_1^2 & r_1 r_2 \\ r_1 r_2 & r_2^2 \end{bmatrix} \right]^{-1} - \Omega^2 \left[\frac{r_2 m_2}{r_2 - r_1} \begin{bmatrix} -1 & 1 \\ 1 & -1 \end{bmatrix} - \begin{bmatrix} m_1 + \frac{r_2}{r_1} m_2 & 0 \\ 0 & 0 \end{bmatrix} \right] \right.$$

$$\left. - \omega^2 \begin{bmatrix} m_1 & 0 \\ 0 & m_2 \end{bmatrix} \right\| = 0$$

The first step is to determine the structural matrix $[S]$. That is find the deflection δ_{s_1} and δ_{s_2} due to loads F_1 and F_2
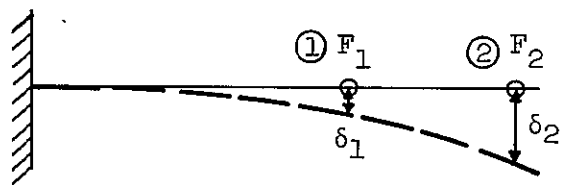
δ_{s_1} , δ_{s_2} due to unit loads at ①
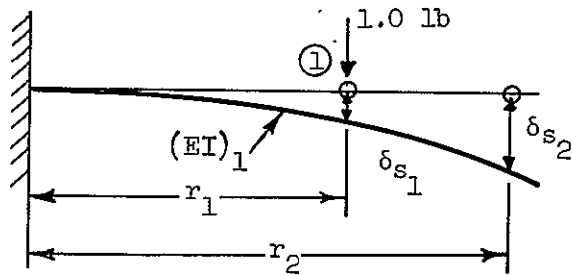
$$\delta_{s_1} \bigg|_{①} = \frac{1.0\ r_1^3}{3(EI)_1}$$

$$\delta_{s_2} \bigg|_{①} = \delta_{s_1} \bigg|_{①} + \frac{1.0\ r_1^2 (r_2 - r_1)}{2(EI)_1}$$

δ_{s_1}, δ_{s_2} due to unit load at ②
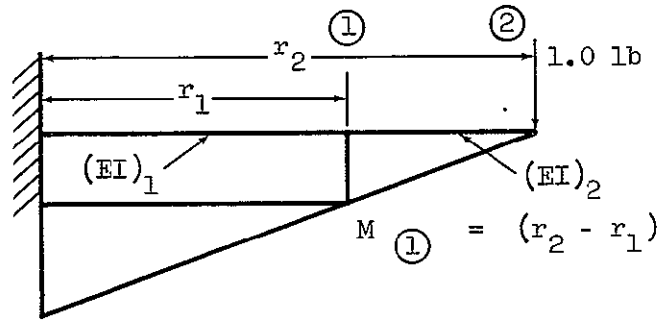
$$\delta_{s_1}\,② = \frac{(r_2 - r_1)\,r_1^2}{2(EI)_1} + \frac{r_1^3}{3(EI)_1}$$

$$\delta_{s_2}\,② = \left(\frac{(r_2 - r_1)\,r_1}{(EI)_1} + \frac{r_1^2}{2(EI)_1}\right)(r_2 - r_1) + \frac{(r_2 - r_1)^3}{3(EI)_2} + \delta_{s_1}\,②$$

The structural matrix $\left[S\right]$ then becomes

$$\left[S\right] = \begin{bmatrix} \dfrac{1.0r_1^3}{3(EI)_1} & \dfrac{1.0r_1^3}{3(EI)_1} + \dfrac{(r_2 - r_1)r_1^2}{2(EI)_1} \\[4em] \dfrac{1.0r_1^3}{3(EI)_1} + & \dfrac{r_1^3}{3(EI)_1} + \dfrac{(r_2 - r_1)\,r_1^2}{2(EI)_1} + \dfrac{(r_2 - r_1)^3}{3(EI)_2} + \\[2em] \dfrac{1.0r_1^2\,(r_2 - r_1)}{2(EI)_1} & \left(\dfrac{(r_2 - r_1)r_1}{(EI)_1} + \dfrac{r_1^2}{2(EI)_1}\right)(r_2 - r_1) \end{bmatrix}$$

253

The stiffness of the shaft acting as a spring to the blade is evaluated as follows:
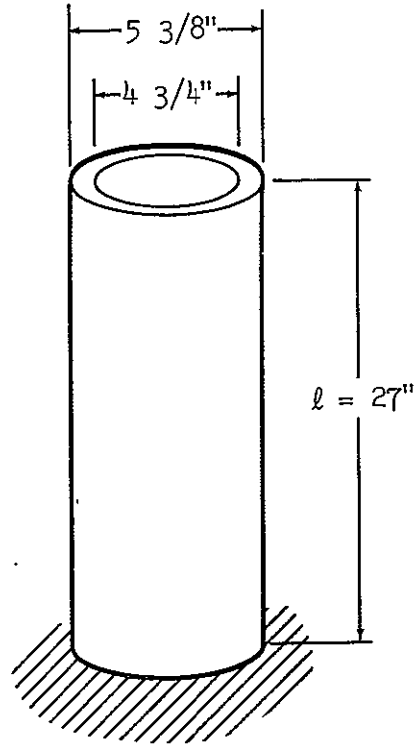
The diametral moment of inertia $I_x = \dfrac{\pi(d_o^4 - d_i^4)}{64}$

$= \dfrac{\pi}{64}(5.375^4 - 4.75^4)$ $I_x = 16\ in^4$ Material: steel $E = 30 \times 10^6$ psi

The change in slope due to a unit bending moment at the top of the shaft, relative to its cantilever end is

$$\frac{d\theta}{dM} = \frac{\ell}{EI} = \frac{27}{30 \times 10^6 \times 16} = .562 \times 10^{-7}\ rad/in.\ lb$$

The value of k to be used must be smaller than that due to the shaft since the analysis is performed for a single blade, but bearing in mind that other blades are also bending at the same time (in phase with the single blade being analyzed). Inspection of the pitch or roll modes shows that the other blades act so as to cause 50 percent greater deflection of the shaft than that supplied by the blade under consideration. The effective k to use for a single blade then becomes

$$\frac{1}{k_\theta} = 1.5 \ \frac{d\theta}{dM} = 1.5 \times .562 \times 10^{-7} = 0.84 \times 10^{-7} \ rad/in. \ lb$$

The next step is to evaluate the data for the blade:

$$m_1, \ m_2, \ (EI)_1, \ (EI)_2, \ r_1, \ r_2$$

and to find the modal frequencies for shapes at some selected range of rotor speeds (rpm).

$$m_1 \quad = \frac{86}{386} = .223 \ \frac{slugs}{12}$$

$$m_2 \quad = \frac{34}{386} = .088 \ \frac{slugs}{12}$$

$$r_1 \quad = 50 \ in.$$

$$r_2 \quad = 160 \ in.$$

$$(EI)_1 = .6 \times 10^8 \ lb \ in.^2$$

$$(EI)_2 = .2 \times 10^8 \ lb \ in.^2$$

$\left. \right\}$ Reference Figure B-1

255
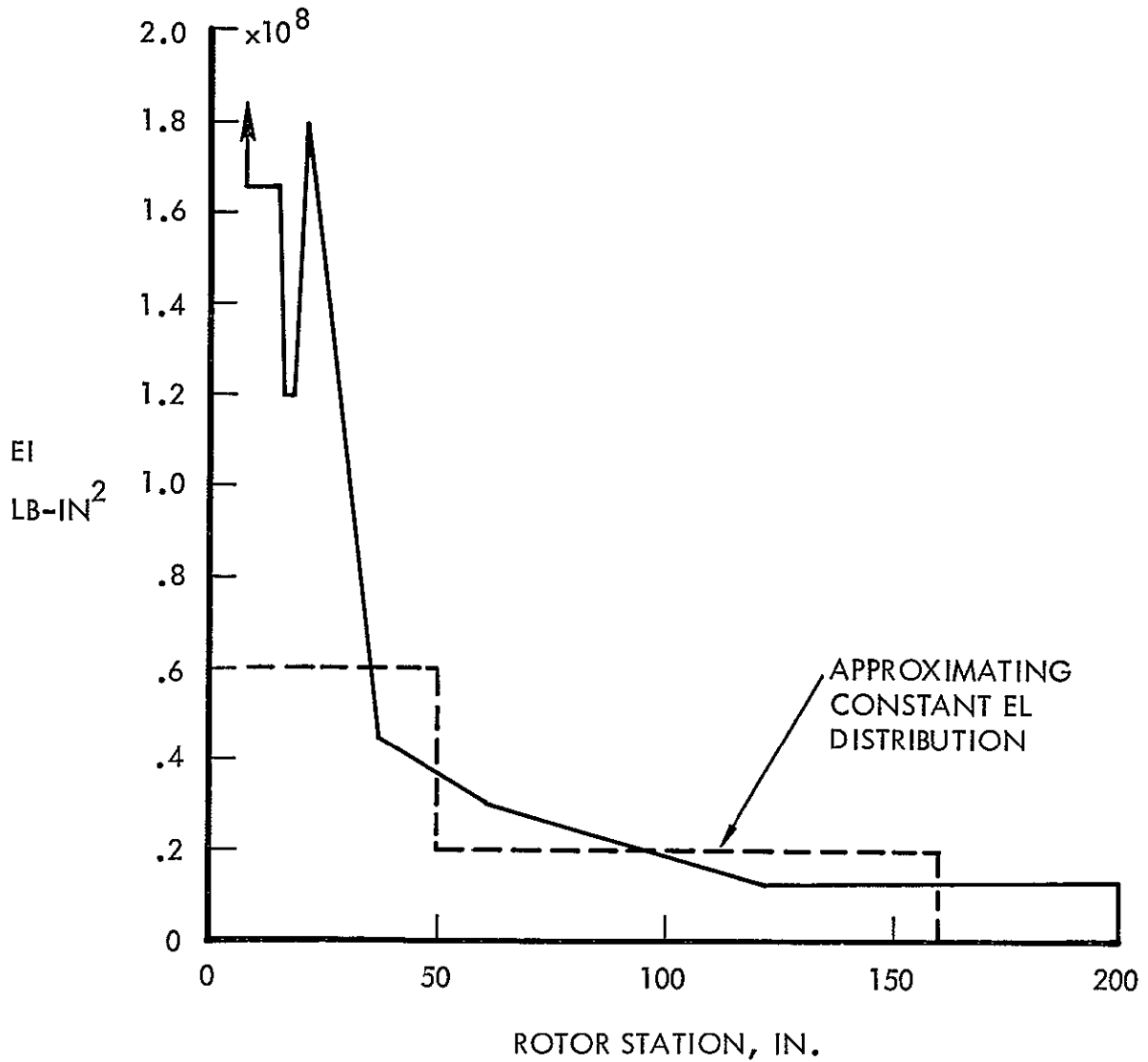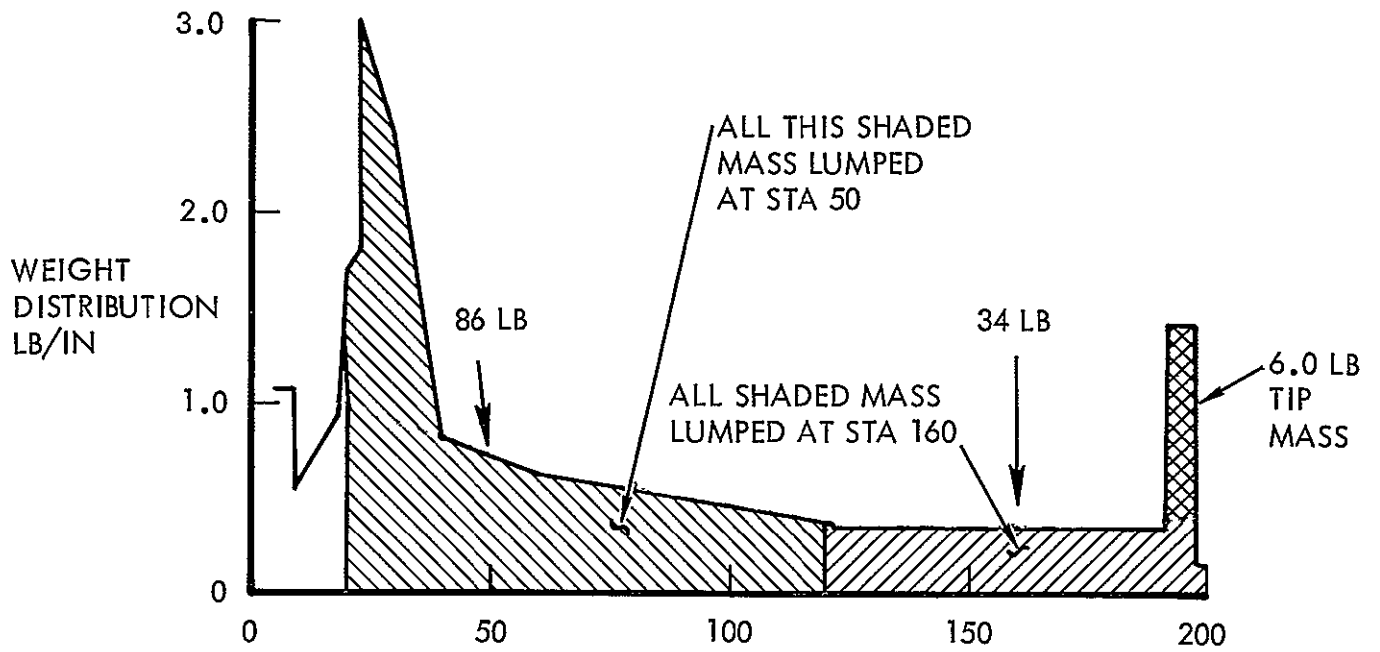
Figure B-1. Blade Mass And Stiffness Distributions

256

The structural influence matrix

$$\begin{Bmatrix} \delta_{s_1} \\ \delta_{s_2} \end{Bmatrix} = \begin{bmatrix} S \end{bmatrix} \begin{Bmatrix} P_1 \\ P_2 \end{Bmatrix}$$

$$\begin{bmatrix} S \end{bmatrix} = \begin{bmatrix} .695 & 2.99 \\ 2.99 & 37.57 \end{bmatrix} \times 10^{-3} \text{ in. per lb}$$

Substituting in equation (2) the resonant frequencies and mode shapes are found, for a rotor speed range varying from 0 to 355 rpm ($0 < \Omega < 37.1$ rad/sec):

$$\left| \begin{bmatrix} .7 & 3.0 \\ 3.0 & 37.6 \end{bmatrix} \times 10^{-3} + .84 \times 10^{-7} \begin{bmatrix} (50)^2 & (50)(160) \\ (50)(160) & (160)^2 \end{bmatrix}^{-1} \right.$$

$$-\Omega^2 \frac{160}{110} (.088) \begin{bmatrix} -1 & 1 \\ 1 & -1 \end{bmatrix} - \begin{bmatrix} .223 + \frac{160}{50}(.088) & 0 \\ 0 & 0 \end{bmatrix}$$

$$\left. -\omega^2 \begin{bmatrix} .223 & 0 \\ 0 & .088 \end{bmatrix} \right| = 0$$

which becomes

$$\left| \begin{bmatrix} .91 & 3.71 \\ 3.71 & 39.75 \end{bmatrix}^{-1} 10^3 \quad -\Omega^2 \begin{bmatrix} -.633 & .128 \\ .128 & -.128 \end{bmatrix} -\omega^2 \begin{bmatrix} .223 & 0 \\ 0 & .088 \end{bmatrix} \right| = 0$$

Inverting the 2 x 2 matrix gives,

$$\left| \begin{bmatrix} 1.78 & -.166 \\ -.166 & .0406 \end{bmatrix} 10^3 \quad -\Omega^2 \begin{bmatrix} -.633 & .128 \\ .128 & -.128 \end{bmatrix} - \omega^2 \begin{bmatrix} .223 & 0 \\ 0 & .088 \end{bmatrix} \right| = 0$$

The roots of the above determinantal equation are calculated for

$$\Omega = 0 \text{ rad/sec}, \quad 0\% \text{ max rpm}$$
$$= 7.42, \quad 20$$
$$= 14.85, \quad 40$$
$$= 26.0, \quad 70$$
$$= 37.1, \quad 100$$

for $\Omega = 0$

$$\left| \begin{bmatrix} 1780 & -166 \\ -166 & 40.6 \end{bmatrix} - \omega^2 \begin{bmatrix} .223 & 0 \\ 0 & .088 \end{bmatrix} \right| = 0$$

$$\begin{vmatrix} 1780 - .223\omega^2 & -166 \\ -166 & 40.6 - .088\omega^2 \end{vmatrix} = 0$$

$$.01965\, \omega^4 - 166\, \omega^2 + 44880 = 0$$

The roots of this are given by

$$\omega^2 = \frac{166 \pm \sqrt{(166)^2 - 4(.01965)\, 44800}}{2(.01965)}$$

$$\omega^2 = \begin{array}{ll} 8150; & \omega = 90.4 \text{ rad/sec} \\ 280; & 16.7 \text{ rad/sec} \end{array}$$

and the two natural frequencies are 14.3 cps

2.66 cps

The roots for all the rotational speeds, are found in a similar way are

Ω	f_1	f_2
.0	2.66	14.3
7.42	2.98	14.6
14.85	3.72	15.0
26.00	5.18	16.1
37.10	6.90	17.8

The variation of the calculated natural frequencies with rpm agrees well with those calculated by more comprehensive analytical techniques as shown in Figure B-2.

The objective of the following analysis is to show the contribution of shaft flexibility to the mode shape. Ground vibration tests (and more comprehensive analyses) showed that the 1st flap mode is essentially parabolic at all values of rpm.

Examining equation (1) and substituting values for $\Omega = 0$ gives:

$$\begin{bmatrix} 1780 - .223\,\omega^2 & -166 \\ -166 & 40.6 - .088\,\omega^2 \end{bmatrix} \begin{Bmatrix} \delta_1 \\ \delta_2 \end{Bmatrix} = 0$$

To obtain the mode shape the equations are divided by δ_1;

$$\begin{bmatrix} 1780 - .223\,\omega^2 & -166 \\ -166 & 40.6 - .088\,\omega^2 \end{bmatrix} \begin{Bmatrix} 1 \\ \dfrac{\delta_2}{\delta_1} \end{Bmatrix} = 0$$

to solve for $\dfrac{\delta_2}{\delta_1}$,

$$-166 + (40.6 - .088\,\omega^2)\,\frac{\delta_2}{\delta_1} = 0$$

The mode shape depends on the value of ω^2 root. For the 1st mode, the root $\omega^2 = 280$, therefore,

$$(40.6 - .088\,(280))\,\frac{\delta_2}{\delta_1} = 166 \qquad \frac{\delta_2}{\delta_1} = \frac{166}{16} = 10.4$$

259
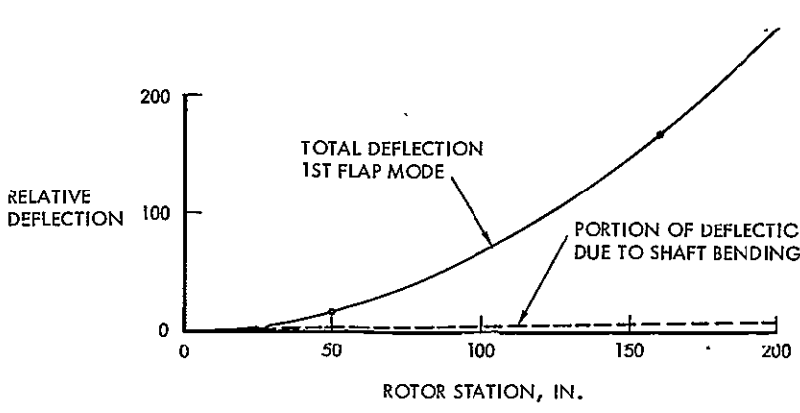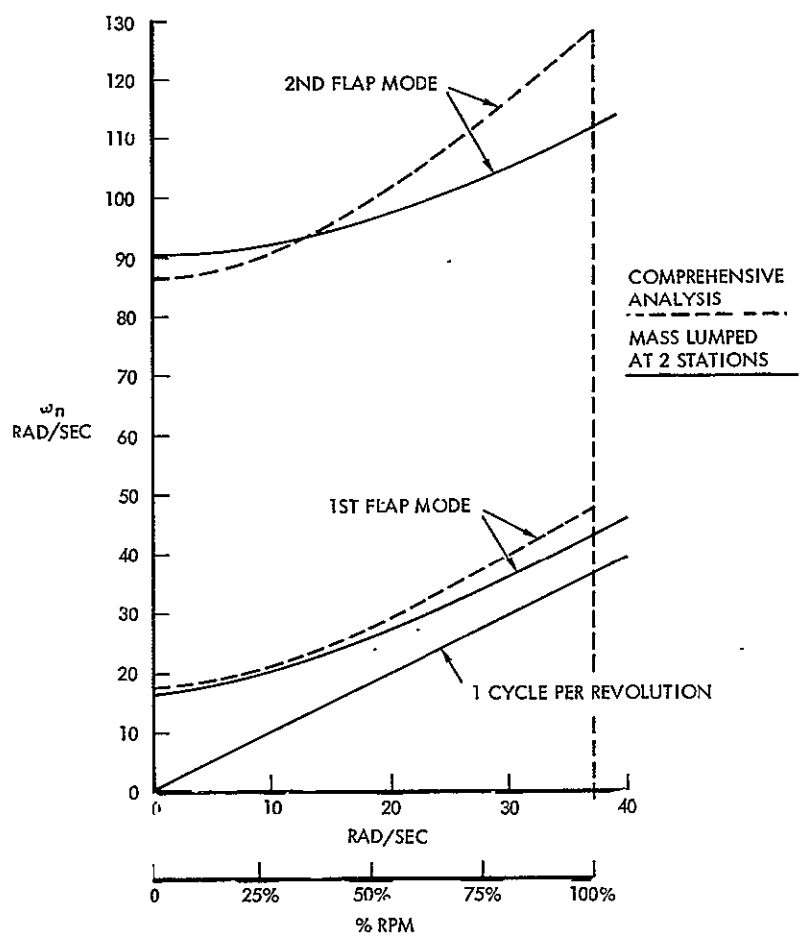
Figure B-2. Blade Vibration Modes and Frequencies

Because of the peak acceleration of point ① or ② (see preceding sketches) is proportional to the displacement, and the force at each point is equal to the mass times the acceleration, the ratio of the forces at the two stations is

$$\frac{F_2}{F_1} = \frac{10.4 \times 34}{1.0 \times 86} = 4.1{:}1.0$$

And the deflections at ① and ② consist of bending deflections and spring displacements

$$\begin{Bmatrix} \delta_1 \\ \delta_2 \end{Bmatrix} = \begin{Bmatrix} \delta_{S_1} \\ \delta_{S_2} \end{Bmatrix} + \begin{Bmatrix} \delta_{\theta_1} \\ \delta_{\theta_2} \end{Bmatrix} = [s] \begin{Bmatrix} F_1 \\ F_2 \end{Bmatrix} + \frac{1}{K} \begin{bmatrix} r_1^2 & r_1 r_2 \\ r_1 r_2 & r_2^2 \end{bmatrix} \begin{Bmatrix} F_1 \\ F_2 \end{Bmatrix}$$

$$\begin{Bmatrix} \delta_1 \\ \delta_2 \end{Bmatrix} = 10^{-3} \begin{bmatrix} .7 & 3.0 \\ 3.0 & 37.6 \end{bmatrix} \begin{Bmatrix} F_1 \\ F_2 \end{Bmatrix} + 10^{-3} \begin{bmatrix} .21 & .71 \\ .71 & 2.15 \end{bmatrix} \begin{Bmatrix} F_1 \\ F_2 \end{Bmatrix}$$

$$\underbrace{\hphantom{XXXXXXXXXXX}}_{\text{bending deflection}} \qquad \underbrace{\hphantom{XXXXXXXXXXX}}_{\text{spring deflection}}$$

Assuming $F_2 = 4,100$ lb, $F_1 = 1,000$ lb for the 1st mode

$$\begin{Bmatrix} \delta_1 \\ \delta_2 \end{Bmatrix} = \begin{bmatrix} .7 + 3.0\ (4.1) \\ 3.0 + 37.6\ (4.1) \end{bmatrix} + \begin{bmatrix} .21 + .71\ (4.1) \\ .71 + 2.15\ (4.1) \end{bmatrix}$$

$$\begin{Bmatrix} \delta_1 \\ \delta_2 \end{Bmatrix} = \underbrace{\begin{Bmatrix} 13 \\ 157 \end{Bmatrix}}_{\text{bending}} + \underbrace{\begin{Bmatrix} 3.1 \\ 9.5 \end{Bmatrix}}_{\text{spring}} = \begin{Bmatrix} 16.1 \\ 166.5 \end{Bmatrix}$$

It is seen in Figure B-2, that the contribution to blade flapping deflection at the outboard mass-lump location to shaft bending is only 5.7 percent of the total deflection. In the rest of the analyses this small shaft bending deflection is neglected.

EFFECTS OF SWASHPLATE AND GYROSCOPE PARAMETERS
ON FIXED-SHAFT STABILITY

The five degree-of-freedom equations which relate swashplate cyclic
feathering to the three rotor degrees of freedom in blade first flapping are
shown on the following page. The effects of rotating damping (primarily
feathering friction), swashplate stationary-axis damping, swashplate spring,
gyroscope diametral moment of inertia, and rotor speed (rpm) on the stability
of the gyroscope precessive mode are shown. Stability is expressed in terms
of the damped (or undamped) natural frequency of the system, and the time for
transient motions to subside to one-half amplitude.

The five degree-of-freedom equations were abstracted from the eight
degree-of-freedom equations derived in Appendix A. In this appendix the
gyroscope's diametral moment of inertia and rpm and the generalized masses
and cross products of inertia have been left in explicit form so that their
effects may be more readily seen.

Effects of Rotating (Feathering) Damping and Swashplate Damping

When the gyroscope's motion is not restrained by springs, the gyro pre-
cessive mode is referred to as the control mode, since it is the dominant one
excited by control moment inputs, and since the system's steady state hub
moment response remains of fairly constant (azimuth and amplitude) as the
rotor rpm changes.

The control mode maintains its advancing precessive character at the
higher rotor speeds as the values of feathering and swashplate damping change
over the modest ranges shown in Figure C-1. The figure shows the effect of
rotating damping on the damped natural frequency and the reciprocal of the
time to half amplitude. C_R and C_S have little effect on the natural frequency
of the mode, especially at low rpm. C_R tends to slightly increase, and C_S
to slightly decrease, the frequency at the higher rpm.

C_R acts strongly to increase the stability of the control mode at high
rotor rpm where it is an advancing precession but at the low rpm feathering

$$[\text{I}]$$

$$
\begin{bmatrix}
I_G + \dfrac{I_R}{k^2} & 0 & 0 & M_{\theta\delta\theta} & 0 \\
0 & I_G + \dfrac{I_R}{k^2} & 0 & 0 & M_{\phi\delta\phi} \\
0 & 0 & M_{\delta_0\delta_0} & 0 & 0 \\
M_{\delta\theta} & 0 & 0 & M_{\delta\theta\delta\theta} & 0 \\
0 & M_{\delta\phi\phi} & 0 & 0 & M_{\delta\phi\delta\phi}
\end{bmatrix}
\begin{bmatrix}
\ddot{\theta} \\ \ddot{\phi} \\ \ddot{\delta}_0 \\ \ddot{\delta}_\theta \\ \ddot{\delta}_\phi
\end{bmatrix}
+
$$

MASS MATRIX

$$[\text{D}]$$

$$
\begin{bmatrix}
C_R + C_S & -2I_G\Omega_G - 2I_R\Omega/k^2 & 0 & 0 & -2\Omega M_{\theta\delta\theta} \\
2I_G\Omega_G + 2I_R\Omega/k^2 & C_R + C_S & 0 & 2\Omega M_{\phi\delta\phi} & 0 \\
0 & 0 & 2\gamma_{\delta_0}\omega_{\delta_0}M_{\delta_0\delta_0} & 0 & 0 \\
0 & -2\Omega M_{\delta\phi} & 0 & 2\gamma_{\delta_\theta}\omega_{\delta_\theta}M_{\delta_\theta\delta_\theta} & -2\Omega M_{\delta_\theta\delta\theta} \\
2\Omega M_{\delta\phi} & 0 & 0 & 2\Omega M_{\delta_\phi\delta_\phi} & 2\gamma_{\delta_\phi}\omega_{\delta_\phi}M_{\delta_\phi\delta\phi}
\end{bmatrix}
\begin{bmatrix}
\dot{\theta} \\ \dot{\phi} \\ \dot{\delta}_0 \\ \dot{\delta}_\theta \\ \dot{\delta}_\phi
\end{bmatrix}
$$

MECHANICAL DAMPING AND GYROSCOPIC MATRIX

$$[\text{S}]$$

$$
\begin{bmatrix}
K_S & -\Omega C_R & 0 & 0 & 0 \\
+\Omega C_R & K_S & 0 & 0 & 0 \\
0 & 0 & M_{\delta_0\delta_0}\omega_{\delta_0}^2 & 0 & 0 \\
0 & 0 & 0 & M_{\delta_\theta\delta_\theta}(\omega_{\delta_0}^2 - \Omega^2) & -2\Omega\gamma_{\delta_\theta}\omega_{\delta_\theta}M_{\delta_\theta\delta\theta} \\
0 & 0 & 0 & 2\Omega\gamma_{\delta_\phi}\omega_{\delta_\phi}M_{\delta_\phi\delta\phi} & M_{\delta_\phi\delta_\phi}(\omega_{\delta_\phi}^2 - \Omega^2)
\end{bmatrix}
\begin{bmatrix}
\theta \\ \phi \\ \delta_0 \\ \delta_\theta \\ \delta_\phi
\end{bmatrix}
-
$$

MECHANICAL STIFFNESS MATRIX

$$[\text{B}_r]$$

$$
\begin{bmatrix}
H_{\theta\dot\theta} & H_{\theta\dot\phi} & H_{\theta\dot\delta_0} & H_{\theta\dot\delta_\theta} & H_{\theta\dot\delta_\phi} \\
H_{\phi\dot\theta} & H_{\phi\dot\phi} & H_{\phi\dot\delta_0} & H_{\phi\dot\delta_\theta} & H_{\phi\dot\delta_\phi} \\
H_{\delta_0\dot\theta} & H_{\delta_0\dot\phi} & H_{\delta_0\dot\delta_0} & H_{\delta_0\dot\delta_\theta} & H_{\delta_0\dot\delta_\phi} \\
H_{\delta_\theta\dot\theta} & H_{\delta_\theta\dot\phi} & H_{\delta_\theta\dot\delta_0} & H_{\delta_\theta\dot\delta_\theta} & H_{\delta_\theta\dot\delta_\phi} \\
H_{\delta_\phi\dot\theta} & H_{\delta_\phi\dot\phi} & H_{\delta_\phi\dot\delta_0} & H_{\delta_\phi\dot\delta_\theta} & H_{\delta_\phi\dot\delta_\phi}
\end{bmatrix}
\begin{bmatrix}
\dot{\theta} \\ \dot{\phi} \\ \dot{\delta}_0 \\ \dot{\delta}_\theta \\ \dot{\delta}_\phi
\end{bmatrix}
-
$$

AERO DAMPING

$$[\text{B}]$$

$$
\begin{bmatrix}
H_{\theta\theta} & H_{\theta\phi} & H_{\theta\delta_0} & H_{\theta\delta_\theta} & H_{\theta\delta_\phi} \\
H_{\phi\theta} & H_{\phi\phi} & H_{\phi\delta_0} & H_{\phi\delta_\theta} & H_{\phi\delta_\phi} \\
H_{\delta_0\theta} & H_{\delta_0\phi} & H_{\delta_0\delta_0} & H_{\delta_0\delta_\theta} & H_{\delta_0\delta_\phi} \\
H_{\delta_\theta\theta} & H_{\delta_\theta\phi} & H_{\delta_\theta\delta_0} & H_{\delta_\theta\delta_\theta} & H_{\delta_\theta\delta_\phi} \\
H_{\delta_\phi\theta} & H_{\delta_\phi\phi} & H_{\delta_\phi\delta_0} & H_{\delta_\phi\delta_\theta} & H_{\delta_\phi\delta_\phi}
\end{bmatrix}
\begin{bmatrix}
\theta \\ \phi \\ \delta_0 \\ \delta_\theta \\ \delta_\phi
\end{bmatrix}
=
\begin{bmatrix}
0 \\ 0 \\ 0 \\ 0 \\ 0
\end{bmatrix}
$$

AERO STIFFNESS

265
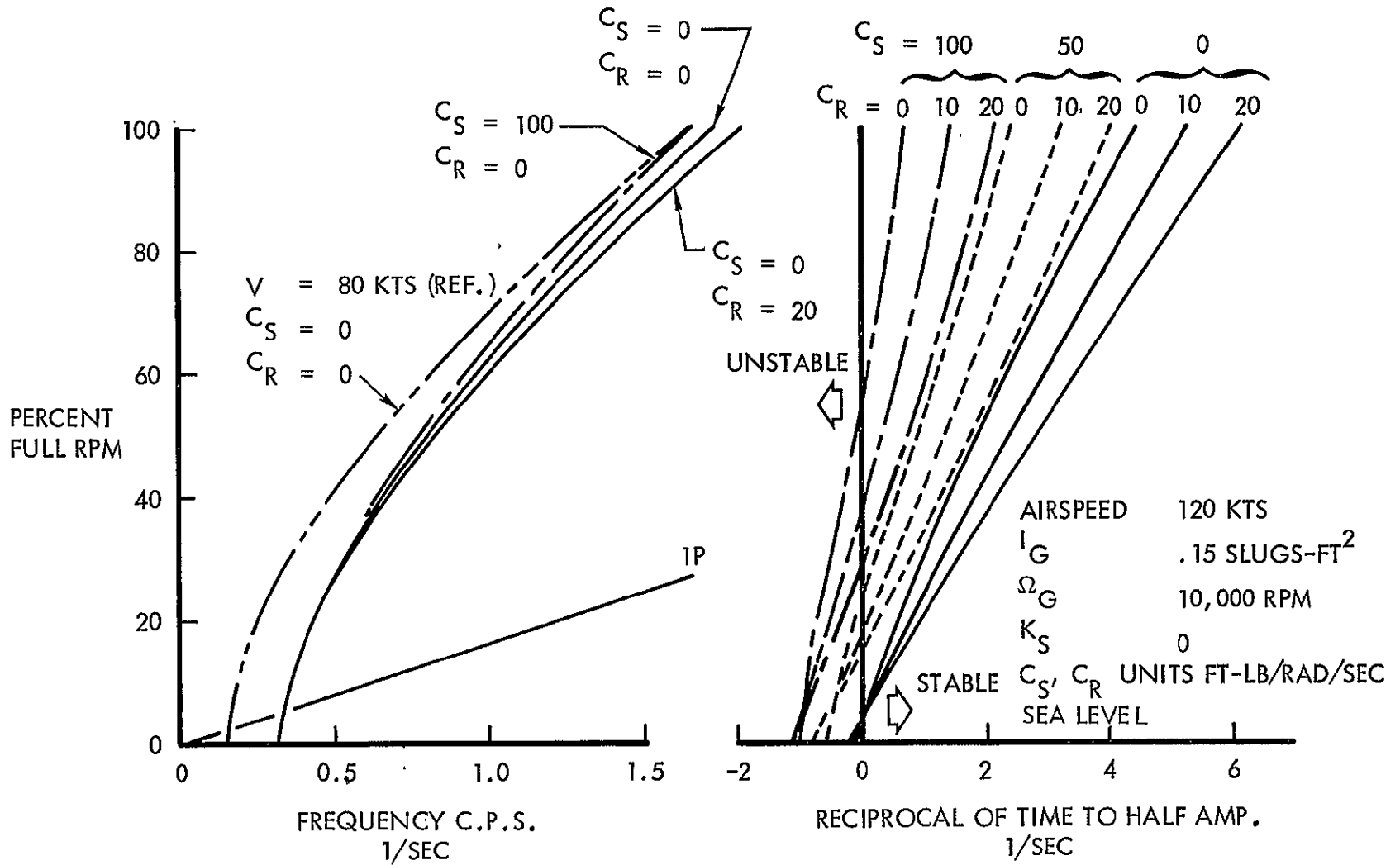
Figure C-1. Fixed-Shaft, Free-Gyro Stability - Effect Of Swashplate Damping And Feathering Damping

divergence stability boundary, with zero swashplate damping, the frequency is close to the rotor rotation rate so that no cyclic feathering takes place and the feathering dampers have no effect. Rotating damping does not effect the feathering divergence instability boundary when $C_S = 0$.

As swashplate damping C_S is increased, while $C_R = 0$, the stability of the advancing precessive mode is reduced and the low rpm stability boundary gradually rises, thus increasing the unstable region. Rotating damping tends to counteract the effect of the swashplate damping; therefore adding rotating damping moves the instability boundary to a lower rotor speed and increases stability at all higher rotor speeds.

The reason for the advancing precessive character of the control mode, and the effects of feathering and swashplate damping on the mode are discussed in physical terms. In the rotor-gyroscope system, the cyclic pitch angles of the blades are geared directly to the gyro tilt, and the gyro tilt plane remains parallel to the swashplate plane. As far as the precessive mode is concerned, the gyroscope and blade feathering inertia act together like a single gyroscope. If no dampers or aerodynamics act on the system, it has a natural frequency of zero (1P in the rotating axes) and is undamped, or neutrally stable. That is, if the gyro were tilted it would maintain its tilted position. In rotating axes the blades would feather nose-up, then nose-down, once per revolution, ad infinitum.

If weak diverging feathering aerodynamic moments are added to such a system, so as to produce a negative spring effect, which when combined with blade feathering centrifugal moments reduces restoring moments (viewed in rotating coordinates), the frequency would reduce below 1P. The period of each control mode oscillation is longer than that of one rotor revolution, and its peak amplitude precesses to a position slightly ahead of its last position, that is, it advances in the direction of rotation. If the feathering diverging moments become strong enough (or the centrifugal moments become weak enough) the frequency in rotating coordinates vanishes and the system statically diverges in feathering. There is no cyclic feathering at this point; therefore, feathering damping cannot prevent the divergence.

268

The effect of feathering damping on dynamic stability is stabilizing, as indicated on Figure C-1. This may be better understood by examining the control system in the absence of aerodynamic forces, and relative to axes rotating with the rotor. From this viewpoint, the blades and gyroscope oscillate at 1P with the inertia forces balanced by centrifugal forces and, in fact, each axis of the gyroscope may be examined independently, as a single degree-of-freedom system. The equation is the same as for a spring-mass system. The introduction of feathering damping, therefore, causes the 1P oscillation to gradually diminish to zero. Viewed in the stationary axes the swashplate attains a level position.

Swashplate damping (stationary axis damping) acts on the precessing gyroscope. Precession-induced damper moments cause the gyroscope to precess about an axis lagged 90 degrees behind the damper axis. If the driving precession is regressive, the damper-induced precession diminishes the driving precession and stabilizes the motions as shown in Figure C-2. If, on the other hand, the driving precession is advancing, the damper-induced precession augments it and destabilizes the motion.

The effects of C_R and C_S on control mode stability at speeds lower than 120 knots (those shown on Figure C-1) are qualitatively the same. The main effect of reducing the forward speed is a reduction in precessive mode frequency. This is illustrated by the reference curve (for 80 knots) shown on the figure.

Effects of Gyroscope Inertia and Rotor Speed

The equations summarized in this appendix show that gyro speed Ω_G is in the equations only in a product with gyro diametral moment of inertia I_G. Where I_G exists without Ω_G its effect is rendered insignificant by being combined with the much larger rotor feathering inertia term. It would be expected, therefore, that stability would vary according to $\Omega_G I_G$ and this, in fact, was shown to be the case in tests. Control mode stability was checked by varying first I_G and then Ω_G. The effects were the same. Figure C-3 shows the effect of doubling and halving $\Omega_G I_G$.

NOTE:
ONE DAMPER SHOWN FOR CLARITY-
DAMPERS ARRANGED FOR POLAR SYMMETRY

GYRO ROTATION

DAMPER INDUCED
TILT VELOCITY

DAMPER INDUCED
TILT VELOCITY

REGRESSIVE
PRECESSION

ADVANCING
PRECESSION

DAMPER FORCE
DUE TO PRECESSIVE
MOTION

REGRESSIVE PRECESSION
STABILIZING

ADVANCING PRECESSION
DESTABILIZING
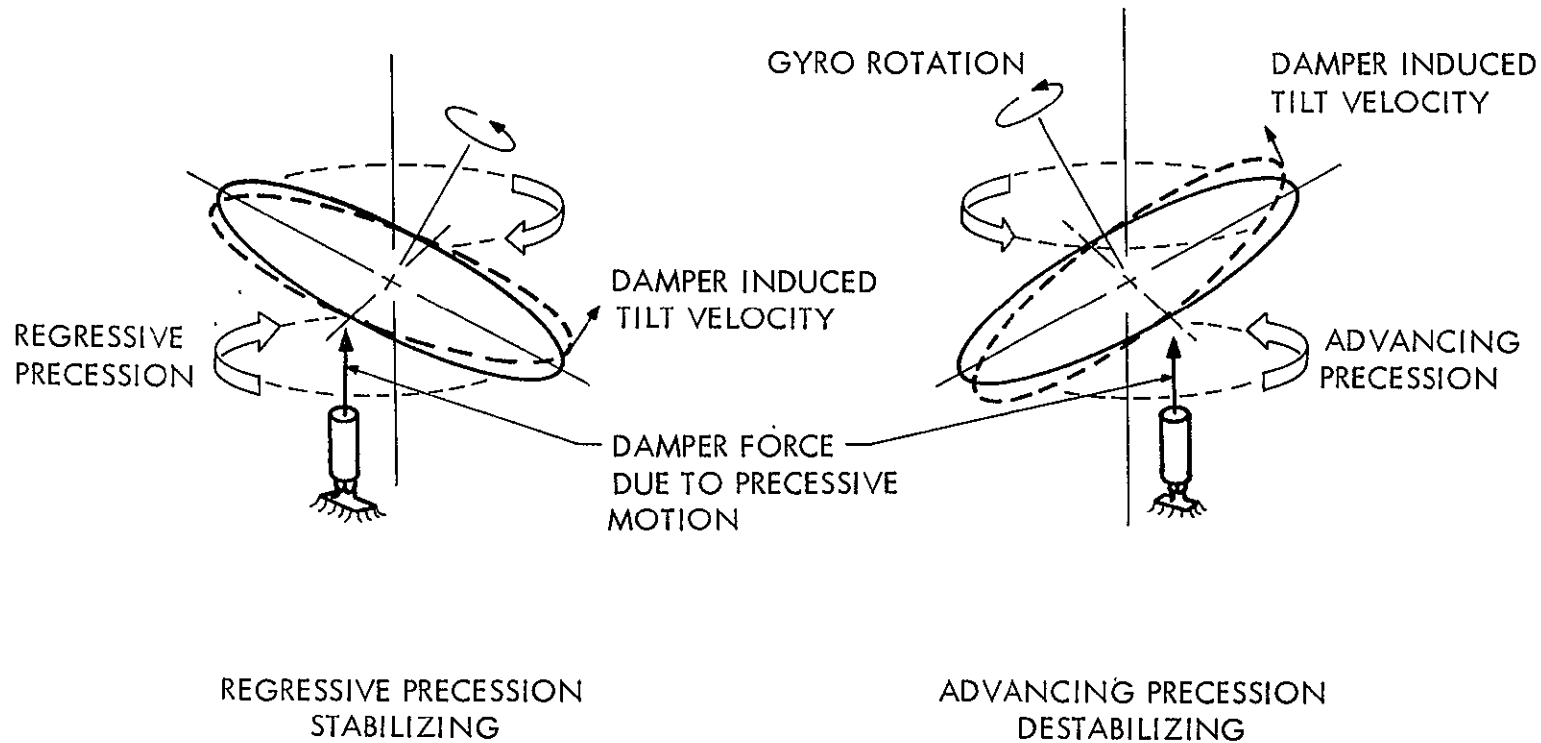
Figure C-2. Swashplate Damping Effect on Stability
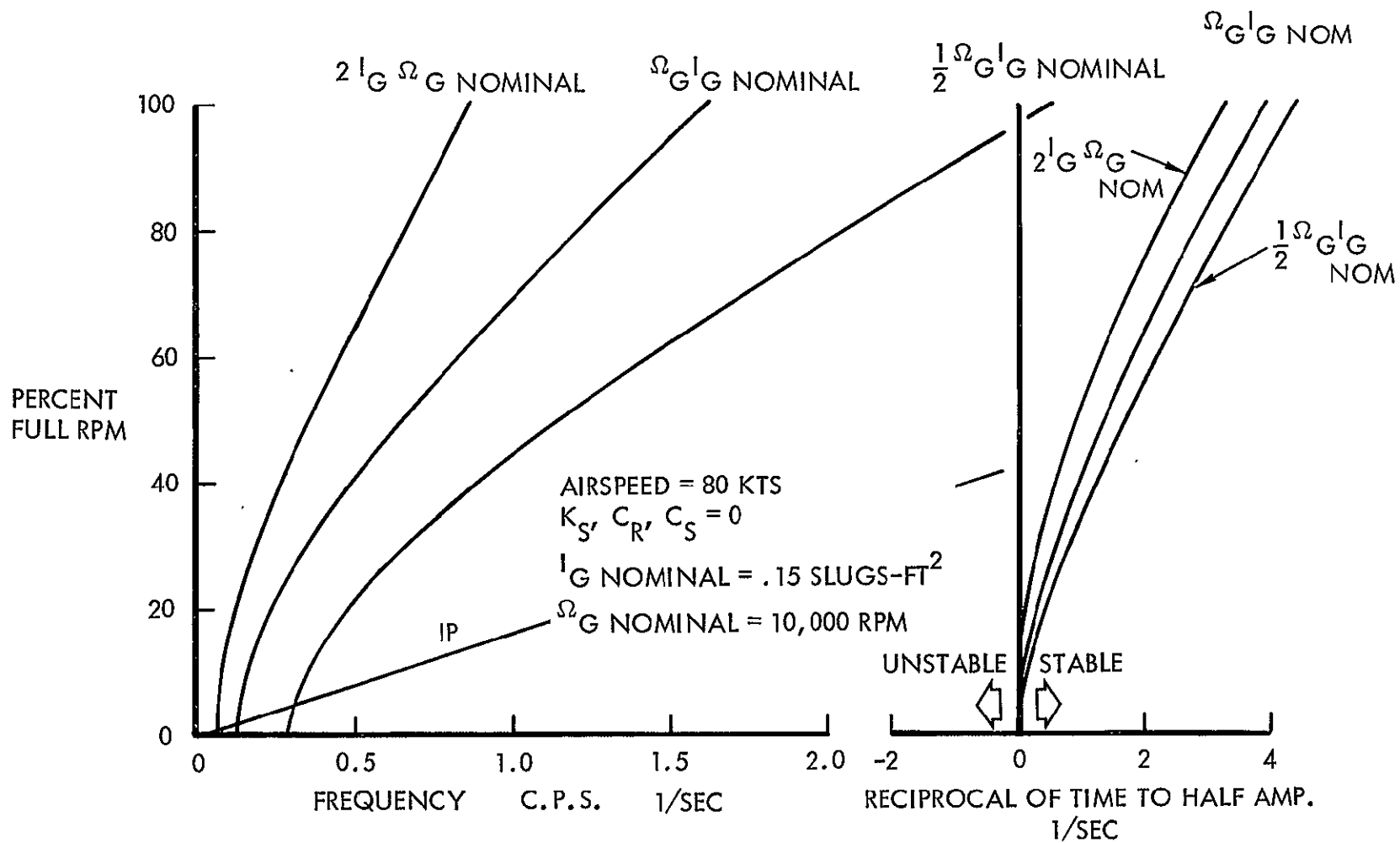
Figure C-3. Fixed-Shaft, Free-Gyro Stability - Effect Of Gyroscope RPM

271

The control mode natural frequency is affected almost inversely propor-
tioned to $\Omega_G I_G$. The time to half amplitude is only slightly affected. Increas-
ing $\Omega_G I_G$ increases the time to half amplitude slightly. Increasing the $\Omega_G I_G$
tends to reduce the rpm of feathering divergence.

The requirements of stability and handling qualities oppose each other.
A large gyroscope reduces the feathering divergence boundary but also reduces
the response time of the system tending to make handling sluggish. The
smallest tolerable stability would give the best system response.

Effects of Swashplate Springs

Figure C-4 illustrates the effect of swashplate springs, K_S, on the gyro-
scope precessive mode stability. With no springs employed, the mode is a
stable advancing precession down to the feathering divergence boundary at
very low rotor speed.

When the swashplate is restrained by springs, the natural frequency and
time to half amplitude decrease and the mode retains its advancing precessive
character at high rpm. As the rotor speed is reduced, the natural frequency
rapidly reduces to zero; and as it is reduced further, the mode becomes
regressive and its frequency increases to a finite value at zero rpm. The
mode remains stable to zero rpm and the feathering divergence vanishes.

It is interesting to note that in the vicinity of the vanishing natural
frequency (in stationary axes) the mode degenerates into two real, stable roots,
and the damped natural frequency remains zero over a small range of rotor
speeds, whereas the undamped natural frequency merely passes through the zero
frequency point.

Effect of Swashplate Damping on the Stability of the
Spring-Restrained Swashplate

Figure C-5 shows the effect of increasing swashplate damping on the
stability of the precessive mode of the spring-restrained gyro. Swashplate
damping causes an increase to the high rpm advancing precessive mode natural
frequency and a reduction in stability. It causes a decrease in the regressive

272
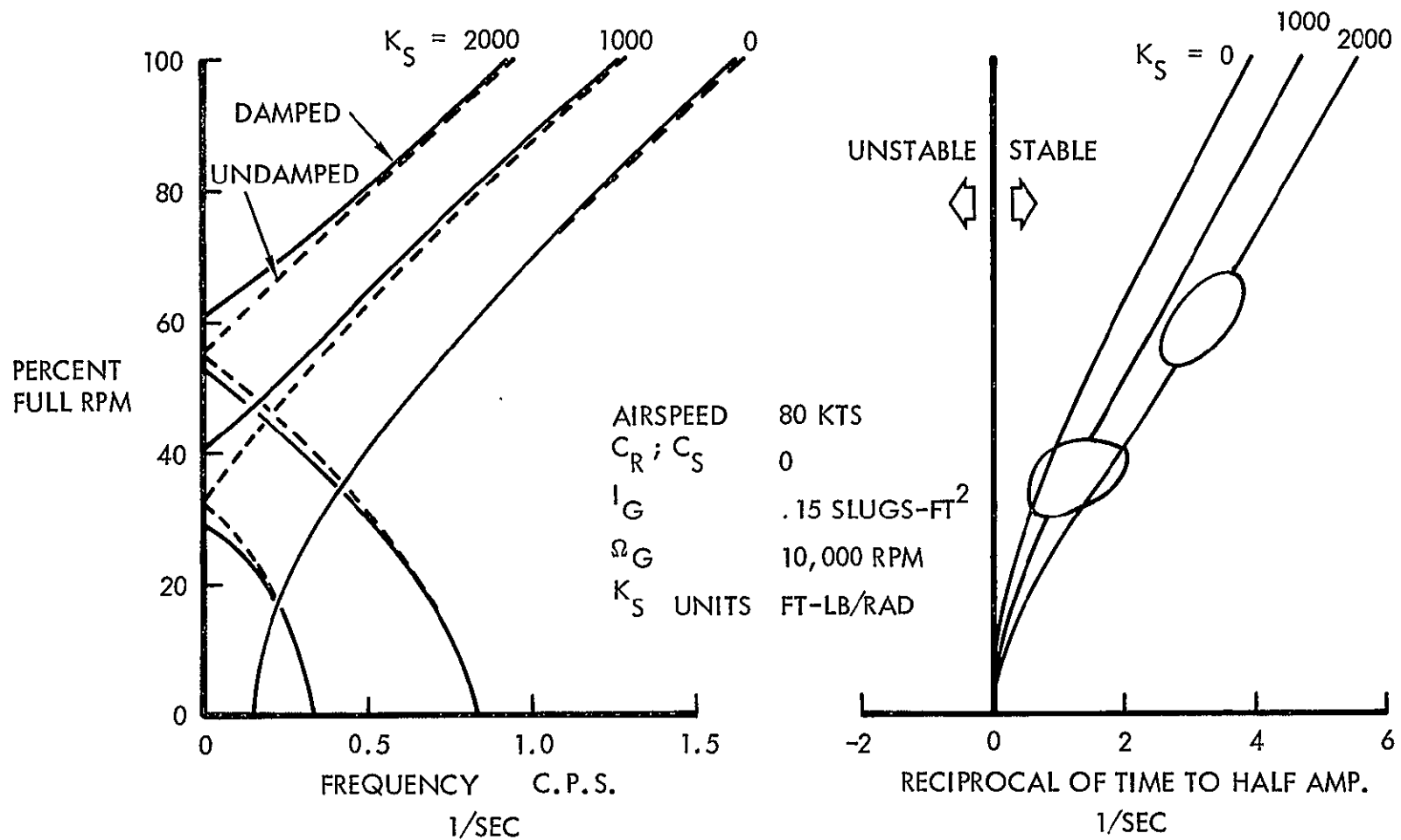
Figure C-4. Fixed-Shaft Stability - Effect Of Swashplate Springs
On The Gyroscope Precessive Mode
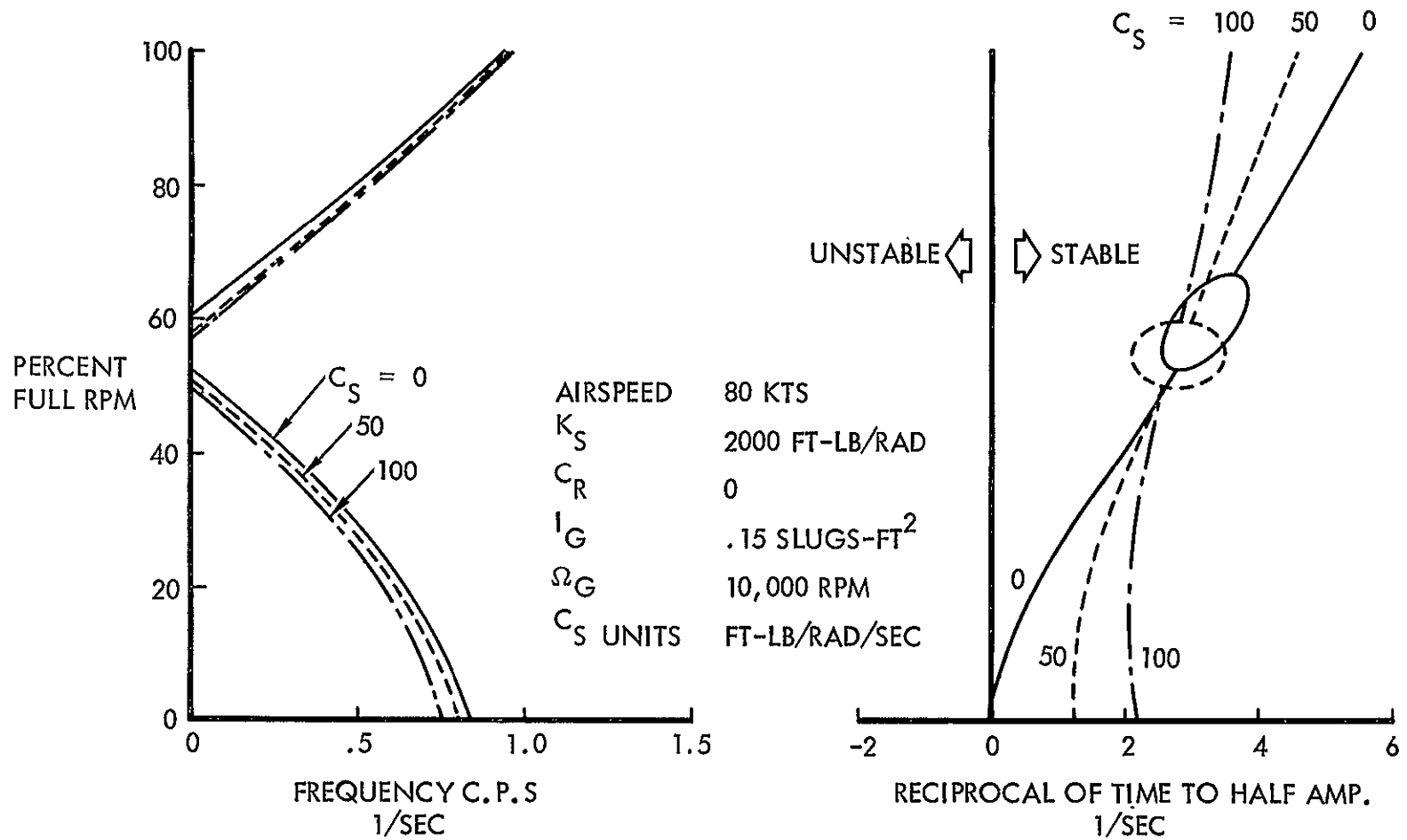
Figure C-5. Fixed-Shaft Stability - Effect Of Swashplate Damping On The
Gyroscope Precessive Mode, With The Swashplate Spring Restrained

precessive mode frequency and stability at low rotor speeds. The effects on frequency are small, but the effects on stability are large. The effect of C_S on stability depends on the advancing or regressing character of the mode as shown in Figure C-2.

APPENDIX D

REDUCED EXPERIMENTAL DATA

Computer printouts of the reduced test data are shown on the following pages. The methods of data reduction employed are those discussed previously in the section entitled Wind Tunnel Tests. The lift data shown here were not used in the plots of the lift derivatives; wind tunnel balance data was used instead.

The following data are shown:

1. Dimensional derivatives.

2. Data samplings and their deviations from least-squares-planes of best fit.

3. Hub or swashplate trimmed angles and moments.

4. Control moments.

5. Nondimensionalized derivatives; these are grouped according to forward speed.

Two tabular forms are employed. The first: (pages 278-306) presents the mean data recorded for various values of cyclic pitch θ_{1c}, θ_{1s} (and corresponding swashplate tilt θ and ϕ) for a collective angle $\theta_{.75R} = 1.50$ and $\alpha = 0$ for nominal forward speed ranging from 50 to 120 KTS at approximately sea level density. The second tabular form (pages 307-310) presents nondimensionalized derivatives corresponding to the cases shown in the first tabular presentation.

In the first form, there are four tables:

1. ROTOR AND SWASHPLATE DERIVATIVES DUE TO CYCLIC ANGLE. These are rates of change of LIFT, hub roll moment (L_h), hub pitch moment (M_h), swashplate roll moment (L_{sp}), and swashplate pitch moment (M_{sp}) with respect to unit changes in cyclic pitch θ_{1c} (TC), θ_{1s}(TS), and corresponding swashplate tilt angles θ(TH) and ϕ(PHI), all angles expressed in degrees. The first row (RW1) consists of values of the forces (1b) and moments (in-1b) occurring at zero cyclic pitch

The second (RW2), third (RW3) etc. rows contain the rates of change of the forces and moments with respect to angles in degrees.

2. The main table consists of the complete set of mean data from which the above derivatives were obtained by a least-squares fit of a plane. The first four columns contain the cyclic pitch θ_{1c}(T1C), θ_{1s}(T1S) and corresponding swashplate tilt θ(THT), ϕ(PHI) in degrees that were actually held during each of the test runs. The following columns contain the mean values of forces and moments experimentally measured, LIFT, hub roll moment (L_h) in-lb, hub pitch moment (M_h) in.-lb, etc. The deviations of the measured forces from the best fit plane through the data $D(LIFT)$, $D(L_h)$, $D(L_{sp})$ etc. are also shown. These deviations allow an appreciation of the scatter in the test data, and more important an appraisal of the applicability of the linear approximation to be made. The rms value of the deviations, SIGMA is also shown.

3. The third table HUB OR SWASHPLATE TRIMMED ANGLES AND MOMENTS presents the θ_{1c}, θ_{1s} (and θ and ϕ) for hub moment trim $L_h = M_h = 0$. Residual swashplate and hub moments are also shown.

4. The fourth table, CONTROL MOMENTS, presents the control effectiveness data. The hub roll and pitch moments for zero swashplate moments (in in-lb), L_h, M_h $(L_{sp} = M_{sp} = 0)$, and the rate of change of hub roll and pitch moments with respect to unit swashplate moment are given.

$$\frac{d\ (L_h,\ M_h)}{d\ (L_{sp},\ M_{sp})}$$

TABLE III. REDUCED EXPERIMENTAL DATA, NOMINAL VELOCITY = 50 KNOTS

ROTOR AND SWASHPLATE DERIVATIVES DUE TO CYCLIC ANGLES

RW1:d(0)	RW2:d(TC)	PW3:d(TS)	RW4:d(TH)	RW5:d(PH)
d(LIFT)	d(Lh)	d(Mh)	d(Lsp)	d(Msp)
138.00	4086.68	15421.03	-80.41	510.69
-10.31	755.93	-5012.99	88.71	-47.66
40.23	4118.31	1671.26	22.45	124.20
34.78	2772.63	3437.85	-21.66	114.32
9.73	2359.62	-3048.42	76.56	18.15

LOCKED GYRO MODE
V = 49.38 kts
q = 7.94 psf
μ = 0.488

"	T1C	T1S	THT	PHI	LIFT	D(LIFT)	Lh	D(Lh)	Mh	D(Mh)	Lsp	D(Lsp)	Msp	D(Msp)
1	1.750	-.652	-1.661	1.377	95.	1.	1810.	-920.	4686.	-827.	92.	31.	281.	-65.
2	.382	.051	-.169	.410	145.	9.	4284.	-301.	13418.	-172.	-42.	3.	500.	1.
3	1.507	-.734	-1.597	1.079	105.	12.	2900.	696.	6264.	-376.	42.	5.	367.	19.
4	2.317	-1.190	-2.518	1.624	70.	4.	8.	-930.	1155.	-660.	84.	-14.	230.	-22.
5	2.918	-1.716	-3.387	1.920	45.	6.	-450.	324.	-1940.	135.	148.	8.	174.	16.
6	1.665	-.808	-1.762	1.194	85.	-3.	1182.	-837.	4761.	-964.	42.	-7.	343.	12.
7	1.177	-1.801	-2.471	.137	70.	17.	-2920.	-479.	6761.	252.	0.	16.	220.	-11.
8	.597	-2.336	-2.669	-.749	45.	7.	-4132.	949.	9501.	975.	-113.	-33.	211.	19.
9	1.708	-.693	-1.672	1.303	11.	-82.	2984.	459.	5670.	-31.	70.	14.	337.	-6.
10	2.219	.041	-1.235	2.234	130.	13.	6480.	546.	5275.	908.	127.	10.	445.	35.
11	2.616	.701	-.806	3.009	155.	16.	9446.	494.	4238.	760.	134.	-33.	475.	?.
SIGMA						26.		673.		651.		19.		26.

HUB OR SWASHPLATE TRIMMED ANGLES AND MOMENTS

T1C	T1S	THT	PHI	Lh	Mh	Lsp	Msp
2.587	-1.467	-2.949	1.733	0.	0.	116.	205.
1.774	-3.429	-4.435	-.204	-8692.	798.	0.	0.

CONTROL MOMENTS

Lh(Lsp,Msp=0)	dLh/dLsp	dLh/dMsp	Mh(Lsp,Msp=0)	dMh/dLsp	dMh/dMsp
-8585.76	22.69	28.69	1009.19	-41.06	20.15

278

TABLE III. CONTINUED

ROTOR AND SWASHPLATE DERIVATIVES DUE TO CYCLIC ANGLES

RW1:d(0)   RW2:d(TC)   RW3:d(TS)   RW4:d(TH)   RW5:d(PH)

LOCKED GYRO MODE
V = 48.04 kts
q = 7.51 psf
μ = 0.771

d(LIFT)	d(Lh)	d(Mh)	d(Lsp)	d(Msp)
84.00	3582.99	10127.53	-57.51	440.53
-10.05	310.00	-2451.06	54.10	-14.68
26.58	2658.09	911.20	7.55	57.37
24.38	1866.88	1751.78	-17.83	49.58
3.90	1389.01	-1449.58	44.02	13.89

N	T1C	T1S	THT	PHI	LIFT	D(LIFT)	Lh	D(Lh)	Mh	D(Mh)	Lsp	D(Lsp)	Msp	D(Msp)
1	2.276	-1.001	-2.396	1.640	41.	0.	1630.	242.	4045.	401.	120.	63.	343.	-2.
2	1.249	-.401	-1.118	1.013	77.	16.	2269.	-634.	6272.	-428.	63.	56.	380.	-10.
3	-.115	.344	.400	.083	92.	-2.	4331.	-131.	10302.	-421.	-113.	-52.	440.	-22.
4	2.200	-1.208	-2.408	1.496	32.	2.	798.	-256.	3722.	87.	40.	-3.	332.	-7.
5	3.388	-1.841	-3.782	2.316	6.	5.	-81.	180.	607.	403.	84.	-28.	224.	-61.
6	4.210	-2.775	-5.190	2.606	-29.	3.	-3025.	-539.	-3657.	-914.	134.	-16.	223.	4.
7	2.249	-1.364	-2.052	1.456	12.	-13.	467.	-187.	3570.	199.	56.	2.	322.	-7.
8	1.693	-2.007	-2.072	.532	17.	3.	-797.	430.	4037.	-113.	28.	9.	343	42.
9	.708	-3.437	-3.831	-1.271	-23.	-0.	-5201.	133.	5585.	325.	-63.	-18.	240	7.
10	2.670	-.504	-2.037	2.370	37.	-7.	3809.	738.	3243.	110.	90.	16.	414.	42.
11	3.450	.780	-1.207	3.884	62.	-8.	6749.	24.	2575.	192.	106.	-29.	440.	14.
SIGMA						8.		387.		412.		33.		27

HUB OR SWASHPLATE TRIMMED ANGLES AND MOMENTS

T1C	T1S	THT	PHI	Lh	Mh	Lsp	Msp
3.480	-1.754	-3.748	2.458	0.	0.	117.	289.
2.062	-7.152	-8.309	-2.059	-14788.	-1443.	0.	0.

CONTROL MOMENTS

Lh(Lsp,Msp=0)	dLh/dLsp	dLh/dMsp	Mh(Lsp,Msp=0)	dMh/dLsp	dMh/dMsp
-12377.23	11.17	37.86	-1726.48	-31.96	20.78

279

TABLE III. CONCLUDED

ROTOR AND SWASHPLATE DERIVATIVES DUE TO CYCLIC ANGLES

RW1:d(O)   RW2:d(TC)   RW3:d(TS)   RW4:d(TH)   RW5:d(PH)

d(LIFT)	d(Lh)	d(Mh)	d(Lsp)	d(Msp)
51.28	4798.77	9622.07	-21.43	477.52
-9.01	-226.85	-1754.52	19.60	-20.95
23.28	2166.06	896.54	2.06	46.19
21.45	1729.75	1437.88	-6.97	43.89
3.33	770.83	-931.46	15.65	4.31

LOCKED GYRO MODE
V = 50.03 kts
q = 8.14 psf
μ = 1.055

N	T1C	T1S	THT	PHI	LIFT	D(LIFT)	Lh	D(Lh)	Mh	D(Mh)	Lsp	D(Lsp)	Msp	D(Msp)
1	3.297	-2.088	-3.970	2.083	-25.	2.	-703.	-230.	1744.	-220.	42.	3.	201.	-21.
2	2.475	-1.572	-2.989	1.561	-10.	-2.	1488.	656.	4696.	825.	49.	25.	330.	-23.
3	1.162	-.582	-1.248	.822	29.	2.	3006.	-267.	6010.	-151.	14.	14.	380.	-46.
4	3.308	-1.911	-3.806	2.196	-21.	2.	479.	570.	1995.	-110.	35.	-4.	327.	7.
5	3.459	-3.689	-5.664	1.324	-61.	5.	-3607.	370.	292.	47.	70.	31.	292.	57.
6	4.716	-2.126	-4.829	3.475	-51.	-10.	-1454.	-578.	-385.	174.	63.	-4.	219.	-62.
7	5.041	-3.289	-6.174	3.130	-66.	5.	-3335.	134.	-2130.	41.	84.	13.	101.	-59.
8	3.291	-2.052	-3.916	2.109	-16.	10.	-795.	-446.	1515.	-512.	42.	3.	250.	-65.
9	2.734	-2.820	-4.381	1.101	-61.	-22.	-1735.	196.	2210.	-86.	0.	-26.	282.	-8.
10	1.851	-4.198	-5.245	-.570	-61.	2.	-5169.	-455.	2793.	182.	-14.	-20.	204.	40.
11	3.216	-1.984	-3.825	2.062	-16.	8.	-251.	-23.	1920.	-281.	21.	-17.	350.	32.
12	3.882	-1.215	-3.442	3.168	-11.	1.	1484.	197.	1619.	-103.	42.	-10.	419.	79.
13	4.730	.073	-2.653	4.762	9.	-1.	3758.	-123.	1567.	195.	63.	-9.	441.	59.
SIGMA						8.		370.		307.		17.		49.

HUB OR SWASHPLATE TRIMMED ANGLES AND MOMENTS

T1C	T1S	THT	PHI	Lh	Mh	Lsp	Msp
4.598	-1.734	-4.371	3.583	0.	0.	65.	301.
2.081	-9.394	-10.553	-3.329	-16021.	-2451.	0.	0.

CONTROL MOMENTS

Lh(Lsp,Msp=0)	dLh/dLsp	dLh/dMsp	Mh(Lsp,Msp=0)	dMh/dLsp	dMh/dMsp
-10046.54	27.15	27.23	-539.96	-38.66	12.77

TABLE IV. REDUCED EXPERIMENTAL DATA, NOMINAL VELOCITY = 60 KNOTS

ROTOR AND SWASHPLATE DERIVATIVES DUE TO CYCLIC ANGLES

RW1:d(0)   RW2:d(TC)   RW3:d(TS)   RW4:d(TH)   RW5:d(PH)

LOCKED GYRO MODE
V = 60.91 kts
q = 12.18 psf
μ = 0.402

d(LIFT)	d(Lh)	d(Mh)	d(Lsp)	d(Msp)
32.03	7653.98	26892.74	-76.31	496.29
21.88	2884.47	-10307.33	188.74	-69.66
74.30	10368.41	4695.34	65.01	213.35
46.44	6553.82	8016.73	-33.10	190.94
48.78	6679.64	-5720.58	170.39	40.29

N	T1C	T1S	THT	PHI	LIFT	D(LIFT)	Lh	D(Lh)	Mh	D(Mh)	Lsp	D(Lsp)	Msp	D(Msp)
1	2.062	-.989	-2.170	1.485	0.	-4.	2173.	-1179.	853.	-147.	374.	125.	152.	10.
2	1.311	-.717	-1.468	.894	0.	-7.	4608.	602.	11053.	1039.	212.	87.	329.	77.
3	.822	-.462	-.933	.553	28.	12.	4345.	-888.	14950.	-1201.	60.	20.	291.	-49.
4	.217	-.297	-.420	.046	28.	13.	5669.	466.	23184.	-77.	-61.	-6.	407.	-11.
5	2.203	-1.587	-2.848	1.282	-28.	10.	-1271.	1176.	-3054.	237.	175.	-61.	20.	16.
6	3.210	-2.300	-4.151	1.878	-55.	14.	-7226.	-225.	-17882.	-756.	429.	39.	-243.	-22.
7	1.866	-1.127	-2.196	1.211	-55.	-44.	1187.	-165.	2827.	463.	168.	-35.	135.	9.
8	1.645	-1.828	-2.767	.587	-83.	-15.	-7381.	-826.	1015.	-338.	99.	-16.	-34.	-26.
9	.997	-2.899	-3.461	-.074	-138.	24.	-18706.	826.	3874.	860.	-114.	-37.	-181.	11.
10	1.599	-.947	-1.863	1.048	0.	3.	3451.	1006.	6677.	708.	130.	-34.	183.	0.
11	2.101	-.142	-1.349	2.011	28.	-39.	10448.	-1798.	2938.	-1633.	260.	-51.	302.	-18.
12	2.803	.986	-.604	3.419	194.	26.	25690.	-450.	1847.	-166.	406.	-32.	508.	1.
13	3.234	1.502	-.363	4.085	222.	8.	34015.	1454.	1700.	1000.	633.	1.	594.	2.
SIGMA					21.		967.		826.		53.		28.	

HUB OR SWASHPLATE TRIMMED ANGLES AND MOMENTS

T1C	T1S	THT	PHI	Lh	Mh	Lsp	Msp
2.017	-1.299	-2.454	1.262	0.	0.	220.	70.
1.084	-1.972	-2.528	-.055	-9671.	6462.	0.	0.

CONTROL MOMENTS

Lh(Lsp,Msp=0)	dLh/dLsp	dLh/dMsp	Mh(Lsp,Msp=0)	dMh/dLsp	dMh/dMsp
-9121.37	27.05	39.86	5992.48	-38.96	33.03

TABLE IV. CONTINUED

ROTOR AND SWASHPLATE DERIVATIVES DUE TO CYCLIC ANGLES

LOCKED GYRO MODE
V = 59.96 kts
q = 11.81 psf
μ = 0.799

RW1:d(0)   RW2:d(TC)   RW3:d(TS)   RW4:d(TH)   RW5:d(PH)

d(LIFT)	d(Lh)	d(Mh)	d(Lsp)	d(Msp)
64.57	7353.73	16609.57	-79.67	376.83
-44.34	190.37	-3715.34	65.76	-47.11
64.91	4104.55	1764.31	17.37	92.66
68.16	3008.12	2943.79	-15.50	90.25
-5.17	1927.75	-2030.79	57.07	4.81

I	T1C	T1S	THT	PHI	LIFT	D(LIFT)	Lh	D(Lh)	Mh	D(Mh)	Lsp	D(Lsp)	Msp	D(Msp)
1	2.425	-.842	-2.233	1.931	-83.	15.	4207.	-154.	6034.	-82.	99.	34.	189.	4.
2	1.808	-.613	-1.651	1.449	-55.	0.	5528.	347.	8822.	13.	46.	17.	231.	-4.
3	1.222	-.037	-.740	1.196	-28.	-36.	6519.	-915.	11277.	-720.	15.	15.	309.	-7.
4	.521	.638	.336	.886	111.	28.	10159.	87.	16010.	211.	-69.	-35.	437.	26.
5	1.875	-1.809	-2.880	.827	-111.	25.	-211.	-494.	6362.	-90.	15.	3.	127.	5.
6	2.488	-2.340	-3.761	1.132	-222.	-24.	-1987.	-210.	2939.	-299.	38.	-5.	71.	28.
7	3.272	-2.914	-4.783	1.583	-249.	21.	-4268.	-285.	-778.	-92.	61.	-24.	-39.	8.
8	1.879	-1.590	-2.664	.957	-138.	-16.	1170.	-14.	6641.	-183.	15.	-1.	152.	11.
9	1.269	-2.545	-3.264	-.200	-138.	19.	-2814.	35.	7341.	-65.	-38.	2.	63.	-18.
10	.517	-3.539	-3.822	-1.520	-222.	-34.	-6903.	172.	8627.	183.	-114.	-7.	12.	-13.
11	1.768	-1.602	-2.612	.840	-111.	7.	1983.	867.	7010.	606.	23.	14.	151.	6.
12	2.233	-.721	-2.002	1.810	-55.	26.	4777.	-44.	6937.	-103.	61.	6.	170.	-35.
13	2.973	.042	-1.667	2.985	-55.	9.	9041.	947.	6409.	769.	107.	-10.	233.	-8.
14	3.402	.665	-1.294	3.771	-83.	-40.	10389.	-341.	4011.	-233.	145.	-11.	273.	-5.

SIGMA · · · · · · · · 24. · 475. · 368. · 17. · 16.

HUB OR SWASHPLATE TRIMMED ANGLES AND MOMENTS

T1C	T1S	THT	PHI	Lh	Mh	Lsp	Msp
3.542	-1.956	-3.985	2.403	0.	0.	119.	29.
2.015	-3.042	-4.180	.258	-4750.	3754.	0.	0.

CONTROL MOMENTS

Lh(Lsp,Msp=0)	dLh/dLsp	dLh/dMsp	Mh(Lsp,Msp=0)	dMh/dLsp	dMh/dMsp
-4639.78	29.37	38.12	3822.75	-34.87	25.23

TABLE IV. CONCLUDED

ROTOR AND SWASHPLATE DERIVATIVES DUE TO CYCLIC ANGLES

RW1:d(θ)   RW2:d(TC)   RW3:d(TS)   RW4:d(TH)   RW5:d(PH)

LOCKED GYRO MODE
V = 60.02 kts
q = 11.83 psf
μ = 1.112

d(LIFT)	d(Lh)	d(Mh)	d(Lsp)	d(Msp)
93.54	7786.86	14007.22	-15.10	290.05
-39.50	-208.21	-2742.50	31.45	-25.07
50.38	3163.16	1101.00	24.51	60.48
55.14	2511.62	2021.36	4.78	56.83
-7.88	1150.58	-1586.56	34.33	6.74

N	T1C	T1S	THT	PHI	LIFT	D(LIFT)	Lh	D(Lh)	Mh	D(Mh)	Lsp	D(Lsp)	Msp	D(Msp)
1	2.623	-1.994	-3.494	1.406	-83.	28.	124.	-575.	4355.	-353.	23.	4.	52.	-51.
2	1.943	-1.529	-2.640	1.056	-55.	5.	3067.	697.	7995.	810.	38.	29.	159.	11.
3	1.128	-.889	-1.534	.612	-28.	-32.	4161.	-477.	9837.	-187.	8.	9.	229.	21.
4	.274	-.089	-.249	.222	55.	-23.	8113.	689.	13568.	320.	-23.	-14.	272.	-6.
5	2.678	-2.187	-3.718	1.419	-111.	12.	-13.	-84.	4279.	-66.	23.	7.	70.	-20.
6	3.433	-2.853	-4.815	1.779	-104.	-8.	-2451.	-190.	1615.	73.	23.	0.	16.	-13.
7	4.202	-3.487	-5.923	2.240	-305.	-54.	-3663.	850.	-1008.	423.	31.	-2.	-12.	18.
8	2.633	-1.981	-3.487	1.483	-111.	-1.	3.	-732.	3793.	-903.	31.	12.	65.	-37.
9	1.959	-3.075	-4.101	.183	-166.	-27.	-3069.	-541.	4816.	-521.	-15.	14.	57.	13.
10	1.383	-4.051	-4.831	-.951	-138.	27.	-5277.	163.	6448.	605.	-53.	18.	17.	7.
11	.413	-5.098	-5.314	-2.520	-166.	14.	-7947.	514.	7820.	467.	-158.	-41.	-7.	21.
12	2.529	-1.993	-3.430	1.373	-111.	-4.	32.	-668.	3919.	-1048.	15.	-1.	87.	-18.
13	3.000	-1.270	-2.980	2.258	-55.	34.	2900.	30.	4121.	-352.	46.	-2.	146.	10.
14	3.763	-.585	-2.746	3.411	-55.	30.	4924.	110.	3170.	45.	76.	-13.	185.	28.
15	4.096	.138	-2.219	4.158	-55.	7.	6513.	-488.	2818.	-108.	107.	-10.	198.	5.
16	4.877	1.012	-1.786	5.440	-55.	-7.	10265.	731.	2720.	384.	152.	-11.	237.	11.
SIGMA						24.		541.		549.		10.		22.

HUB OR SWASHPLATE TRIMMED ANGLES AND MOMENTS

T1C	T1S	THT	PHI	Lh	Mh	Lsp	Msp
4.315	-2.055	-4.528	3.116	0.	0.	70.	55.
3.169	-3.450	-5.259	1.172	-4072.	1608.	0.	0.

CONTROL MOMENTS

Lh(Lsp,Msp=0)	dLh/dLsp	dLh/dMsp	Mh(Lsp,Msp=0)	dMh/dLsp	dMh/dMsp
-3917.52	25.05	40.72	1998.90	-47.50	35.44

283

TABLE V. REDUCED EXPERIMENTAL DATA, NOMINAL VELOCITY = 70 KNOTS

ROTOR AND SWASHPLATE DERIVATIVES DUE TO CYCLIC ANGLES

RW1:d(θ)   RW2:d(TC)   RW3:d(TS)   RW4:d(TH)   RW5:d(PH)

LOCKED GYRO MODE
V = 69.19 kts
q = 15.58 psf
μ = 0.492

d(LIFT)	d(Lh)	d(Mh)	d(Lsp)	d(Msp)
298.62	3051.74	29252.01	-100.74	585.62
-31.62	1402.45	-10123.24	165.09	-91.70
79.74	8620.57	4151.28	68.03	165.26
73.79	5886.70	7527.01	-20.55	164.31
10.80	4807.68	-5818.47	153.89	2.79

N	T1C	T1S	THT	PHI	LIFT	D(LIFT)	Lh	D(Lh)	Mh	D(Mh)	Lsp	D(Lsp)	Msp	D(Msp)
1	1.060	-.970	-1.500	.502	181.	-6.	2854.	1752.	15101.	736.	-64.	17.	272.	-54.
2	.501	-.576	-.913	.258	231.	-3.	4374.	462.	22298.	1420.	-134.	-2.	482.	46.
3	.080	-.360	-.404	-.108	266.	-1.	4982.	-73.	27115.	103.	-205.	-3.	472.	-47.
4	1.252	-.816	-1.533	.778	186.	-8.	5160.	2396.	13672.	484.	-35.	5.	307.	-29.
5	1.476	-1.307	-2.151	.721	146.	-2.	-1071.	81.	8754.	-100.	-29.	7.	296.	-28.
6	1.966	-1.272	-2.307	1.226	120.	-9.	575.	745.	5454.	1384.	49.	2.	170.	-25.
7	.971	-1.194	-1.747	.281	176.	3.	-1202.	-375.	14570.	107.	-92.	20.	355.	56.
8	.725	-1.863	-2.273	-.349	116.	-11.	-7270.	-259.	12812.	-1363.	-183.	15.	105.	-16.
9	.701	-2.667	-3.060	-.835	81.	17.	-15447.	-1467.	10027.	-154.	-282.	-20.	112.	31.
10	1.106	-.888	-1.521	.501	191.	-2.	715.	-1225.	13050.	-1314.	-85.	-17.	370.	33.
11	1.462	-.176	-1.016	1.355	256.	18.	8026.	-555.	13063.	-660.	28.	-11.	434.	12.
12	2.009	.710	-.440	2.414	296.	4.	15588.	-1481.	11205.	-693.	183.	-7.	542.	22.
SIGMA						9.		1153.		880.		13.		36.

HUB OR SWASHPLATE TRIMMED ANGLES AND MOMENTS

T1C	T1S	THT	PHI	Lh	Mh	Lsp	Msp
2.350	-1.315	-2.661	1.585	0.	0.	108.	153.
2.129	-2.362	-3.577	.762	-9349.	-2106.	0.	0.

CONTROL MOMENTS

Lh(Lsp,Msp=0)	dLh/dLsp	dLh/dMsp	Mh(Lsp,Msp=0)	dMh/dLsp	dMh/dMsp
-7547.99	33.23	34.72	-360.51	-35.52	36.30

TABLE V. CONTINUED

ROTOR AND SWASHPLATE DERIVATIVES DUE TO CYCLIC ANGLES

LOCKED GYRO MODE
V = 68.45 kts
q = 15.14 psf
μ = 0.494
α_R = 1.5 DEG

RW1:d(0) RW2:d(TC) RW3:d(TS) RW4:d(TH) RW5:d(PH)

d(LIFT)	d(Lh)	d(Mh)	d(Lsp)	d(Msp)
377.03	10473.38	32513.23	-133.17	133.91
-18.00	2141.70	-9580.83	171.76	-57.20
79.41	8952.24	3830.32	85.22	172.61
67.06	5810.28	7053.43	-10.40	150.19
20.90	5504.60	-5556.33	166.30	24.43

H	TIC	TIS	THT	PHI	LIFT	D(LIFT)	Lh	D(Lh)	Mh	D(Mh)	Lsp	D(Lsp)	Msp	D(Msp)
1	1.841	-1.375	-2.428	1.043	238.	3.	1309.	-801.	8007.	-683.	84.	18.	-255.	-28.
2	1.277	-.860	-1.600	.772	298.	13.	4083.	-1347.	16160.	-770.	-7.	-10.	-124.	-22.
3	.681	-.553	-.942	.361	310.	-11.	7008.	924.	24860.	006.	-40.	14.	15.	23.
4	1.996	-1.253	-2.305	1.267	253.	12.	3339.	-101.	8361.	-210.	77.	-20.	-240.	-24.
5	2.230	-1.503	-2.770	1.357	202.	-15.	2170.	385.	6673.	1305.	127.	5.	-266.	0.
6	2.761	-1.971	-3.550	1.617	168.	-3.	-1172.	83.	-1138.	374.	169.	-4.	-381.	11.
7	2.013	-1.261	-2.413	1.280	232.	-9.	2642.	-856.	7407.	-885.	106.	1.	-234.	-15.
8	1.668	-1.970	-2.927	.525	188.	-2.	-3514.	133.	8058.	-800.	-7.	8.	-363.	-44.
9	1.392	-2.744	-3.533	-.191	143.	9.	-10616.	492.	9056.	401.	-106.	22.	-398.	35.
10	2.000	-1.366	-2.511	1.207	233.	1.	2380.	-148.	8184.	80.	77.	-17.	-231.	5.
11	2.175	-.734	-1.981	1.744	278.	-1.	9445.	883.	8935.	87.	155.	-23.	-90.	43.
12	2.707	.015	-1.503	2.705	323.	-5.	17370.	774.	6207.	461.	345.	-4.	-35.	17.
13	3.359	.872	-1.063	3.847	393.	8.	25139.	-332.	3377.	-266.	542.	24.	48.	-11.
SIGMA						8.		680.		678.		17.		25.

HUB OR SWASHPLATE TRIMMED ANGLES AND MOMENTS

TIC	TIS	THT	PHI	Lh	Mh	Lsp	Msp
2.668	-1.808	-3.335	1.618	0.	0.	171.	-358.
.972	-.307	-.955	.740	9000.	21667.	0.	0.

CONTROL MOMENTS

Lh(Lsp,Msp=0)	dLh/dLsp	dLh/dMsp	Mh(Lsp,Msp=0)	dMh/dLsp	dMh/dMsp
8875.33	27.51	37.70	21266.20	-38.41	40.32

TABLE V. CONTINUED

ROTOR AND SWASHPLATE DERIVATIVES DUE TO CYCLIC ANGLES

LOCKED GYRO MODE
V = 69.30 kts
q = 15.63 psf
μ = 0.783

RW1:d(0) RW2:d(TC) RW3:d(TS) RW4:d(TH) RW5:d(PH)

d(LIFT)	d(Lh)	d(Mh)	d(Lsp)	d(Msp)
180.72	3698.86	21330.27	-99.42	448.20
-22.78	-520.55	-5375.34	64.52	-55.19
54.05	4809.81	2430.29	27.21	121.41
50.60	3848.27	4166.96	-7.56	115.41
6.35	1699.00	-2991.30	60.42	11.22

N	T1C	T1S	THT	PHI	LIFT	D(LIFT)	Lh	D(Lh)	Mh	D(Mh)	Lsp	D(Lsp)	Msp	D(Msp)
1	1.780	-.902	-1.922	1.254	86.	-5.	3725.	293.	9944.	375.	0.	9.	246.	6.
2	.929	-.547	-1.070	.611	131.	1.	3604.	-1980.	13753.	-1253.	-50.	4.	319.	-12.
3	.322	-.061	-.246	.285	166.	-4.	9070.	834.	20001.	550.	-78.	2.	397.	-26.
4	1.742	-.823	-1.821	1.261	96.	-1.	5849.	2015.	11891.	1923.	7.	16.	273.	21.
5	2.142	-1.122	-2.349	1.488	71.	0.	1318.	-870.	6591.	-498.	7.	-1.	161.	-33.
6	2.760	-1.656	-3.237	1.797	26.	-2.	-648.	57.	2398.	-71.	35.	1.	74.	-21.
7	1.539	-.864	-1.745	1.036	101.	2.	3288.	-454.	10451.	-509.	-35.	-11.	262.	4.
8	1.008	-1.580	-2.153	.095	71.	-1.	2420.	1844.	13912.	1838.	-64.	13.	237.	36.
9	.671	-2.087	-2.465	-.532	61.	8.	-3020.	-1338.	11296.	-1356.	-134.	-21.	156.	-2.
10	1.672	-.798	-1.756	1.206	96.	-4.	4148.	158.	10636.	231.	-7.	6.	285.	26.
11	1.888	-.322	-1.406	1.696	116.	-4.	6089.	-79.	9148.	-1250.	7.	-7.	274.	-31.
12	2.359	.342	-1.016	2.546	156.	11.	9637.	-479.	9504.	21.	49.	-13.	391.	31.
SIGMA						5.		1125.		1043.		11.		24.

HUB OR SWASHPLATE TRIMMED ANGLES AND MOMENTS

T1C	T1S	THT	PHI	Lh	Mh	Lsp	Msp
3.313	-1.450	-3.349	2.460	0.	0.	75.	89.
2.600	-2.510	-3.995	1.146	-4728.	1256.	0.	0.

CONTROL MOMENTS

Lh(Lsp,Msp=0)	dLh/dLsp	dLh/dMsp	Mh(Lsp,Msp=0)	dMh/dLsp	dMh/dMsp
-4382.48	23.02	33.53	1380.85	-50.43	32.42

286

TABLE V. CONTINUED

ROTOR AND SWASHPLATE DERIVATIVES DUE TO CYCLIC ANGLES

RW1:d(0)   RW2:d(TC)   RW3:d(TS)   RW4:d(TH)   RW5:d(P')

LOCKED GYRO MODE
V = 69.40 kts
q - 15.20 psf
μ = 1.125

d(LIFT)	d(Lh)	d(Mh)	d(Lsp)	d(Msp)
123.18	5936.81	16184.33	-79.31	310.31
-18.93	120.36	-3400.46	49.40	-22.60
42.71	3129.64	1185.88	22.77	62.71
40.3c	2304.42	2371.31	-4.33	57.05
4.31	1451.20	-2045.13	47.10	10.24

N	T1C	T1S	THT	PHI	LIFT	D(LIFT)	Lh	D(Lh)	Mh	D(Mh)	Lsp	D(Lsp)	Msp	D(Msp)
1	2.515	-1.998	-3.436	1.356	-8.	2.	-1573.	-1558.	4082.	-1181.	-21.	-20.	45.	-84.
2	2.214	-1.531	-2.798	1.325	22.	6.	1199.	-213.	6747.	-93.	-74.	-9.	162.	-2.
3	1.501	-1.094	-1.953	.866	57.	9.	3434.	740.	10734.	952.	-42.	-12.	206.	-2.
4	2.528	-1.949	-3.394	1.398	-8.	0.	-327.	-470.	5125.	-152.	21.	20.	127.	-4.
5	3.329	-2.440	-4.344	1.913	-48.	-4.	-2483.	-1184.	816.	-1154.	28.	-2.	53.	-29.
6	4.161	-3.052	-5.432	2.380	-78.	8.	-2017.	1008.	-304.	1180.	49.	-8.	41.	16.
7	2.422	-1.884	-3.269	1.320	-8.	-5.	2323.	1992.	7267.	1553.	0.	3.	150.	13.
8	2.003	-2.704	-3.845	.440	-23.	7.	-2399.	-113.	6170.	14.	-35.	7.	88.	-7.
9	1.450	-3.429	-4.269	-.527	-63.	-12.	-4850.	-231.	6018.	-268.	-84.	2.	97.	34.
10	2.484	-1.911	-3.332	1.375	-3.	2.	837.	583.	5357.	-114.	7.	7.	176.	42.
11	2.930	-1.035	-2.715	2.323	17.	-7.	2372.	-679.	4057.	-939.	56.	14.	160.	-19.
12	3.406	-.469	-2.426	3.122	32.	-7.	4913.	35.	4341.	194.	77.	-1.	246.	42.
SIGMA						7.		944.		841.		11.		33.

HUB OR SWASHPLATE TRIMMED ANGLES AND MOMENTS

T1C	T1S	THT	PHI	Lh	Mh	Lsp	Msp
4.044	-2.052	-4.369	2.847	0.	0.	74.	90.
3.332	-3.747	-5.648	1.164	-5390.	409.	0.	0.

CONTROL MOMENTS

Lh(Lsp,Msp=0)	dLh/dLsp	dLh/dMsp	Mh(Lsp,Msp=0)	dMh/dLsp	dMh/dMsp
-4449.27	19.89	34.81	1080.64	-49.87	32.41

TABLE V. CONCLUDED

ROTOR AND SWASHPLATE DERIVATIVES DUE TO CYCLIC ANGLES

LOCKED GYRO MODE
V = 68.66 kts
q = 15.70 psf
μ = 1.960

RW1:d(0) RW2:d(TC) RW3:d(TS) RW4:d(TH) RW5:d(PH)

d(LIFT)	d(Lh)	d(Mh)	d(Lsp)	d(Msp)
55.94	7187.20	13915.62	-16.68	342.05
-11.96	-550.31	-2015.96	18.81	-31.22
28.95	1688.54	633.17	30.62	53.19
27.00	1510.77	1353.21	14.88	53.62
3.58	319.67	-1242.83	27.48	-.39

N	T1C	T1S	THT	PHI	LIFT	D(LIFT)	Lh	D(Lh)	Mh	D(Mh)	Lsp	D(Lsp)	Msp	D(Msp)
1	3.700	-1.611	-3.732	2.758	-39.	-4.	2028.	-402.	5346.	-91.	-7.	-11.	140.	-1.
2	3.078	-1.212	-2.977	2.369	-42.	-26.	3342.	-105.	7268.	325.	7.	3.	188.	7.
3	2.314	-.331	-1.660	2.114	26.	7.	6037.	683.	9190.	148.	63.	46.	317.	65.
4	1.397	.311	-.493	1.570	55.	7.	6818.	-126.	11170.	-127.	14.	-5.	303.	-12.
5	3.835	-1.765	-3.963	2.805	-34.	7.	1739.	-358.	4706.	-361.	7.	6.	94.	-35.
6	4.740	-2.340	-5.057	3.375	-70.	-1.	-482.	-1109.	2394.	-484.	28.	27.	70.	1.
7	5.470	-3.003	-6.137	3.721	-90.	6.	121.	1015.	1358.	372.	14.	20.	59.	48.
8	3.896	-1.677	-3.911	2.916	-39.	0.	2723.	512.	5378.	370.	-21.	-26.	83.	-48.
9	3.319	-2.254	-4.154	2.010	-50.	-1.	1850.	296.	5867.	71.	-42.	-19.	116.	-3.
10	2.761	-2.969	-4.545	1.043	-59.	4.	-81.	-736.	5881.	-589.	-63.	-7.	84.	-14.
11	3.769	-1.611	-3.772	2.827	-34.	2.	2881.	489.	5748.	450.	0.	-5.	148.	9.
12	4.139	-.911	-3.287	3.598	-25.	-5.	4266.	895.	5846.	850.	14.	-19.	166.	2.
13	4.755	-.243	-2.976	4.596	-4.	4.	3107.	-1053.	3233.	-944.	56.	-9.	162.	-19.
SIGMA						9.		684.		478.		20.		29.

HUB OR SWASHPLATE TRIMMED ANGLES AND MOMENTS

T1C	T1S	THT	PHI	Lh	Mh	Lsp	Msp
6.201	-2.236	-5.792	4.890	0.	0.	32.	30.
5.806	-3.023	-6.349	4.044	-1112.	297.	0.	0.

CONTROL MOMENTS

Lh(Lsp,Msp=0)	dLh/dLsp	dLh/dMsp	Mh(Lsp,Msp=0)	dMh/dLsp	dMh/dMsp
-1066.45	-1.59	25.03	576.44	-41.80	35.65

TABLE VI. REDUCED EXPERIMENTAL DATA, NOMINAL VELOCITY = 80 KNOTS

ROTOR AND SWASHPLATE DERIVATIVES DUE TO CYCLIC ANGLES

LOCKED GYRO MODE
V = 80.59 kts
q = 21.23 psf
$\mu = 0.399$

RW1:d(O)   RW2:d(TC)   RW3:d(TS)   RW4:d(TH)   RW5:d(PH)

d(LIFT)	d(Lh)	d(Mh)	d(Lsp)	d(Msp)
468.39	8961.58	45669.88	-411.08	659.70
-34.45	7212.33	-17834.31	417.25	-75.33
169.07	15537.93	9267.72	56.57	378.35
142.29	8565.19	14732.17	-138.79	317.66
47.56	12186.05	-9400.90	338.80	107.76

N	T1C	T1S	THT	PHI	LIFT	D(LIFT)	Lh	D(Lh)	Mh	D(Mh)	Lsp	D(Lsp)	Msp	D(Msp)
1	.529	-.429	-.732	.281	332.	-46.	6867.	755.	31729.	-522.	-130.	84.	402.	-55.
2	3.141	-1.698	-3.497	2.152	0.	-73.	5088.	-149.	-27239.	-1151.	870.	66.	-303.	-84.
3	1.433	-1.116	-1.935	.786	222.	-8.	3050.	1088.	9132.	-639.	153.	29.	85.	-45.
4	2.142	-1.946	-3.170	1.015	55.	-11.	-4934.	889.	-8731.	1843.	397.	24.	-198.	40.
5	1.395	-.871	-1.669	.889	277.	4.	4752.	-742.	15048.	2323.	99.	-23.	211.	-14.
6	1.769	-.861	-1.875	1.267	222.	-40.	7237.	-1101.	4020.	-2115.	298.	20.	170.	-31.
7	2.202	-1.233	-2.494	1.485	194.	10.	4278.	-1417.	-7540.	-2509.	412.	-26.	-25.	-52.
8	1.493	-.919	-1.774	.959	0.	-262.	3946.	-1501.	7170.	-3352.	145.	-15.	148.	-51.
9	1.696	-1.830	-2.798	.637	138.	37.	-8960.	-1715.	-3619.	-2085.	175.	-18.	-202.	-42.
10	1.529	-2.970	-3.837	-.184	28.	114.	-23440.	2711.	-5061.	4065.	15.	-44.	-429.	150.
11	1.337	-.851	-1.616	.842	388.	110.	5606.	224.	13254.	-685.	92.	-7.	265.	28.
12	1.648	-.464	-1.410	1.375	360.	27.	11340.	-2295.	12515.	542.	200.	-44.	355.	-5.
13	1.952	.267	-.857	2.098	499.	53.	27657.	470.	14750.	1424.	360.	-53.	661.	47.
14	2.255	.792	-.508	2.702	609.	84.	40317.	2784.	15653.	2862.	580.	5.	903.	114.
SIGMA						91.		1516.		2149.		40.		66.

HUB OR SWASHPLATE TRIMMED ANGLES AND MOMENTS

T1C	T1S	THT	PHI	Lh	Mh	Lsp	Msp
1.822	-1.422	-2.464	.997	0.	0.	269.	-16.
1.190	-1.507	-2.185	.318	-5872.	10491.	0.	0.

CONTROL MOMENTS

Lh(Lsp,Msp=0)	dLh/dLsp	dLh/dMsp	Mh(Lsp,Msp=0)	dMh/dLsp	dMh/dMsp
-5877.91	24.35	36.98	10236.14	-36.10	29.63

TABLE VI. CONTINUED

ROTOR HUB SWASHPLATE DERIVATIVES

RW1:d(0)	RW2:d(TC)	RW3:d(TS)	RW4:d(TH)	RW5:d(PH)
d(LIFT)	d(Lh)	d(Mh)	d(Lsp)	d(Msp)
157.40	12528.95	37029.13	-242.21	540.26
-4.07	2873.52	-12928.82	220.87	-87.63
77.00	11997.86	6759.10	42.75	298.98
59.75	7785.62	10710.48	-63.82	263.24
30.41	7379.77	-6797.47	184.91	63.99

N	T1C	T1S	THT	PHI	LIFT	D(LIFT)	Lh	D(Lh)	Mh	D(Mh)	Lsp	D(Lsp)	Msp	D(Msp)
1	1.812	-1.255	-2.292	1.083	0.	-53.	2371.	-307.	4917.	-202.	92.	-13.	-1.	-8.
2	1.968	-1.129	-2.257	1.311	40.	-22.	4870.	234.	3563.	-384.	148.	4.	11.	-19.
3	.686	-.431	-.824	.435	137.	16.	7762.	-1563.	25234.	-14.	-100.	9.	347.	-4.
4	1.812	-1.028	-2.066	1.214	27.	-44.	6544.	1144.	7930.	1277.	81.	-33.	96.	22.
5	1.811	-1.126	-2.163	1.156	27.	-36.	3953.	-267.	5599.	-404.	75.	-35.	48.	3.
6	.890	-.820	-1.328	.415	110.	19.	3956.	-1297.	18535.	-1445.	-88.	-7.	188.	-29.
7	.240	-.480	-.617	-.037	82.	-37.	8438.	982.	31788.	1111.	-224.	-14.	328.	-48.
8	1.950	-1.191	-2.307	1.258	55.	-3.	3750.	-97.	2780.	-991.	145.	7.	-7.	-21.
9	2.869	-1.796	-3.438	1.825	55.	48.	-1326.	-554.	-11246.	951.	323.	6.	-291.	-43.
10	1.691	-.927	-1.896	1.152	55.	-24.	6492.	224.	10504.	1608.	63.	-28.	153.	38.
11	1.312	-2.313	-3.058	-.023	0.	26.	-12497.	-1048.	3141.	-1290.	-44.	7.	-266.	0.
12	1.186	-3.514	-4.181	-.840	-55.	63.	-24747.	1474.	-1302.	745.	-95.	35.	-558.	56.
13	1.925	-1.246	-2.348	1.201	0.	-54.	3843.	728.	3789.	74.	135.	5.	5.	6.
14	1.976	-.277	-1.412	1.808	137.	9.	13530.	-1353.	7872.	-1744.	194.	12.	259.	-25.
15	1.644	1.100	.150	2.270	329.	94.	32149.	1701.	23909.	707.	213.	45.	796.	71.
SIGMA						43.		1017.		1018.		22.		33.

HUB OR SWASHPLATE TRIMMED ANGLES AND MOMENTS

T1C	T1S	THT	PHI	Lh	Mh	Lsp	Msp
2.060	-1.538	-2.716	1.168	0.	0.	147.	-100.
1.369	-1.406	-2.187	.555	-405.	9830.	0.	0.

CONTROL MOMENTS

Lh(Lsp,Msp=0)	dLh/dLsp	dLh/dMsp	Mh(Lsp,Msp=0)	dMh/dLsp	dMh/dMsp
-330.61	26.49	35.94	9798.55	-46.26	29.21

TABLE VI. CONTINUED

ROTOR AND SWASHPLATE DERIVATIVES DUE TO CYCLIC ANGLES

LOCKED GYRO MODE
V = 82.78 kts
q = 21.85 psf
μ = 0.807

RW1:d(0)   RW2:d(TC)   RW3:d(TS)   RW4:d(TH)   RW5:d(PH)

d(LIFT)   d(Lh)   d(Mh)   d(Lsp)   d(Msp)

-5.44	13031.94	24265.98	-117.74	409.95
18.28	-52.41	-5735.67	97.33	-59.01
54.92	6764.76	3472.80	26.71	176.63
33.41	5116.90	5108.65	-22.20	158.66
37.65	2901.42	-2809.43	84.90	32.35

N	T1C	T1S	THT	PHI	LIFT	D(LIFT)	Lh	D(Lh)	Mh	D(Mh)	Lsp	D(Lsp)	Msp	D(Msp)
1	1.373	-.931	-1.717	.832	-55.	-24.	6622.	-40.	13366.	206.	-31.	-22.	166.	1.
2	.736	-.521	-.942	.433	0.	21.	9612.	145.	18268.	33.	-49.	11.	264.	-10.
3	2.210	-1.264	-2.530	1.474	-82.	-48.	5057.	693.	7115.	-87.	35.	-29.	59.	2.
4	2.666	-1.554	-3.081	1.762	-82.	-40.	2388.	11.	2497.	-1077.	137.	37.	-18.	4.
5	3.226	-2.109	-3.956	2.001	-55.	7.	-1313.	94.	-547.	1018.	125.	-15.	-159.	-6.
6	1.534	-2.146	-3.020	.294	-110.	-15.	-1811.	-244.	7774.	-240.	-21.	5.	-64.	-5.
7	1.342	-2.931	-3.691	-.349	-110.	32.	-7090.	-223.	6798.	408.	-60.	6.	-172.	15.
8	2.814	-1.106	-2.719	2.166	-27.	-12.	4989.	-415.	3679.	-609.	120.	-7.	35.	-13.
9	2.800	-1.080	-2.686	2.168	55.	69.	5899.	321.	4185.	-268.	134.	8.	51.	-3.
10	2.849	.469	-1.171	3.108	82.	10.	15714.	-342.	10169.	617.	178.	6.	340.	15.
SIGMA						33.		318.		574.		18.		9.

HUB OR SWASHPLATE TRIMMED ANGLES AND MOMENTS

T1C	T1S	THT	PHI	Lh	Mh	Lsp	Msp
3.079	-1.903	-3.665	1.972	0.	0.	131.	-108.
1.692	-1.756	-2.721	.675	1065.	8466.	0.	0

CONTROL MOMENTS

Lh(Lsp,Msp=0)	dLh/dLsp	dLh/dMsp	Mh(Lsp,Msp=0)	dMh/dLsp	dMh/dMsp
1137.73	19.56	35.09	8405.75	-41.95	26.11

TABLE VI. CONTINUED

ROTOR AND SWASHPLATE DERIVATIVES DUE TO CYCLIC ANGLES

RW1:d(0)   RW2:d(TC)   RW3:d(TS)   RW4:d(TH)   RW5:d(PH)

LOCKED GYRO MODE
V = 82.68 kts
q = 21.80 psf
μ = 1.120

d(LIFT)	d(Lh)	d(Mh)	d(Lsp)	d(Msp)
45.52	13083.84	23487.76	-82.45	383.62
-11.20	-571.05	-5016.34	72.65	-64.81
73.54	5428.08	3008.52	30.25	140.30
60.25	4335.80	4446.31	-8.81	133.83
23.54	1929.76	-2469.58	67.86	12.19

N	T1C	T1S	THT	PHI	LIFT	D(LIFT)	Lh	D(Lh)	Mh	D(Mh)	Lsp	D(Lsp)	Msp	D(Msp)
1	2.503	-1.394	-2.828	1.691	-55.	30.	4249.	161.	6836.	97.	66.	9.	18.	-8.
2	2.042	-1.146	-2.315	1.375	-55.	7.	6393.	694.	9961.	163.	55.	23.	70.	-20.
3	1.563	-.790	-1.685	1.102	0.	30.	6602.	-1301.	12392.	-880.	21.	14.	154.	-18.
4	2.295	-1.525	-2.839	1.409	-55.	38.	5149.	1653.	8485.	1099.	35.	-4.	29.	8.
5	2.889	-1.967	-3.621	1.746	-137.	-5.	1754.	999.	3957.	881.	62.	-6.	-77.	3.
6	3.007	-2.940	-5.175	2.201	-192.	23.	-5635.	-528.	-5406.	-448.	134.	22.	-285.	-3.
7	2.630	-1.631	-3.137	1.681	-137.	-33.	2130.	-598.	4732.	-658.	31.	-28.	-43.	-28.
8	2.108	-2.424	-3.627	.706	-137.	20.	-1008.	271.	5825.	207.	3.	5.	-88.	5.
9	1.817	-3.362	-4.394	-.124	-274.	-52.	-6288.	-83.	4435.	178.	-59.	-6.	-165.	41.
10	2.610	-1.127	-2.624	1.952	-82.	-15.	4187.	-1287.	5798.	-1205.	51.	-22.	26.	-30.
11	2.768	-.251	-1.842	2.612	-27.	-23.	9338.	-801.	8919.	71.	90.	-21.	177.	8.
12	2.832	.823	-.809	3.294	55.	-10.	16753.	821.	12251.	404.	162.	14.	357.	42.
SIGMA						28.		895.		659.		17.		22.

HUB OR SWASHPLATE TRIMMED ANGLES AND MOMENTS

T1C	T1S	THT	PHI	Lh	Mh	Lsp	Msp
3.455	-2.047	-4.025	2.264	0.	0.	107.	-127.
1.907	-1.854	-2.942	.833	1934.	8347.	0.	0.

CONTROL MOMENTS

Lh(Lsp,Msp=0)	dLh/dLsp	dLh/dMsp	Mh(Lsp,Msp=0)	dMh/dLsp	dMh/dMsp
1993.86	21.31	33.64	8106.94	-37.24	29.73

TABLE VI. CONTINUED

ROTOR AND SWASHPLATE DERIVATIVES DUE TO CYCLIC ANGLES

LOCKED GYRO MODE
V = 82.88 kts
q = 21.91 psf
μ = 2.129

RW1:d(0)   RW2:d(TC)   RW3:d(TS)   RW4:d(TH)   RW5:d(PH)

d(LIFT)	d(Lh)	d(Mh)	d(Lsp)	d(Msp)
144.93	11004.34	17396.04	13.95	178.62
-23.34	14.17	-2015.78	36.79	-19.92
40.85	3594.56	1705.21	41.74	118.41
40.91	2700.68	2160.42	15.43	97.82
.18	1573.35	-776.64	45.85	36.48

N	T1C	T1S	THT	PHI	LIFT	D(LIFT)	Lh	D(Lh)	Mh	D(Mh)	Lsp	D(Lsp)	Msp	D(Msp)
1	3.862	-2.227	-4.439	2.566	-27.	9.	3011.	-43.	5962.	149.	41.	-22.	-175.	-13.
2	3.013	-1.281	-3.008	2.264	27.	5.	6377.	-67.	9291.	152.	64.	-7.	-25.	8.
3	2.589	-.891	-2.376	2.066	55.	7.	8374.	536.	11163.	505.	69.	-3.	31.	10.
4	1.981	-.379	-1.517	1.755	82.	-1.	9090.	-579.	12248.	-509.	75.	4.	95.	1.
5	3.276	-1.659	-3.535	2.309	-27.	-28.	7010.	1922.	9091.	1126.	82.	17.	-76.	7.
6	4.317	-2.741	-5.212	2.724	-55.	13.	707.	-506.	3751.	-269.	67.	9.	-219.	13.
7	3.271	-1.596	-3.471	2.340	27.	24.	4710.	-602.	7509.	-480.	60.	-8.	-89.	-14.
8	2.847	-2.675	-4.303	1.298	-27.	4.	281.	-1150.	6457.	-639.	4.	-3.	-220.	-25.
9	2.673	-3.758	-5.280	.501	-82.	-11.	-1731.	735.	5890.	289.	-41.	4.	-305.	15.
10	4.161	-1.339	-3.726	3.374	-27.	-20.	5525.	-726.	6243.	-483.	122.	11.	-66.	-3.
11	4.822	-.770	-3.539	4.360	0.	-1.	8787.	481.	6524.	160.	157.	-2.	-6.	3.
SIGMA						14.		829.		512.		10.		12.

HUB OR SWASHPLATE TRIMMED ANGLES AND MOMENTS

T1C	T1S	THT	PHI	Lh	Mh	Lsp	Msp
6.020	-3.085	-6.534	4.222	0.	0.	107.	-307.
1.110	-1.320	-1.958	.355	6274.	12890.	0.	0.

CONTROL MOMENTS

Lh(Lsp,Msp=0)	dLh/dLsp	dLh/dMsp	Mh(Lsp,Msp=0)	dMh/dLsp	dMh/dMsp
6339.26	13.52	25.66	12704.37	-37.33	27.70

TABLE VI. CONTINUED

ROTOR AND SWASHPLATE DERIVATIVES DUE TO CYCLIC ANGLES

RW1:d(0)   RW2:d(TC)   RW3:d(TS)   RW4:d(TH)   RW5:d(PH)

d(LIFT)	d(Lh)	d(Mh)	d(Lsp)	d(Msp)
240.56	10953.69	41377.8d	-391.63	523.48
73.39	6816.50	-16508.33	388.25	-37.79
136.34	16184.52	9455.81	61.52	406.85
70.77	9224.18	14297.35	-122.46	322.80
114.54	12169.07	-8320.62	319.11	148.41

FREE GYRO MODE
V = 81.67 kts
q = 21.28 psf
μ = 0.404

N	T1C	T1S	THT	PHI	LIFT	D(LIFT)	Lh	D(Lh)	Mh	D(Mh)	Lsp	D(Lsp)	Msp	D(Msp)
1	1.606	-1.201	-2.120	.908	194.	-1.	1708.	-746.	1536.	-1974.	135.	-23.	-74.	-48.
2	.461	-1.198	-1.458	-.230	83.	-28.	-7280.	-1979.	22149.	-292.	-325.	-39.	-71.	-89.
3	.177	-1.399	-1.496	-.628	28.	-35.	-10177.	309.	27534.	2319.	-410.	-1.	-64.	-12.
4	1.673	-1.042	-2.000	1.067	194.	-27.	3842.	-1647.	1429.	-2467.	144.	-50.	-45.	-81.
5	3.580	-.885	-2.940	3.056	332.	-51.	20156.	-868.	-24649.	1441.	932.	-12.	-37.	-65.
6	1.570	-1.195	-2.093	.876	166.	-27.	2560.	251.	2412.	-1749.	233.	89.	32.	55.
7	2.086	-2.453	-3.643	.667	111.	52.	-13699.	832.	-14064.	2189.	203.	-64.	-511.	42.
8	1.975	-3.248	-4.371	.099	-28.	29.	-26178.	1978.	-21096.	846.	240.	65.	-784.	89.
9	1.673	-1.128	-2.085	1.018	221.	11.	3886.	-225.	1634.	-1457.	207.	18.	-43.	-45.
10	1.648	-.107	-1.054	1.580	360.	13.	19390.	-1969.	12665.	-502.	250.	8.	445.	27.
11	1.424	.312	-.508	1.598	470.	82.	30310.	4601.	24558.	3740.	216.	36.	756.	159.
12	1.762	-1.143	-2.151	1.097	194.	-20.	3027.	-1437.	-607.	-2095.	195.	-27.	-41.	-33.
SIGMA						38.		1759.		1976.		44.		73.

HUB OR SWASHPLATE TRIMMEL ANGLES AND MOMENTS

T1C	T1S	THT		Lh	Mh	Lsp	Msp
1.707	-1.396	-2.372	.89	0.	0.	185.	-109.
1.195	-1.176	-1.858	.514	71.	10534.	0.	0.

CONTROL MOMENT.

Lh(Lsp,Msp=0)	dLh/dLsp	dLh/dMsp	Mh(Lsp,Msp=0)	dMh/dLsp	dMh/dMsp
158.85	20.42	35.75	10489.47	-39.40	29.27

TABLE VI. CONCLUDED

ROTOR AND SWASHPLATE DERIVATIVES DUE TO CYCLIC ANGLES

RW1:d(0)   RW2:d(TC)   RW3:d(TS)   RW4:d(TH)   RW5:d(PH)

FREE GYRO MODE
V = 81.26 kts
q = 21.07 psf
μ = 0.520

d(LIFT)	d(Lh)	d(Mh)	d(Lsp)	d(Msp)
18.10	11870.22	34963.06	-330.18	399.17
61.54	3208.65	-11646.87	258.79	-44.25
90.57	11309.25	6103.26	26.80	260.14
41.45	7121.38	9659.30	-92.33	215.13
85.71	7332.77	-6117.23	206.53	79.77

N	T1C	T1S	THT	PHI	LIFT	D(LIFT)	Lh	D(Lh)	Mh	D(Mh)	Lsp	D(Lsp)	Msp	D(Msp)
1	1.917	-1.377	-2.473	1.117	28.	17.	2824.	376.	3470.	-768.	136.	7.	-33.	11.
2	.490	-1.397	-1.674	-.315	-69.	9.	-3987.	-1627.	20069.	-653.	-225.	16.	-24.	-37.
3	-.003	-1.306	-1.299	-.754	-138.	-38.	-4341.	-1430.	27327.	300.	-384.	-18.	-40.	-99.
4	1.888	-1.592	-2.671	.965	0.	10.	2171.	2252.	5036.	1779.	126.	10.	-44.	55.
5	3.130	-1.078	-2.874	2.498	124.	11.	10476.	757.	-6471.	1606.	432.	-19.	-13.	7.
6	3.971	-.500	-2.781	3.667	208.	-9.	17216.	-1744.	-15320.	-988.	723.	39.	10.	-84.
7	1.904	-1.498	-2.587	1.035	-14.	-14.	2205.	1165.	3581.	-61.	128.	6.	-46.	29.
8	3.445	-.742	-2.720	3.005	124.	-39.	13092.	-1444.	-10214.	-523.	508.	-34.	-3.	-57.
9	1.910	-1.583	-2.675	.992	0.	8.	936.	840.	4932.	1881.	75.	-47.	-48.	50.
10	1.952	-2.710	-3.822	.387	-83.	24.	-12235.	274.	-4961.	-646.	100.	-3.	-378.	14.
11	1.910	-3.391	-4.476	-.047	-194.	-23.	-21774.	-1425.	-9725.	-1742.	114.	41.	-598.	-31.
12	1.913	-1.685	-2.778	.937	0.	17.	402.	1445.	3275.	880.	103.	-17.	-74.	50.
13	1.891	.068	-1.020	1.922	180.	39.	19023.	320.	13534.	181.	143.	-18.	452.	119.
14	1.431	959	.132	1.977	180.	-13.	27554.	242.	22902.	-1246.	103.	37.	560.	-25.
SIGMA						22.		1254.		1117.		26.		58.

HUB OR SWASHPLATE TRIMMED ANGLES AND MOMENTS

T1C	T1S	THT	PHI	Lh	Mh	Lsp	Msp
2.135	-1.055	-2.876	1.174	0.	0.	178.	-126.
1.410	-1.295	-2.100	.660	1753.	10641.	0.	0.

CONTROL MOMENTS

Lh(Lsp,Msp=0)	dLh/dLsp	dLh/dMsp	Mh(Lsp,Msp=0)	dMh/dLsp	dMh/dMsp
1728.78	19.52	40.49	10563.77	-39.91	26.50

TABLE VII. REDUCED EXPERIMENTAL DATA, NOMINAL VELOCITY = 90 KNOTS

ROTOR AND SWASHPLATE DERIVATIVES DUE TO CYCLIC ANGLES

RW1:d(0)   RW2:d(TC)   RW3:d(TS)   RW4:d(TH)   RW5:d(PH)

LOCKED GYRO MODE
V = 89.80 kts
q = 26.22 psf
μ = 0.493

d(LIFT)	d(Lh)	d(Mh)	d(Lsp)	d(Msp)
442.03	9403.61	47941.88	-431.24	695.99
-20.71	4315.51	-17244.57	329.32	-90.83
150.32	13024.64	8722.06	74.57	367.04
122.20	7931.94	14064.88	-87.01	315.88
49.76	8912.02	-9194.03	280.41	91.16

N	T1C	T1S	THT	PHI	LIFT	D(LIFT)	Lh	D(Lh)	Mh	D(Mh)	Lsp	D(Lsp)	Msp	D(Msp)
1	1.898	-1.236	-2.322	1.180	242.	25.	770.	-727.	4582.	146.	98.	-4.	-47.	-117.
2	1.513	-1.402	-2.266	.701	178.	-22.	-3655.	-1332.	8802.	-830.	-57.	-19.	1.	-43.
3	.362	-.691	-.896	-.036	305.	-26.	2576.	606.	36889.	1216.	-324.	39.	433.	23.
4	1.974	-1.654	-2.783	1.015	178.	26.	-1646.	1978.	2888.	3425.	77.	-19.	-43.	47.
5	3.183	-1.918	-3.741	2.068	76.	-12.	-2252.	-414.	-23085.	598.	450.	-24.	-326.	-29.
6	3.571	-1.865	-3.911	2.485	76.	-12.	1309.	787.	-28633.	1281.	661.	55.	-303.	10.
7	2.220	-1.184	-2.456	1.530	227.	9.	2490.	-1070.	-2324.	-1661.	211.	0.	31.	-28.
8	2.420	-2.009	-3.392	1.255	61.	-29.	-7476.	-1157.	-14192.	-2882.	190.	-26.	-213.	48.
9	2.189	-1.304	-2.557	1.431	221.	20.	3356.	1488.	-907.	272.	218.	26.	84.	65.
10	1.722	-.985	-1.971	1.148	287.	29.	4441.	435.	8667.	-998.	63.	1.	171.	-7.
11	1.860	-.317	-1.386	1.671	377.	21.	12344.	-958.	11563.	-1531.	140.	-18.	433.	22.
12	2.000	.199	-.952	2.107	401.	-30.	20996.	365.	16148.	962.	231.	-11.	595.	8.
SIGMA						23.		1053.		1616.		25.		48.

HUB OR SWASHPLATE TRIMMED ANGLES AND MOMENTS

T1C	T1S	THT	PHI	Lh	Mh	Lsp	Msp
2.068	-1.407	-2.591	1.251	0.	0.	145.	-8.
1.647	-1.489	-2.430	.784	-2881.	6562.	0.	0.

CONTROL MOMENTS

Lh(Lsp,Msp=0)	dLh/dLsp	dLh/dMsp	Mh(Lsp,Msp=0)	dMh/dLsp	dMh/dMsp
-2685.31	20.88	30.11	6565.04	-43.15	31.98

TABLE VII. CONTINUED

ROTOR AND SWASHPLATE DERIVATIVES DUE TO CYCLIC ANGLES

LOCKED GYRO MODE
V = 89.37 kts
q = 26.01 psf
μ = 1.072

RW1:d(0)   RW2:d(TC)   RW3:d(TS)   RW4:d(TH)   RW5:d(PH)

d(LIFT)   d(Lh)   d(Mh)   d(Lsp)   d(Msp)

d(LIFT)	d(Lh)	d(Mh)	d(Lsp)	d(Msp)
167.36	14490.53	32884.23	-151.97	531.39
-1.72	-1053.07	-7209.37	78.60	-72.52
45.63	6407.46	4390.53	42.78	151.84
35.11	5282.87	6440.41	-1.95	145.87
18.54	1992.55	-3520.21	77.79	11.40

N	T1C	T1S	THT	PHI	LIFT	D(LIFT)	Lh	D(Lh)	Mh	D(Mh)	Lsp	D(Lsp)	Msp	D(Msp)
1	2.176	-1.010	-2.257	1.586	102.	-16.	5941.	211.	11665.	-1101.	-21.	3.	158.	-62.
2	1.602	-.788	-1.706	1.142	137.	8.	8263.	511.	18108.	233.	-29.	31.	312.	16.
3	1.101	-.527	-1.158	.793	107.	-34.	10101.	146.	22075.	-560.	-106.	-18.	361.	-11.
4	2.123	-1.060	-2.276	1.505	203.	88.	4634.	-832.	11439.	-1488.	-43.	-13.	203.	-14.
5	2.156	-1.198	-2.434	1.459	97.	-12.	4607.	66.	12486.	410.	-21.	13.	240.	47.
6	2.561	-1.493	-2.959	1.692	47.	-48.	2713.	483.	7816.	-54.	-21.	-6.	114.	-5.
7	1.924	-1.085	-2.187	1.292	97.	-18.	6199.	689.	15011.	761.	-49.	-2.	189.	-38.
8	1.616	-1.833	-2.755	.556	60.	-21.	384.	-662.	13107.	-80.	-120.	-17.	183.	47.
9	1.304	-2.178	-2.919	.047	87.	21.	-898.	-63.	14282.	358.	-134.	9.	84.	-22.
10	1.950	-1.168	-2.285	1.271	127.	16.	5361.	407.	14404.	709.	-50.	-1.	225.	12.
11	2.070	-.590	-1.778	1.723	157.	20.	7690.	-839.	15624.	256.	-7.	7.	310.	18.
12	2.406	.090	-1.293	2.448	162.	-5.	12417.	-117.	16493.	556.	35.	-6.	381.	10.
SIGMA						34.		505.		681.		13.		31.

HUB OR SWASHPLATE TRIMMED ANGLES AND MOMENTS

T1C	T1S	THT	PHI	Lh	Mh	Lsp	Msp
3.538	-1.680	-3.708	2.558	0.	0.	54.	20.
3.046	-2.045	-3.788	1.858	-1819.	1945.	0.	0.

CONTROL MOMENTS

Lh(Lsp,Msp=0)	dLh/dLsp	dLh/dMsp	Mh(Lsp,Msp=0)	dMh/dLsp	dMh/dMsp
-372.28	23.36	30.83	3712.35	-42.46	37.65

TABLE VII. CONTINUED

ROTOR AND SWASHPLATE DERIVATIVES DUE TO CYCLIC ANGLES

RW1:d(0)   RW2:d(TC)   RW3:d(TS)   RW4:d(TH)   RW5:d(PH)

LOCKED GYRO MODE
V = 89.56 kts
q = 25.79 psf
μ = 1.079
α_R = 1.0 DEG

d(LIFT)	d(Lh)	d(Mh)	d(Lsp)	d(Msp)
326.27	16761.49	34171.09	-122.60	180.41
-31.93	46.16	-5671.78	95.53	-54.23
80.46	6691.00	4671.92	30.00	151.02
74.47	5018.51	5983.87	-18.94	137.30
10.93	2943.58	-2240.02	84.98	24.82

N	T1C	T1S	THT	PHI	LIFT	D(LIFT)	Lh	D(Lh)	Mh	D(Mh)	Lsp	D(Lsp)	Msp	D(Msp)
1	2.863	-1.961	-3.599	1.723	81.	4.	35125	-260.	7603.	-1171.	113.	21.	-283.	-12.
2	2.133	-1.405	-2.626	1.316	132.	-13.	6351.	-1105.	15896.	386.	35.	-4.	-168.	-21.
3	1.388	-.873	-1.667	.881	221.	9.	10715.	-271.	21208.	-1012.	-7.	9.	-43.	-16.
4	2.804	-1.752	-3.358	1.785	81.	-15.	4182.	-985.	9144.	-937.	84.	-9.	-235.	1.
5	3.367	-2.242	-4.169	2.065	31.	-7.	1345.	-573.	4078.	-521.	141.	9.	-356.	-15.
6	3.938	-2.817	-5.071	2.303	-18.	8.	-2298.	-390.	-1725.	-396.	169.	0.	-476.	-17.
7	2.733	-1.555	-3.120	1.828	122.	8.	8290.	1806.	12860.	1455.	99.	7.	-149.	54.
8	2.376	-2.543	-3.800	.904	46.	0.	-906.	-840.	8472.	-341.	21.	-7.	-346.	-13.
9	2.254	-3.162	-4.446	.427	2.	2.	-3043.	1251.	8035.	1423.	-7.	-5.	-383.	36.
10	2.604	-1.874	-3.364	1.515	91.	-1.	5038.	694.	10382.	-266.	63.	-7.	-262.	-18.
11	2.821	-1.029	-2.647	2.218	157.	4.	10200.	193.	14114.	752.	106.	-10.	-119.	9.
12	3.297	-.622	-2.515	2.927	172.	1.	13243.	489.	13192.	628.	169.	-5.	-80.	13.
SIGMA						8.		872.		873.		9.		23.

HUB OR SWASHPLATE TRIMMED ANGLES AND MOMENTS

T1C	T1S	THT	PHI	Lh	Mh	Lsp	Msp
3.939	-2.532	-4.787	2.467	0.	0.	178.	-416.
1.490	-.659	-1.514	1.105	12418.	22637.	0.	0.

CONTROL MOMENTS

Lh(Lsp,Msp=0)	dLh/dLsp	dLh/dMsp	Mh(Lsp,Msp=0)	dMh/dLsp	dMh/dMsp
12376.57	22.68	30.44	22552.57	-37.42	38.10

TABLE VII CONCLUDED

ROTOR AND SWASHPLATE DERIVATIVES DUE TO CYCLIC ANGLES

RW1:d(0)   RW2:d(TC)   RW3:d(TS)   RW4:d(TH)   RW5:d(PH)

d(LIFT)	d(Lh)	d(Mh)	d(Lsp)	d(Msp)
126.37	9915.97	21690.48	-139.55	289.95
-19.23	-338.74	-2942.87	51.56	-30.34
46.87	3076.24	1590.98	58.72	109.89
43.66	2463.78	2477.44	21.80	95.94
5.90	1082.27	-1524.44	64.35	24.92

N	TIC	TIS	THT	PHI	LIFT	D(LIFT)	Lh	D(Lh)	Mh	D(Mh)	Lsp	D(Lsp)	Msp	D(Msp)
1	3.244	-2.210	-4.066	1.960	-46.	-6.	1534.	-484.	8272.	-302.	-113.	-11.	-23.	28.
2	2.726	-1.607	-3.258	1.740	-1.	5.	2945.	-828.	10449.	-525.	-106.	-7.	-3.	-24.
3	1.890	-1.125	-2.207	1.236	34.	-3.	6047.	231.	14352.	7.	-99.	9.	81.	-28.
4	3.305	-2.287	-4.178	1.977	-37.	7.	868.	-894.	7510.	-822.	-113.	-9.	-92.	-30.
5	3.590	-2.521	-4.575	2.125	-56.	5.	1766.	823.	7710.	589.	-99.	4.	-116.	-20.
6	4.316	-2.979	-5.440	2.585	-101.	-5.	-673.	38.	4294.	38.	-78.	14.	-183.	-15.
7	3.186	-2.125	-3.948	1.952	-36.	-2.	1143.	-1157.	7348.	-1591.	-148.	-48.	-121.	-81.
8	2.820	-2.548	-4.160	1.344	-46.	1.	1370.	248.	9426.	84.	-148.	-4.	-83.	-7.
9	2.340	-3.055	-4.389	.574	-66.	-4.	70.	345.	11107.	1159.	-183.	15.	-64.	53.
10	3.054	-1.980	-3.728	1.903	-22.	3.	4243.	1453.	10011.	453.	-78.	20.	24.	44.
11	3.396	-1.708	-3.654	2.400	-16.	3.	3233.	-278.	8796.	-189.	-57.	8.	51.	52.
12	3.804	-.877	-3.060	3.285	8.	-4.	6434.	503.	10265.	1158.	14.	9.	105.	27.
SIGMA						4.		731.		758.		17.		39.

HUB OR SWASHPLATE TRIMMED ANGLES AND MOMENTS

TIC	TIS	THT	PHI	Lh	Mh	Lsp	Msp
5.986	-2.564	-5.906	4.488	0.	0.	18.	-173.
4.347	-1.438	-3.932	3.502	4019.	6616.	0.	0.

CONTROL MOMENTS

Lh(Lsp,Msp=0)	dLh/dLsp	dLh/dMsp	Mh(Lsp,Msp=0)	dMh/dLsp	dMh/dMsp
4091.66	9.71	19.82	7086.00	-30.95	30.44

TABLE VIII. REDUCED EXPERIMENTAL DATA, NOMINAL VELOCITY = 100 KNOTS

ROTOR AND SMASHPLATE DERIVATIVES DUE TO CYCLIC ANGLES

LOCKED GYRO MODE
V = 101.91 kts
q = 33.16 psf
μ = 0.410

RW1:d(0)   RW2:d(TC)   RW3:d(TS)   RW4:d(TH)   RW5:d(PH)

d(LIFT)   d(Lh)   d(Mh)   d(Lsp)   d(Msp)

d(LIFT)	d(Lh)	d(Mh)	d(Lsp)	d(Msp)
703.93	14292.28	63184.32	-423.32	659.18
37.85	12598.30	-28496.51	592.62	-3.09
222.23	23753.95	14265.30	34.57	583.79
150.89	12410.65	23130.84	-231.60	440.96
125.11	10813.77	-15257.28	461.29	250.46

N	T1C	T1S	THT	PHI	LIFT	D(LIFT)	Lh	D(Lh)	Mh	D(Mh)	Lsp	D(Lsp)	Msp	D(Msp)
1	1.735	-1.433	-2.425	.904	401.	-50.	1405.	-701.	-7764.	-1072.	595.	40.	-245.	-62.
2	.721	-1.041	-1.452	.110	428.	-72.	-1295.	57.	28012.	229.	-2.	30.	45.	-4.
3	.975	-.860	-1.418	.477	481.	-69.	2456.	-3683.	23474.	353.	103.	-22.	120.	-34.
4	.209	-.911	-1.027	-.316	508.	-1.	-7155.	-2440.	41807.	-2347.	-316.	15.	85.	-42.
5	1.482	-1.250	-2.007	.757	535.	53.	7045.	4383.	5111.	1078.	300.	-42.	-21.	54.
6	2.292	-1.486	-2.708	1.428	508.	48.	6867.	-985.	-21440.	1072.	850.	-33.	-250.	-43.
7	3.016	-2.441	-4.166	1.601	201.	-75.	-8104.	-2509.	-60350.	-2700.	1310.	30.	-789.	-14.
8	1.303	-1.081	-1.826	.076	588.	75.	6828.	1304.	11614.	967.	307.	-4.	28.	4.
9	1.655	-2.107	-3.050	.437	374.	76.	-12100.	2712.	-13153.	864.	457.	-17.	-400.	77.
10	1.420	-1.168	-1.985	.752	508.	10.	5100.	557.	7547.	1740.	356.	-27.	-12.	15.
11	1.217	-.153	-.853	1.124	722.	6.	26784.	795.	24477.	-1827.	318.	25.	615.	49.
SIGMA						56.		2297.		1651.		20.		43.

HUB OR SMASHPLATE TRIMMED ANGLES AND MOMENTS

T1C	T1S	THT	PHI	Lh	Mh	Lsp	Msp
1.514	-1.405	-2.270	.700	0.	0.	425.	-166.
.780	-1.125	-1.569	.130	-2605.	24909.	0.	0.

CONTROL MOMENTS

Lh(Lsp,Msp=0)	dLh/dLsp	dLh/dMsp	Mh(Lsp,Msp=0)	dMh/dLsp	dMh/dMsp
-2533.90	21.28	39.37	24985.61	-48.28	26.50

TABLE VIII. CONTINUED

ROTOR AND SWASHPLATE DERIVATIVES DUE TO CYCLIC ANGLES

RW1:d(0)   RW2:d(TC)   RW3:d(TS)   RW4:d(TH)   RW5:d(PH)

LOCKED GYRO MODE
V = 101.87 kts
q = 33.13 psf
μ = 0.512

d(LIFT)	d(Lh)	d(Mh)	d(Lsp)	d(Msp)
430.37	23083.47	55673.83	-304.37	739.21
4.35	5068.40	-18548.64	358.33	-43.45
124.03	17143.65	12753.82	-35.68	449.21
91.51	10706.40	17667.87	-182.65	357.16
57.19	11269.66	-8423.29	254.33	162.57

N	T1C	T1S	THT	PHI	LIFT	D(LIFT)	Lh	D(Lh)	Mh	D(Mh)	Lsp	D(Lsp)	Msp	D(Msp)
1	1.637	-1.584	-2.519	.719	267.	26.	4539.	322.	4901.	-206.	388.	49.	-23.	21.
2	1.209	-1.339	-2.029	.434	267.	-3.	6935.	683.	15806.	-372.	210.	34.	86.	1.
3	.372	-1.073	-1.283	-.247	321.	22.	6223.	-349.	35300.	209.	-124.	9.	209.	-32.
4	1.791	-1.396	-2.421	.981	294.	29.	7854.	-367.	4876.	235.	369.	-18.	24.	-10.
5	2.531	-2.036	-3.483	1.350	201.	12.	650.	-350.	-18190.	-949.	720.	45.	-326.	-41.
6	1.924	-1.675	-2.775	.953	241.	10.	5044.	933.	-244.	1130.	407.	-38.	-89.	8.
7	2.010	-2.900	-4.044	.334	53.	-26.	-17457.	-1014.	-18298.	287.	487.	-32.	-632.	19.
8	1.479	-1.516	-2.360	.601	227.	-22.	6181.	1596.	7808.	-1104.	274.	-6.	4.	10.
9	1.583	-.985	-1.892	1.011	294.	-21.	13891.	-330.	15293.	1552.	273.	-25.	233.	5.
10	1.132	-.482	-1.131	.851	348.	-28.	19443.	-1123.	27744.	-782.	101.	-18.	493.	19.
SIGMA						22.		822.		823.		31.		20.

HUB OR SWASHPLATE TRIMMED ANGLES AND MOMENTS

T1C	T1S	THT	PHI	Lh	Mh	Lsp	Msp
1.725	-1.856	-2.841	.651	0.	0.	380.	-170.
.692	-1.579	-1.970	-.218	-472.	22701.	0.	0.

CONTROL MOMENTS

Lh(Lsp,Msp=0)	dLh/dLsp	dLh/dMsp	Mh(Lsp,Msp=0)	dMh/dLsp	dMh/dMsp
-327.48	18.49	39.30	22301.35	-47.50	24.99

TABLE VIII. CONTINUED

ROTOR AND SWASHPLATE DERIVATIVES DUE TO CYCLIC ANGLES

FREE GYRO MODE
V = 102.93 kts
q = 33.33 psf
μ = 0.413

RW1:d(0)　RW2:d(TC)　RW3:d(TS)　RW4:d(TH)　RW5:d(PH)

d(LIFT)	d(Lh)	d(Mh)	d(Lsp)	d(Msp)
840.19	10373.26	66067.44	-309.59	809.84
41.39	12270.63	-23080.54	531.48	-49.86
290.17	25561.09	20600.33	104.69	745.85
200.52	13913.99	25550.69	-152.22	583.33
157.32	20352.58	-8431.59	445.74	286.71

N	T1C	T1S	THT	PHI	LIFT	D(LIFT)	Lh	D(Lh)	Mh	D(Mh)	Lsp	D(Lsp)	Msp	D(Msp)
1	1.664	-1.157	-2.110	.992	428.	-145.	2298.	1078.	5531.	1733.	513.	59.	-92.	44.
2	1.211	-1.255	-1.946	.484	562.	36.	-3881.	2972.	16697.	4434.	200.	-2.	-92.	95.
3	.729	-1.121	-1.535	.082	575.	30.	-8020.	1305.	26228.	74.	-5.	35.	-96.	-33.
4	1.707	-1.200	-2.182	1.007	615.	54.	1427.	924.	6403.	4585.	439.	-32.	-91.	83.
5	2.161	-1.008	-2.246	1.573	655.	18.	10754.	-375.	-7751.	-3162.	764.	31.	-105.	-55.
6	2.427	-1.115	-2.506	1.776	669.	52.	14923.	3257.	-9416.	3516.	917.	53.	-120.	22.
7	1.656	-1.022	-1.970	1.062	589.	-23.	2299.	-2275.	4468.	-2327.	397.	-66.	-90.	-55.
8	1.795	-1.755	-2.781	.778	401.	-4.	-13177.	-705.	-10785.	757.	377.	-84.	-539.	50.
9	1.626	-1.580	-2.509	.711	401.	-48.	-13401.	-3418.	-9721.	-5690.	369.	-20.	-562.	-112.
10	1.525	-1.098	-1.970	.888	642.	57.	150.	-876.	6479.	-1761.	465.	79.	-117.	-32.
11	1.589	-.805	-1.716	1.120	669.	-3.	8465.	-832.	10292.	-2495.	475.	24.	96.	-34.
12	1.675	-.200	-1.162	1.554	829.	-23.	24770.	-1055.	23602.	333.	484.	-76.	604.	27.
SIGMA						55.		1898.		3080.		53.		60.

HUB OR SWASHPLATE TRIMMED ANGLES AND MOMENTS

T1C	T1S	THT	PHI	Lh	Mh	Lsp	Msp
1.750	-1.246	-2.247	1.026	0.	0.	490.	-207.
.786	-1.033	-1.481	.189	-6392.	26633.	0.	0.

CONTROL MOMENTS

Lh(Lsp,Msp=0)	dLh/dLsp	dLh/dMsp	Mh(Lsp,Msp=0)	dMh/dLsp	dMh/dMsp
-6274.88	25.65	30.41	25502.88	-37.76	33.49

302

TABLE VIII. CONCLUDED

ROTOR AND SWASHPLATE DERIVATIVES DUE TO CYCLIC ANGLES

FREE GYRO MODE
V = 102.95 kts
q' = 33.28 psf
μ = 0.520

RW1:d(0) RW2:d(TC) RW3:d(TS) RW4:d(TH) RW5:d(PH)

d(LIFT)	d(Lh)	d(Mh)	d(Lsp)	d(Msp)
487.82	15504.08	62470.91	-306.39	796.43
45.52	5104.37	-20554.10	396.03	-141.53
204.00	17024.74	12027.68	99.97	432.63
133.83	10601.22	17992.91	-96.89	387.32
122.96	11245.05	-10249.15	341.69	81.50

H	T1C	T1S	THT	PHI	LIFT	D(LIFT)	Lh	D(Lh)	Mh	D(Mh)	Lsp	D(Lsp)	Msp	D(Msp)
1	1.978	-1.304	-2.437	1.220	334.	22.	3963.	571.	6078.	-47.	342.	-5.	-18.	30.
2	1.250	-1.426	-2.139	.425	267.	13.	-3132.	-737.	10005.	-618.	52.	6.	-25.	-28.
3	.892	-1.554	-2.000	-.005	214.	3.	-6507.	-113.	24834.	-613.	-84.	24.	-31.	-29.
4	2.568	-1.043	-2.516	1.958	401.	9.	10201.	-650.	-2742.	128.	576.	-30.	-30.	-12.
5	3.210	-.776	-2.619	2.751	481.	5.	18681.	8.	-13747.	-805.	930.	43.	-26.	-33.
6	1.948	-1.112	-2.227	1.301	294.	-56.	3579.	-2945.	7243.	-1811.	292.	-62.	-51.	-90.
7	2.200	-2.084	-3.340	.993	160.	-3.	-8861.	-116.	-6640.	1162.	325.	-31.	-364.	52.
8	2.197	-2.541	-3.794	.727	80.	11.	-15625.	914.	-12307.	930.	331.	21.	-593.	21.
9	1.809	-1.375	-2.461	1.101	294.	0.	4113.	2320.	8087.	1180.	327.	19.	-26.	41.
10	1.792	-.570	-1.598	1.457	415.	-38.	13761.	-1192.	15903.	-2882.	368.	22.	248.	-48.
11	1.676	.085	-.879	1.719	615.	34.	27448.	1939.	32504.	3466.	360.	-6.	691.	95.
SIGMA						24.		1395.		1618.		29.		51.

HUB OR SWASHPLATE TRIMMED ANGLES AND MOMENTS

T1C	T1S	THT	PHI	Lh	Mh	Lsp	Msp
2.132	-1.550	-2.770	1.233	0.	0.	383.	-176.
1.144	-1.467	-2.110	.296	-3627.	21310.	0.	0.

CONTROL MOMENTS

Lh(Lsp,Msp=0)	dLh/dLsp	dLh/dMsp	Mh(Lsp,Msp=0)	dMh/dLsp	dMh/dMsp
-3603.95	24.81	33.20	21103.92	-38.33	36.50

TABLE IX. REDUCED EXPERIMENTAL DATA, NOMINAL VELOCITY = 120 KNOTS

ROTOR AND SWASHPLATE DERIVATIVES DUE TO CYCLIC ANGLES

FREE GYRO MODE
V = 120.54 kts
q = 46.83 psf
μ = 0.365

RW1:d(0)   RW2:d(TC)   RW3:d(TS)   RW4:d(TH)   RW5:d(PH)

d(LIFT)	d(Lh)	d(Mh)	d(Lsp)	d(Msp)
1882.30	-4926.97	78877.55	-475.29	664.12
67.40	30133.22	-33622.27	730.13	68.13
614.15	30029.25	32834.72	-64.69	964.31
433.17	9513.17	39342.60	-366.13	696.54
317.75	35746.26	-11044.41	521.69	470.52

N	T1C	T1S	THT	PHI	LIFT	D(LIFT)	Lh	D(Lh)	Mh	D(Mh)	Lsp	D(Lsp)	Msp	D(Msp)
1	1.275	-1.055	-1.784	.663	1188.	-132.	-179.	-1974.	2720.	1340.	615.	91.	-297.	-31.
2	.773	-.914	-1.354	.244	1241.	-132.	-11536.	-2447.	18286.	-4612.	484.	336.	-294.	-130.
3	1.227	-1.142	-1.843	.566	1293.	29.	-3535.	-1293.	4660.	4558.	352.	-143.	-315.	39.
4	.675	-1.073	-1.457	.056	1372.	103.	-15100.	1702.	22077.	1142.	-95.	-182.	-257.	68.
5	1.366	-1.001	-1.782	.785	1267.	-93.	2360.	-3808.	-3788.	-3879.	491.	-96.	-312.	-104.
6	1.714	-1.298	-2.278	.961	1293.	92.	12811.	5043.	-15263.	6108.	901.	41.	-310.	160.
7	1.936	-.990	-2.099	1.359	1320.	-85.	20113.	-3566.	-25790.	-7074.	1099.	97.	-313.	-154.
8	1.266	-1.016	-1.740	.676	1372.	28.	3525.	828.	-441.	-3408.	528.	14.	-290.	-61.
9	1.281	-1.557	-2.287	.380	1134.	122.	-13085.	13.	-14098.	1207.	535.	-25.	-713.	37.
10	1.167	-1.856	-2.519	.096	765.	-56.	-24059.	1418.	-22914.	-1612.	513.	16.	-1037.	9.
11	1.340	-1.043	-1.809	.735	1320.	-12.	2489.	-1630.	712.	1127.	528.	-42.	-285.	-35.
12	1.439	-.547	-1.372	1.119	1662.	19.	20141.	-1861.	14419.	1883.	535.	-76.	233.	-2.
13	1.379	-.527	-1.318	1.070	1768.	116.	28366.	7574.	18434.	3219.	535.	-30.	452.	202.
SIGMA						89.		3202.		3704.		125.		101.

HUB OR SWASHPLATE TRIMMED ANGLES AND MOMENTS

T1C	T1S	THT	PHI	Lh	Mh	Lsp	Msp
1.266	-1.106	-1.830	.625	0.	0.	520.	-316.
.586	-.730	-1.064	.164	-9186.	35192.	0.	0.

CONTROL MOMENTS

Lh(Lsp,Msp=0)	dLh/dLsp	dLh/dMsp	Mh(Lsp,Msp=0)	dMh/dLsp	dMh/dMsp
-5015.13	31.02	34.86	28976.66	-38.46	28.80

304

TABLE IX. CONTINUED

ROTOR AND SWASHPLATE DERIVATIVES DUE TO CYCLIC ANGLES

FREE GYRO MODE
V = 119.92 kts
q = 46.1 psf
μ = 0.503

RW1:d(0)   RW2:d(TC)   RW3:d(TS)   RW4:d(TH)   RW5:d(PH)

d(LIFT)	d(Lh)	d(Mh)	d(Lsp)	d(Msp)
1092.32	12935.90	78940.44	-550.03	883.59
-3.35	9392.78	-28798.41	517.89	-105.75
265.49	20946.27	15622.81	60.16	585.73
201.38	11689.96	24284.28	-179.84	487.05
112.89	16179.22	-14894.50	416.15	175.00

N	T1C	T1S	THT	PHI	LIFT	D(LIFT)	Lh	D(Lh)	Mh	D(Mh)	Lsp	D(Lsp)	Msp	D(Msp)
1	1.938	-1.480	-2.588	1.079	739.	46.	1614.	1476.	3929.	3917.	411.	46.	-144.	44.
2	1.454	-1.390	-2.220	.649	713.	-5.	-3181.	-663.	14117.	-1241.	161.	42.	-131.	-47.
3	1.170	-1.401	-2.008	.360	713.	-4.	-8709.	-3290.	20270.	-3082.	-15.	13.	-133.	-72.
4	.994	-1.626	-2.191	.055	660.	3.	-10988.	804.	26595.	1686.	-101.	-28.	-143.	31.
5	1.947	-1.567	-2.680	1.038	686.	16.	3214.	4817.	3826.	5436.	454.	90.	-149.	91.
6	2.403	-1.086	-2.463	1.709	739.	-57.	11435.	-1319.	-13732.	-6597.	709.	140.	-139.	-132.
7	2.993	-1.128	-2.845	2.332	818.	35.	16977.	-439.	-22758.	2121.	902.	-30.	-83.	11.
8	1.933	-1.380	-2.486	1.132	660.	-60.	3627.	1437.	807.	-915.	381.	13.	-131.	-2.
9	2.145	-2.077	-3.302	.942	475.	-59.	-15283.	-4861.	-21735.	-6444.	366.	-70.	-871.	-116.
10	2.236	-2.744	-4.019	.649	369.	13.	-23173.	371.	-25748.	2595.	374.	-67.	-871.	89.
11	1.854	-1.355	-2.415	1.007	818.	92.	5505.	3534.	5124.	731.	337.	9.	-84.	22.
12	1.859	-.703	-1.769	1.447	871.	-28.	13876.	-1785.	14328.	-95.	315.	-55.	208.	-7.
13	1.924	-.145	-1.251	1.833	1055.	8.	27886.	-77.	23065.	1798.	337.	-101.	683.	88.
SIGMA						42.		2493.		3492.		66.		71.

HUB OR SWASHPLATE TRIMMED ANGLES AND MOMENTS

T1C	T1S	THT	PHI	Lh	Mh	Lsp	Msp
1.935	-1.485	-2.592	1.073	0.	0.	363.	-191.
1.212	-1.290	-1.981	.465	-2696.	23891.	0.	0.

CONTROL MOMENTS

Lh(Lsp,Msp=0)	dLh/dLsp	dLh/dMsp	Mh(Lsp,Msp=0)	dMh/dLsp	dMh/dMsp
-2671.08	24.83	33.15	22739.46	-45.87	31.78

305

TABLE IX. CONCLUDED

ROTOR AND SWASHPLATE DERIVATIVES DUE TO CYCLIC ANGLES

FREE GYRO MODE
V = 119.98 kts
q = 46.15 psf
μ = 0.787

RW1:d(0)	RW2:d(TC)	RW3:d(TS)	RW4:d(TH)	RW5:d(PH)
d(LIFT)	d(Lh)	d(Mh)	d(Lsp)	d(Msp)
652.00	22325.48	57164.11	-492.34	1097.90
-12.70	2010.75	-13284.34	269.83	-154.62
195.84	14851.94	11179.65	22.64	486.51
153.00	10309.93	14193.88	-100.26	433.58
75.58	7970.85	-5143.42	213.03	95.07

N	T1C	T1S	THT	PHI	LIFT	D(LIFT)	Lh	D(Lh)	Mh	D(Mh)	Lsp	D(Lsp)	Msp	D(Msp)
1	2.791	-1.557	-3.155	1.884	343.	31.	3752.	-1059.	918.	-1767.	227.	2.	-207.	-116.
2	2.036	-2.023	-3.186	.865	237.	7.	-2760.	866.	7180.	-320.	59.	48.	-192.	9.
3	1.336	-1.955	-2.715	.206	237.	-15.	-6444.	-2421.	16486.	-1080.	-198.	-22.	-109.	-49.
4	2.799	-1.820	-3.422	1.741	290.	30.	2884.	1956.	2465.	2821.	183.	-39.	-145.	.75.
5	3.649	-.967	-3.061	3.079	317.	-99.	8739.	-6564.	-4206.	-4206.	425.	-45.	-127.	-190.
6	3.606	-1.552	-3.619	2.699	396.	94.	9436.	2911.	-6266.	1828.	520.	74.	-109.	106.
7	2.644	-1.803	-3.316	1.597	370.	105.	1126.	256.	1754.	-130.	205.	25.	-151.	37.
8	2.823	-2.014	-3.629	1.653	158.	-64.	-133.	1778.	1752.	-1097.	149.	-75.	-308.	10.
9	2.776	-2.169	-3.757	1.517	132.	-60.	-6949.	-2637.	-4726.	-767.	212.	5.	-437.	-50.
10	2.732	-1.682	-3.247	1.754	237.	-51.	2248.	-586.	-832.	-2889.	205.	-2.	-138.	5.
11	2.532	-1.329	-2.779	1.758	343.	-17.	7412.	-272.	8504.	-170.	198.	37.	17.	-43.
12	2.696	-1.029	-2.575	2.094	422.	6.	12834.	370.	11544.	1704.	220.	8.	212.	32.
13	2.837	-1.026	-2.653	2.235	448.	33.	18190.	5399.	11233.	3223.	234.	-16.	335.	175.
SIGMA						58.		2815.		2125.		39.		90.

HUB OR SWASHPLATE TRIMMED ANGLES AND MOMENTS

T1C	T1S	THT	PHI	Lh	Mh	Lsp	Msp
2.727	-1.872	-3.433	1.640	0.	0.	201.	-235.
1.962	-1.633	-2.755	1.015	2013.	12846.	0.	0.

CONTROL MOMENTS

Lh(Lsp,Msp=0)	dLh/dLsp	dLh/dMsp	Mh(Lsp,Msp=0)	dMh/dLsp	dMh/dMsp
2242.79	22.88	28.85	12513.88	-33.67	24.27

306

TABLE X. REDUCED EXPERIMENTAL DATA, NONDIMENSIONALIZED DERIVATIVES (a) LOCKED SWASHPLATE

Vkt	MU	RPM	dCL/dT1C	(dCl)h/dT1C	(dCm)h/dT1C	(dCl)sp/dT1C	(dCm)sp/dT1C
49.38	.488	98.7	-.151817E-02	.5621835E-03	-.372815E-02	.6597344E-04	-.354446E-04
48.04	.771	60.8	-.156462E-02	.2437467E-03	-.192722E-02	.4253774E-04	-.115426E-04
50.03	1.055	46.3	-.129414E-02	-.164570E-03	-.127277E-02	.1421833E-04	-.151977E-04

Vkt	MU	RPM	dCL/dT1S	(dCl)h/dT1S	(dCm)h/dT1S	(dCl)sp/dT1S	(dCm)sp/dT1S
49.38	.488	98.7	.5923955E-02	.3062778E-02	.1242913E-02	.1669602E-04	.9243421E-04
48.04	.771	60.8	.4138065E-02	.2090002E-02	.7165053E-03	.5936412E-05	.4510887E-04
50.03	1.055	46.3	.3343804E-02	.1571315E-02	.6503727E-03	.1494376E-05	.3350739E-04

Vkt	MU	RPM	dCL/dT1C	(dCl)h/dT1C	(dCm)h/dT1C	(dCl)sp/dT1C	(dCm)sp/dT1C
60.91	.402	147.9	.2100305E-02	.1398414E-02	-.499708E-02	.9150266E-04	-.337717E-04
59.96	.799	73.3	-.438963E-02	.9518437E-04	-.185766E-02	.3287978E-04	-.235548E-04
60.02	1.112	52.7	-.390979E-02	-.148852E-03	-.136892E-02	.1569831E-04	-.129630E-04

Vkt	MU	RPM	dCL/dT1S	(dCl)h/dT1S	(dCm)h/dT1S	(dCl)sp/dT1S	(dCm)sp/dT1S
60.91	.402	147.9	.7132204E-02	.5026688E-02	.2276338E-02	.3151737E-04	.1034338E-03
59.96	.799	73.3	.6426048E-02	.2052262E-02	.8821492E-03	.8684943E-05	.4632970E-04
60.02	1.112	52.7	.4979155E-02	.1578896E-02	.5495657E-03	.1223420E-04	.3018868E-04

TABLE X. CONTINUED (b) LOCKED SWASHPLATE

Vkt	MU	RPM	dCL/dT1C	(dCl)h/dT1C	(dCm)h/dT1C	(dCl)sp/dT1C	(dCm)sp/dT1C
69.19	.492	137.4	-.237288E-02	.5315413E-03	-.383680E-02	.6257061E-04	-.347551E-04
68.45	.494	135.3	-.139700E-02	.8353375E-03	-.374026E-02	.6699050E-04	-.262096E-04
69.30	.783	86.4	-.170403E-02	-.196662E-03	-.203079E-02	.2437544E-04	-.208506E-04
69.40	1.125	60.2	-.145609E-02	.4675797E-04	-.132103E-02	.1919112E-04	-.877974E-05
68.66	1.960	34.2	-.890664E-03	-.206978E-03	-.758227E-03	.7074670E-05	-.117422E-04

Vkt	MU	RPM	dCL/dT1S	(dCl)h/dT1S	(dCm)h/dT1S	(dCl)sp/dT1S	(dCm)sp/dT1S
69.19	.492	137.4	.5983992E-02	.3270685E-02	.1573373E-02	.2578399E-04	.6263504E-04
68.45	.494	135.3	.6132415E-02	.3491587E-02	.1493916E-02	.3323783E-04	.6732202E-04
69.30	.783	86.4	.4043142E-02	.1817130E-02	.9181554E-03	.1027985E-04	.4586829E-04
69.40	1.125	60.2	.3285248E-02	.1215816E-02	.4606957E-03	.8845787E-05	.2436185E-04
68.66	1.960	34.2	.2155913E-02	.6350805E-03	.2381429E-03	.1151655E-04	.2000541E-04

Vkt	MU	RPM	dCL/dT1C	(dCl)h/dT1C	(dCm)h/dT1C	(dCl)sp/dT1C	(dCm)sp/dT1C
80.59	.399	197.2	-.189724E-02	.2006054E-02	-.496048E-02	.1160549E-03	-.209525E-04
82.76	.527	153.2	-.217883E-03	.7769242E-03	-.349561E-02	.5971744E-04	-.236928E-04
82.78	.807	100.2	.9781534E-03	-.141638E-04	-.155006E-02	.2630343E-04	-.159474E-04
82.68	1.120	72.1	-.600681E-03	-.154680E-03	-.135877E-02	.1967869E-04	-.175551E-04
82.88	2.129	38.0	-.124549E-02	.3818955E-05	-.543273E-03	.9915268E-05	-.536864E-05

Vkt	MU	RPM	dCL/dT1S	(dCl)h/dT1S	(dCm)h/dT1S	(dCl)sp/dT1S	(dCm)sp/dT1S
80.59	.399	197.2	.9311053E-02	.4321756E-02	.2577745E-02	.1573451E-04	.1052351E-03
82.76	.527	153.2	.4122117E-02	.3243906E-02	.1827483E-02	.1155847E-04	.8083632E-04
82.78	.807	100.2	.2938741E-02	.1828176E-02	.9385240E-03	.7218376E-05	.4773425E-04
82.68	1.120	72.1	.3944113E-02	.1470303E-02	.8149172E-03	.8193811E-05	.3800303E-04
82.88	2.129	38.0	.2179877E-02	.9687694E-03	.4595709E-03	.1124934E-04	.3191266E-04

TABLE X. CONTINUED (c) LOCKED SWASHPLATE

Vkt	MU	RPM	dCL/dT1C	(dCl)h/dT1C	(dCm)h/dT1C	(dCl)sp/dT1C	(dCm)sp/dT1C
89.80	.493	177.7	-.923485E-03	.9718886E-03	-.388362E-02	.7416559E-04	-.204557E-04
89.37	1.072	81.4	-.773162E-04	-.239075E-03	-.163672E-02	.1784429E-04	-.164640E-04
89.56	1.079	81.0	-.144754E-02	.1056894E-04	-.129863E-02	.2187286E-04	-.124167E-04
88.28	2.018	42.7	-.889022E-03	-.790924E-04	-.687131E-03	.1203874E-04	-.708409E-05

Vkt	MU	RPM	dCL/dT1S	(dCl)h/dT1S	(dCm)h/dT1S	(dCl)sp/dT1S	(dCm)sp/dT1S
89.80	.493	177.7	.6702955E-02	.2933257E-02	.1964280E-02	.1679378E-04	.8266045E-04
89.37	1.072	81.4	.2051126E-02	.1454664E-02	.9967670E-03	.9712197E-05	.3447172E-04
89.56	1.079	81.0	.3647631E-02	.1531993E-02	.1069698E-02	.6868896E-05	.3457802E-04
88.28	2.018	42.7	.2166848E-02	.7182712E-03	.3714779E-03	.1371053E-04	.2565821E-04

Vkt	MU	RPM	dCL/dT1C	(dCl)h/dT1C	(dCm)h/dT1C	(dCl)sp/dT1C	(dCm)sp/dT1C
101.91	.410	242.6	.1334546E-02	.2243456E-02	-.507451E-02	.1002419E-03	-.550251E-06
101.87	.512	194.1	.1535147E-03	.9033717E-03	-.330604E-02	.6386733E-04	-.774436E-05

Vkt	MU	RPM	dCL/dT1S	(dCl)h/dT1S	(dCm)h/dT1S	(dCl)sp/dT1S	(dCm)sp/dT1S
101.91	.410	242.6	.7835567E-02	.4229980E-02	.2540307E-02	.6156047E-05	.1039583E-03
101.87	.512	194.1	.4377111E-02	.3055617E-02	.2273191E-02	-.635946E-05	.8006543E-04

TABLE X.   CONCLUDED (d) FREE SWASHPLATE

Vkt	MU	RPM	dCL/dT1C	(dCl)h/dT1C	(dCm)h/dT1C	(dCl)sp/dT1C	(dCm)sp/dT1C
81.67	.404	197.2	.4032250E-02	.1891502E-02	-.458088E-02	.1077350E-03	-.104863E-04
81.26	.520	152.6	.3414878E-02	.8992384E-03	-.326409E-02	.7252705E-04	-.124013E-04

Vkt	MU	RPM	dCL/dT1S	(dCl)h/dT1S	(dCm)h/dT1S	(dCl)sp/dT1S	(dCm)sp/dT1S
81.67	.404	197.2	.7490898E-02	.4491023E-02	.2623881E-02	.1707111E-04	.1128963E-03
81.26	.520	152.6	.5025764E-02	.3169468E-02	.1710466E-02	.7510819E-05	.7290539E-04

Vkt	MU	RPM	dCL/dT1C	(dCl)h/dT1C	(dCm)h/dT1C	(dCl)sp/dT1C	(dCm)sp/dT1C
102.93	.413	243.4	.1451919E-02	.2173945E-02	-.409069E-02	.9416048E-04	-.883352E-05
102.85	.520	193.1	.1599194E-02	.9056823E-03	-.364697E-02	.7026868E-04	-.251121E-04

Vkt	MU	RPM	dCL/dT1S	(dCl)h/dT1S	(dCm)h/dT1S	(dCl)sp/dT1S	(dCm)sp/dT1S
102.93	.413	243.4	.1017887E-01	.4528570E-02	.3649689E-02	.1854757E-04	.1321397E-03
102.85	.520	193.1	.7166863E-02	.3020746E-02	.2134104E-02	.1773795E-04	.7676272E-04

Vkt	MU	RPM	dCL/dT1C	(dCl)h/dT1C	(dCm)h/dT1C	(dCl)sp/dT1C	(dCm)sp/dT1C
120.54	.365	322.4	.1682744E-02	.3799005E-02	-.423955E-02	.9206469E-04	.8590754E-05
119.92	.503	232.9	-.849623E-04	.1203124E-02	-.368880E-02	.6633667E-04	-.135455E-04
119.98	.787	148.8	-.321747E-03	.2572785E-03	-.169975E-02	.3452515E-04	-.197839E-04

Vkt	MU	RPM	dCL/dT1S	(dCl)h/dT1S	(dCm)h/dT1S	(dCl)sp/dT1S	(dCm)sp/dT1S
120.54	.365	322.4	.1533319E-01	.3786495E-02	.4140247E-02	-.815699E-05	.1215933E-03
119.92	.503	232.9	.6733324E-02	.2683013E-02	.2001130E-02	.7705910E-05	.7502031E-04
119.98	.787	148.8	.4961488E-02	.1900328E-02	.1430453E-02	.2896822E-05	.6224968E-04

REFERENCES

1. Abbot, I. H. and Von Doenhoff, A. E., "Theory of Wing Sections," Dover Publications, New York, 1959

2. Harris, F. D., Tarzanin, F. J. and Fisher, R. K. "Rotor High Speed Performance, Theory vs. Test," Proc. V/STOL Tech. and Planning Conference, Las Vegas, 1969

3. Fung, Y. C., "The Theory of Aeroelasticity," John Wiley & Sons, Inc., New York, 1955

4. Gessow, A. and Meyers, G. C., "Aerodynamics of the Helicopter," Frederick Ungar Publishing Co., New York, Republished 1967

5. Cardinale, S. V.; Donham, R. E., "Full-Scale Wind Tunnel Tests and Analysis of a Stopped/Folded Rotor," Lockheed Report 21016 for Naval Air Systems Command, May 1968

6. Perkins, C. D.; Hage, R. E., "Airplane Performance Stability and Control," John Wiley & Sons, Inc., New York, 1949